THE DIFFUSION OF ADATOMS ON TUNGSTEN SINGLE CRYSTAL SURFACES

THESIS SUBMITTED IN ACCORDANCE WITH THE REQUIREMENTS OF THE UNIVERSITY OF LIVERPOOL FOR THE DEGREE OF DOCTOR IN PHILOSOPHY.

By

M.A. Morris.

The Department of Industrial, Physical and Inorganic Chemistry,

University of Liverpool,

Liverpool, 1983.

ORIGINAL COPY TIGHTLY BOUND

TEXT BOUND CLOSE TO THE SPINE IN THE ORIGINAL THESIS

PAGE NUMBERS CLOSE TO THE EDGE OF THE PAGE.

SOME ARE CUT OFF

And I'll tell it and think it and speak it and breathe it,

And reflect it from the mountains so all souls can see it,

B.Dylan.

ACKNOWLEDGEMENTS.

I would like to extend my thanks to Professor D.A.King for all the help he has given me over the years.I would like to extend the same gratitude to all the members of the Liverpool Surface Science group who as well as being valued colleagues have also been valued friends, which may be of greater importance in the end.Of all these three deserve special mention, K.Griffiths,C.Barnes, and N.Palmer, the first two because they have had to survive considerable lengths of time in my presence for the sake of Science. Nick is included on the grounds that he was, is,and always will be a very dear friend.

I would also like to thank Professor A.Ledwith for extending to me the facilities of the department of I.P.I.Chemistry at Liverpool during the course of this study.

Last but most importantly,I must thank my wife Annette,she has been the most important inspiration for me over the years.She has never failed to give me a level of support of which I am most undeserving.

FOREWORD.

Foreword

This Thesis follows the same type of structure that has been adopted by most Ph.D students. It differs slightly in that the experimental chapters are written in the style of academic papers . These chapters are arranged in this form because they are also intended as drafts for future publications. In this way co-authors' names also appear. It should be emphasised that these chapters were written without their assistance.

CHAPTER I: INTRODUCTION.

I. Introduction.

I.I. General Introduction.

Surface Chemistry is having an ever more obvious impact on our lives. Soaps, lubricants and adhesives are all surface active reagents. The problem of corrosion is well known to everybody in the modern world. Heterogeneous catalysis is important in the production of many of our essential chemicals. Latterly the microchip industry has revolutionised life for most of us and many believe that its' impact will alter the whole fabric of society.

Over the recent years scientists have begun to apply themselves in solving the fundamental problems associated with solid surfaces. The reason for the sudden development is mainly technological rather than scientific. The ability to produce clean, well-characterised surfaces and maintain them for long enough to study them is relatively new (less than thirty years). This occurred only with the advent of techniques capable of producing ultra high vacuum. This co-incided with and spurred the advance of quantitative experimental techniques which can now be performed with a sensitivity of less than one per cent of a monolayer. Thus it has came to pass that scientists have been handed the "Tools of the trade".

As well as a practical approach there exists a need to produce a reliable data base within a discipline that is in its infancy. To this objective a large number of surface scientists have worked with simple systems, e.g. low molecular weight gases on single crystal planes. These "simple" systems are of great importance to the physicist and the theortician. Why do molecules adsorb? How is energy dissipated in the process of adsorption? Are the surfaces themselves perfectly stable? The answers to these questions are providing a great impetus to all surface scientists.

I.2. Ultra-High Vacuum, (U.H.V.).

The purpose of this study is to investigate the diffusion of adspecies across a single crystal surface. It will be seen that in order to do this the species of interest has to be deposited on to part of the surface ensuring that the rest of the surface is atomically clean. The preparation of the clean surface, the dosing time and the time needed to perform the experiments necessitates that a state of near perfect cleanliness must be maintained for periods of up to an hour. This experimental requisite could not be achieved until the development of U.H.V. The kinetic theory of gases shows that the rate of arrival of N molecules of a gas is given by

$$N = 2{\cdot}89 \times 10^{22} P(MT)^{-\frac{1}{2}} \text{ molecules cm}^{-2} \text{ s}^{-1}$$

where P is the pressure in Torr,

M is the molecular weight of the impinging gas,

T is the temperature of the gas.

Conventional diffusion pumped systems normally achieve pressures around 10^{-6} Torr. Assuming that all the gas molecules that collide with the surface adsorb (i.e. the sticking probality is equal to one) and that a monolayer of gas corresponds to $\sim 10^{15}$ atoms cm^{-2}, it can be seen that a monolayer of gas is collected in about 3 seconds at this pressure. In order to maintain the surface at the cleanliness level necessary for experiments to be meaningful, pressures of 10^{-10} Torr or below are necessary

I.3. The Gas-Solid Interaction.

When a gas particle collides with a surface and sticks, a gradual accumulation of the particles occurs. This process is known as adsorption. The incoming particles are known as adsorbates, the reacting surface as the adsorbent. In many cases adsorbate particles may be

transferred from the surface layer to the interior of the solid. This is known as absorption.

How and why do molecules adsorb? It is well known that for adsorption the process occurs spontaneously i.e. the free energy of the gas/solid system is lowered; the change of free energy ΔG is given by,

$$\Delta G = \Delta H - T\Delta S.$$

Since the adsorbent is more ordered than the gas phase when it is adsorbed on the surface, the free entropy change ΔS must be negative. This means that ΔH is negative i.e. the adsorption process is exothermic. As early as 1924[2] the process could be described in terms of an interaction potential. The basics of the model are still used today. For a gas-metal system where the interaction is strong enough to form a chemisorbed bond it was shown that an incoming particle passes through two energy minima. This is seen in Fig.I(a). The second deeper well is due to the formation of a chemical bond. The well is known as the chemisorbed well, the process bringing gas particles into equilibrium in this well is known as chemisor-ption. The first shallow well is the physisorbed well and its existence has been attributed to the existence of weak Van der Waals forces between the gas and the solid. It has been shown,[3,4] that the depth of the well is often greater than is predicted solely by these rather weak forces. However the concept of a two stage adsorption process is still believed to be true for many of the systems investigated today.

The impression may have been given that all molecules incident on the surface will automatically adsorb. This is not true. Incoming particles always have kinetic energy to dump before they can be accommodated into the wells. Hence a number of events can be performed by these

partides before they adsorb. A recent review has detailed these events[5]. These events allow the molecule to lose energy and are summarised here.

The particle may be elastically scattered losing no energy to the surface or may lose a proportion of its energy and be non-elastically scattered. It may be partially accommodated, diffuse across the surface from one well to the next before either leaving the surface again or, in fact, being fully accommodated. It may also pass into the chemisorbed well where a number of similar events may be performed. All of these events can be assigned a certain probability. It is an overall probability equal to the individual probabilities multiplied together that defines the probability of adsorption. This is the sticking probability defined as, s

$$s = \text{Rate of adsorption} \Big/ \text{Rate of gas arrival.}$$

There is another reason why particles do not have to adsorb. Fig.I(a) shows this explicitly. Here it can be seen that the crossover of the potential wells is below the energy zero. In Fig.I(b) it is above. In this case the adsorption is said to be activated. Particles that are to reach the chemisorbed well have to climb above the energy zero and so are preferentially scattered into the gas phase. For such systems the rate of chemisorption is normally very low[6]. This despite the fact that the chemisorption energy is of the same order of magnitude as in a non-activated case.

I.4. Surface structure of W{110} and W{100}.

In order to fully understand adsorption processes it has proved necessary to look at the simplest surfaces possible. This was made feasible because bulk single crystal surfaces of most metals became commercially available.

In this study W{110} and W{100} were used as adsorbents. W is a metal that adopts a body-centered cubic arrangement. The surface unit mesh of W{110} is shown in Fig.2. The surface is two fold symmetric and the surface density is 14·2 atoms $cm^{-2} \times 10^{14}$. This plane is fairly smooth and is the most closely packed plane of a B.C.C. metal. Also shown in Fig.2. is the W{100} surface unit mesh. It is four fold symmetric and the surface atom density is 10·0 atoms $cm^{-2} \times 10^{14}$.

Apart from the rather obvious differences in symmetry and corresponding differences in surface density, there are other marked differences between the two surfaces. It has been shown[14] that the W{100} surface undergoes a surface reconstruction at room temperature and below. This causes enhanced stability of the surface. However small amounts of Nitrogen[15] have been shown to lift this surface reconstruction. It has been pointed at that[16] this does not alter the simple picture of the surface as a simple square array. The W{110} surface does not display the same tendancy, due to its more closely packed structure. The difference is emphasised by the adsorption properties of H_2[17], N_2[18] and O_2[19]. All of these gases cause surface reconstructions when adsorbed to high surface concentrations. The W{100} surface is a landmark, being the first surface where such effects were quantitatively investigated.

I.5. Low Energy Electron Diffraction.

The experimental arrangement necessary to observe the diffraction of electrons from surfaces is described in the following chapter, the aim here is to outline the information that can be obtained from a L.E.E.D. system. A description of how and why electrons diffracted from the surface carry information is also included.

Since its discovery in 1927[7] L.E.E.D. techniques have remained almost

unchanged for about 50 years . Since X-rays diffract strongly from materials it is to be expected that electrons of a similar wavelength should also diffract. The electron wavelength is given by,

$$\lambda = \left(\frac{150.4}{V}\right)^{1/2} \text{ A}^{\circ}$$

here V is the voltage through which the electron is accelerated. This puts the useful voltages in the range of 20 to 1000 volts. Because of the strong elastic and inelastic scattering of these slow electrons, they can only penetrate 3-5 atomic layers and so are highly sensitive to the surface, unlike X-rays which penetrate the bulk of the crystal. Higher energies can be used but the angle of incidence is limited to less than 5° rather than normal in L.E.E.D. Thus the energy normal to the surface is still low enough to ensure a high surface sensitivity. The technique is known as Reflection High-Energy Electron diffraction or R.H.E.E.D.

So in a L.E.E.D. experiment a primary beam of electrons is diffracted from the surface, i.e. we observe a number of discrete beams emerging from the surface. The spatial distribution of these beams is determined by the distances between rows of atoms in the atomic planes. The geometry of the diffraction is then described in terms of a unit mesh, this can be defined by unit vectors a_1^* and a_2^* and an interaction angle γ^*. The diffraction geometry can be pictured using a Ewald Sphere construction. The surface layer is represented as a 2D set of atoms. Again this can be described in terms of a unit mesh which repeats over space to form the net. There are only five possible unit meshes. The square, the rectangle, centered rectangle, the 120° degree rhombus and the parallelogram. The unit meshes are made up of two vectors a_1 and a_2 with an angle of γ degrees between them. Because of the physics of diffraction a distance that is large on the surface appears to be small when viewed in the diffraction pattern. The surface net is said to be in real space, the diffraction

pattern in reciprocal space. The surface net, the reciprocal net and an observed L.E.E.D. pattern for a B.C.C.{110} crystal plane are shown in Fig.3. A Ewald sphere construction for a square lattice is shown in Fig.4. The surface can be considered as a 2D-array of point scatterers as scattering from the second layer is negligible. Because of this, effectively , the distance between atoms in the direction normal to the surface plane is infinite, transposed in reciprocal space to zero. Hence it is a continuum. The reciprocal lattice thus consists of a set of rods perpendicular to the surface as shown. These rods are numbered as shown, the general notation being (h,k).[9] The incident electron beam makes the same angle with the surface normal as in real space and is represented by the wave vector $K_o = 2\pi/\lambda$, terminating at the origin (0,0). The Ewald Sphere is drawn with radius K_o. The points where the Ewald Sphere intersect the rods determine the directions of the diffracted beams. Observed L.E.E.D. patterns are simply sections of the reciprocal lattice perpendicular to the rods. It can be seen that as the primary beam energy increases (K_o increases) the radius of the circle increases and cuts more rods. This in a L.E.E.D. experiment means that the higher the beam energy, the higher the number of observed beams. The relation between the surface net and the L.E.E.D. pattern is shown in Fig.5. The indexing of the beams is simply, then, the number taken from the Ewald Sphere construction.

The vectors K drawn from the centre of the sphere to the intersections satisfy the conditions of energy conservation,

$$K^2 = K_o^2 .$$

Momentum conservation is also maintained, but due to translational symmetry (i.e. the existence of unit cells) momentum parallel to the surface is multivalued,

$$K_{//} = K_{o//} + \bar{g}\,(h,k);$$

where $\bar{g}(h,k)$ is a reciprocal lattice vector to go from one point scatterer to the next. This equation is the physics of the L.E.E.D. process. It is only a restatement of Bragg's law.

When new periodic surface structures form new diffraction beams are observed. Since electrons do penetrate more than one layer usually in many cases, the diffraction beams are no longer determined by a single layer reciprocal net. The superposition of two nets results in a pattern of diffraction beams described by,

$$M_a a^* + M_b b^* = M_c c^*$$

a^* and b^* are matrices describing the substrate and surface reciprocal nets. M_a, M_b and M_c are integer row matrices such that if M_b is zero, $M_c c^*$ describes the original surface net. When M_a is zero $M_c c^*$ describes the new surface structure. If both are non-zero, beams resulting from double diffraction are described. This diffraction is called "incoherent". However, it is more frequently seen that a and b are related and that the superposition can be described by a third net c, (the nets being referred to are real space nets)

$$c = Pa = Nb.$$

It is useful at this point to show explicitly why matrix notation is so powerful. P and N are 2×2 transformation matrices. We illustate here how this type of notation is used. a_1 and a_2 are the translation vectors of the surface net, and c_1 and c_2 the translations of the new net.

Then, $c = Pa$

$$P = \begin{bmatrix} P_{11} & P_{12} \\ P_{21} & P_{22} \end{bmatrix} \qquad \text{a } (2 \times 2) \text{ matrix}$$

So $c_1 = P_{11} a_1 + P_{12} a_2$

$c_2 = P_{21} a_1 + P_{11} a_2$.

In this case,

$c_1 = 2a_1$ and $c_2 = 2a_2$

and thus,

$$P = \begin{bmatrix} 2 & 0 \\ 0 & 2 \end{bmatrix}$$

More complicated examples than this are of course possible. Adsorbate structures have been separated into three categories. These are shown in Fig.6. "Simple" means that the two nets are related directly- the ratio of the two unit cells is an integer. A "coincidence site" superposition has a ratio of areas that is a rational fraction. The last case is an "incoherent" superposition when the surface net shows no relation to the substrate.

So far we have only discussed real space structures when experimentally we observe the reciprocal space structure. At present there is no unambiguous method of determining the real space surface net, b. Frequently several possible structures exist that could result in the same observed reciprocal net. For example, all the structures shown in Fig.7. produce the same L.E.E.D. pattern. This is due to the fact that the L.E.E.D. pattern is produced by electrons that carry only 2D symmetry information. The most general method of cataloguing structures is to list the transformation matrices P. The reciprocal net c , is obtained from the diffraction pattern as,

$$c^* = P^* a^*$$

where P is given by,

$$P = P^{*-1} = \frac{1}{\det P} \begin{bmatrix} P_{22}^* & -P_{21}^* \\ -P_{12}^* & P_{11}^* \end{bmatrix}$$

It is more likely in the literature that structures will be classified according to Woods-notation [10]. The structure is indicated by $(c_2/a_2 \times c_2/a_1)R$, where R is the rotation of the net c with respect

to a.

Throughout this section it has been assumed that the surface and hence the surface net show perfect order, and the order is repeated through space. In real terms this is never true. As well as molecules adsorbing on the sites to give the required L.E.E.D. pattern, it may be that other sites are filled in a random manner. The intensities of the L.E.E.D. spots are highly sensitive to such effects.In general the greater the order of the surface the more intense are the spots. Disorder may also be apparent at low surface concentrations (coverages) where although ad-species may occupy the correct sites, the long range order is still small. The surface layer may also be thermally disordered. These type of effects are discussed in greater detail elsewhere in this thesis.

L.E.E.D. is now recognised as a most powerful tool in the hand of a surface scientist. This is even greater than is indicated here. It is noticeable that if the incident beam energy is varied, that the intensity of the spots shows distinct maxima. The reason for this variation is two-fold. Firstly the registry of the surface perpendicular to the surface is felt to some extent so weak variations are to be expected as the third diffraction condition is met. Secondly this is further distorted by "multiple scattering" of the electrons. (Due to an electrons strong interaction with matter) Using ever more powerful and quicker computing techniques it is possible to find the registry of the surface net to the bulk net and the spacing between them. It should be pointed out that often these experiments are very time consuming and that the computer work is very involved and may take an equally long time. These techniques have been fully described by Pendry [11].

I.6 Auger Electron Spectroscopy. (A.E.S.)

When electrons are incident onto a surface most of them undergo some energy loss to the surface and are inelastically scattered, as shown in Fig.8. The diagram is divided into three distinct regions. the first is the elastically scattered electrons used in L.E.E.D., the second shows electrons which have lost discrete amounts of energy(e.g. to plasmon excitation to the substrate.). The third region shows a broad peak due to the production of secondary electrons. Superimposed on this peak are subsidiary maxima due to the production of Auger electrons. The Auger process is an alternative to X-ray emission and occurs after an atomic core level has been ionised by the incident electrons (or photons). The hole in the inner shell is filled by a less tightly bound electron, the Kinetic energy gained during this process may be passed to a second electron which is lost into the vacuum. The process is shown diagrammatically in Fig.9. It can be seen that the kinetic energy of the escaping electron is given by,

$$E_{KE} \sim E_K - E_{L_1} - E_{L_{2,3}}$$

the electron being a $KL_1L_{2,3}$ Auger electron. The approximation sign is used because as the ionisation takes place the screening of the nucleus is reduced and so the energy levels shift [12]. Every element will show a number of Auger transitions and the energy where these occur is typical of the element. So with the development of A.E.S. it became possible to characterise the surface chemical composition.

In the normal Auger systems electron beams of between 0 and 5 Kv at beam currents of upto 50μA are usually used. Such high energy electrons have the capability of probing more than one layer. The sensitivity of the technique is governed by the mean free path of the incident electrons through the sample and the escape depth of produced Auger electrons. For 2Kv the mean free path is between 5 and 20 Å and thus the technique is sensitive to the surface. Escape depth effects have been discussed in

depth by Seah[20]. Use of equations formulated by Seah will be illustrated in later chapters.

Fig.10. shows a typical experimental spectrumfor a clean and CO covered W{110} sample. The method for obtaining such a spectrum and its form will be discussed in the following chapter.

As well as being used to monitor the chemical composition of a surface it can also be used to measure the kinetics of adsorption. This is due to the fact that the intensity of the Auger signal is usually directly proportional to the amount of material at the surface. It does suffer from the disadvantage that to obtain quantitative information for the surface coverage it must be used in conjunction with another technique.

A.E.S. is now an extremely common technique in very widespread use both in research institutions and in Industry. A number of reviews are available explaining the theory and the practicalities of A.E.S.[13].

References for chapter I.

I. See for example, J. Yarwood, "High Vacuum Technique", Chapman and Hall, London 1967.

2. J.F. Lennard-Jones, Proc.Roy.Soc.A, 106(1924)463.

3. G. Ehrlich in, Transactions of the Eigth American Vacuum Symposium, Pergamon Press, Oxford, 1961.

4. T. Engel and R. Gomer, J.Chem.Phys., 52(1970)5572.

5. M.A. Morris, M. Bowker and D.A. King, Kinetics of Adsorption, Desorption and Diffusion at Metal Surfaces, to be published in: Comprehensive Chemical Kinetics, ed. by C.H. Bamford and C.F.H. Tipper, Elsevier, Amsterdam, Volume 19.

6. J. Pritchard, Trans.Far.Soc., 59(1963)437.

7. C.J. Davison and L.H. Germer, Phys. Rev.,30(1927)705.

8. W.Ehrenberg, Phil.Mag., 18(1934)878.

9. See M.W. Roberts and C.S. McKee, Chemistry of the Metal-Gas Interface, Clarendon Press, Oxford, 1978.

10. E.A. Wood, J. Appl.Phys., 35(1967)1306.

11. J.B. Pendry, Low Energy Electron Diffraction, Academic Press, London and New York, 1974.

12. M.F. Chung and L.H. Jenkins, Surf.Sci., 22(1970)479.

13. See for instance ,
G. Ertl and J. Kueppers, Low Energy Electrons and Surface Chemistry, Verlag Chemie,Weinheim, 1974., and references therein.

14. M.K. Debe and D.A. King, Surf.Sci., 81(1979)193.

15. K. Griffiths and D.A. King, J.Phys.C.,Solid State Physics, 12(1979) L755.

16. P. Alnot and D.A. King, Surf. Sci., to be published.

17. G. Thomas and D.A. King, Surf.Sci., 92(1980)201.

18. K. Griffiths, C. Kendon,D.A. King and J.B. Pendry, Phys.Rev.Letts., 46(1981)L755.

19. E. Bauer, Surf.Sci., 58(1978)517.

20. M.P. Seah, and W.A. Dench, Surface and Interface Analysis, I(1972)2.

Fig.I.

Potential Energy Wells for adsorption. Two cases are illustrated. I(a) where adsorption is non-activated and I(b) where the adsorption is activated.

FIG.1.

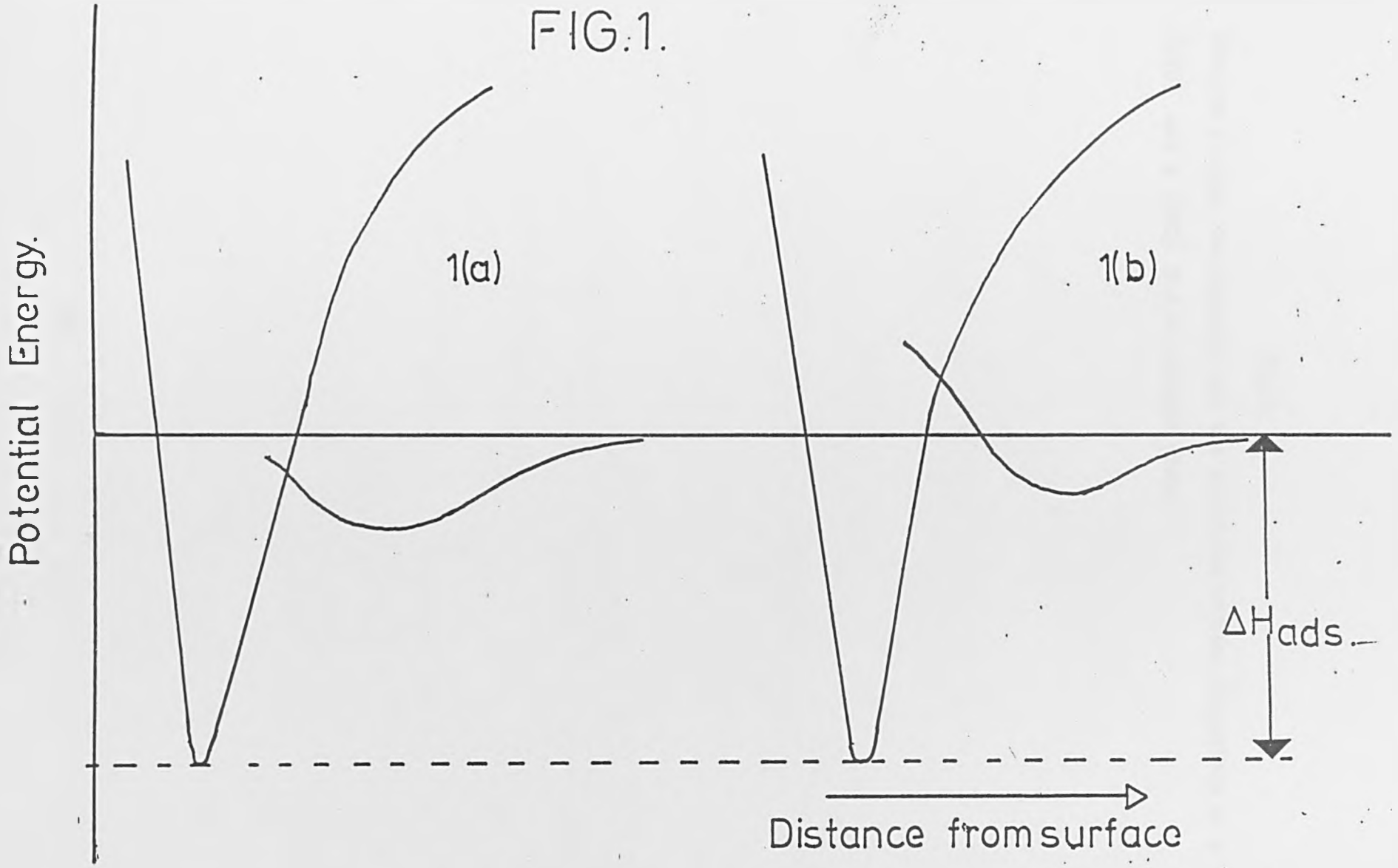

Fig.2.

Diagram showing the symmetry and the principle crystal directions of a {110} and a {100} B.C.C. crystal plane.

FIG. 2

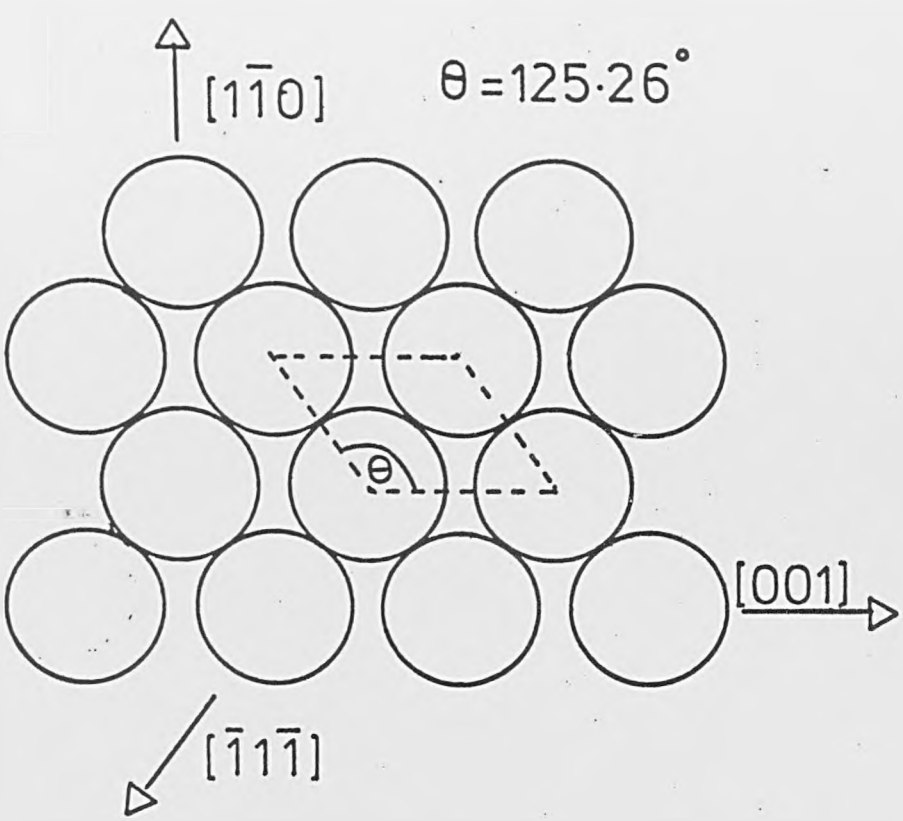

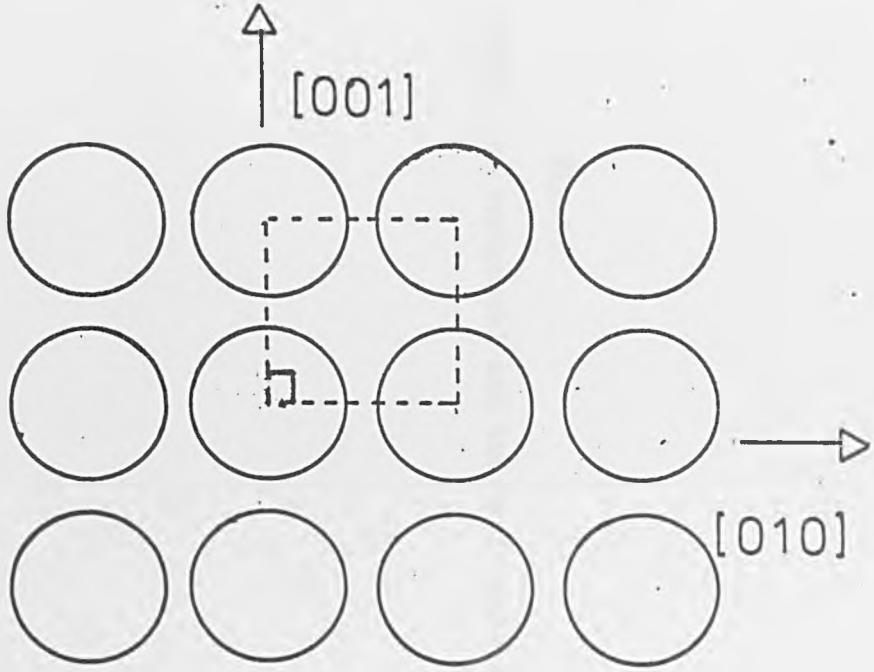

Fig.3.

The relationship between the reciprocal and the real space nets.

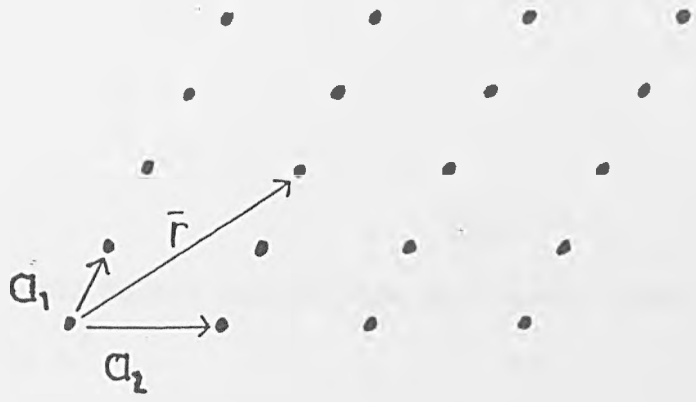

REAL SPACE

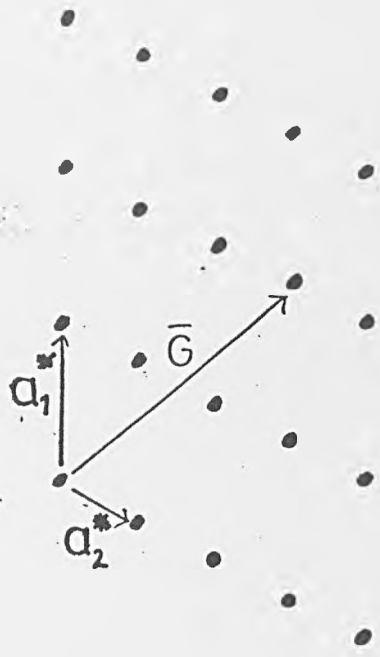

RECIPROCAL SPACE

(LEED pattern)

FIG. 3

Fig.4.

Ewald Sphere construction in a plane normal to the surface and parallel to a_1^*.

FIG 4

Fig.5.

The L.E.E.D. geometry.

FIG. 5.

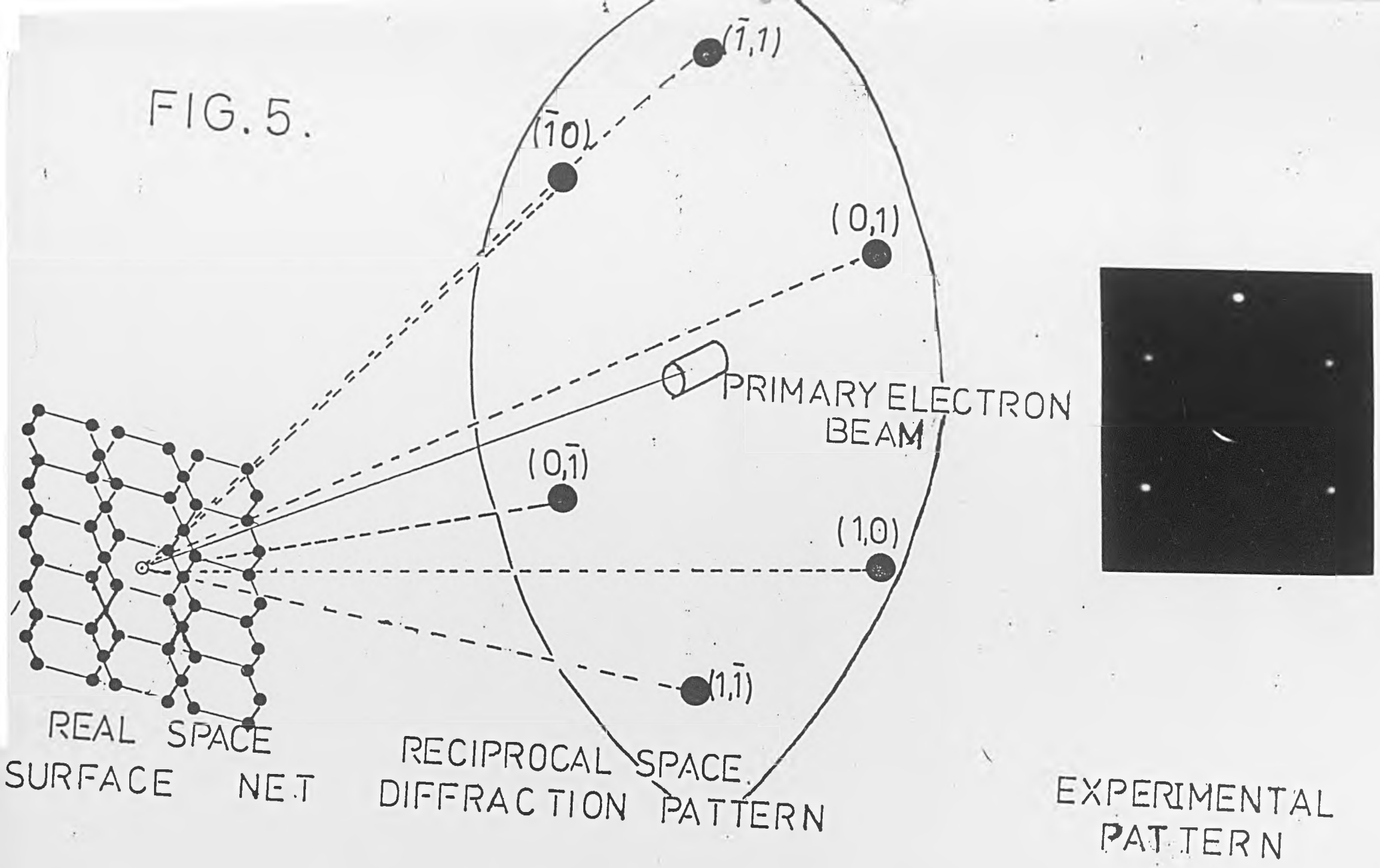

EXPERIMENTAL PATTERN

Fig.6.

Three different surface structures.

FIG. 6.

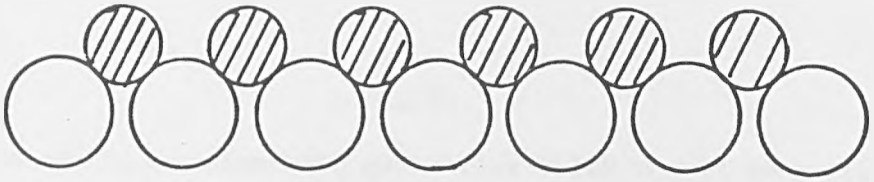

SIMPLE

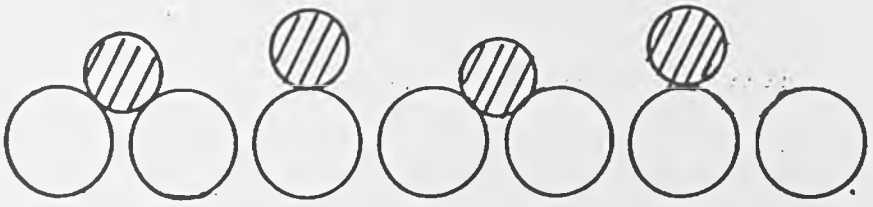

COINCIDENCE-SITE

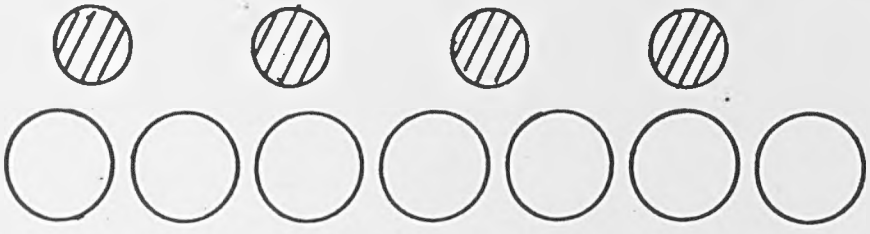

INCOHERENT

Fig.7.

Three different adsorbate geometries which result in a c(2x 2) L.E.E.D. pattern.

FIG. 7

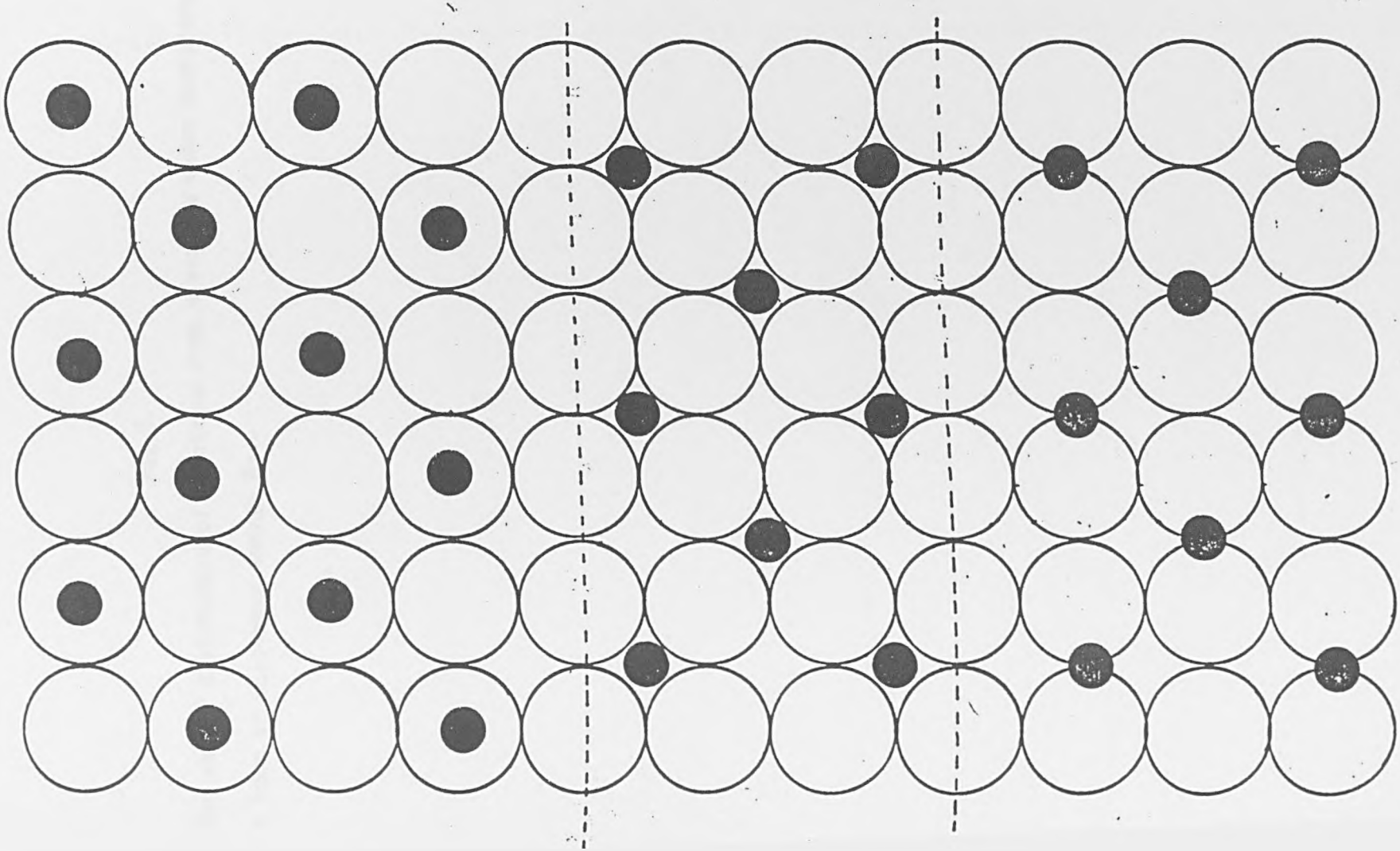

Fig.8.

The energy distibution of electrons from a surface under bombardment by a beam of electrons energy E_p .

FIG. 8

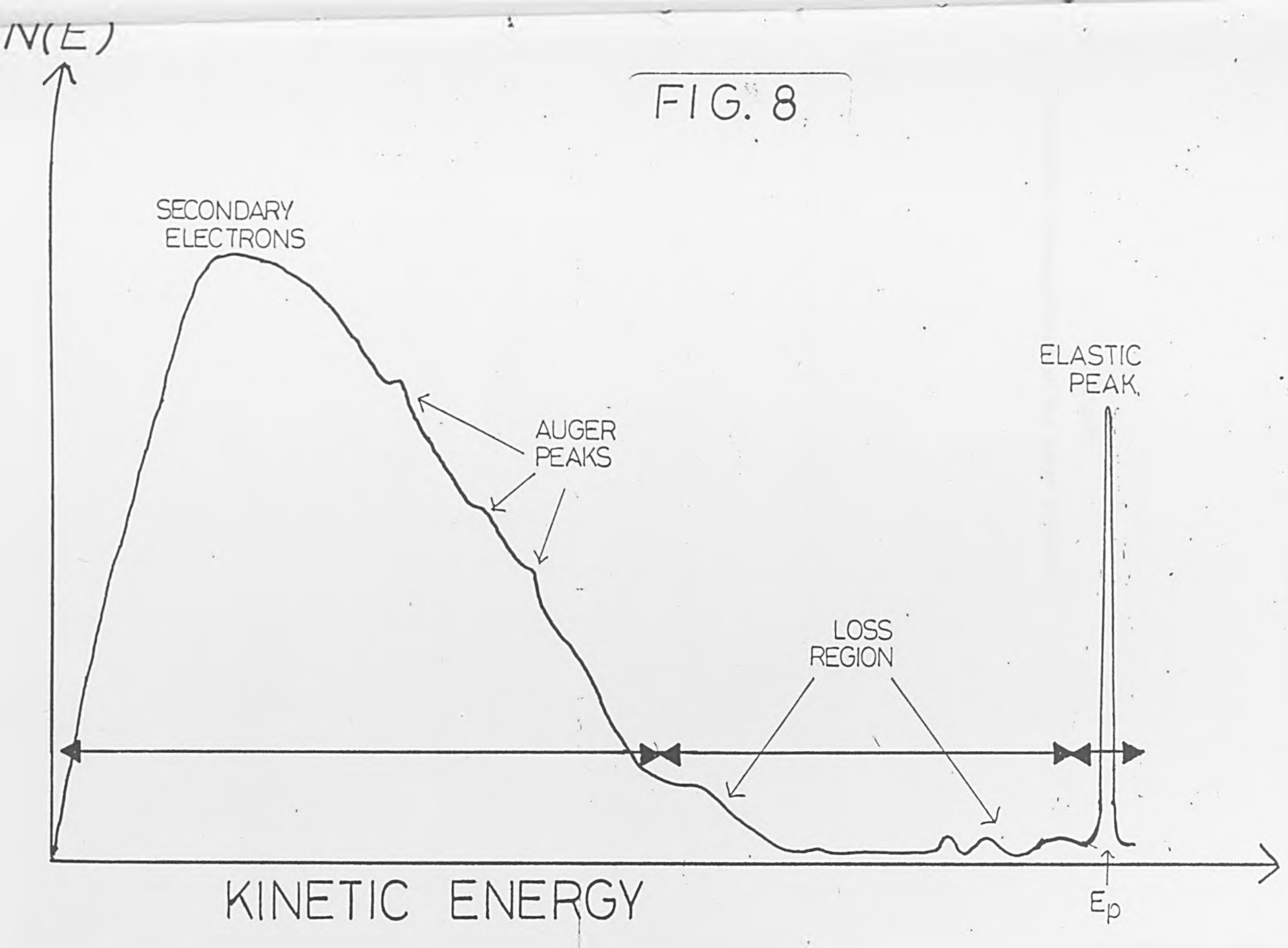
N(E)
SECONDARY ELECTRONS
AUGER PEAKS
ELASTIC PEAK
LOSS REGION
KINETIC ENERGY
Ep

Fig.9.

Schematic representation of the Auger process.

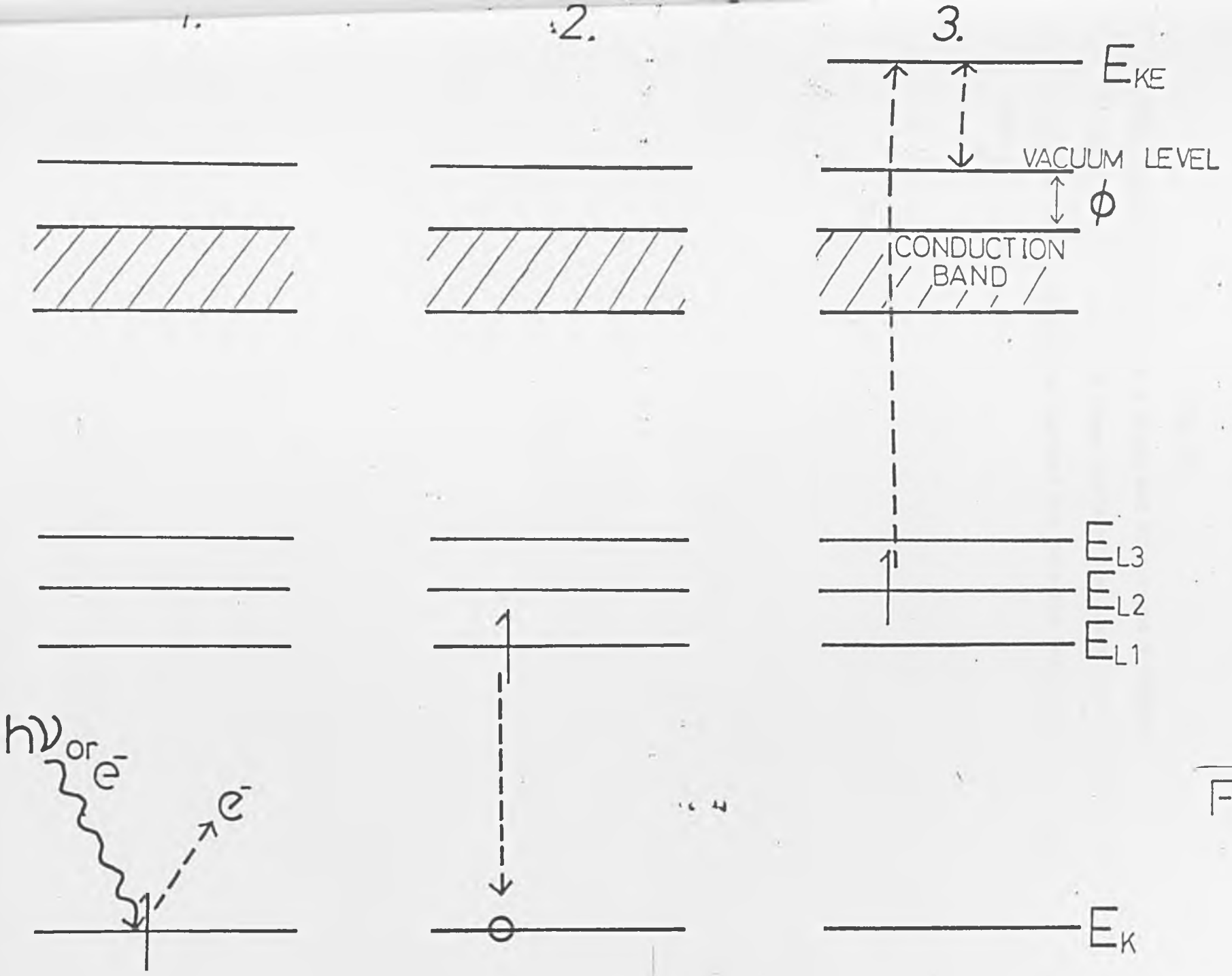
1.
2.
3.
E_{KE}
VACUUM LEVEL
ϕ
CONDUCTION BAND
E_{L3}
E_{L2}
E_{L1}
E_K
$h\nu$ or e^-
e^-

FIG. 9.

Fig.IO.

Auger electron sectra from a clean and CO covered W sample.

The upper spectrum is from a clean surface, the lower spectrum (displaced vertically) from a CO covered surface and here the sensitivity has been multiplied by two.

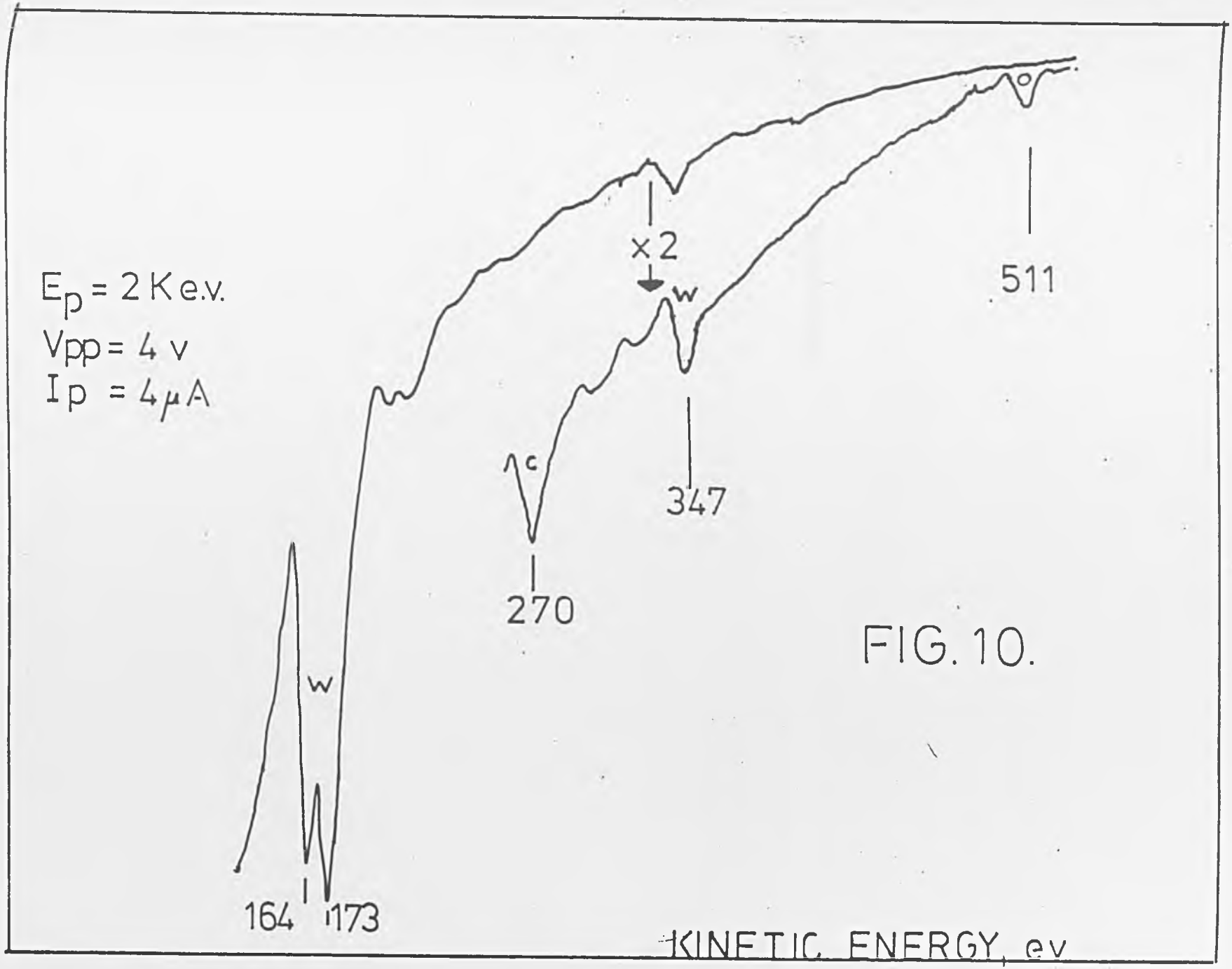
E_p = 2 K e.v.
Vpp = 4 v
Ip = 4 μA
dN(E)/dE
×2
w
511
347
c
270
w
164
173
KINETIC ENERGY, ev

FIG. 10.

CHAPTER 2: EXPERIMENTAL.

2.I. Introduction.

This chapter describes how results presented in this thesis were obtained. It outlines how U.H.V. was obtained on a routine basis, how kinetic measurements were made, how L.E.E.D. spots were obtained, and how Auger spectra were collected.

2.2 The U.H.V. Chamber-basic design.

The experiments were carried out in a 24 inch Vacuum Generators (V.G.) stainless steel U.H.V. system shown in Figs.I. and 2. Pumping of the main bell was carried out by a 220 ls^{-1} sputter ion pump combined with a titanium sublimation pump.[2] The sublimation pump fired over a liquid-nitrogen-cooled shroud. Total pressure measurements were made with a nude Bayard-Alpert ionisation gauge. A vacuum quadrupole mass spectrometer (V.G. model Q8K) was used for residual gas analysis. Gas samples were introduced into the system via an all-metal valve or a molecular beam dosing arrangement, discussed elsewhere. In order to maintain the purity of the samples entering the system, they were handled in a glass U.H.V. line pumped by an Edwards ED50 rotary pump and a mercury diffusion pump. Between this line and the main chamber was a liquid-nitrogen-cooled trap to remove impurities. For accurate calibrations of gas fluxes there was another Bayard-Alpert ionisation gauge connected to the trap.

2.3. Obtaining U.H.V.

A schematic showing the gas dosing line and the U.H.V. chamber is seen in Fig.2. Starting at atmospheric pressure the rotary pump was switched on and allowed to pump until a pressure of 0.0I Torr was measured with the valve MVI open. The rotary pump was liquid nitrogen trapped to prevent pump oil contaminating the system. After this pressure had been reached the mercury diffusion pump DI was switched on. This

pump consisted of two seperate pumps, a small Jencons pump ($30ls^{-1}$), and a Klemperer pump ($90ls^{-1}$). The smaller pump backed the large pump. Pumping continued until the pressure reached 10^{-6} Torr. At this pressure the ion pump was switched on and the valve MVI was closed. Pumping then continued until the pressure in the chamber reached 10^{-8} Torr. The whole of this process took upto 24 hours. This was a convenient point to test the system for any air leaks. This was done using the mass spectrometer. Mass 32, if present, was diagnostic of a leak, since at these pressures only contaminants adsorbed on the walls should be detected. The leak could then be isolated by tuning in to mass 4 and probing the vessel walls with He.

In order to reach U.H.V. in both the gas line and the main chamber it was imperative to bake the system. The parts that were enclosed in large ovens, to this effect, are shown in Fig.2, between the dotted lines. Baking was continued until the pressure went through a large maximum which at a temperature of about 160c took around six hours. The ovens were then switched off and the gas line was allowed to cool more quickly. The gas line trap was slowly cooled with liquid nitrogen so that gases were condensed near the bottom of the trap. When the temperature of the main chamber fell to around 70c the ovens were removed and any instruments in the chamber that used a heated filament were degassed. On cooling the pressure reached about 10^{-10} Torr within a few hours. After a few days the pressure reached 10^{-11} Torr; below this, pressures could not be read.

2.4. The Gas Dosing Line.

The following section describes explicitly how this was used to introduce pure gas into the chamber. The gas line was constructed of "pyrex" glass. The gas bulbs G_1 to G_4 were connected to a high pressure

line shown in Fig.2. The gases were obtained from the British Oxygen Company at a purity of 99.999% . During pump down the high pressure line was initially pumped via a rotary pump but then it was closed off and pumped only by the mercury pump. The required pressure of gas to be used behind the molecular beam was obtained by isolating the high pressure branch(H.P.B.) from the pumping lines and allowing the gas to flow from the gas bottle into the line. Pressure was monitored on a mercury manometer, M, and could be readily adjusted using a viton seal all glass leak valve to the rotary pump. Gas was then admitted to the low pressure section of the gas line through a capillary so that pressures of between 10^{-5} and 10^{-7} Torr were measured at the ionisation gauge, B.A.G.I. Incorporated in the H.P.B. was a two litre ballast bulb. This ensured that there was only a very small pressure drop in opening the valve M.V.I. into the system.

The above is only a brief description of the U.H.V. and gas handling techniques. It does not pretend to give a full descrition of the back-up electronics or a step-by-step guide to U.H.V. techniques. A number of reviews are easily accesible.

2.5. Bayard-Alpert Ionisation Gauges,(B.A.G.).

Before the advent of these gauges it was impossible to measure high vacuum and so they have been important in the development of surface science. There have been very few changes to the basic design since their introduction[3]. The gauges essential features are described below. Emission of electrons from a hot cathode are accelerated by an applied potential towards a spiral anode. Inside this anode gas molecules are ionised by the electrons and are collected by a fine wire. The pressure is then given by the ion current ratioed to the electron current multiplied by some constant. These gauges have a pumping effect due to the trapping of ions

or free radicals formed by the dissociation of gas at the cathode. This can be prevented by lowering the workfunction of the cathode and filaments such as rhenium/lanthanum boride or thoriated tungsten are often used.

2.6. Sample manipulator and preparation.

2.6.I. Degrees of freedom.

The sample manipulator was a Varian model 981-2527[4], which had been adapted by M.K. Debe[5] so that the crystal was 2.5 inches from the axis of rotation. The sample could then be turned towards the various instrument ports. More importantly it allowed the sample to be in the centre of curvature of the L.E.E.D. grids. The sample mounting arrangement allows various degrees of freedom. These are,

a) vertical translation- z motion,

b) horizontal motion in two orthagonal planes- x and y motion,

c) rotation about the axis of the manipulator-indicated by θ,

d) offset flip motion providing 100^{o} of rotation about an axis normal to the central shaft.

The movements x,y,z, were controlled using accurate micrometers which could be read to a tenth of a millimetre. The θ setting could be read to a tenth of a degree. Two stops were provided on the manipulator so that the sample could be accurately swung between any two positions. The flip motion had an important use in allowing the sample to be exactly at normal incidence in L.E.E.D. and A.E.S. experiments. These motions are shown in Fig.3.

2.6.2. Cooling the sample.

The manipulator had the facilities for liquid nitrogen cooling of the sample. This has been modified from the original design[6]. Cooling is now performed by a V.G. liquid nitrogen tank[4(b)]. Liquid nitrogen was fed

into the tank as shown in Fig.4. The inlet and outlet pipes were on the same mini-conflat flange. Stainless steel tubes 0.I mm in diameter coiled around the manipulator shaft and fed the tank. Before cooling dry nitrogen was passed through the tubes to remove any water so as to prevent ice formation. To pass the liquid, dry nitrogen gas at around I0 p.s.i. was flowed through several tubes immersed in liquid nitrogen. The tube diameter was 5mm and the total immersed length I0 metres. The gas is liquefied in the tubes and flows into the tank. After 20 minutes the outlet pipe was seen to be emitting liquid. The tank was connected to the sample mount with an annealed copper tape (I5 x I x 0.25 cm). Within 20 minutes the sample temperature fell to 220K.

2.6.3. The sample holder.

Sample holders have to be carefully designed. The holder used here was designed to maximise the cooling rate and allow prolonged heating times of upto 5minutes at 2500K. The crystal was heated by two methods,

a) electron bombardment-700K upwards,

b) reistive heating-700K,and below.

This necessitated complex electrical isolation of the sample, mounting blocks and the wires carrying voltages and current. The wires were insulated with either "Teflon" or "Refrasil". In order to allow free rotation these wires made several coils around the manipulator. The design is illustrated in Fig.4. The crystal was held by two 0.25 mm W wires passing through holes drilled in the edge of the sample. These were bent in such a way to prevent the crystal moving. The two wires were clamped to two stainless steel blocks using screws. Resistive heating was carried out by passing current down two copper braids attached to each of the blocks. A small electron bombardment filament behind the crystal was fed by two gold wires attached to the mounting block supporting arms. The

temperature of the sample was measured using a W-3%Re/ W-25%Re thermocouple inserted into a hole drilled into the edge of the crystal. A temperature curve, calibrated using a disappearing filament optical pyrometer, is shown in Fig.6. For comparison the E.M.F. of a standard thermocouple is also shown[6]. E.M.F. readings were made with a high insulation multimeter. It can be seen that the two curves agree quite well up to very high temperatures. The divergence after this is explained as an emission effect. The filament is in direct line of sight with the thermocouple producing a secondary E.M.F., thus altering the reading. At low temperatures emission is small and the effect small. This particular thermocouple was used because of its almost linear output and compared to the 0%/25% combination[6], does not pass through a minimum below room temperature. Fig.7. shows the calibration of the thermocouple below room temperature taken from the work of Sandstrom and Withrow[7]. This was used in this work because it is expected to be exact at these temperatures.

2.6.4. Temperature sample control.

The temperature of the sample was usually controlled using an electron bombardment unit. This could raise the temperature of the sample to a given desired value at any rate up to a maximum of 180 $Ksec^{-1}$. The final temperature could then be held to within 2K for an indefinite time. The unit displays the temperature and using a feedback circuit changes the current through the filament to keep this constant.

2.7. Gas adsorption at the sample.

2.7.1. Gas adsorption from a partial pressure of active gas.

As described earlier the gas line could be filled to up to 10^{-2} Torr. Fine adjustment of this pressure was possible using a fine bore valve, V4. If a pressure of 10^{-6} Torr was produced in the line and M.V.I. was

opened a pressure of 1.5×10^{-9} Torr was produced in the chamber. This facility was seldom used. Its main use was during cleaning work when it was thought that beam dosing may leave the back of the sample dirty and later contamination may spread to the front of the crystal.

2.7.2. Gas adsorption from a Molecular Beam.

The molecular beam is clearly described in Fig.8. It consists of a length of stainless steel tubing 10mm internal diameter. This is mounted on a bellows arrangement. At the end of the tube is a stainless steel cap with a cylindrical orifice length 0.685 and radius 0.55 mm. This produces a flux of gas with enhanced velocity in the forward direction. The bellows allow about 7cm of linear motion towards the centre of the chamber and operation of the thumbwheels allows a small amount of angular variation. Combination of these two movements allowed the sample to be set at a pre-determined position without using the manipulator micrometers.

In order to measure sticking probabilities and coverage, the flux and its spatial distribution had to be known. This, off course, varied with pressure. These parameters could be evaluated with formulae derived by Dalton[8]. These formulae have been adopted for use with this system by Marsh[9]. Given the molecular weight of a gas, its temperature and the pressure, a computer program develped by Marsh[9], calculates the total flux leaving the orifice and the fraction, f, intercepted by the sample. With a pressure of 10^{-6} Torr behind the beam the flux at the sample is about 5×10^{12} molecules $cm^{-2}\ s^{-1}$ at a distance of 5mm away. Dosing the crystal in this way was very useful. Although high fluxes could be produced at the sample the background pressure rise was very small. Even with a pressure of 10^{-5} Torr behind the beam the background pressure did not rise above 3×10^{-10} Torr.

2.7.3. The adaptation of the molecular beam to deposit an adsorbate boundary on the surface.

In the oxygen diffusion work it was necessary to produce a gas boundary at the surface between clean and covered W. The experimental arrangement is shown in Fig.8. A shield was held on a pivot so that it could be swung in and out of the beam. In the centre of the shield a hole was cut to exactly match the size of the crystal. At either side of this were cut two more holes so that half of the sample, in either the perpendicular or the horizontal direction, could be covered. These were cut so that the boundary was deposited 90^{o} to the crystal edge.

The molecular beam does not give a completely homogeneous flux until the sample is some distance from the beam. The further away the sample, the greater the homogeneous nature of the flux. Also as the beam to sample distance is increased, "shadow" effects at the boundary edge are decreased. There is, however, a drawback. The greater this distance the greater the amount of gas that is lost into the chamber, i.e. the greater the background pressure. Thus the boundary is smeared by random gas adsorption. Experimentally some compromise has to be found. A typical boundary is shown in Fig.18.

2.7.4. Scanning the Adsorbate Boundary

The shape of the boundary edge was measured using A.E.S. The height of the Auger derivative signal was calibrated against coverage. The Auger signal as a function of distance could then be used to obtain coverage profiles. This was done by positioning the sample in front of the Auger beam and using the accurate micrometers described earlier, the sample could be moved across the beam, recording the Auger signal as a function of distance. Usually after this, the sample would be heated for

a time. Diffusion was measured by re-scanning the profile. It should be pionted out that this process took some time and particular attention had to be paid to the vacuum conditions during these experiments.

2.7.5. Sticking Probability and Surface Coverage measurements.

The following method was used to measure the sticking probability, s, and the surface coverage.N. The crystal is swung away from the beam source and the beam valve opened so that a known flux of gas enters the system. The mass spectometer is then used to measure this pressure,P'. The crystal can then be positioned in front of the beam and provided that the sample is free to adsorb,the background pressure measured at the mass spectrometer decreases to ,P. s is then given by the relationship

$$s = \frac{I}{f} \frac{(P'-P)}{P} ,$$

where f is the fraction of flux intercepted by the crystal and this can be calculated.If a plot of s against t is made then the coverage is evaluated from the equation,

$$N = \int_o^t Q \, s \, dt.$$

Q is the impinging flux of molecules. In this way s versus N plots can be constructed.

2.8. Experimental Aspects of L.E.E.D. and A.E.S.

2.8.I. L.E.E.D. Display.

The L.E.E.D./A.E.S. retarding field analyser (R.F.A.) is a multi-purpose Varian model number 981-0137. The electron optics assembly is a set of four concentric grids in front of a fluorescent screen. The grids are made from hydrogen-fired nickel-plated tungstenmesh of 98% transparency, and the screen is a spherical surface, coated with a PII phosphor layer, which is biased at around 5kV producing an intense blue image when impacted by electrons. Through the centre of the grid assembly is an

off-axis electron gun, producing a finely controlled primary electron beam in the energy range of 2-I.500 eV. The beam current is regulated at 0.5μA for voltages > 45eV. In front of the final grid is a moveable faraday cup, allowing the current in a diffracted electron beam to be measured.

The experimental technique is shown in Fig.IO. The crystal is held at earth potential as is the first grid, ensuring a field free region between the two. Magnetic fields are eliminated by use of three Helmholz coils at 90° to each other surrounding the chamber. The two centre grids are held at a potential just below the primary beam energy such that only elastically scattered electrons are passed through the optics. The fourth grid is held at earth potential. The electronics provide an auto-focussing facility ensuring that the beams remain in focus over the energy range.

2.8.2. Measurement of the L.E.E.D. Intensity and Spot Width.

These measurements could be made in one of two ways.

a- The intensity of the L.E.E.D. spot could be measured using the Faraday cup; by sweeping the primary beam voltage the beam is made to scan across the aperture of the cup, thus providing a measure of the intensity as a function of distance. However this method could not be used if the I-V spectra are rapidly changing in this voltage range.

b- A second method became available during the course of these experiments. A video L.E.E.D. system was bought from the "Data-Quire Corp."[IO]. Briefly this consists of a low level video camera pionting at the screen, interfaced to a small microcomputer. The image of the L.E.E.D. screen is divided into a number of small windows and the microcomputer can measure the intensity of any of these windows. Software allows the operator to measure the intensity average of a spot, the maximum intensity and the distribution of the intensity of any given spot. It allows rapid collection of I-V spectra.

2.8.3. The collection of A.E.S. spectra.

It was shown in 1967 that in principle an R.F.A. could be used to detect Auger electrons [11]; the basic L.E.E.D. display had become a spectrometer, an important event. Harris soon showed that differentiating the signal led to enhanced sensitivity [12] and Weber and Peria [13] then developed the techniques of phase sensitive detection to do this electronically. The electrical circuit and the necessary equipment is shown in Fig.II. Modulating the crystal rather than the second grid led to superior signal to noise ratios. The primary electron beam is a focussed 2keV beam of between 4 and 10μA. The oscillator provides a 4kHz sine wave modulation to the crystal at about 5 volts peak-to-peak and also to the reference of the lock-in-amplifier.

The back scattered electrons leave the crystal and move in a field free region towards the first grid. Grids 2 and 3 are at a negative voltage which can be ramped between 0 and 1000 v. Electrons with energy greater than this pass through the optics and are collected at the screen (held at 350V positive to rapidly discharge the phosphor). The signal is then fed to the lock-in. The signal reaching the screen is shown in Fig.12(a) and represents the total number of electrons arriving in the energy range, between that of the primary beam to the retarding energy. The lock-in amplifier allows this to be differentiated into the normal N(E)/E curve (Fig.12.(b)) and double differentiation allows the small Auger peaks to be emphasised so producing a dN(E)/dE curve (Fig.12(c)). The spectra were collected in this form.

2.9. The Potassium Source.

The arrangement used is shown in Fig.13. Potassium ions are obtained

from a zeolite source, a large cage like molecule capable of storing positive ions which are released on heating the zeolite. The potassium zeolite was commercially available (B.D.H.[14]) and was coated onto a Pt/Rh(10%) filament as described by Weber and Cordes[15]. A series of plates capable of being floated, focus the emitted ions into a beam directed at the sample. There was direct line of sight between the filament and the crystal. The final shield is arranged in such a way so as to cover part of the crystal and produce an adsorbate boundary, unfortunately the boundaries were not as sharp as those for oxygen. In these experiments the ion energy was between 3and 8 eV, a recent study by Overbosch et al has shown that potassium ions of this energy are fully accomadated at the surface[16].

It has been noticed[17] that zeolite sources are prone to the production of high levels of oxygen contamination, presumably due to the breakdown of the cage structure. This was never noticed in this series of experiments as demonstrated by the A.E.S. spectrum in Fig.14. In order to produce cleanliness of this level the source was run for about 100 hours at the operation temperatures,in the range 1300-1500K. The coverage profile of a typical deposit is shown in Fig.15.

2.10. The Indium Source.

Indium belongs to a group of metals which evaporate at significant rates at temperatures far in excess of their melting point. The difference between indiums melting point and boiling point is the greatest for any material. The experimental arrangement for the dosing of indium is shown in Fig.16.Two stainless steel tubes, diameter 1mm, were filled with indium wire of 99.999% purity (Koch Light Laboratories[18]) and sealed at one end. The sealed end of each tube was spot welded to two feedthroughs mounted

on a flange. The open ends of the tubes were then bound together with W wire so that resistive heating of the tubes was possible. A shield was placed in front of the tubes to prevent evaporation onto the whole chamber. There was a small hole cut into the shield to allow crystal dosing.

Temperatures between 1100 and 1400K were used to deposit indium, the evaporation rate varied between these temperatures from about a monolayer per hour to 5 monolayers per minute. After an initial degassing period of 2 hours no contamination was detectable by A.E.S., as evidenced by the spectra shown in Fig.19. Very careful checks were made to ensure that evaporation was not taking place from the stainless steel but no evidence for this could ever be found.

The source arrangement used here produced profiles similar to the potassium coverage profiles, as can be seen in Fig.17. The source proved to be extremely stable. Over the entire life of the source no deterioration was ever noticed in the amount of material given off in a given time at a preset temperature.

REFERENCES.

I. P.A. Redhead.J.P. Hobson and E.V. Kornelsen. The Physical Basis of Ultrahigh Vacuum, Chapman and Hall, London, I968.

2. A.E. Barrington, High Vacuum Engineering, Prentice-Hall, Englewood Cliffs, New Jersey, I963.

3. R.T. Bayard and D. Alpert, Rev.Scient.Instrum.,2I(I950)572.

4. Varian, Vacuum Div., Palo Alto, California, U.S.A.

5. M.K. Debe and D.A. King, Surf.Sci.,8I(I979)I93.

6. D.A. Davies, J.Sci.Instrum.,37(I960)I5.

7. D.R. Sandstron and S.P. Withrow, J.Vac.Sci.Tech., I4(I977)748.

8. B.B Dayton, Trans.3rd.A.V.S. National Vac. Symp.(I956).

9. F.S. Marsh, Ph.d. Thesis, L'pool Univ.,(I977).

I0. Data-Quire Corporation, Palo Alto, California, U.S.A.

II. L.N. Thorpe and E.J. Scheiber, Surf.Sci.,8(I968)247.

I2. L.A. Harris, J.Appl.Phys.?39(I968) I4I9.

I3. R.F.Weber and W.J. Peria, J.Appl.Phys., 38(I967)4355.

I4. Linde Laboratories, British Drug Houses, Poole, U.K.

I5. R.F. Weber and L.F. Cordes,Rev.Sci. Instrum.,36(I965)II2.

I6. E.G. Overbosch, A. Hurtmans, D.R. Olarrider and J. Los, Surf. Sci., 54(I976)I54.

I7. E. Bauer,in "The physics of Solid Surfaces and Heterogeneous Catalysis" eds. D.A. King and D.P. Woodruff. Elsevier(Amsterdam), Vol.3B,in press

I8. Koch Light Laboratories, Coinbrook. U.K.

Fig.I. Schematic representation of the U.H.V. chamber.

FIG. 1.

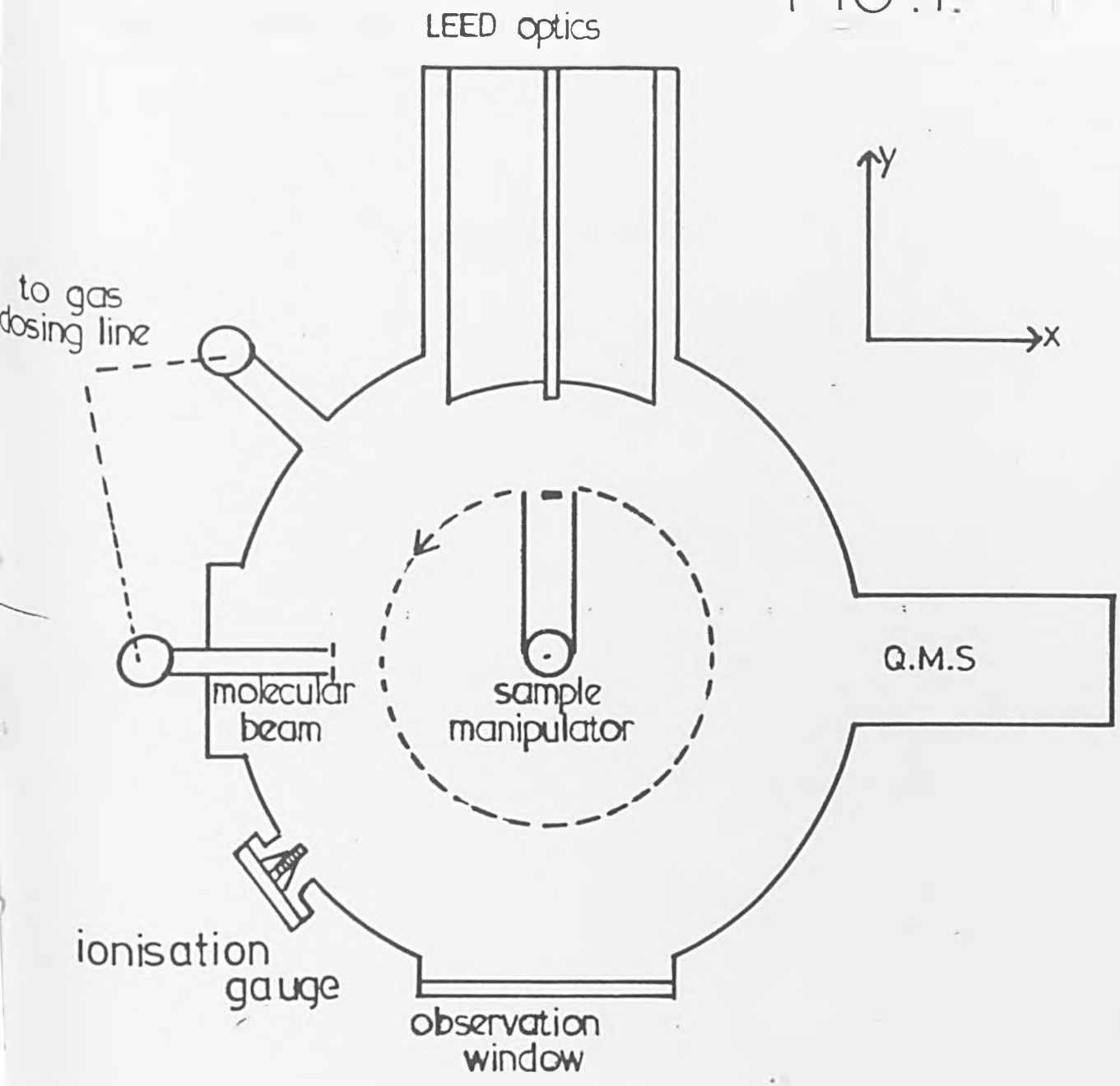
LEED optics
y
x
to gas
dosing line
molecular
beam
sample
manipulator
Q.M.S
ionisation
gauge
observation
window

Fig,2. The valve layout of the gasline and the U.H.V. chamber.

fig. 2.

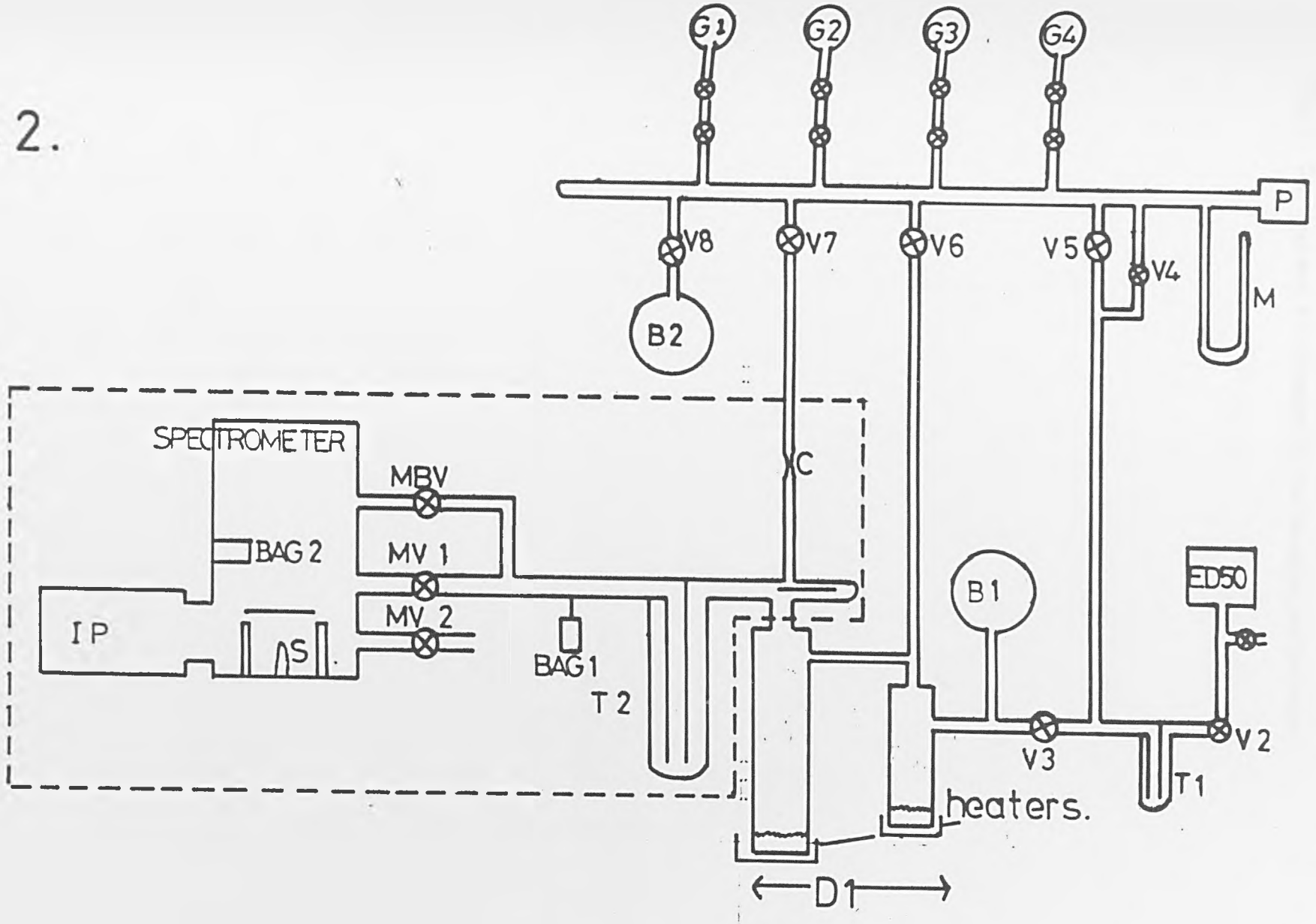
G1
G2
G3
G4
P
V8
V7
V6
V5
V4
M
B2
SPECTROMETER
MBV
C
BAG 2
MV 1
MV 2
IP
S
BAG 1
T 2
B1
ED50
V3
V2
T1
heaters.
D1

Fig.3. The degrees of freedom at the sample manipulator.

FIG. 3.

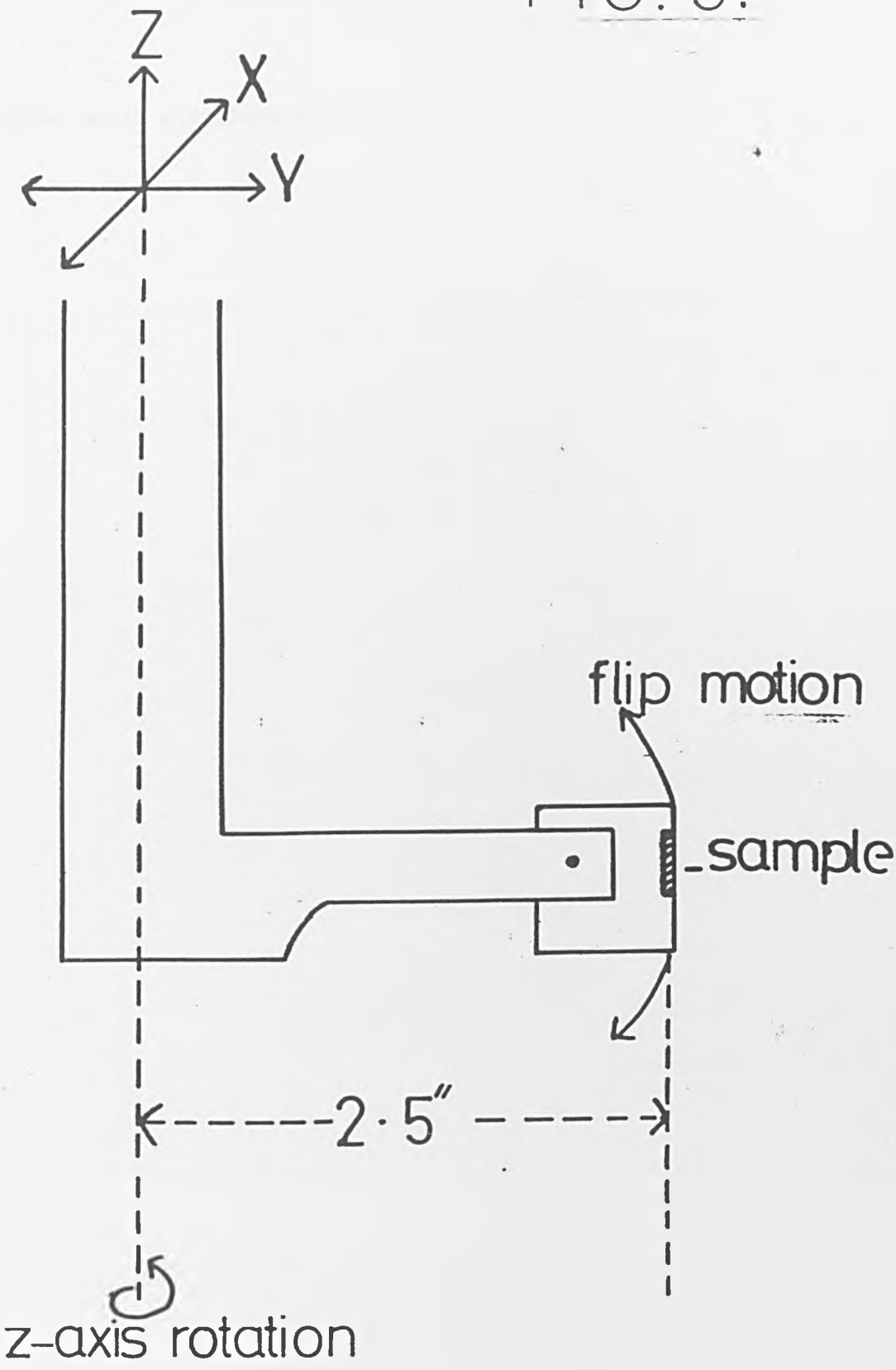

Fig.4. The sample mount and electrical contacts.

FIG.4.

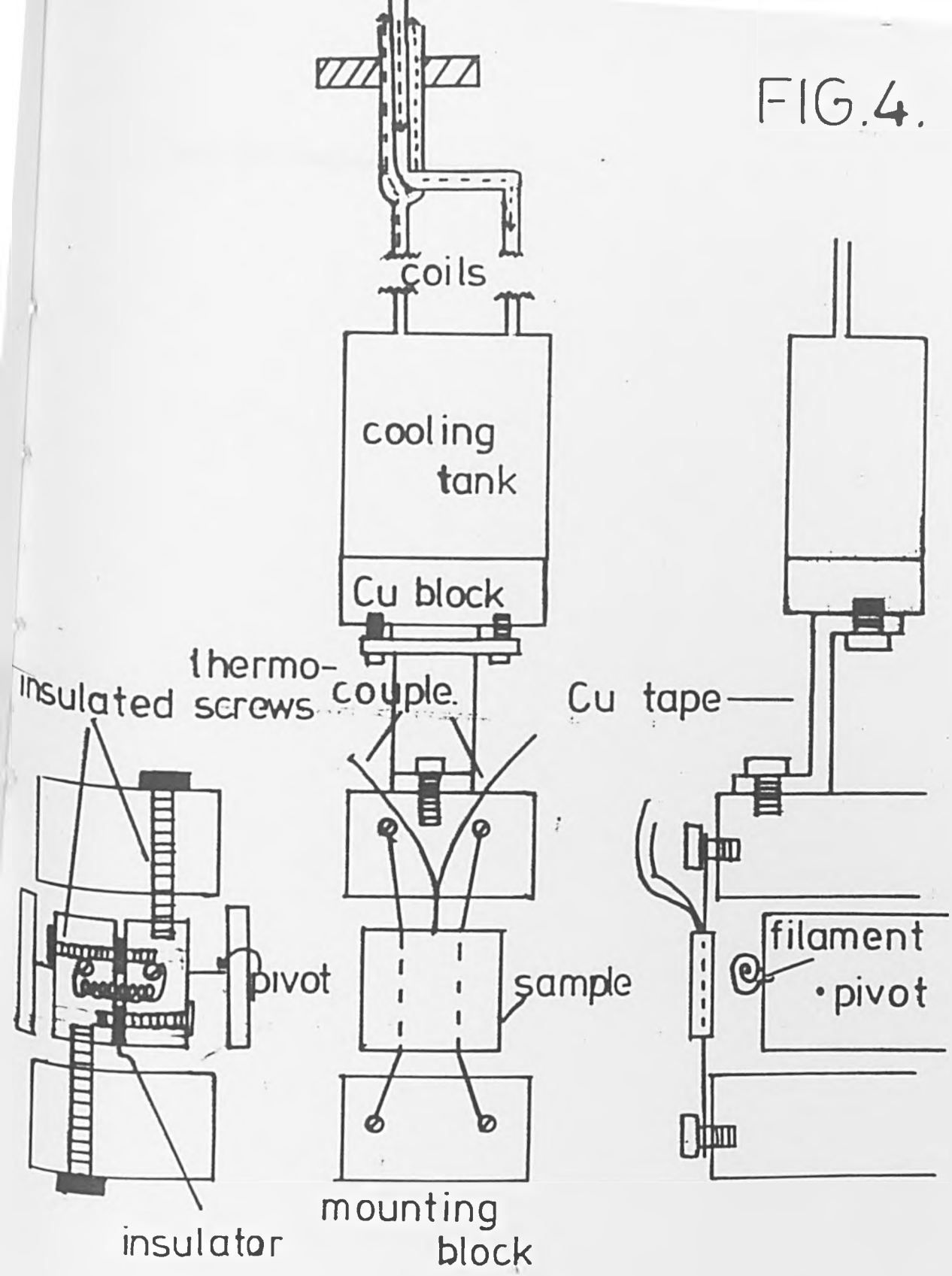
coils
cooling tank
Cu block
thermo-couple.
insulated screws
Cu tape
pivot
sample
filament
pivot
insulator
mounting block
(a)
(b)
(c)

Fig.5. The cooling arrangement.

FIG.5.

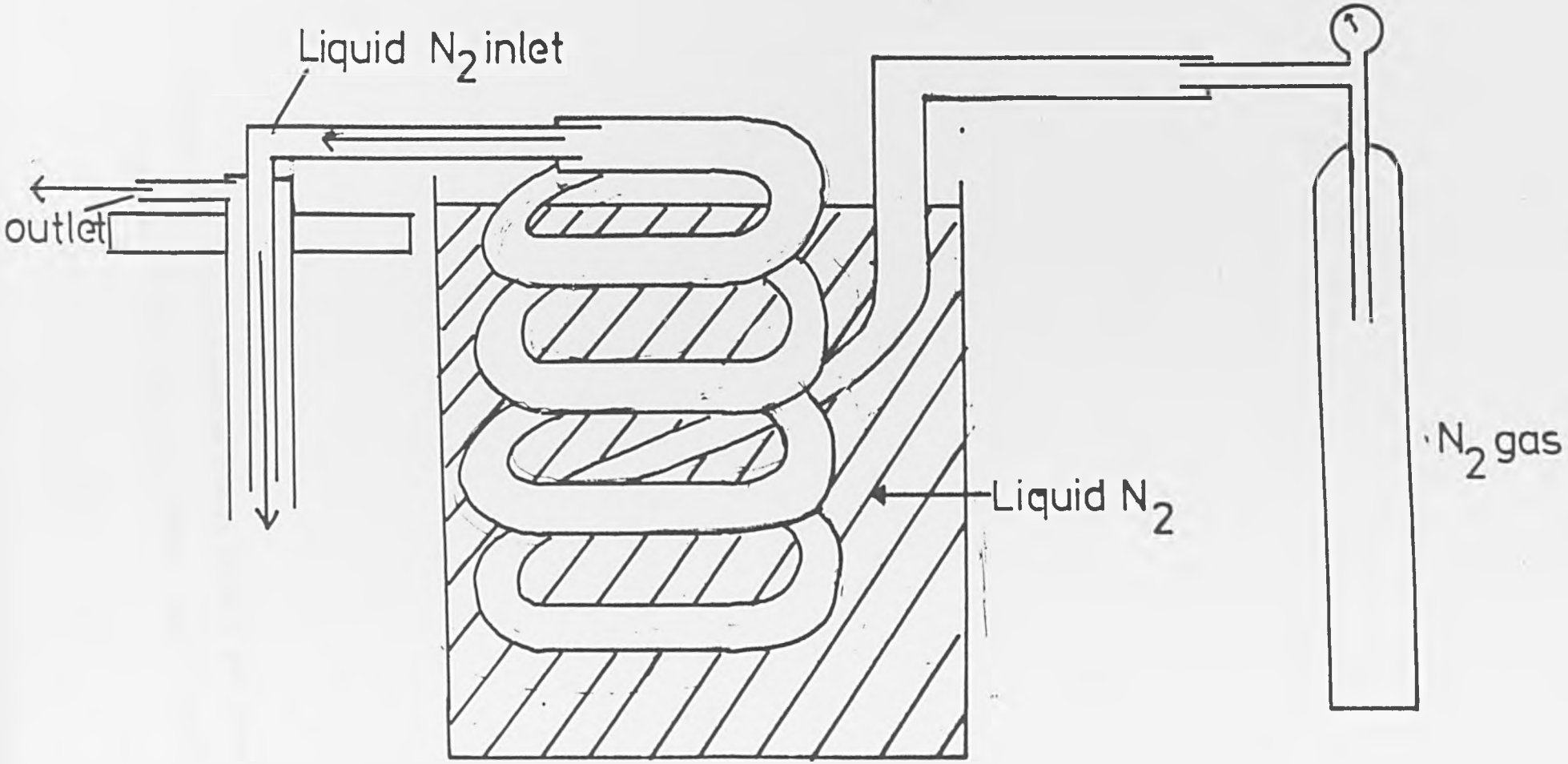

Fig.6. Thermocouple output versus temperature from (dashed line) the experimental arrangement and (solid line) standard thermocouple tables.

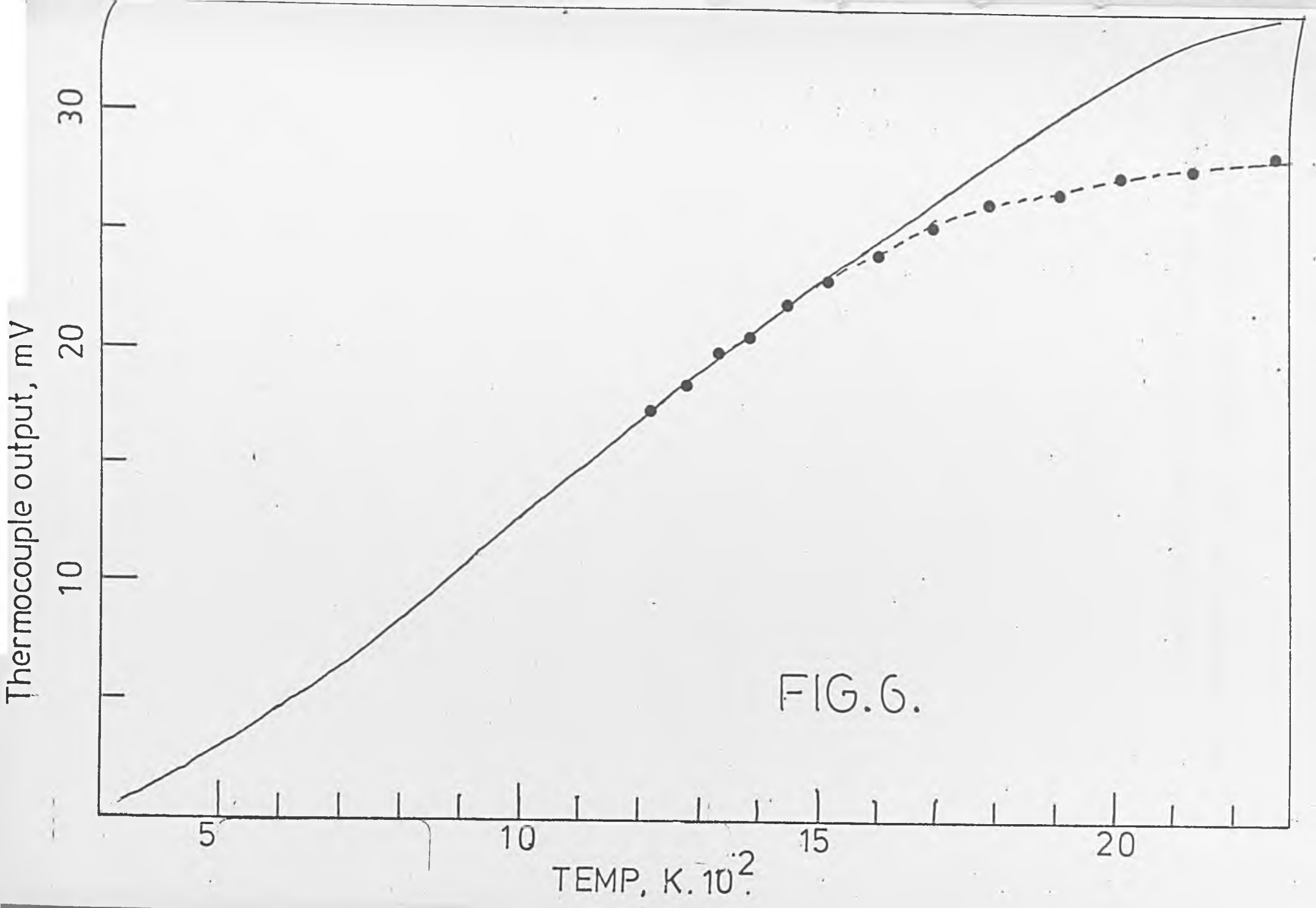

FIG. 6.

Fig. 7. The variation of thermocouple output versus temperature at low temperatures. Taken from the work of Sandstrom and Withrow [7].

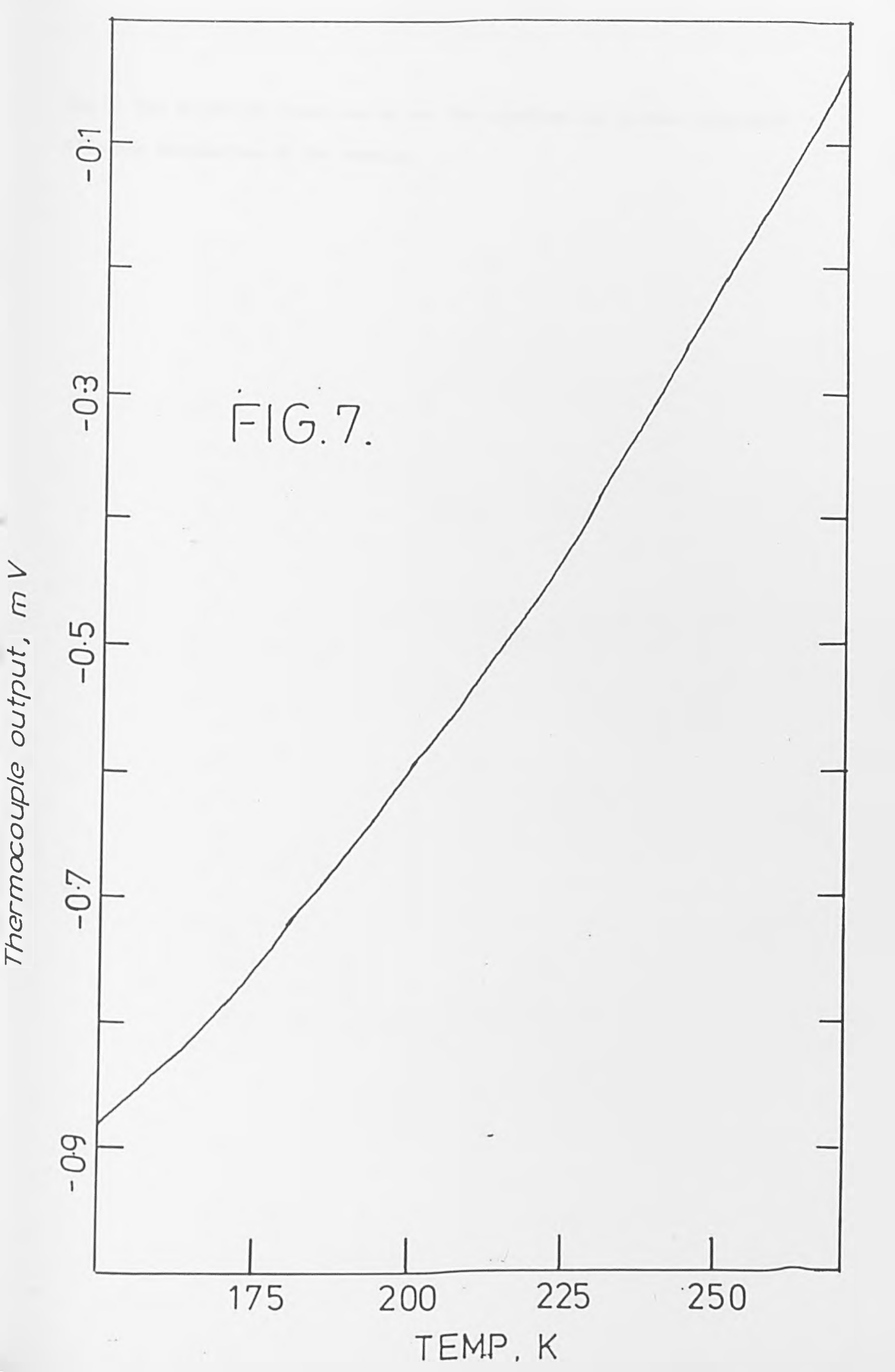
FIG. 7.
-0·1
-0·3
-0·5
-0·7
-0·9
Thermocouple output, m V
175
200
225
250
TEMP, K

Fig.8. The molecular beam source and its adaption to produce adsorbate coverage boundaries at the sample.

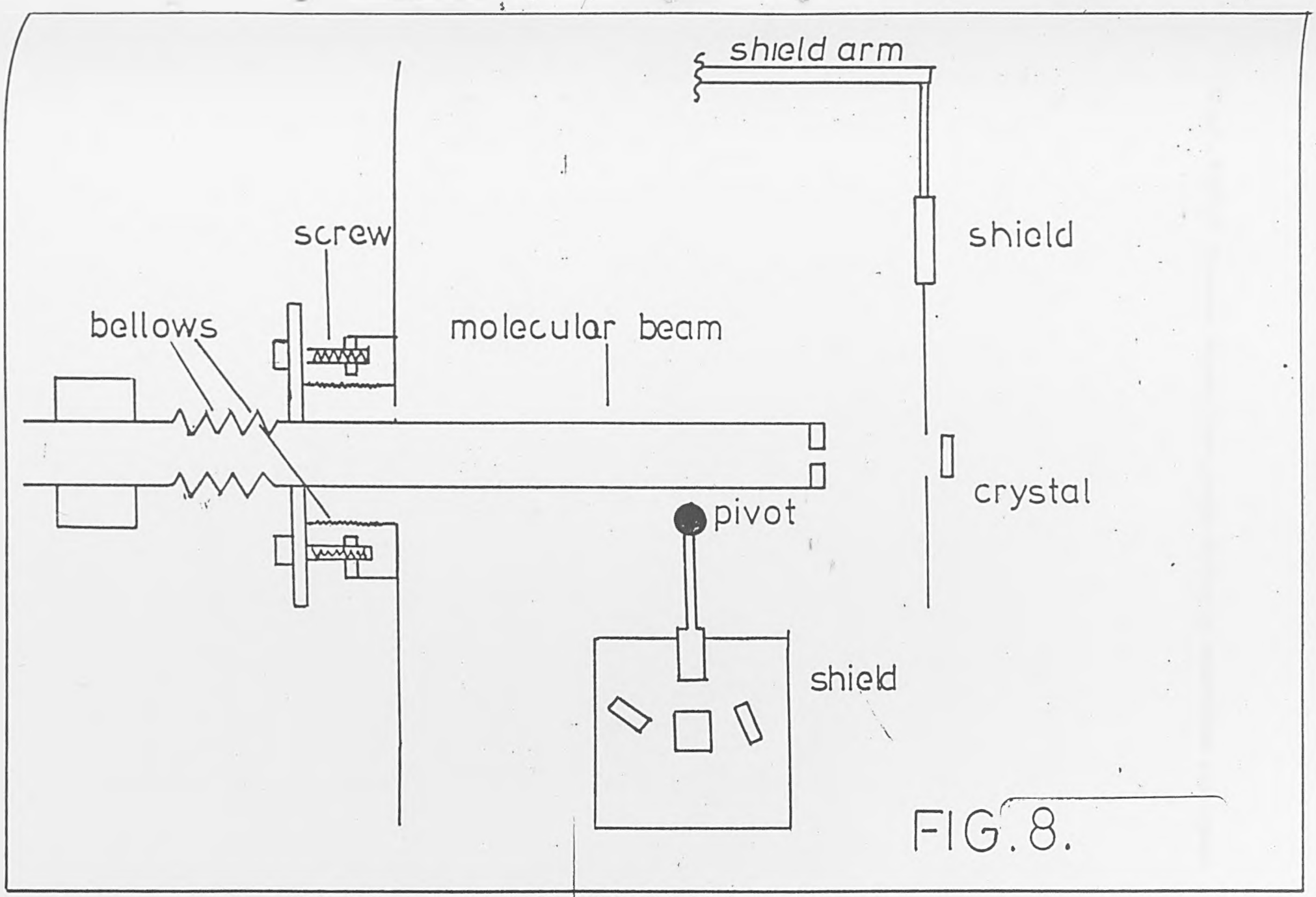
shield arm
screw
shield
bellows
molecular beam
crystal
pivot
shield

FIG. 8.

Fig.9. Typical pressure versus time graphs during an adsorption experiment.

fig .9.

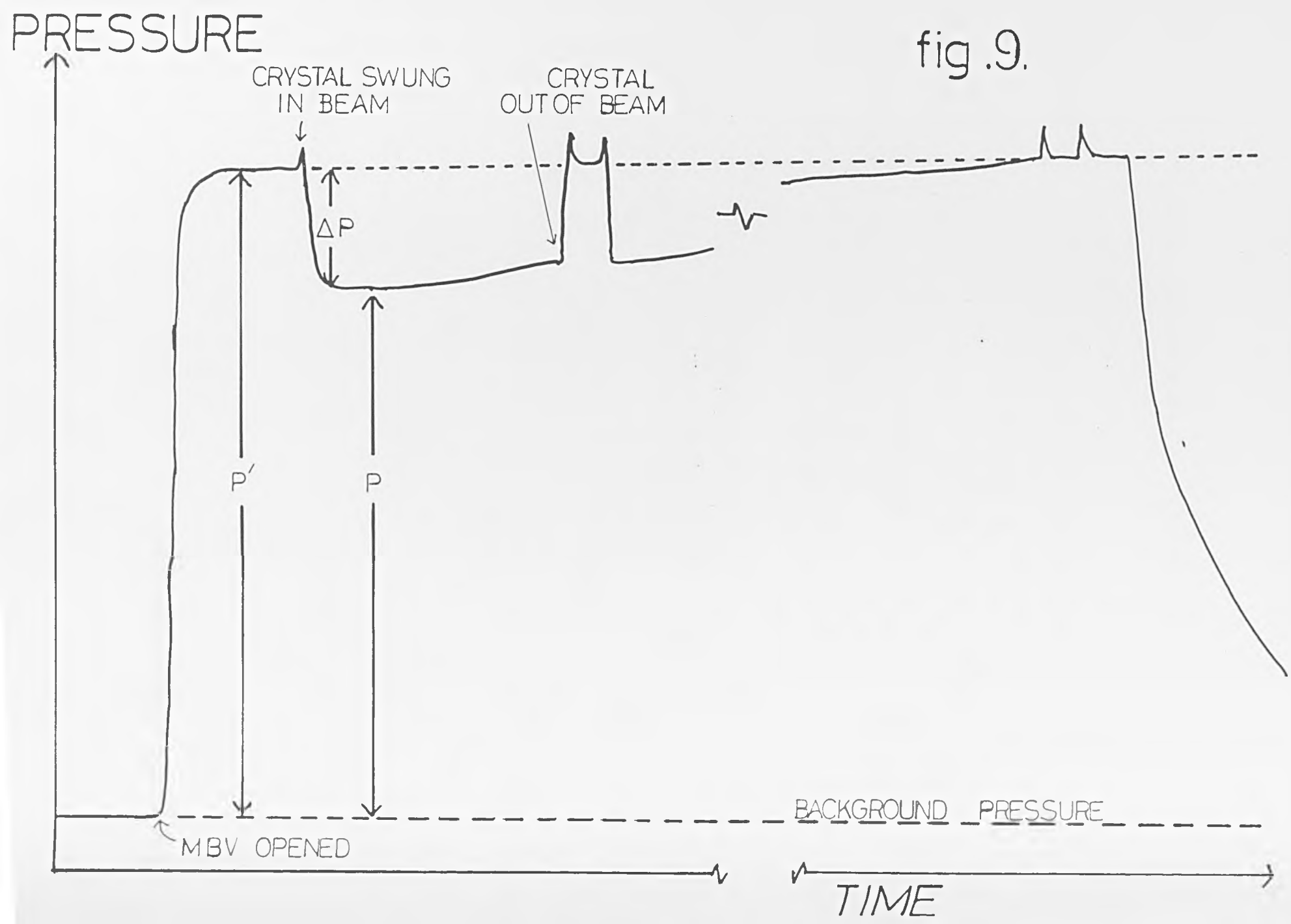
PRESSURE
CRYSTAL SWUNG IN BEAM
CRYSTAL OUT OF BEAM
ΔP
P′
P
BACKGROUND PRESSURE
MBV OPENED
TIME

Fig.IO. The L.E.E.D. experiment.

fig 10.

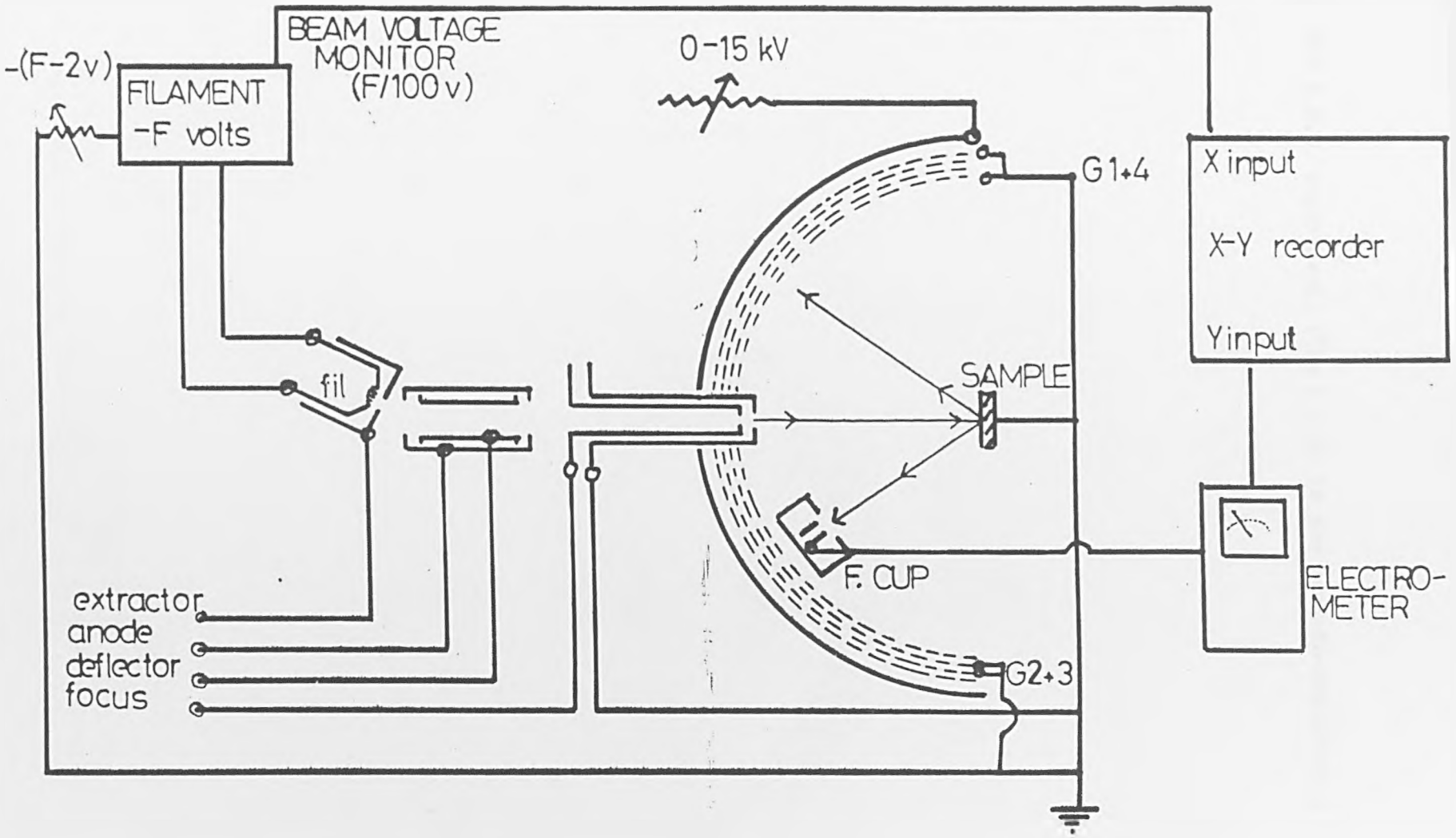
BEAM VOLTAGE
MONITOR
(F/100 v)
-(F-2v)
FILAMENT
-F volts
0-15 kV
G1+4
X input
X-Y recorder
Y input
fil
SAMPLE
F. CUP
ELECTRO-
METER
extractor
anode
deflector
focus
G2+3

Fig.II. The A.E.S. experiment. (The L.I.A. is the lock-in-amplifier.)

fig .11.

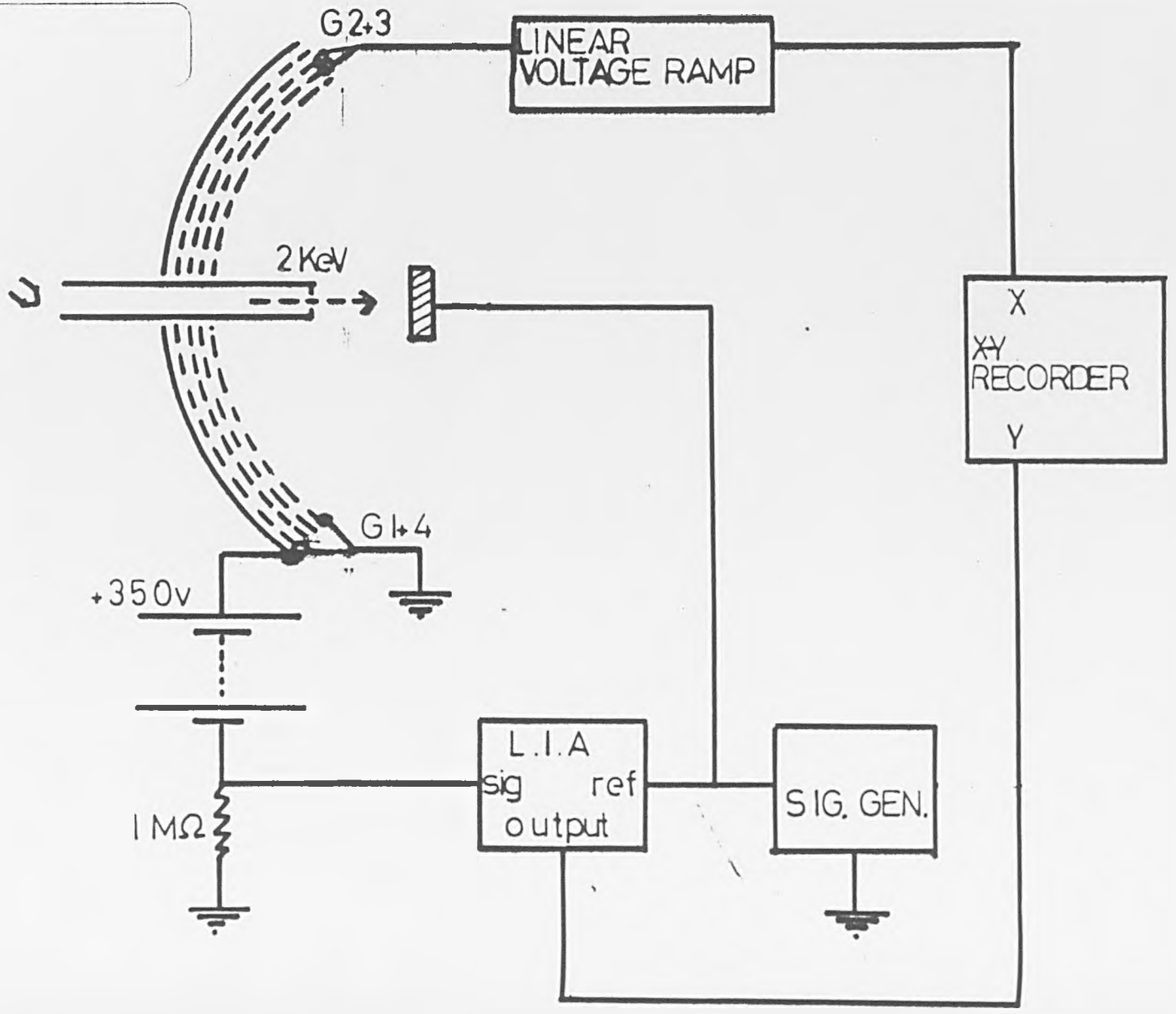
G2+3
LINEAR VOLTAGE RAMP
2KeV
X
X-Y RECORDER
Y
G1+4
+350v
L.I.A
sig ref
output
SIG. GEN.
1 MΩ

Fig.I2. The use of differentiation in R.F.A. Auger experiments.

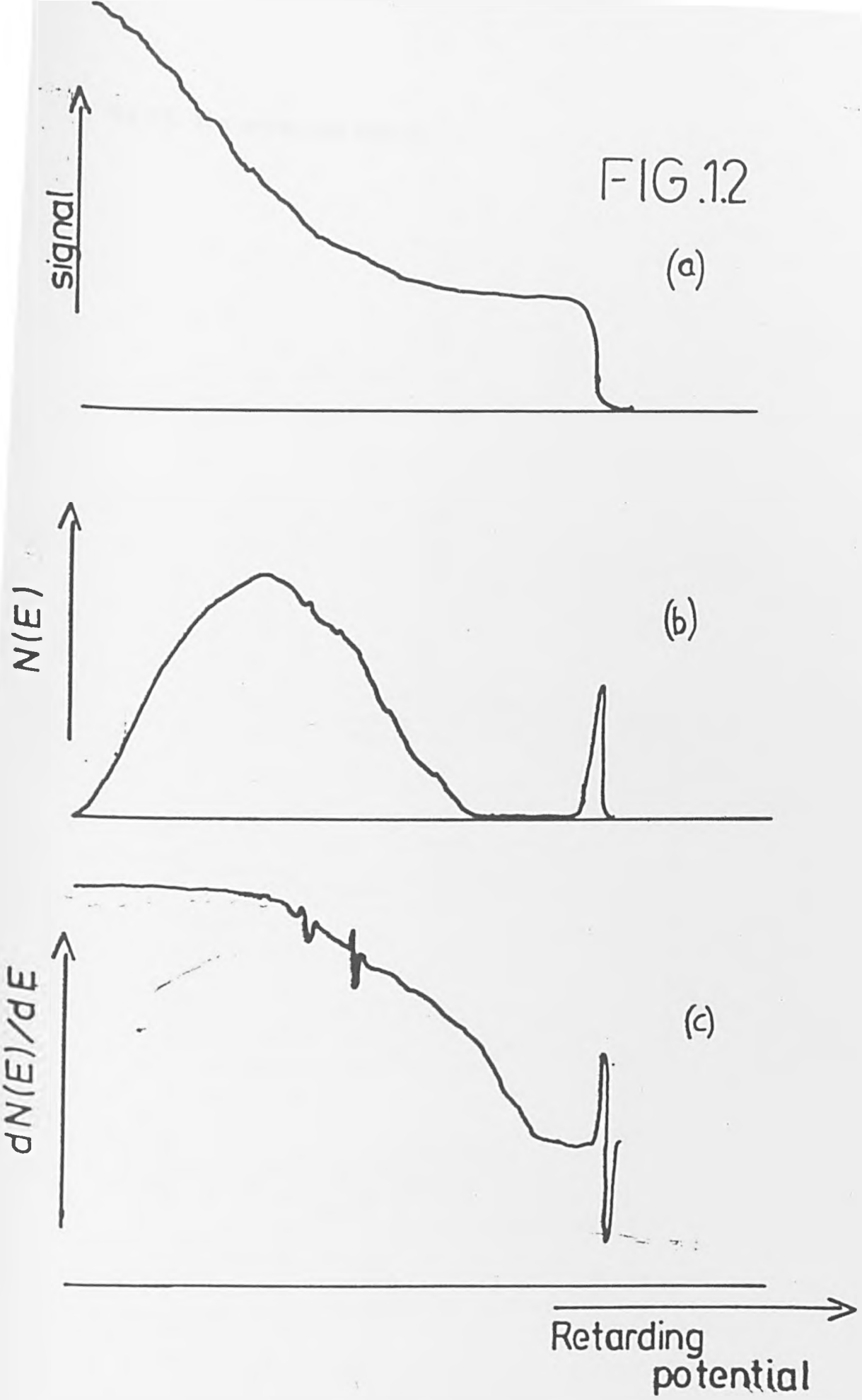

FIG.1.2

Fig.13. The potassium source.

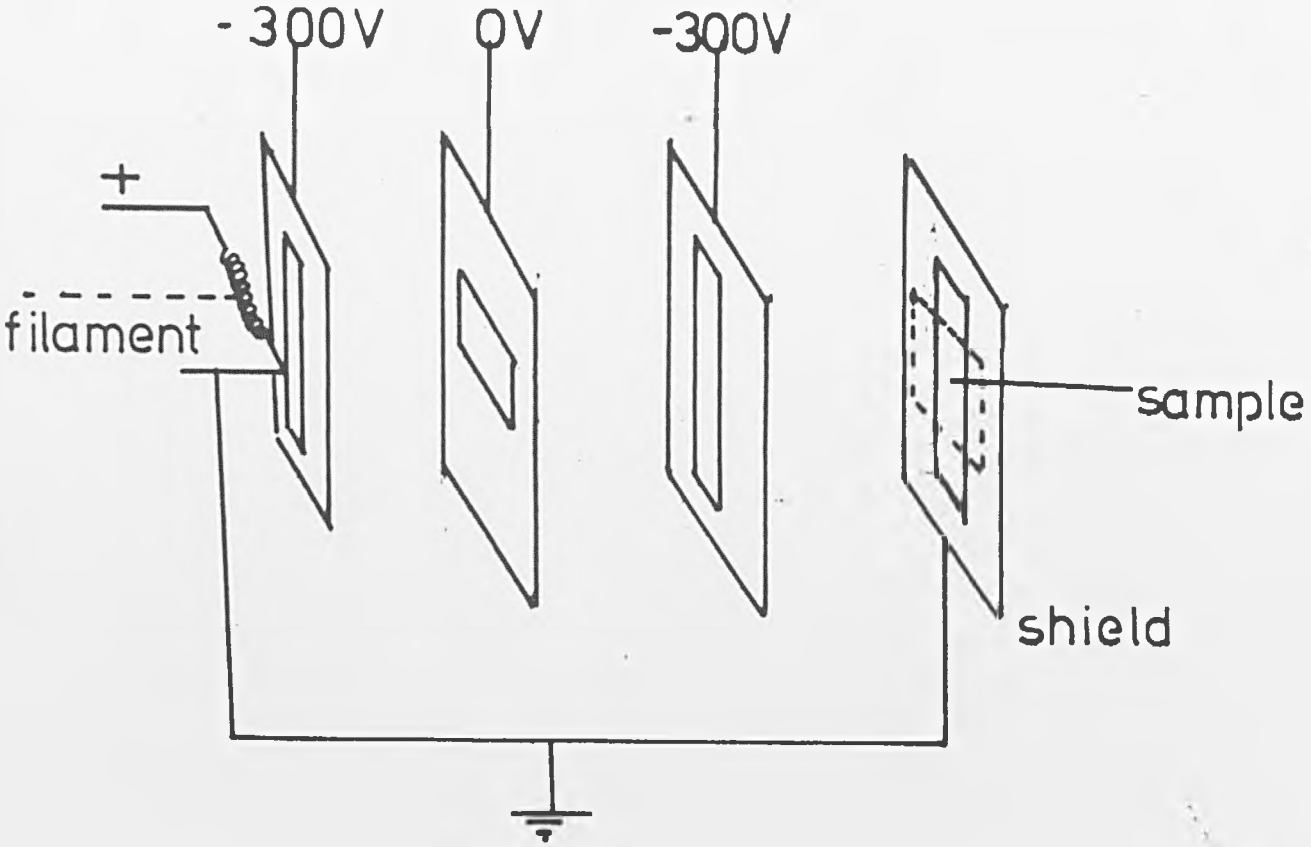

FIG.13.

Fig.14 Typical A.E.S. spectrum from the K dosed surface.

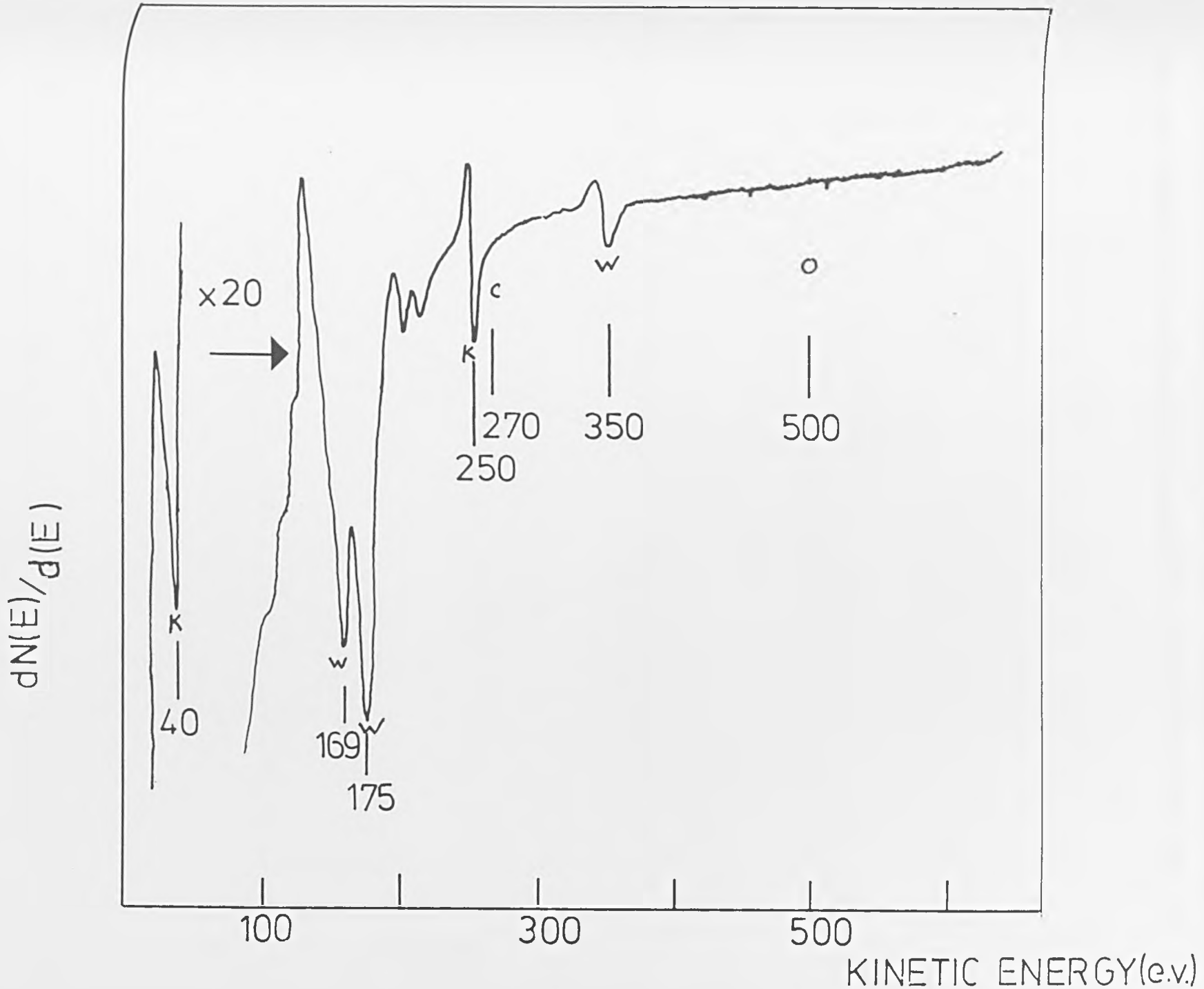
dN(E)/d(E)
×20
K
40
W
169
W
175
K
C
250
270
W
350
O
500
100
300
500
KINETIC ENERGY(e.v.)

Fig.15. Typical coverage versus distance profiles for K.
The time shown on the graphs indicates the number of minutes the initial patch has been heated for in diffusion experiments. The heating temperature was 610K.

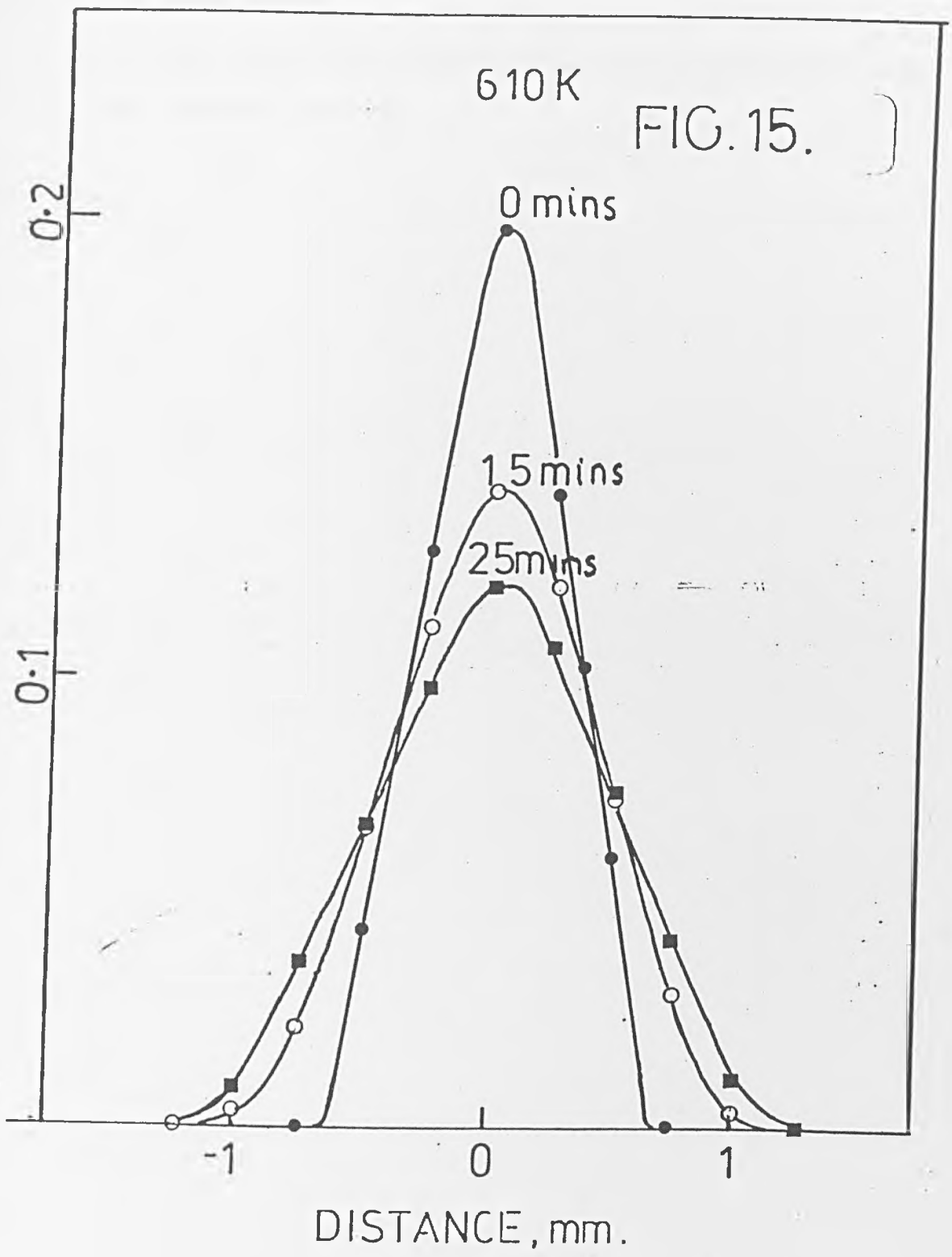
610 K
0 mins
15 mins
25 mins
0·2
0·1
-1
0
1
COVERAGE, MONOLAYERS
DISTANCE, mm.

FIG. 15.

Fig.16. The indium source.

T is the indium loaded tubes, S the shield and W the tungsten wire used to bind the two tubes together.

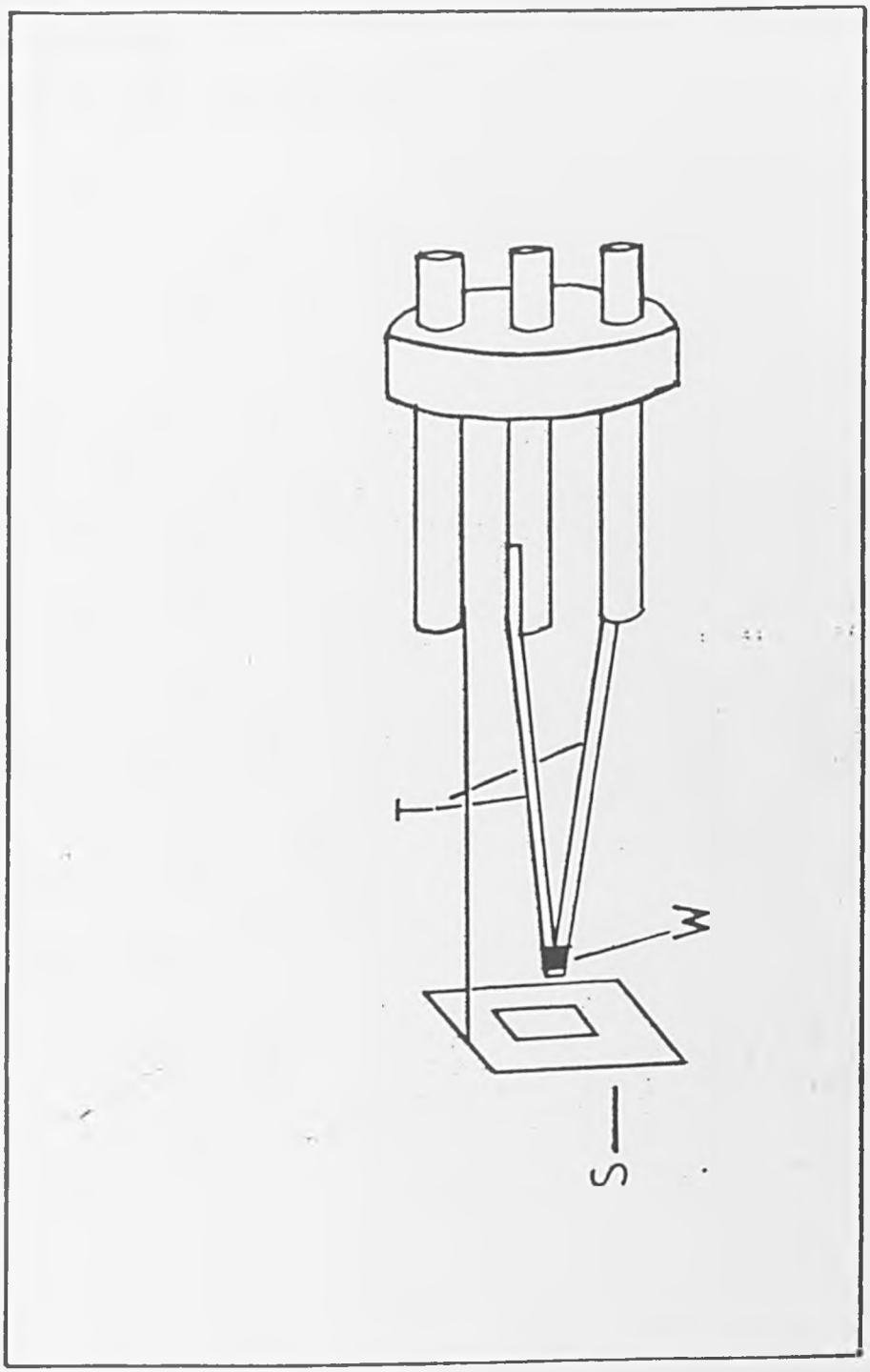
W
S

Fig.17. The type of coverage versus distance profiles obtained for indium adsorption. Four curves are shown. These are the result of heating the patch for the time and temperatures shown.

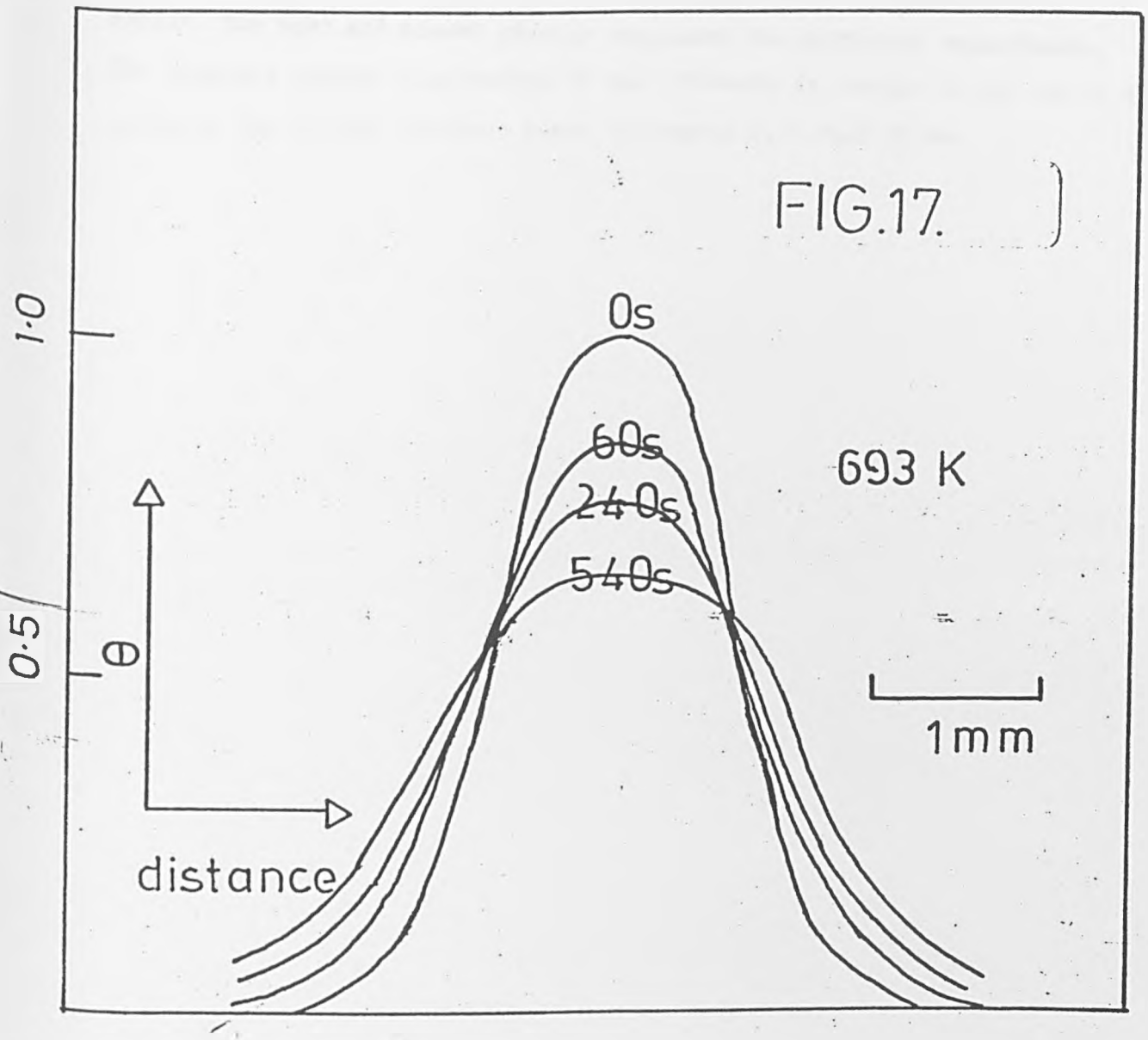
FIG.17.
1·0
0·5
θ
0s
60s
240s
540s
693 K
1mm
distance

Fig.I8. The boundary between zero and a half monolayer obtained for oxygen. The open and closed circles represent two different experiments. The apparent spatial distrbution of the boundary is thought to be due to the width of the primary electron beam; estimated as 0.I5-0.25 mm.

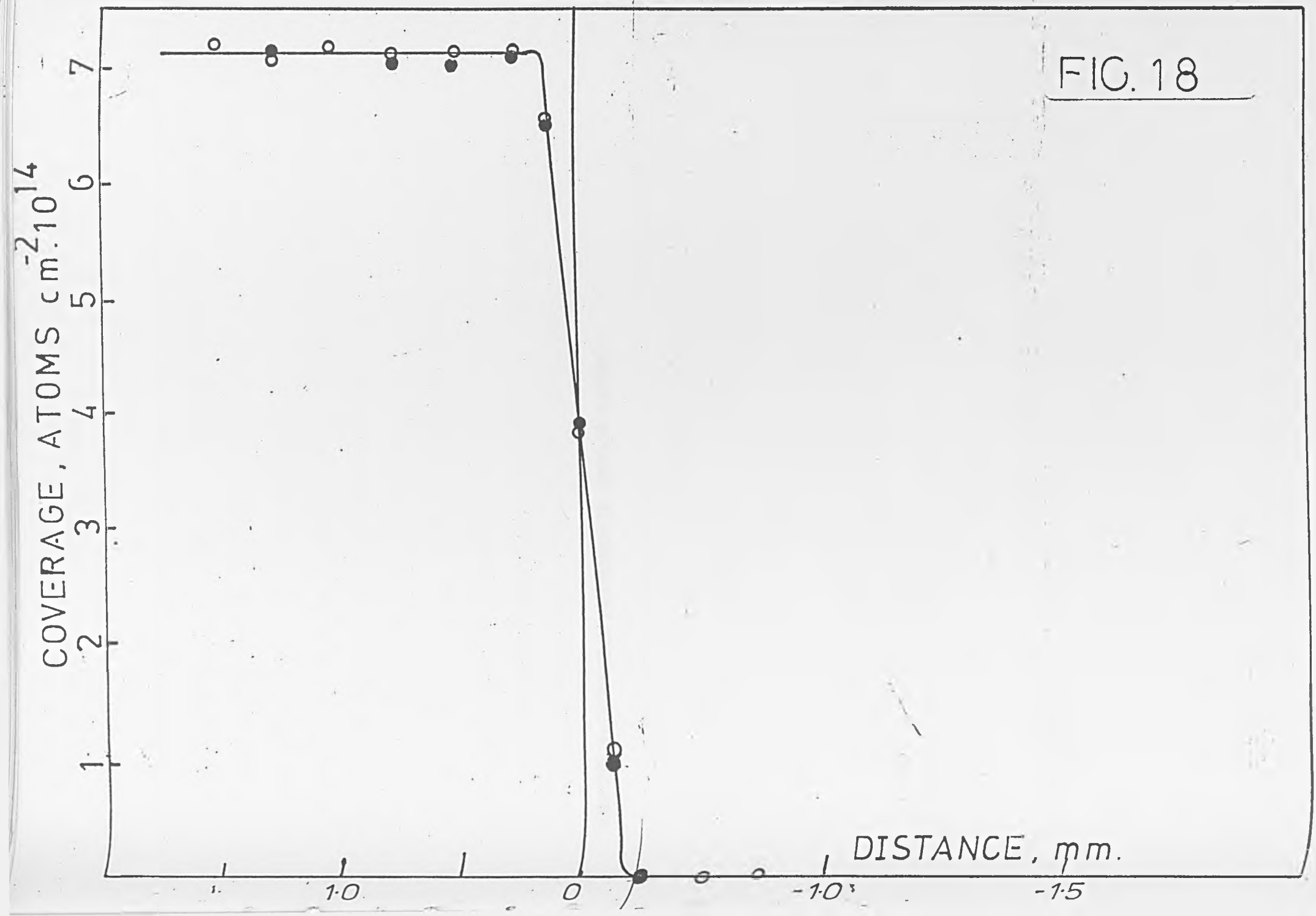
FIG. 18
COVERAGE, ATOMS cm^{-2}.10^{14}
1
2
3
4
5
6
7
1·0
0
-1·0
-1·5
DISTANCE, mm.

CHAPTER 3; DIFFUSION PROCESSES IN SURFACE LAYERS.

3.I. Introduction.

Surface diffusion has been one of the most neglected fields of study in recent years. However, the subject has undergone something of a revival. It has long been known that the movement of reaction intermediates over substrates is one of the most important steps in many catalytic processes[1]. Crystal and thin film growth is also dependent on the diffusion of species across the surface.[2] Mobility in surface layers is also important in less applied fields. It is now a well known fact that mobility in the physisorbed layer leads to increased efficiency of chemisorption. Migration of the chemisorbed species allow the adspecies to find sites of minimum energy and so produce ordered structures. The principle reason for the lack of experimental data is mainly associated with the diffuculty in measuring the diffusion parameters. The development of surface sensitive techniques capable of measuring surface coverages quickly and easily has alleviated these problems to some extent. However, diffusion studies still tend to be very time consuming and the work experimentally very exacting.

The aim of this chapter is to briefly present an overview of surface diffusion studies, both theoretically and experimentally. Migration of electronegative and electropositive adsorbates will be reviewed but self-diffusion will be largely ignored.

3.2. Experimental Techniques in Surface Diffusion.

These can be divided into 2 types; those which measure the diffusion kinetics by noting the change in coverage of a deposited layer and those which observe Brownian motion in an equilibrium distribution over the surface.[4] The first of these methods is based on Ficks second law which

relates the change in surface coverage with time to the diffusion coefficient, D,

$$\frac{\delta N}{\delta t} = \frac{\delta}{\delta x} D \frac{\delta N}{\delta x} \quad \text{.....I}$$

N is the coverage, t the time and x is the distance moved at coverage N.

3.2.I. Coverage sensitive methods.

a) Primary photon beam.

This technique is restricted to species which drastically change the work function of the sample and thus is very useful when investigating alkali metal migration. In these experiments the photoemission of electrons from the surface is measured and this will vary with the work function of the surface. The method was first used by Bosworth in the 1930's [5,6], but has recently been rediscovered [7]. Bosworths method makes use of a focussed light beam which can be accurately scanned across the sample. Provided that the photoemission current can be calibrated with coverage then the results can be readily treated to yield coverage/distance profiles.

b) Primary Electron Beam.

Scanning Auger electron spectroscopy (SAES) may well prove to be the most important development in the study of surface diffusion. This can be applied to any system with a convenient Auger transition. Recent studies include work on the N/W(IIO) system [8]. This work was notable in that the electron beam was used to produce a line deposit on the surface. This was done by adsorbing the molecular γ state over the whole of the surface held at 90K. A part of this strip was converted into the β state using the electron beam. The γ state could then be desorbed by gentle heating. Scanning Auger has also been successfully used by Butz and Wagner [9] to study Pd and Au diffusion on W {IIO} .

The secondary electron emission properties of surfaces have also been used to study diffusion [10,11]. The simplest way to monitor such effects is to measure the drain current at the sample,

$$I_t = I_p + I_s ,$$

where I_s is the secondary electron current and I_p the primary beam current and are opposite in sign. Secondary electrons at energies of greater than 200eV originate only from the first 3 or 4 layers of the surface due to escape depth considerations and hence are very sensitive to surface effects. The investigators who have made use of these techniques found it easy to calibrate drain current changes with coverage (due to the large work function change for the O/W {110} system studied) and hence using scanning techniques to produce coverage versus distance profiles [10,11].

c) Other techniques.

An extremely novel technique was developed by Butz and Wagner [13] to study the diffusion of O on W {110}. They deposited a sharp boundary on the surface, between covered and uncovered areas, and then measured the coverage versus distance profiles. This was done by monitoring the contact potential of the surface as a function of distance. The vibrating capacitor method was used, and in this work the reference plate was a small wire (diameter 6×10^{-6} m) held a distance of 10^{-6} m above the surface. This could be scanned across the surface, so measuring the contact potential as a function of distance which could be rapidly converted into coverage profiles by using a coverage calibration. The distance resolution was quoted as 5×10^{-6} m. A similar technique has been used to measure the diffusion of Cs across polycrystalline W samples [14]. Here the work function as a function of distance was measured using a scanning electron microscopy instrument.

3.2.2. Field Emission Techniques.

These techniques have been used over the last 20 years to provide the bulk of the available diffusion data. The field emission microscope, devised by Müller in the 1930's, produces a highly magnified image of a sharply pointed sample on a fluorescent screen[15]. The image is formed by electrons which are emitted under the very high field densities produced by biasing the sample at large voltages. Gomer[16] has described how sharp adsorbate boundaries can be produced on field emitter tips. This consists of an effusion source pointing at the tip and keeping the walls of the chamber at very low temperature. The field emission microscope provides a resolution of about 20 Å enabling individual low-index crystal planes to be viewed. A typical example of the early work is a study of Ba diffusion on W[17]. This metal increases electron emission very greatly and thus the field emission displays become brighter and so diffusion is easily followed. However, it is very difficult to seperate and understand some of the effects in a field emission display. This is because the field emission microscope shows the results of a number of different effects, e.g. the possibility of coverage dependent parameters[18,19] or the possibility of different adsorption sites[20]. Probe hole field emission microscopy allowed individual planes to be studied and planes of high work function to be studied and so alleviated some of the problems.

By far the most dramatic improvement of the technique came with the observation that current fluctuations in field emission were related to the diffusion process[21,22], the so-called "flicker noise technique". When the adsorbate is in a mobile state on the surface, localised variations in adsorbate density occur with time and these appear as rapidly appearing and disappearing points of light on the screen. If a current measuring system is used they appear as a spikey noise level. The level of the noise

and its frequency is strongly coverage, temperature and crystal plane dependent. The adsorbate density fluctuations build up and decay with a characteristic time given by:

$$\tau = r^2 / 4D$$

where r is the radius of the area probed. With $r = 50\text{Å}$, diffusion coefficients between 10^{-13} and 10^{-10} $cm^2 s^{-1}$ yield $0.6 \geq \tau \geq 0.0006$s. The amplitude of the flicker noise is related to the mean square displacement, $\bar{x}$, of the diffusing species. The particular use of this method is that it extends the substrate temperatures useful in diffusion studies downwards so that processes such as desorption and absorption are well seperated.

Field emission techniques are beset with problems. The high electric field at the sample may affect the diffusion process in some way and recent work has indicated that the flicker noise technique does not measure diffusion directly although the measured values do relate to diffusion in some way.[65]

The flicker noise technique observes Brownian motion in an equilibrium layer and the technique described below belongs in the same category. After the development of the field emission microscope, Müller quickly discoverd that the same apparatus could be used to obtain even greater resolution[23] and the Field Ion Microscope was born. Here high pressures of an inert gas (He at 0.1 Pa) are admitted to the vacuum chamber and the potential on the tip and screen is reversed compared to field emission. Atoms on the tip, adsorbed from the background gas, make a number of of hops until they slow down and ionised by quantum mechanical tunneling from the gas to the tip, the positive charge on the tip then repels these ions from the tip towards the screen where they impact and cause a bright spot. Resolutions of the order of about 3Å are obtained due to the minimisation

of the impinging ion energy parallel to the surface compared to the transverse velocity of an electron in field emission. The very high fields in this technique tend to strip gaseous molecules or atoms from the surface so only metal adsorbates can be studied [24]. In this technique Brownian motion of individual adatoms is observed and the diffusion coefficient can be found simply from the random walk relationship,

$$a^2 = 4Dt$$

where a is the mean square displacement in a random walk process.

3.2.3. Other Methods.

One of the earliest studies of surface diffusion was made by Langmuir [25] when studying the Cs/W system. A polycrystalline W wire was surrounded by a concentric electrode divided into three parts. Cs layers on the surface could be stripped by biasing the centre section negative and immersing the cell in liquid air. If the outer sections of the electrode were positive an area on the wire depleted in Cs could be produced. This central region could be filled with Cs by diffusion from the outer parts of the wire. The field desorption process could be repeated and if the desorption flux was monitored, diffusion could be measured.

Other methods include monitoring the thermionic emission of W as a function of thorium coverage [26], by monitoring the Cu^+ signal in a secondary ion mass spectrometry experiment as diffusion carried Cu into a clean area of sample from a high Cu coverage region. A similar method was used to study physisorbed tritium on a Ni(III) surface [27, 28] but this time the β radiation from transported particles was measured. There was a problem in this work in that the diffusion was accompanied by desorption, but a relationship was used in an attempt to seperate the two events.

3.3. Surface Diffusion Processes.

Diffusion is an activated process and follows an Arrhenius relationship of the following form,

$$D = D_o \exp(-E_m/RT) \quad \ldots\ldots\ldots 2$$

This relationship breaks down if more than one diffusion process occurs at the same time and, effectively, only single site hopping can be treated in this way. D_o is the pre-factor, known as the diffusivity, and E_m the activation energy for diffusion. The diffusion process is illustrated in Fig. 1. The adspecies lies in the bottom of a potential energy well seperating it from the next site. By gaining energy E_m it can reach the transition state # from which it can reach the second site or refill the original site. The lifetimes in the transition state are very small; an instantaneous picture of the sample would show most of the molecules in the wells. Assuming that diffusion proceeds by hopping from well to well with a mean square jump distance a^2 over the barrier E_m with an activation entropy $\Delta S_m^{\#}$ then the mean jump frequency can be expressed in terms of absolute rate theory as,[29]

$$\Gamma = (kT/h) \exp(\Delta S_m^{\#}/k) \exp(-E_m/kT) \quad \ldots\ldots\ldots 3$$

provided that the transmission coefficient at the barrier is unity.

Equation 3 is sometimes expressed as,

$$\Gamma = \nu \exp(-E_m/kT) \exp(\Delta S_m^{\#}/k) \quad \ldots\ldots\ldots 4$$

with $\nu = (kT/h)$ $\ldots\ldots\ldots 5$

The diffusion coefficient is related to the jump frequency through the expression,

$$D = a^2 \Gamma/2\alpha \quad \ldots\ldots\ldots 6$$

where $\alpha = 1$ for diffusion in one dimension and $\alpha = 2$ for two dimensions.

If random walk is assumed it can be shown that,

$$\langle x^2 \rangle^{\frac{1}{2}} = (\Gamma t)^{\frac{1}{2}} a \quad \ldots\ldots\ldots 7$$

where $\langle x^2 \rangle^{\frac{1}{2}}$ is the root mean square displacement in time t. By combining

these expressions, it can be written that,

$$D_o = \frac{\gamma a^2}{2\alpha} (\Delta S_m^{\#}/k) \quad \ldots\ldots\ldots 8$$

For diffusion in 2D i.e. $\alpha = 2$ and assuming that $\Delta S_m^{\#}$ is O and $a = 3\text{A}^{o}$, then at a temperature of 500K, D_o evaluates to 3×10^{-4} cm^2 s^{-1}.

D can be expressed using equations 6 and 7 as,

$$D = \langle x^2 \rangle / t \quad \ldots\ldots\ldots 9$$

and experimentally this is approximated to [30],

$$\bar{x} = (Dt)^{\frac{1}{2}} \quad \ldots\ldots\ldots 10$$

where $\bar{x}$ is the average distance travelled by a boundary in time t. If D varies with coverage then the D values found refer to some average D value over that coverage range.

It will be seen later that D is often dependent on coverage due to coverage dependent interactions on the surface. These will strongly influence the kinetics of the diffusion. The first examples of coverage dependence discussed here is due to the adsorption of multilayers. These layers are often weakly bound to the surface compared to the first layer and are highly mobile. The second example of coverage dependence occurs when lateral interactions exist between the adspecies. This is shown in Fig.2. Repulsive interactions between the adspecies will reduce the barrier height, while attractive interactions will increase it. Bowker and King [31] developed both an analytical method and a Monte-Carlo routine to determine the consequential results of lateral interactions on the diffusion process. The results are indicated in Fig.3, where diffusion from a square boundary is represented. The point where the diffusing boundary crossed the position of the original boundary was found to be sensitive to the interaction. For attractive interactions the crossoverp point, θ_c, is below the half coverage position, for repulsive interactions it is above. With no lateral interactions

the crossover point is at the half coverage point exactly.

3.4. Survey of Experimental results.

3.4.I. Metallic Adsorbates: Strongly Charged Atomic Species.

Early investigations by Taylor and Langmuir[25] showed that Cs diffusion on a W polycrystalline wire was extremely coverage dependent. They found that as the coverage dropped from 2.73 to I.73 10^{13} atoms cm^{-2} the diffusion coefficient dropped from 3.45 to I.4 10^{-5} cm^{2} s^{-1}. This was thought to be due to repulsive interactions on the surface. Shortly after this it was showed that very similar effects existed for the diffusion of Th on W[26]. Work continued with the systems Na/W[5] and K/W[6], and the results all gave good support for the effects seen by Langmuir[25]. A different effect was seen for the migration of Na than had been noticed for the other adsorbates.[5] Bosworth noticed[5] that a patch of Na deposited on the surface followed by temperature annealing was accompanied only by loss of Na from the surface; there was no sign of the patch spreading. However, if this process was repeated many times then the Na began to spread in a diffusion like manner but unlike the other alkali metals there was no coverage dependence in the measurements. Bosworth postulated that the initial behaviour was produced by diffusion into a microstructure of the surface. Eventually this was filled and diffusion across the surface began. For K[6] this effect was less important and the profiles of deposited patches after heating resembled those expected of a diffusion process. These are illustrated in Fig.4. For K, a very strong variation of E_m with surface coverage was found, at the lowest coverages measured E_m was measured as 69kJ mol^{-1} but decreased to a value of 28kJ mol^{-1} at near the monolayer point.

Suddenly in the I950's the effect of substrate structure on diffusion could be examined using the field emission microscope. Also, by this time

vacua were approaching those obtained in modern UHV systems, thus ensuring that most of the recorded data was from at least fairly clean surfaces. Drechsler[17] used this technique to study Ba diffusion on W. The diffusion energies varied markedly from plane to plane, decreasing in the order,

$$\{112\}>\{100\}>\{111\}\sim\{012\}>\{122\}>\{110\}$$

The $\{210\}$ plane showed the most interesting results. This plane is made up of rows of lattice atoms in the $\langle 001 \rangle$ direction seperating flat terraces. Diffusion across the rows needed an activation energy of three times greater than that needed for diffusion along the rows and this type of result was soon repeated for Hg and Cs diffusion on W[32].

It must be remembered that the field emission technique is to be treated with some caution; diffusion is observed taking place over planes of vastly different character and it is to be expected that certain sites or planes act as "feeder" sites for other planes by adsorbing gas very quickly. This sort of effect will be the norm rather than the exception and may dominate some work. Work by Schmidt and Gomer[33] and by Meclewski[34] seems to have suffered from this type of effect. Both laboratories showed that the diffusion of K on W occured with an increasing activation energy as a function of coverage. This strongly contradicts the observed variation in the desorption energy which falls with coverage.

The only work that can be viewed as being in any way reliable is a recent study by Love and Wiederick for Cs diffusion on polycrystalline tungsten and a $\{110\}$ sample. For the polycrystalline sample they found two effects (presumably the same effects seen by Bosworth[5]), diffusion into the bulk via grain boundaries and the normal diffusion behaviour. The former had an activation energy of 170kJ mol^{-1}, the latter an activation energy of 17kJ mol^{-1}. For Cs on the $\{110\}$ plane the absorption effect was very much

less important and they found that the low coverage surface diffusion regime could be described by,

$$D = 0.23 \pm 0.1 \exp(-57 \text{ kJ mol}^{-1} / RT) \quad \text{cm}^2 \text{ s}^{-1}.$$

Unfortunately, even in this work the variation as a function of coverage was not measured.

3.4.2. Metallic Adsorbates: More Weakly Charged Atomic Species.

These studies are usually limited to the investigation of the transition metals as adsorbates and self diffusion experiments. The most common technique is field ion microscopy. These experiments have been of great importance in the study of surface diffusion. The first quantitative study using FIM was made in 1966 by Ehrlich and Hudda for W self diffusion. The work showed that motion was extremely directional on channelled surfaces and this has now been found many times. A review has been published that documents the E_m and D_o values for many metal adsorbates on W[36] and this will not be reproduced here.

On many surfaces the diffusion is seen to be I-dimensional. All these surfaces are channelled and include the W {211} and the W {321}[35], the Rh {110}, {331} and {311}[37] and the diffusion takes place only along the channels and has been seen for self diffusion[35,37] and adatom diffusion such as Mo on W {211} and W {321}. On smooth surfaces the diffusion is seen to be 2-dimensional and these include the {110} and {111} planes of W[35] and Rh[37]. The activation energies vary widely from one plane to another and this variation is predicted from pairwise interaction potentials[35,37] which show that E_m is greater for rough surface planes. This trend is followed for Rh[37], however, it is not for W[35] where the {110} plane, the most close packed for a BCC metal, has the highest E_m value. This anomaly has now been explained in terms of surface relaxation and changes in field strength.[39]

Recent FIM experiments have shown that adatoms may jump across the channels on the {110} plane of Pt[40], indeed on Ir, the cross channel jumps dominate the diffusion mechanism.[41] The atom probe technique, which gives chemical enviroment information, has shown that the cross-channel motion for W adsorbed on Ir {110}[23], occurs by the incorporation of the adatom into the lattice and the removal of the lattice atom to the adjacent site.

One of the most amazing observations in recent years was that clusters are important in the diffusion process. Using FIM, Bassett noticed the association of adatoms to form clusters[42] and quantitative studies[43-50] quickly followed. Results have been collected for the diffusion of Re dimers on W {211} showing that the dimers diffuse more quickly than the adatoms[43]. This effect is explained in terms of an attractive interaction between the adatoms which peaks near the saddle point in the energy versus distance curves. Even more suprisingly the rates of migration of Re trimers on W {211} has been shown to occur at rates similar to the dimer.[44] Obviously these effects are very dependent on the interactions of the adatoms and e.g. the migration of Ir dimers on W {211} was observed but[45] the activation energy for surface diffusion is higher for the dimer than the adatom[50]. Dimer studies have been performed for W on W {211}[36] and Pt on W {110}[50].

Recent studies using scanning AES have been made for the diffusion of Pd and Au on single crystal planes of W[9]. This study is one of the most elegant ever made in the field of surface diffusion. The role of lateral interactions played an important part in the diffusion of these elements. To this effect the profiles observed had distinct kinks at various coverages corresponding to the position of various ordered structures. These kinks in the coverage distance profiles occur because of the extra stability of the ordered structures and have been observed for other

systems, notably for the spreading of Th on W {113} [46], Ba on W {110} [47] and Ba on Mo {110} [48]. For Pd and Au diffusion the dominating influence on the profiles proved to be the presence of second layer atoms. These atoms are free to "roll" over the first layer and extend the width of the adsorbed patch; in doing so the second layer atoms are converted into more strongly bound first layer atoms and the energy of the system is lowered. This mechanism is very similar to the diffusion of physisorbed gases which roll across the chemisorbed atoms until they reach an empty site when they transfer to the deeper well [49]. The process is known as the "unrolling carpet". In these studies results were obtained in strong support of the FIM observations that diffusion was sensitive to the anisotropy of the surface. This was done by comparing the diffusion on a stepped W {110} plane in different directions. It was found that Pd could not spread in a direction perpendicular to the steps as fast as it could in a direction parallel to the steps (110 terraces). Thus it was seen that circular patches of adsorbate assumed oval shapes under heat treatment.

3.4.3. The Diffusion of Gaseous Adsorbates.

We shall divide this section into two separate sections. Firstly a brief review of the diffusion of physisorbed species is given. The second section will be longer and the diffusion of chemisorbed species will be reviewed. Particular reference will be made to the system O/W {110}, since this is the only system which has been examined by a number of different techniques, so that work on field emitter tips and bulk single crystal planes can be compared. The relationship between the structure of the surface as viewed by LEED and surface diffusion will be examined.

a)Physisorbed Species.

It has been observed that when gaseous adsorbates are condensed onto

W field emitter tips at 4.2K, then, when the tip temperature is raised to between 20k and 40K a sharp boundary is observed to move across the tip [49,51]. The process has been discussed in the previous section; the unrolling carpet. The boundary displacement $\bar{x}$ at time t is given by,

$$\bar{x} \sim (Dt \times N/N_t)^{\frac{1}{2}} \quad \ldots\ldots\ldots II$$

where N is the surface coverage and N_t the density of trap sites. In many studies it has been impossible to control such low temperatures or to measure them so that data collection at only very few temperatures is possible. Usually D is found from use of equation II and using a calculated estimate of D_o, E_m can be found from equation 2. This type of analysis is less accurate than Arrhenius methods but results on W [53] show that E_m varies from 0.4kJ mol^{-1} to 3.7kJ mol^{-1} (for the adsorbates H and CO respectively). This work was also notable in that it showed that the diffusion of H took place in certain preferred directions.

In this type of study it is usually found that the lifetime of the physisorbed [4] species is of the same order of magnitude as the time of the experiment and so desorption as well as diffusion is observed. Such processes are described by the equation [30,51],

$$\bar{x} = \left\{ a^2 \exp(-E_m/kT) \exp(E_d/kT) \right\}^{\frac{1}{2}} \quad \ldots\ldots I2$$

where E_d is the desorption energy. If, E_m is measured where the lifetime is long, then, E_d can be found. For O on W [54] the measured value of E_d was 9.3kJ mol^{-1}. For the γ state of N on W at 77K no migration was observed [55], implying that the desorption and the diffusion energies had about the same value or the diffusion process took place with an activation energy that was about equal to an energy that converted it into a more strongly bound state.

b) Chemisorbed Species.

Using the method described earlier, [8] Polak and Ehrlich investigated the diffusion of the β state of N over a W {110} surface.

The equation :- $D = 4.7 \times 10^{-2} \exp(-87.9 \text{ kJ mol}^{-1}/RT) \text{ cm}^2 \text{ s}^{-1}$

was found to fit his results (illustrated in Fig.5)over an experimental temperature range of 100K. This value was found to be insensitive to the initial coverage of β N, not too surprising a result since lateral interactions on this surface are very weak between the N adatoms. Evidence for this is the observation that N forms only a very weak c(2×2) pattern on W {110} [56] and desorbs from the surface over a very narrow temperature range [57].

Chen and Gomer [58] have used the flicker noise technique to study the diffusion of CO on the same surface; this system is much more complicated than N discussed above. Firstly,below 300K the CO is adsorbed as a molecular, virgin state and no diffusion of this species could be seen, presumably because the mobility of this state leads to the formation of a more strongly bound β state. Further adsorption onto the β state produces a molecular α state and this again was not observed to diffuse because of similar desorption and diffusion energies. Measurements at 650K did show that the β state did diffuse and could be described by,

$$D = 2 \times 10^{-5} \exp(-94 \text{ kJ mol}^{-1}/RT) \text{ cm}^2 \text{ s}^{-1}$$

and like N no significant change in this relationship could be found as a function of coverage. This is something of a surprise since the diffusing species is thought to be O adatoms which form a p(2×1) structure on the surface and O atoms,when on the surface from oxygen adsorption, show coverage dependent diffusion parameters. This contradiction has been explained in terms of a very strong C-O interaction compared to a weaker O-O interaction. There is some evidence for this in photoemission experiments [59].

Chen and Gomer have extended their studies with this technique to study the system O/W {110} [60]. Here there was a very noticeable effect of coverage on the diffusion parameters. The results are shown in Fig.6.

At $\theta < 0.2$, E_m was found to be 60 kJ mol^{-1}. As the coverage rises to a value of $\theta = 0.6$, E_m also increases to a value of 96 kJ mol^{-1}. During this increase the D_o value was found to increase from 10^{-7} to 10^{-4} $cm^2 s^{-1}$. If D is plotted as a function of coverage (at constant temperature) a distinct maximum is seen to occur. However, this work has a number of puzzling features. The magnitude and the increase of D_o can not be explained and may be due to the technique rather than any surface property.[65] Also it has been shown that as the temperature increases, the current fluctuations should also increase if repulsive interactions exist between the molecules, and this was observed. This is in apparent contradiction with the increasing value of E_m they found.

The O/W {110} system had been investigated three years earlier by Butz and Wagner[13] but in this work the sample was a bulk single crystal rather than a field emitter tip. The authors could deposit a very sharp initial coverage profile and then diffuse it. Their results could be treated using the Matano analysis[61]. This is based on the equation,

$$D(N) = -\frac{I}{2t}\frac{dx}{dN}\int_{N_1}^{N} x\,dN$$

where $\int_{N_1}^{N_o} x\,dN = 0$ and when $t = 0$ if $x > 0$, $N = N_o$

$t = 0$ if $x < 0$, $N = N_1$

This assumes a perfectly square boundary between two coverages N_o and N_1 at an initial position of $x = 0$. This is a very useful analysis method and allows the evaluation of coverage dependent diffusion parameters to be performed very easily. Typical results from Butz and Wagner are shown in Fig.7 and it is quickly seen that material gained on the left hand side of the boundary does not equal the amount lost from the right hand side. Thus the results violate the boundary conditions above. Despite this, the authors continued with the analysis and found that the activation energy did not vary with coverage; a constant value of 113 kJ mol^{-1} was reported. However, D did vary with coverage and is shown in Fig. 8, displaying a

large peak just below $\theta = \frac{1}{2}$. D_0 also showed a large variation, changing from 0.02 to 0.38 in the coverage range $\theta = 0.4$ to 0.9.

Experiments at Liverpool[10] coupled with theory[51] are in strong support of these findings and have helped to form a coherent theory for the O/W {110} system by providing an explanation of the diffusion results using a number of LEED observations[62-64]. It is clear that the increasing E_m value with coverage noticed by Chen and Gomer[58] is due to the presence of adatom lateral interactions on the surface. The work of Lagally[62-64] shows that at the coverage and temperature where the E_m value was found to be at its lowest, the adatoms are randomly distributed across the surface and the diffusion energy is the value for an isolated adatom. At the high coverage region, the temperature was low enough to allow the surface adatoms to form an ordered p(2 × 1) surface phase because of next-nearest-neighbour attractive lateral interactions between the adatoms and thus the E_m value should be expected to increase. Butz and Wagner[13] may not have seen this because their experimental curves clearly showed some non-diffusion linked effect. The peak observed at near $\theta = 0.5$ in D versus coverage plots can also be shown to be due to these interactions. A Monte-Carlo simulation[51] shows that a distinct maximum in D should occur at $\theta = 0.5$ provided that nearest-neighbour and next-nearest-neighbour interactions are taken into account. This system emphasises that there is a strong relationship between the surface structure, as observed by LEED, and the surface diffusion of adspecies.

3.5. Concluding Remarks.

It is hoped that this review illustrates the importance of surface diffusion in the field of gas/solid interactions. It is clear that there is a dreadful scarcity of reliable data in this area of surface science, and most of the data has been collected on W, presumably because of the

ease of producing W field emitter tips. However, techniques are available that can produce bulk single crystal planes of almost any metal and surface science is certainly capable of measuring diffusion of adspecies across these planes. Two measuring techniques may assume primary importance, scanning AES and scanning secondary ion mass spectroscopy, because of the ease of scanning and producing very small diameter electron and ion beams. It is to be hoped that future investigators are more adventurous in their choice of systems and possibly look at systems important industrially. as well as theoretically.

REFERENCES.

I. J.C. Carberry, in Catalysis Reviews, published by Marcel Dekker Inc., New York, 1970.

2. G.C. Kuczynski,ed,Sintering and Catalysis, Plenum Press, New York,(1975)

3. M.A. Morris, M. Bowker and D.A. King, Kinetics of Adsorption,Desorption and Migration at Single Crystal Metal Surfaces, in Comprehensive Chemical Kinetics, eds C.H.F. Tipper and C. Bamford, Elsevier, North Holland.

4. W. Jost, Diffusion in Solids,Liquids and Gases, Academic Press, New York, 1980.

5. R.C. Bosworth, Proc.Roy.Soc., London, Ser.A.,150(1935)58.

6. R.C. Bosworth, Proc.Roy.Soc., London, Ser.A.,154(1936)112.

7. H.M. Love and H.D. Wiederick, Can.J.Phys.,47(1969)657.

8. A. Polak and G. Ehrlich, J.Vac.Sci.Tech.,14(1977)407

9. R. Butz and H.Wagner, Surf.Sci.,87(1979)69,85.

10. M. Bowker and D.A. King, Surf.Sci.,94(1980)564.

11. M.G. Wells and D.A. King,J.Phys.C.,7(1974)4053.

12. R.G. Muskett, J.Less Common Metals,22(1970)175.

13. R. Butz and H. Wagner, Surf.Sci.,63(1977)448.

14. P. Akhter and J.A. Venables,Surf.Sci.,103(1981)301.

15. E.W. Muller, Ergeb.Exakten Naturwiss.,27(1953)290.

16. R. Gomer,Field Emission and Field Ionisation,Harvard Univ.Press, Cambridge,(1961)

17. M. Drechsler, Z.Elekrochem,58(1954)340.

18. L. Schmidt and R. Gomer,J.Chem.Phys.,42(1965)3573.

19. G. Vladimirov,B. Medvedev and J. Sokolskaya, Sov.Phys.Sol.St., 12(1970)1118.

20. T. Engel and R.Gomer, J.Chem.Phys.,50(1969)2428, 52(1970)1832.

21. Ch. Kleint, Surf.Sci.,25(1971)373.

22. R. Gomer,Surf.Sci.,38(1973)373.

23. E.W. Muller and T.T. Tsong, Field Ion Microscopy, American Elsevier, New York,(1969).

24. A. van Oostrom, C.R.C.Crit.Revs.Sol.St.Sci.,4(1974) 353.

25. I. Langmuir and J.A Becker, Phys.Rev.,40(1932)463.

26. W. Brittain and J.A. Becker, Phys.Rev.,43(1933)428.

27. A. Abremenkov, V. Slezov, L.Tantrarov and Y. Fogel, Sov.Phys.Sol.St., 12(1971)411.

28. M. Renard and D. Deloche, Surf.Sci.,35(1973)487.

29. T.L. Hill, An Introduction to Statastical Thermodynamics, Addison-Wesley, Reading, Mass.,(1970).

30. R. Gomer, R. Wortman and R. Lundy, J.Chem.Phys.,26(1957)1147.

31. M. Bowker and D.A. King, Surf.Sci.,71(1978)583.

32. L.W. Swanson, R.W. Strayer and L.E. Davis,Surf. Sci.,9(1968)165.

33. L.D. Schmidt and R.Gomer, J.Chem.Phys.,42(1965)3573.

34. R. Meclewski,Acta Phys.Polon.,A37(1970)41.

35. G. Ehrlich and F.G. Hudda,J. Chem.Phys.,44(1966)1039.

36. G.L. Kellogg, T.T. Tsong and P. Cowan,Surf.Sci.,70(1978)485.

37. G. Ayrault and G. Ehrlich, J. Chem. Phys.,60(1974)281

38. T. Sakata and S. Nakamura, Surf.Sci.,51(1975)313.

39. P.W. Wynblatt,Surf.Sci.,22(1970)125.

40. D.W. Bassett and P.R. Webber,Surf.Sci.,70(1978)520.

41. J.D. Wingley, R.S. Chambers and G. Ehrlich, Atom Probe Studies on Adsorbates, 26th Int. Field Emission Symp.,West Berlin,(1975).

42. D.W. Bassett, Surf.Sci.,23(1970)240.

43. K. Stadt, W.R. Grahm and G. Ehrlich, J.Chem.Phys.,65(1976)3206.

44. K. Stadt and G. Ehrlich. Fall Meeting,TH S-AIME,Milwaukee,(1979).

45. D.A. Reed and G. Ehrlich, Philos.Mag.,32(1975)1095.

46. Yu.S. Vedula and A.G. Naumovets,in Poverkhnostraya Diffuziya i Rastekanie, (izd. Nauka, Moscow,(1969)).

47. A.G. Fedorus, A.G. Naumovets and Yu.S. Vedula,Phys.Stat.Sol.,AI3(I972) 445.

48. Yu.S. Vedula, A.T. Loburets and A.G. Naumovets, Pisma Zh. Exper. Tear. Fiz.,28(I978)258.

49. R.Gomer, R. Wortman and R.Lundy, J.Chem.Phys.,26(I957)II47.

50. D.W. Bassett,J.Phys.C.,9(I976)249I.

5I. R. Gomer, Field Emission and Field Ionisation, Harvard Univ.Press, Cambridge,Mass.,(I96I)

52. H. Fujita, J.Chem.Phys.,2I(I953)700.

53. H. Folman and R. Klein,Surf.Sci.,II(I968)430.

54. R. Galmer and J.K. Hulm, J.ChemPhys.,27(I957)I47.

55. G. Ehrlich and F.G. Hudda, J.Chem.Phys.,35(i96I)I42I.

56. C. Somerton and D.A. King, Surf.Sci.,89(I979)39I.

57. T.E. Madey and J.T. Yates Jr.,Nouvo Cimento Suppl.,5(I967)486.

58. J.R. Chen and R. Gomer, Surf.Sci.,8I(I979)589.

59. E.W. Plummer, Photoemission and Field Emission Spectroscopy, in Interactions on Metal Surfaces, ed. R. Gomer, Springer-Verlag,New York, (I975).

60. J.R. Chen and R. Gomer, Surf.Sci.,79(I979)4I3.

6I. C.Matáno, Jap.J.Appl.Phys.,8(I933)I09.

62. T.M. Lu, G.C. Wang and M.G. Lagally, Phys.Rev.Lett.,39(I977)4II.

63. G.C. Wang, T.M Lu and M.G. Lagally, J.Chem.Phys.,69(I978)479:

64. J.C. Bucholz,&M.G. Lagally, Phys.Rev.Lett.,35(I975)422.

65. Ch.Kleint, J. Beben and R. Meclewski, Surf.Sci.,93(I980)33.

Fig.I. Potential energy plots as a function of distance for a molecule travelling across the surface.

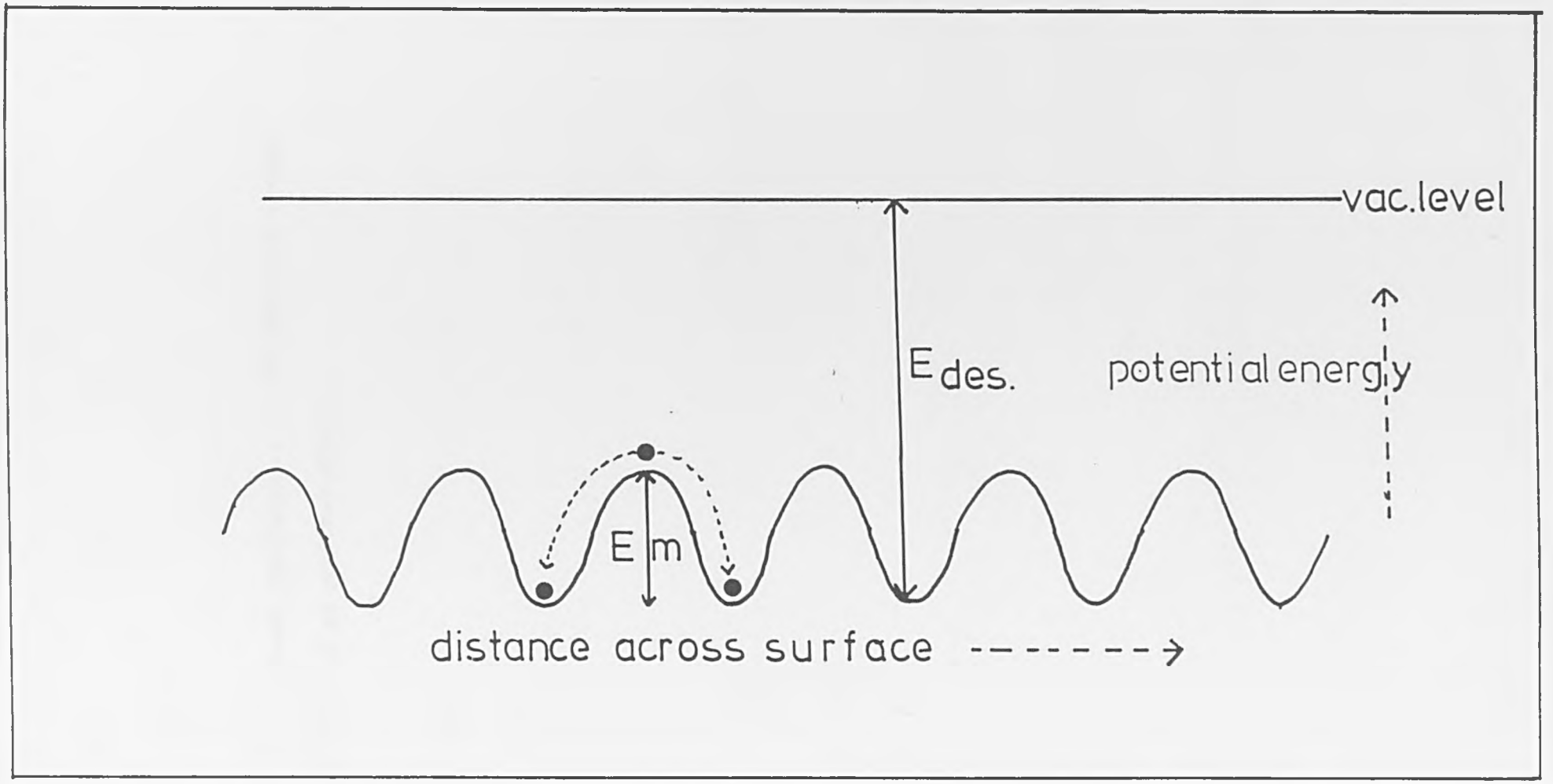
vac.level
E des.
potential energy
E m
distance across surface

FIG. 1.

Fig. 2. The effect of lateral interactions on the potential energy wells for the migration of an adsorbed adatom.

FIG. 2.

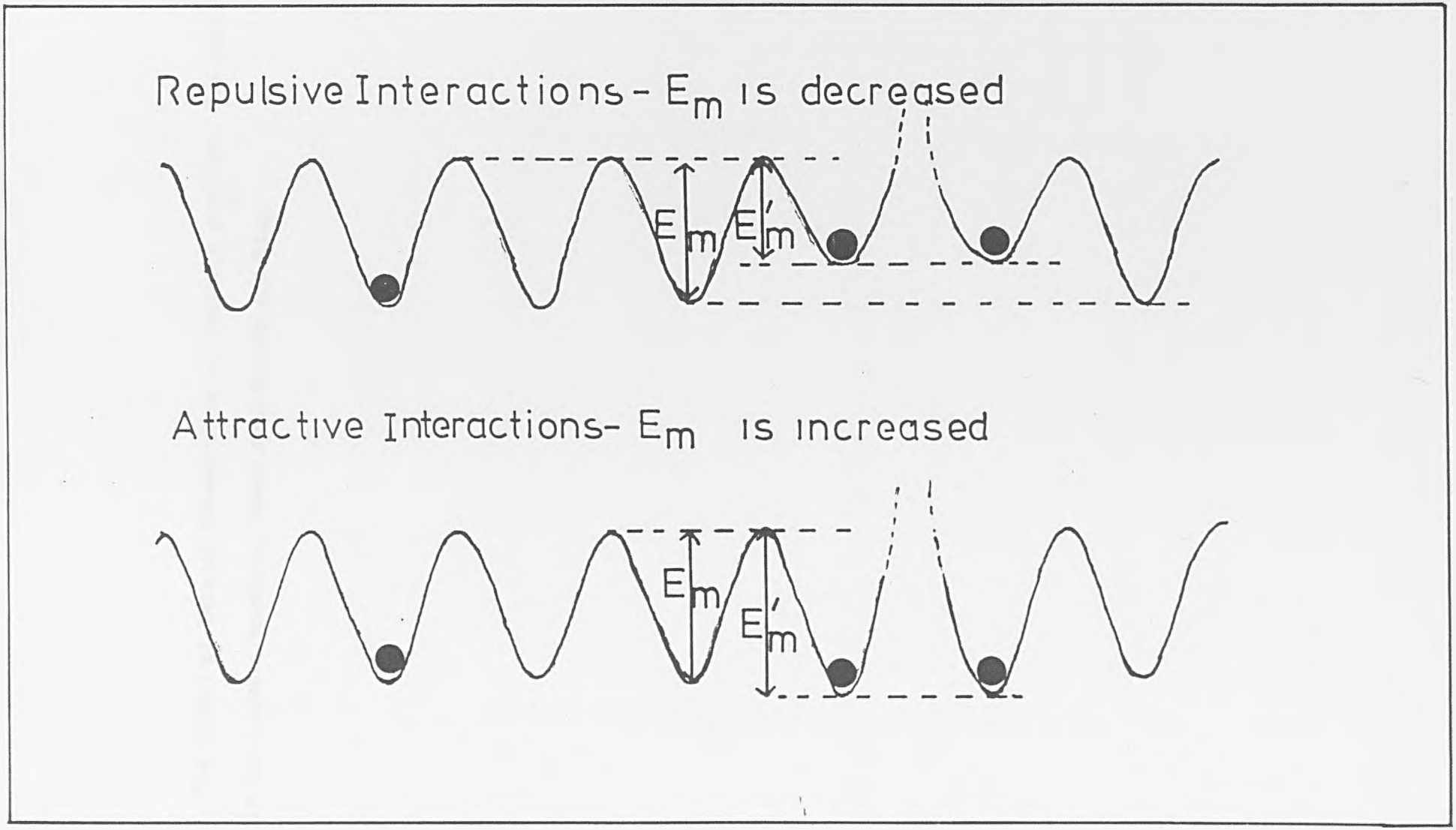
Repulsive Interactions- E_m is decreased
E_m
E'_m
Attractive Interactions- E_m is increased
E_m
E'_m

Fig.3. The effect of lateral interactions on coverage profiles. The initial profile was a square boundary. Taken from Bowker and King [51].

FIG.3.

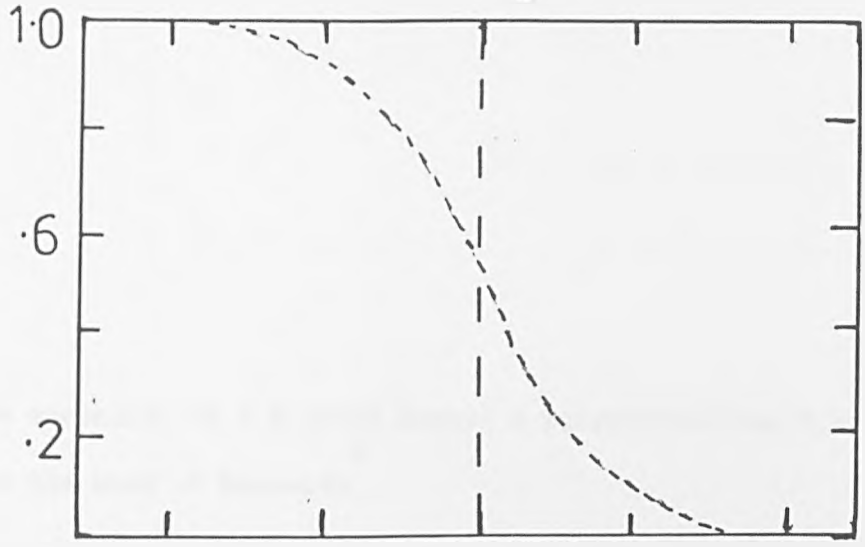

No Interactions - $\theta_c = 0.5$

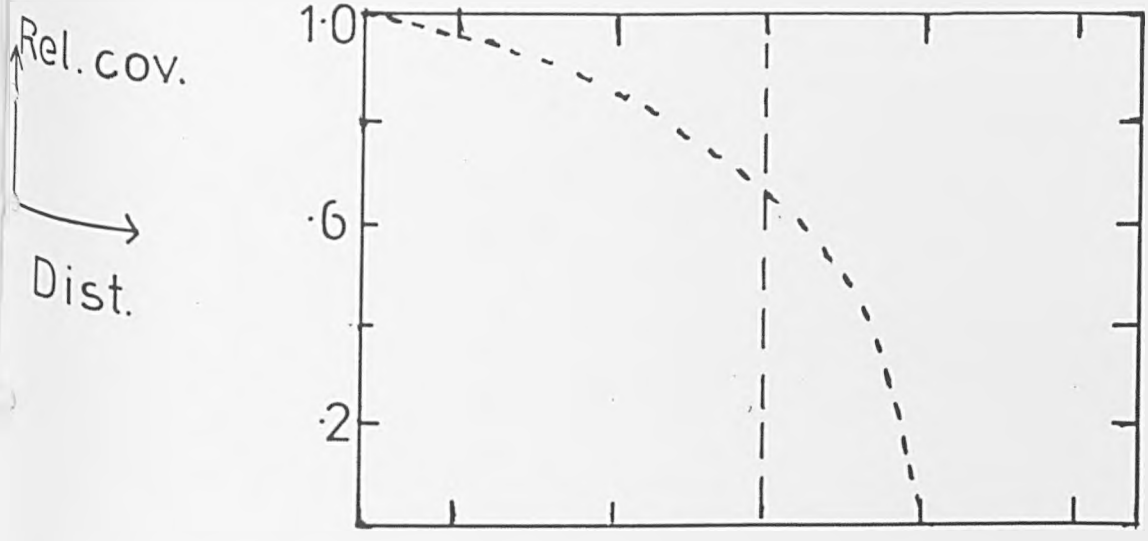

Repulsive Interactions - $\theta_c > 0.5$

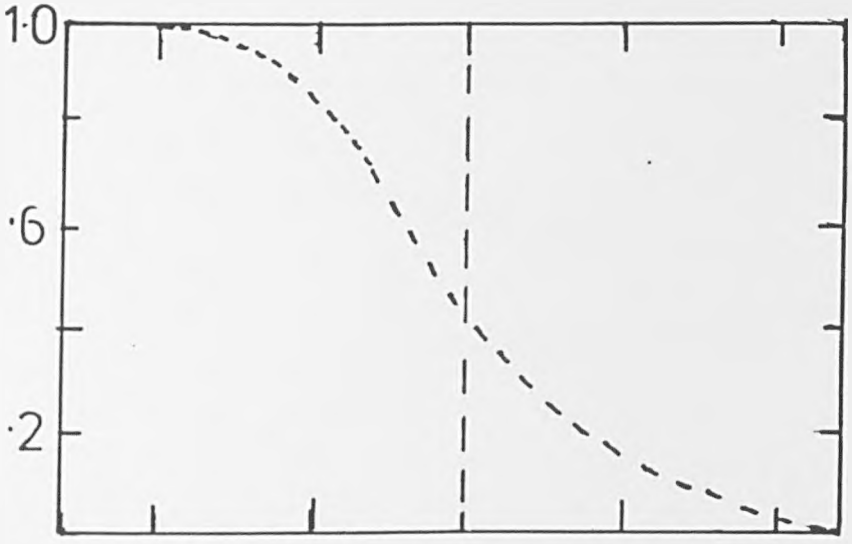

Attractive Interactions - $\theta_c < 0.5$

Fig.4. The spreading of a K patch across a polycrystalline W surface, taken from the work of Bosworth [6].

FIG. 4.

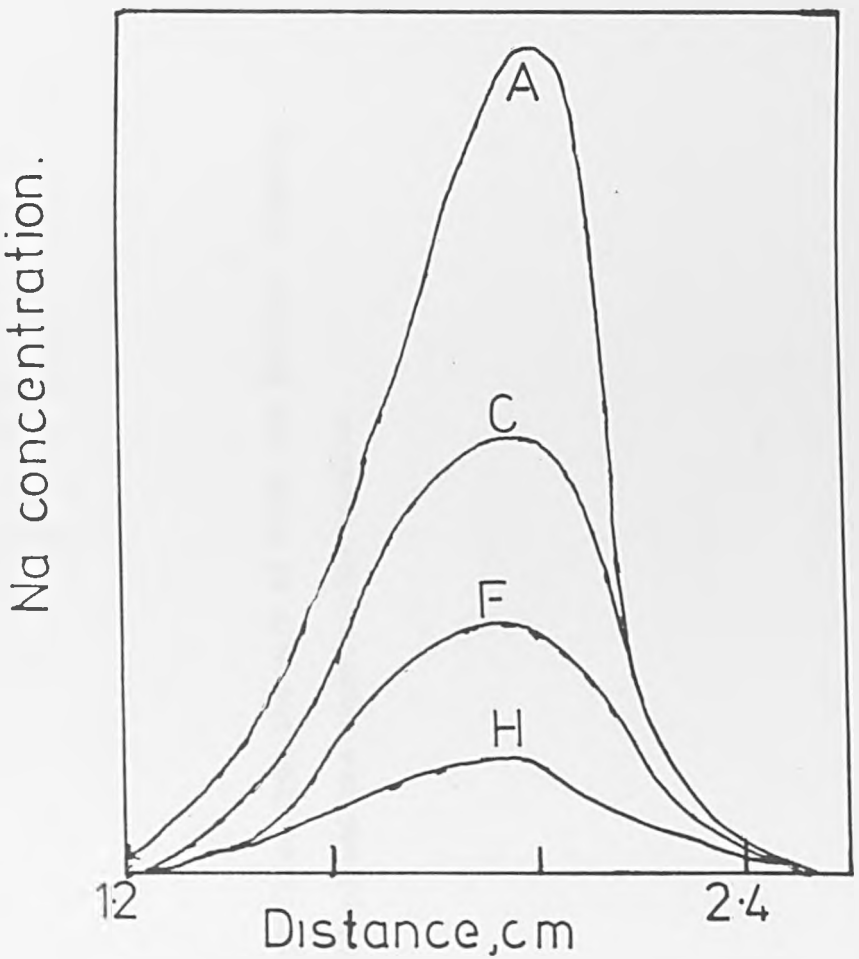

Na-W

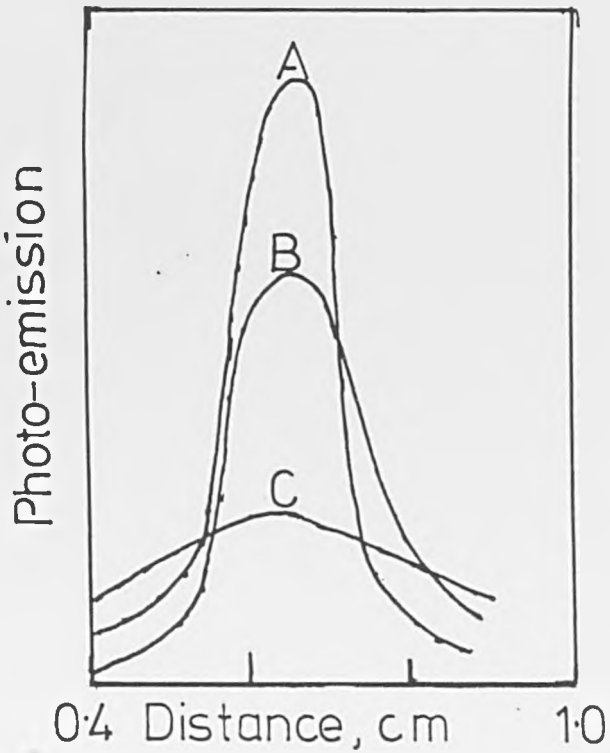

K-W

A = 5 mins at 295°K
B = 10 " " "
C = 20 " " "
F = 1 " " 415K
H = 11 " " "

Fig.5. Diffusion profiles from the work of Polak and Ehrlich[8] showing theoretical curves(top) and the experimental results.

FIG.5.

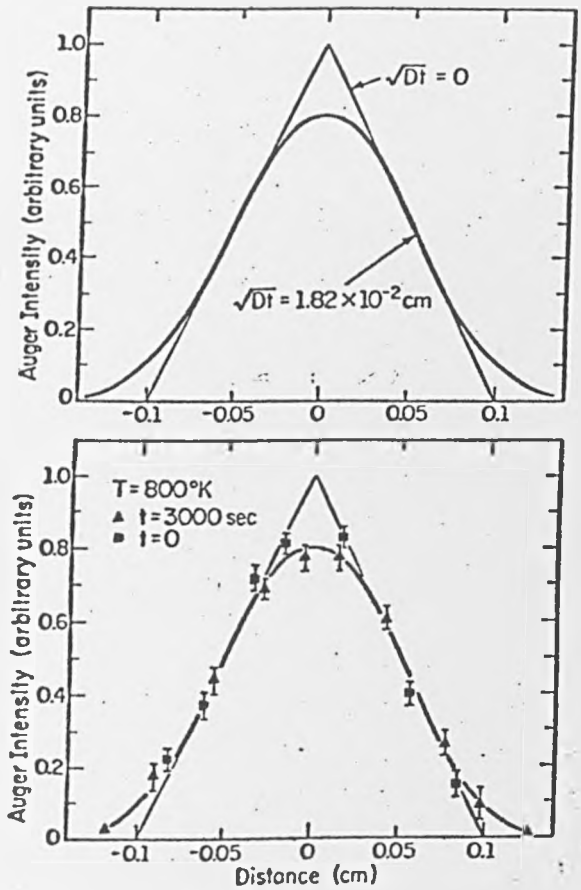
Auger Intensity (arbitrary units)
1.0
0.8
0.6
0.4
0.2
0
√Dt = 0
√Dt = 1.82×10⁻²cm
-0.1
-0.05
0
0.05
0.1
T = 800°K
▲ t = 3000 sec
■ t = 0
Distance (cm)

Fig.6.The variation of E_m and D_o versus coverage for O on W {110} .
Taken from the work of Chen and Gomer [60] .

FIG. 6.

Fig.7. Coverage versus distance plots for O on W{110} after heating an initial square boundary (at x = 0) for different times at 880°c. Taken from Butz and Wagner[13].

FIG. 7

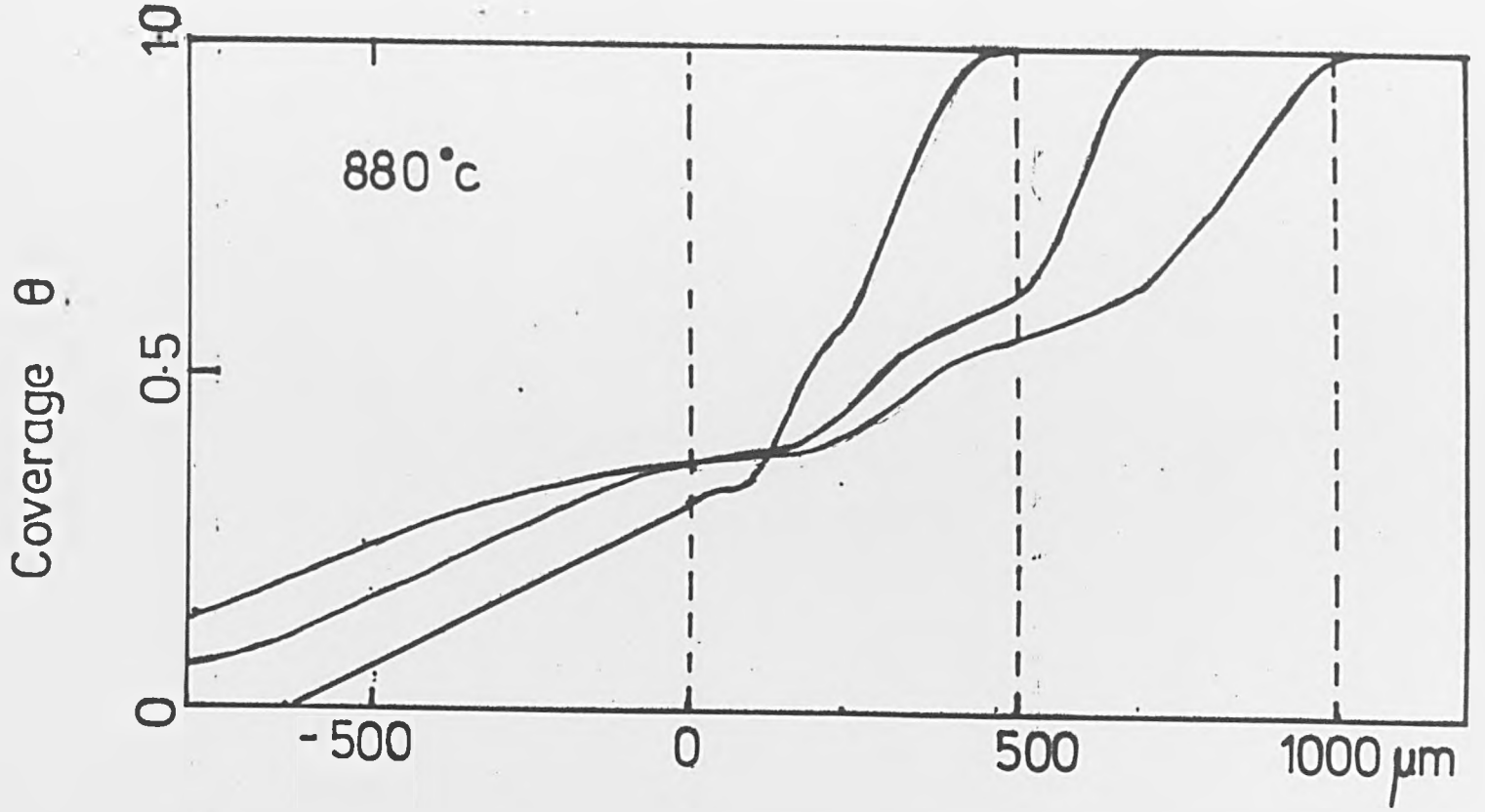

Fig.8. Variation of D versus coverage for two different temperatures, as measured by Butz and Wagner.[13]

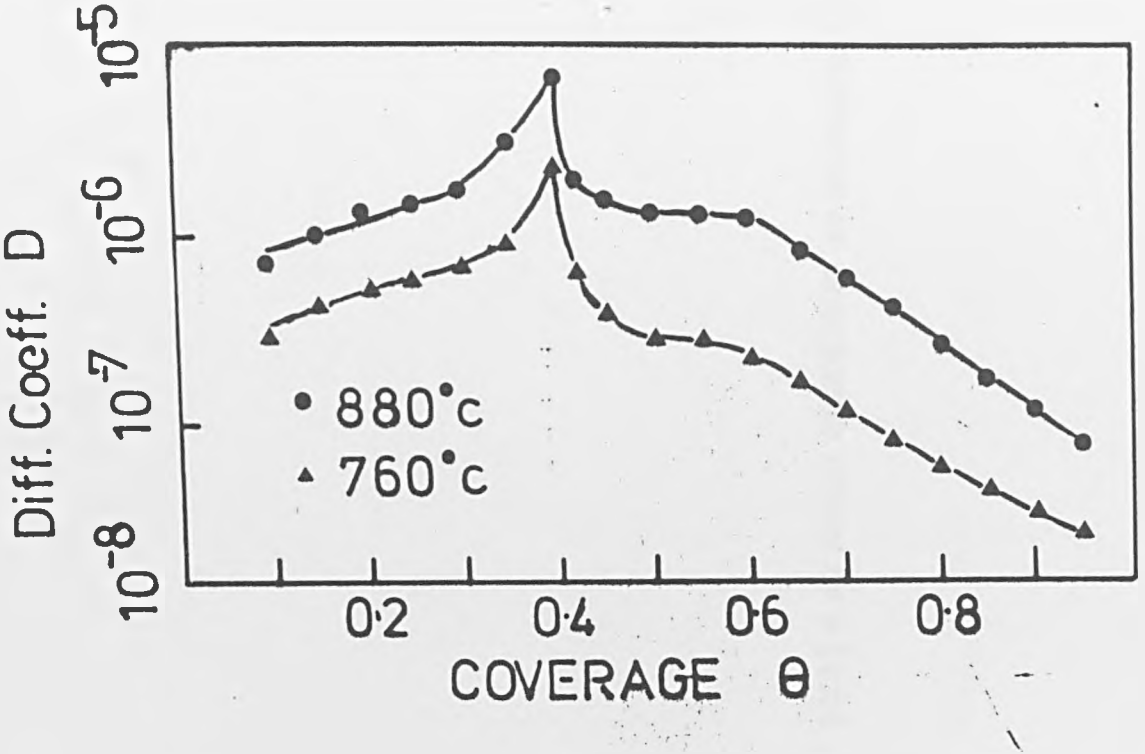

FIG. 8.

CHAPTER 4: SURFACE DIFFUSION OF CHEMISORBED OXYGEN ON W{110}.

Suface Diffusion of Chemisorbed Oxygen on W{110}.

M.A. Morris, C.J. Barnes and D.A. King.

The Donnan Laboratories, University of Liverpool, Liverpool L69 3BX.

I. Introduction.

Quantitative diffusion studies of adsorbed species on single crystal surfaces are relatively rare, although several promising techniques are now available[I-3]. On macroscopic single crystals(as distinct from field emitter tips) a recurring difficulty arises from competition between diffusion and other processes, particularly desorption, absorption and surface reconstruction, at the temperatures required to shift a diffusion boundary detectable distances. This is a major reason why oxygen on W{110} has become a favoured system: diffusion over distances of a mm in short times (~100 secs) occurs at ~1000K. Desorption occurs at temperatures in excess of 1800K, provided that the coverage does not exceed half a monolayer[9]. No oxygen incorporation has been observed under these conditions. Moreover, detailed structural studies of the O/W{110} system have been reported[4,5], the phase diagram determined[6], and lateral interaction energies have been estimated[4]. The relationship between the coverage dependence of diffusion coefficients and lateral interactions between diffusing species has been theoretically investigated[8]. The O/W{110} system provides an opportunity to test the conclusions from these studies. The object of the present work was to obtain more detailed results concerning the coverage dependence of the diffusion parameters for this system than previously obtained, and to re-examine the validity of results obtained using the field-emission flicker-noise techniques(or density fluctuation) for the same system.

During oxygen adsorption at 300K on W{110}, islands of a p(2x1) structure are formed at low coverage, covering the surface at a fractional coverage of $\theta = 0.5$ (relative to the density of W atoms in the surface)[9]. The domain structure which has been obtained[4] is shown in Fig.I. No reconstruction of the surface occurs up to 1700K[11]. The overlayer disordering temperature, T_c, is strongly dependent on coverage: at

$\theta < 0.35$, T = 450K corresponds to island dissolution; and at $\theta > 0.35$, T = 700K is an order-disorder transition.[6] Various estimates of lateral interactions have been made on the basis of these results. Pairwise interactions fail to explain the formation of a p(2×2) structure observed at $\theta = 0.75$, but not at $\theta = 0.25$, and for this reason 3-body (trio) interactions have been included.[10] Pairwise interactions are indicated in Fig.I., to which are added trio interactions between adatoms forming the smallest triangle. Good agreement has been obtained[7] with: $\omega_1 = 7 kJ\ mol^{-1}$; $\omega_2 = -5.4 kJ\ mol^{-1}$; $\omega_3 = 0$; $\omega_4 = 4.7 kJ\ mol^{-1}$; $\omega_5 = 2.3 kJ\ mol^{-1}$. Theoretical calculations provide support for the importance of trio interactions.

2. Experimental.

The uhv chamber, pumped by a combination of ion and liquid-nitrogen-cooled titanium-sublimation pumps and routinely producing pressures in the low 10^{-11} torr range, has been previously described.[12] It is equipped with Varian four-grid LEED/AES optics, with a Faraday cup, and a quadrupole mass spectrometer, and a calibrated directional source of gas. The retarding field analyser was used to monitor oxygen coverages by AES, and diffusion profiles were measured by scanning the crystal across the electron beam, using accurate micrometer gauges on the manipulator. In this way diffusion distances were absolutely calibrated and the incidence beam and analyser conditions were maintained constant. The mounting of the W{110} crystal, via W wires passed through spark-drilled holes in the sample, is as described previously for a W{100}[12] crystal. Crystal heating and control was achieved by resistive heating of the support wires for temperatures up to 700K, for temperatures above this electron bombardment was used. Temperatures were measured with a

W-Re 3% / W-Re 25% thermocouple housed in a spark-drilled pit in the crystal edge. The crystal was cut and polished to within $\frac{1}{2}^{o}$ of W{110} and has the dimensions 5x5x1.5 mm. The crystal was cleaned in situ by repeated heat treatment in high fluxes of oxygen to about 1800K, with the occasional flash up to 2500K. All traces of carbon were removed.

A localised patch of adsorbed oxygen was formed on the W{110} sample using the directional oxygen beam and shielding shown in Fig.2. A small diameter hole, of measured length (0.685mm) and diameter (0.55mm) acts as a source for a directional flux of gas at the crystal which can be calculated for a given pressure behind the source. The shield, S, can be interposed between the source and the sample, either to cut of the gas supply to the crystal completely (useful in absolute sticking probability measurements) or, by aligning one of the slots in the shield with the crystal, to deposit an appropriate adsorbate patch on the crystal. The slots were cut in two orthogonal directions so that directional effects in diffusion could be studied. The boundary produced by oxygen adsorption on W{110} at 300K, with a source to crystal distance of 5 cm, determined by scanning the crystal across the $\langle 1\bar{1}0 \rangle$ direction in front of the electron beam, is shown in Fig.3. A good step function is produced, an essential prerequisite for detailed studies of diffusive coverage profiles.

3. Absolute Sticking Probability, Surface Coverage and LEED Intensities.

The directional flux oxygen source provides a convenient and accurate means of measuring the absolute sticking probability and surface coverage. During dosing the randomised flux of oxygen in the uhv chamber is measured with a mass spectrometer, giving a pressure P, with the crystal out of the gas beam, and a smaller pressure P' with the crystal in the beam. The sticking probability, s, is then simply:

$$s = \frac{I}{f} \frac{(P-P')}{P}$$

where f is the fraction of the flux leaving the source which is intercepted by the crystal. From the absolute intensity of the flux at the sample, the coverage, N, is obtained from,

$$N = \int_0^t Q \, . \, s \, dt.$$

The variation of s with N for oxygen adsorption on the W{110} sample used for the remainder of this work is shown in Fig.4. With the crystal at 300K the zero coverage sticking probability is 0.41(±0.015); s is almost independent of coverage up to 6.5×10^{14} atoms cm^{-2}, and then decreases quite precipitously towards zero at 7.5×10^{14} atoms cm^{-2}, corresponding very closely to half a monolayer defined in terms of the density of surface W atoms (14.7×10^{14} atoms cm^{-2}); superimposed on this figure is the observed variation in intensity of the $(\frac{1}{2},0)$ LEED beam from the p(2×1) structure at a primary beam energy of 65eV, the $(\frac{1}{2},\frac{1}{2})$ from the p(2×2) at 96eV, and the (1,0) integral order beam at 72eV, corresponding to the (1×1) structure. Above the half monolayer position, coverages were estimated from AES peak-to-peak height, calibrated at θ = 0.5. The maximum intensity of the p(2×1) structure occurs at θ = 0.5, of the p(2×2) structure at θ = 0.75; and the (1×1) at θ = 1. The initial sticking probability, functional dependence of s on N, and maximum intensity in p(2×1) beams are all in agreement with the literature. 4-7,9,13.

We note here that we obtained very different results from another W{110} face, also cut to within $\frac{1}{2}^{o}$, and cleaned and polished to give good Auger spectra and LEED pattern. The initial sticking probability was 0.62 (±0.015); and the coverage at the maximum intensity from the p(2×1) LEED beams, where s falls rapidly, was found to be 13×10^{14} atoms cm^{-2}. We have no explanation for the behaviour of this particular crystal face, which was regarded as anomalous by comparison with the literature, and hence discarded. The most likely explanation is the presence of a high density of defect sites, although we could find no evidence of these.

The sensitivity of oxygen to such effects may explain discrepancies previously observed in the literature for this system particulary in electron stimulated desorption studies.[14] No anomaly was found for CO adsorption on the same face: the initial sticking probability (0.88) and saturation coverage (11.5×10^{14} molecules cm^{-2}) at 300K agree well with the literature.[15]

4. Surface Diffusion.

A typical set of results showing the spread of boundary profiles as a function of time, at 1063K, is shown in Fig.5. The initial boundary is a $\theta = 0.5/\theta = 0$ step, which is readily obtained because of the sharp fall in s at $\theta = 0.5$. To obtain data at higher coverages, much higher beam fluxes were employed; under this condition the background pressure in the uhv chamber was sufficiently high to produce a coverage of $\theta = 0.5$ on the shielded part of the crystal. $\theta = 0.75/\ \theta = 0.5$ steps could be produced in this way, and a set of data at temperatures between 990K and 1313K are shown in Fig.6. Higher coverages could not be achieved without losing the sharp edge at the adsorption temperature. Care was taken that during the diffusion step effects were unimportant.

Diffusion profiles of this sort can be readily analysed to yield the diffusion parameters. Diffusion is governed by the equation,

$$\frac{\partial N}{\partial t} = \frac{\partial}{\partial x} D_{(N)} \frac{\partial N}{\partial x}$$

where N is the coverage, t the heating time and x the distance moved at the coverage N. $D_{(N)}$ is the coverage dependent diffusion coefficient. If the diffusion process is of the random walk type, it can be shown,

$$x = (Dt)^{\frac{1}{2}}.$$

Thus curves taken as a function of heating time can be treated to yield a single curve at one constant temperature. An example of this is shown in Fig.7. for T = 1063K and illustrates the quality of the data. The

diffusion process is an activated process described by the equation,

$$D_{(\omega)} = D_{o(\omega)} \exp\ (-E_\omega / RT)$$

where D_o is the preexponential of the process and E_ω is a coverage dependent activation energy. For boundaries that are initially perfectly square before diffusion takes place , D can be calculated at any coverage from the equation, [16]

$$D = \frac{-I}{2t} \frac{dx}{dN} \int_{N_1}^{N_o} x\,dN \quad .$$

The initial boundary is at position $x = 0$ between two coverages N_1 and N_o; N is the coverage at any point between these two values. Note that N_o is the coverage at $t = 0$ and $x > 0$ and that N_1 is the coverage at $t = 0$ and $x < 0$. This analysis has the important boundary condition,

$$\int_{N_1}^{N_o} x\,dN = 0 \ .$$

This equation is very important, it states that any material lost from the high coverage side of the boundary must equal the material gained at the low coverage side. A similar analysis for this system has been reported in the literature but this boundary condition is clearly not met [17] ; in the present work this was always found to be true.

Using this analysis plots of D versus coverage can be drawn up and examples of these are shown in Fig.8. The logarithmic values of D at a particular coverage for various temperatures, is used to find the activation energy and the preexponential for diffusion, utilising an Arrhenius type plot. Fig. 9 shows these plots, and the E_ω and D_o values extracted from these are shown in table I.

5. Discussion of the Surface Diffusion results.

It can be seen that the activation energy increases strongly with coverage, in agreement with the results obtained by Chen and Gomer [18] .

The value of the activation energy for diffusion agrees well with the high coverage results presented by previous authors; 123 ± 10 kJ mol^{-1} here, 113 kJ mol^{-1} measured by Butz and Wagner[17], and 101 kJ mol^{-1} as determined by Bowker and King[19]. The value of the preexponential is also of the same order of magnitude as reported by these authors.

The variation of E_m and D_o are shown in Fig.10., also shown are the values obtained by Chen and Gomer[18] for comparison. The variation in E_m noticed by these authors has been confirmed here; other authors have been unable to confirm the results because of experimental difficulties, and these have been overcome in the present work. The variation of E_m has been attributed to the presence of lateral interactions between the adatoms[1]. The E_m graph shown can be extrapolated to zero coverage yielding a value of 63 kJ mol^{-1}, in very good agreement with the value of 56 kJ mol^{-1} as found by Chen and Gomer[18]. This value of the activation energy is associated with the diffusion of a single isolated adatom, one that does not feel any lateral interactions with another adatom. The increase in E_m for Chen and Gomers results has been explained[1] using the phase diagram for the system. For $\theta < 0.35$ the island dissolution temperature is 450K and at the temperatures were the experiments were carried out (above this) the adatoms should be randomly distributed and have the isolated adatom diffusion energy. For $\theta > 0.35$ the transition becomes an order-disorder transition at $T = 700$K above the diffusion temperatures used by Chen and Gomer; hence the increase in E_m is due to the attractive interactions between molecules in a $p(2 \times 1)$ island. The results presented here, since all experiments were carried out above 700K, would seem to indicate that there is enough short range order between the adatoms to make a contribution to the diffusion energy. This contribution

may be expected to increase as the coverage increases and so produce the variation of E_m observed here. If we write the difference in energy between the two regimes, we can equate this to the interaction energy between the adatoms, i.e.,

$$E_m^{2x1} - E^i = 2(\omega_1 + \omega_2) .$$

Using the values of E_m^{2x1} and E^i found here, $(\omega_1 + \omega_2) = 11.7$ kJ mol^{-1}, in good agreement with the interaction energies reported by W.Y.Ching et al.[7] Butz and Wagner[17] report that they see no evidence in their activation energy plots for an increasing value for E_m. However, if their high coverage boundaries are examined(a step profile between $\theta = 1$ and $\theta = 0.5$) it can be seen that at the $x = 0$ position the crossover of the diffused boundary is below $\theta = 0.75$. It has been shown[20] that this is indicative of attractive interactions between the adatoms. The crossover of the low coverage boundaries does not show a similar effect, presumably then, we would expect the sort of variation in E_m noted here; this is explicitly shown when the coverage profiles are examined, Figs.5 &6, which show exactly the same effects.

The variation of D_o shown in Fig.10. is not as easily explained. A strong variation of D_o was also found by Chen and Gomer[18]; it seems likely that these results are almost certainly incorrect. The absolute values reported by these authors are a factor of 10^4 too low. This difference is ascribed to the fact that the field emission fluctuation technique used by these authors leads to D_o values which are likely to be misleading[21]. Bowker and King[19] and Butz and Wagner[17] report similar effects of the same order of magnitude but at different coverages. It can be shown that,

$$D_o = \frac{\nu a^2}{4} \exp(\Delta S_m/k)$$

where ν is the vibrational frequency of an adatom, and a the mean square

jump distance. ΔS_m is the entropy change associated with surmounting the energy barrier. We can only surmise that the diffusion process occurs through a number of different routes, possibly as clusters and individual adatoms.

Butz and Wagner[17] and Chen and Gomer[18] both report a large peak in the diffusion coefficient as a function of coverage. Fig. 8 shows that the same effect has been noticed in the present work. Using a Monte-Carlo analysis Bowker and King[8] have shown that this is due to the presence of attractive next-nearest-neighbour as well as repulsive nearest-neighbour lateral interactions on the surface. and should produce a peak in D at $\theta = 0.5$. The previous work shows that the peak is below this coverage. However this may not be so; Froitzheim et al[22] have proposed that the saturation coverage for this system is greater than one, this would ensure that the results of Butz and Wagner were shifted to higher coverage. In the present work (unlike Butz and Wagner) we are able to measure absolute surface coverages and so have confidence in our values. It can be seen that the peak reported here is slightly above the half coverage position; a recent theoretical study[23] supports this. The theory again models the surface with the lateral interactions discussed earlier.

5. The Directional Effect in Surface Diffusion of O on W {110} .

The results above refer to a boundary moving in the $\langle 1\bar{1}0 \rangle$ direction. Results were also obtained by depositing the boundary 90 degrees to the one used above and scanning in the $\langle 001 \rangle$ direction. No differences were observed, as illustrated in Fig. 11 where an activation energy plot at a coverage of 4×10^{14} atoms cm^{-2} for both directions is shown; the agreement is very good indicating that diffusion is isotropic for this system. Presumably the agreement of E_m values recorded by other authors is because of this property.

6. Conclusions.

a) The diffusion of O on W {110} is dominated by the interactions between the adsorbed adatoms. These lateral interactions are the same ones that result in the complex phase diagram for the system. The dominant interaction is the next-nearest-neighbour attractive interaction which cause the activation energy for surface diffusion to increase as the coverage increases.

b) All the effects predicted for a system where attractive next-nearest-neighbour interactions are important, are observed in the same study. These are I) An increasing activation energy for diffusion as the coverage increases.

II)A strong increase of the diffusion coefficient near the half coverage position.

III) The point where a diffusing boundary passes through the initial boundary position occurs below the half coverage position.

c) The magnitude of E_m and D_o measured here agree well with previous work. It seems likely that D_o measurements using the flicker noise field emission technique are misleading. The agreement between the measurements would seem to indicate that the large number of defect sites (although a small percentage of the total number of sites) present on any bulk single crystal, have no, or a very small, effect on the measured values.

d- There is evidence that the attractive lateral interactions between the adatoms are still felt by the adatoms when the p(2×1) islands are disordered by LEED.

e) Diffusion is isotropic on the W {110} face.

REFERENCES.

I. D.A. King, J.Vac.Sci.Tech., I7(I980)24I.

2. G. Ehrlich, C.R.C.Crit.Reviews in Solid State and Material Sciences, I0(I982)39I.

3. M.A. Morris, M.Bowker and D.A.King, The Kinetics of Adsorption, Desorption and Migration at Single Crystal Metal Surfaces, in Comprehensive Chemical Kinetics, eds. C.H.F.Tipper and C.Bamford, Elsevier.

4. M.G. Lagally, J.C.Bucholz and G.C. Wang, J.Vac.Sci.Tech.,I2(I975)2I3.

5. M.A. Van Hove and S.Y. Tong, Phys.Rev.Letts., 35(I975)I092.

6. T.M. Lu, G.C. Wang and M.G. Lagally, Surf. Sci.,92(I980)I33.

7. W.Y. Ching, D.L. Huber, M.G.Lagally, and G.C. Wang, Surf.Sci., 77(I975)550.

8. M. Bowker and D.A. King, Surf.Sci.,72(I978)208, 7I(I978)583.

9. T. Engel, H.Niehus and E.Bauer, Surf.Sci.,52(I975)237.

I0. T.L. Einstein,Surf. Sci.,84(I978)L497.

II. E. Bauer and T. Engel, Surf.Sci., 7I(I978)695.

I2. M.K.Debe and D.A.King, Surf.Sci., 8I(I979)I93.

I3. T.E. Madey, Surf.Sci.,94(I980)483.

I4. S-l. Weng, Phys. Rev.B.,28(I98I)I699.

I5. C.Kohrt and R.Gomer, Surf.Sci,40(I973)7I.

I6. C. Matano, Jap.J.App.Phys.,8(I933)I09.

I7. R. Butz and H.Wagner, Surf.Sci.,63(I977)448.

I8. J.R. Chen and R. Gomer, Surf.Sci.,79(I979)4I3.

I9. M. Bowker and D.A. King, Surf.Sci.,94(I980)564.

20. M.Bowker and D.A. King, Surf.Sci.,53(I978)583.

2I. J. Beben, Ch. Kleint and R.Meclewski, Surf.Sci.,93(I980)33.

22. H. Froitzheim, H. Ibach and S. Lehwald, Phys.Rev.B.,I4(I976)I362.

23. M. Asada and M. Masuda, Surf.Sci.,99(I980)L429.

TABLE I.

COVERAGE atoms $cm^{-2} \times 10^{14}$.	E_{m-1} $kJ\ mol^{-1}$.	D_{o-1} $cm^{2}\ s^{-1}$.
2	76.6 ± 5	0.019 ± 30%
4	89.5	0.10
6	100.5	0.05
7.5	111.4	0.019
8.5	117.8	0.40
9.5	123.1	0.63.

Fig.I. Domain Structure for $p(2\times 1)$-O islands on W{ 110} .

Also shown are the two-body lateral interactions that exist between the adatoms.

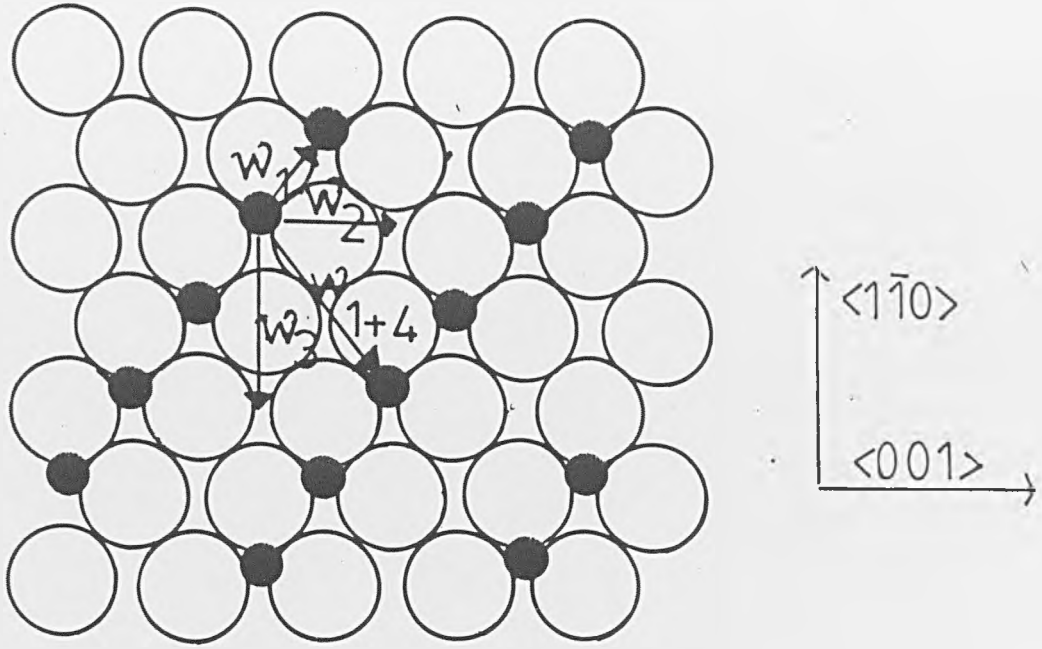
w2
w2
w2
w2
1+4
<1$\bar{1}$0>
<001>

Fig.2. Schematic illustrating how adsorbate boundaries were deposited on the crystal.

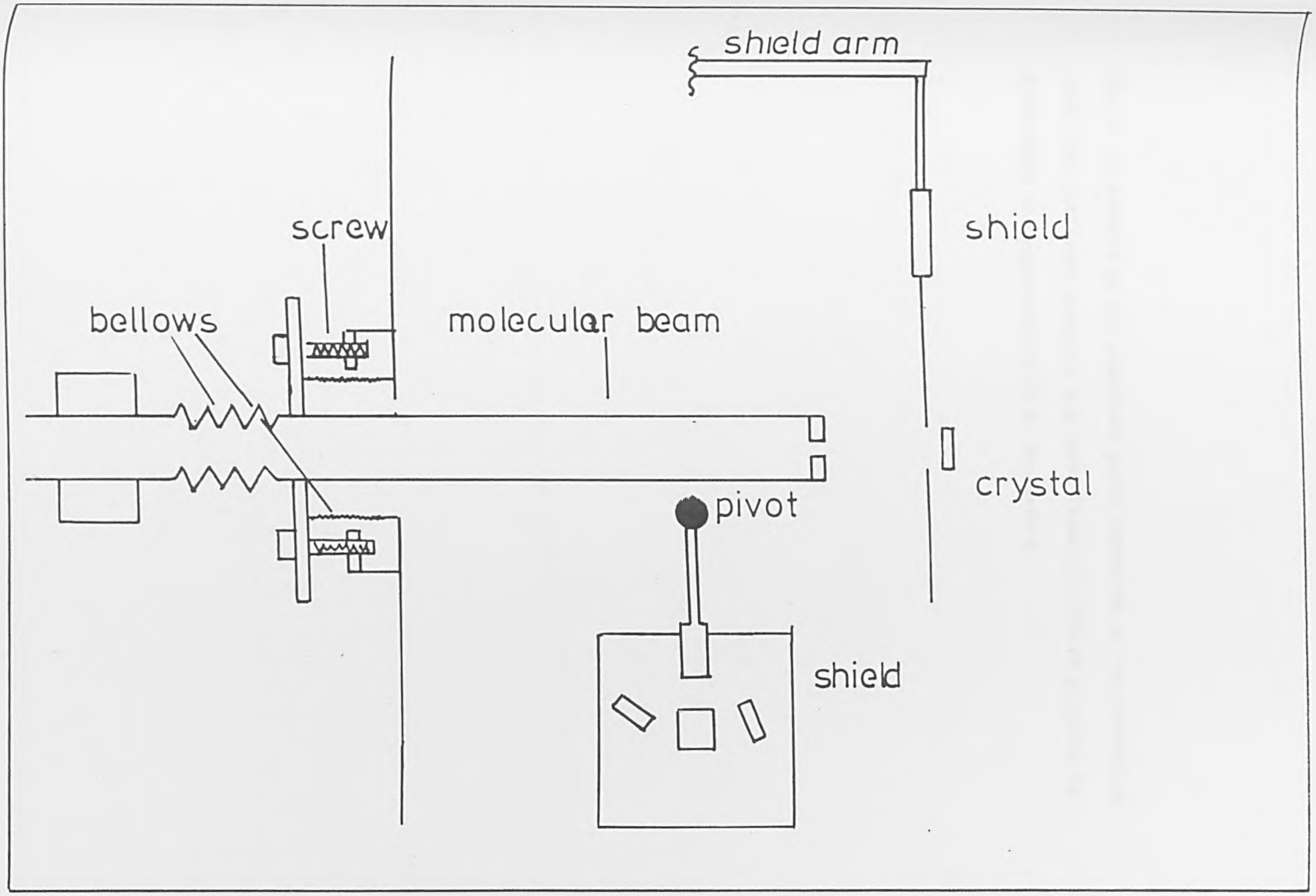
shield arm
screw
shield
bellows
molecular beam
crystal
pivot
shield

Fig.3. An example of the adsorbate patch deposited on the crystal at 300K. Two different examples are shown (open and filled circles) to illustrate the reproducibility of the method.

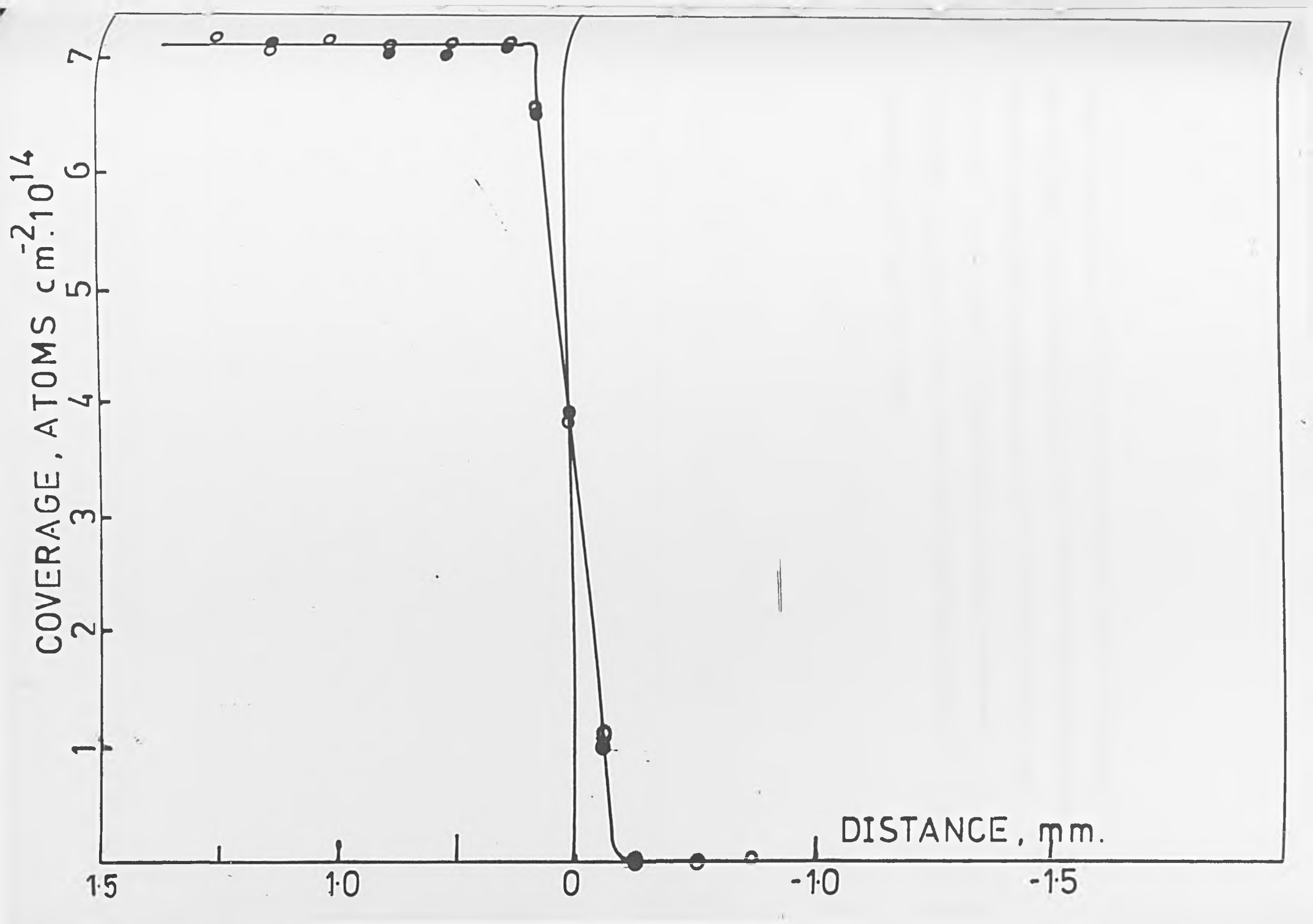
COVERAGE, ATOMS cm^{-2}.10^{14}
7
6
5
4
3
2
1
DISTANCE, mm.
1·5
1·0
0
-1·0
-1·5

Fig.4. Sticking Probability and Leed intensity as a function of coverage for O/W $\{110\}$. Half filled circles and the LEED data refer to adsorption onto the crystal used in these experiments. The half filled circles are data from a second crystal. Open squares are intensity measurements of a (1,0) LEED beam (72eV); filled squares from a $(\frac{1}{2},0)$ beam (65eV); and half filled from the $(\frac{1}{2},\frac{1}{2})$ beam (96eV).

STICKING PROBABILITY
S →
1·0
·9
·8
·7
·6
·5
·4
·3
·2
·1
O2 (b)
O2 (a)
2
4
6
10
12
COVERAGE, PARTICLES cm-2. 10^14

Fig.5. The spreading of an adsorbate boundary, a $\theta = 0.5$ / $\theta = 0$ step, as a function of time at 1063K.

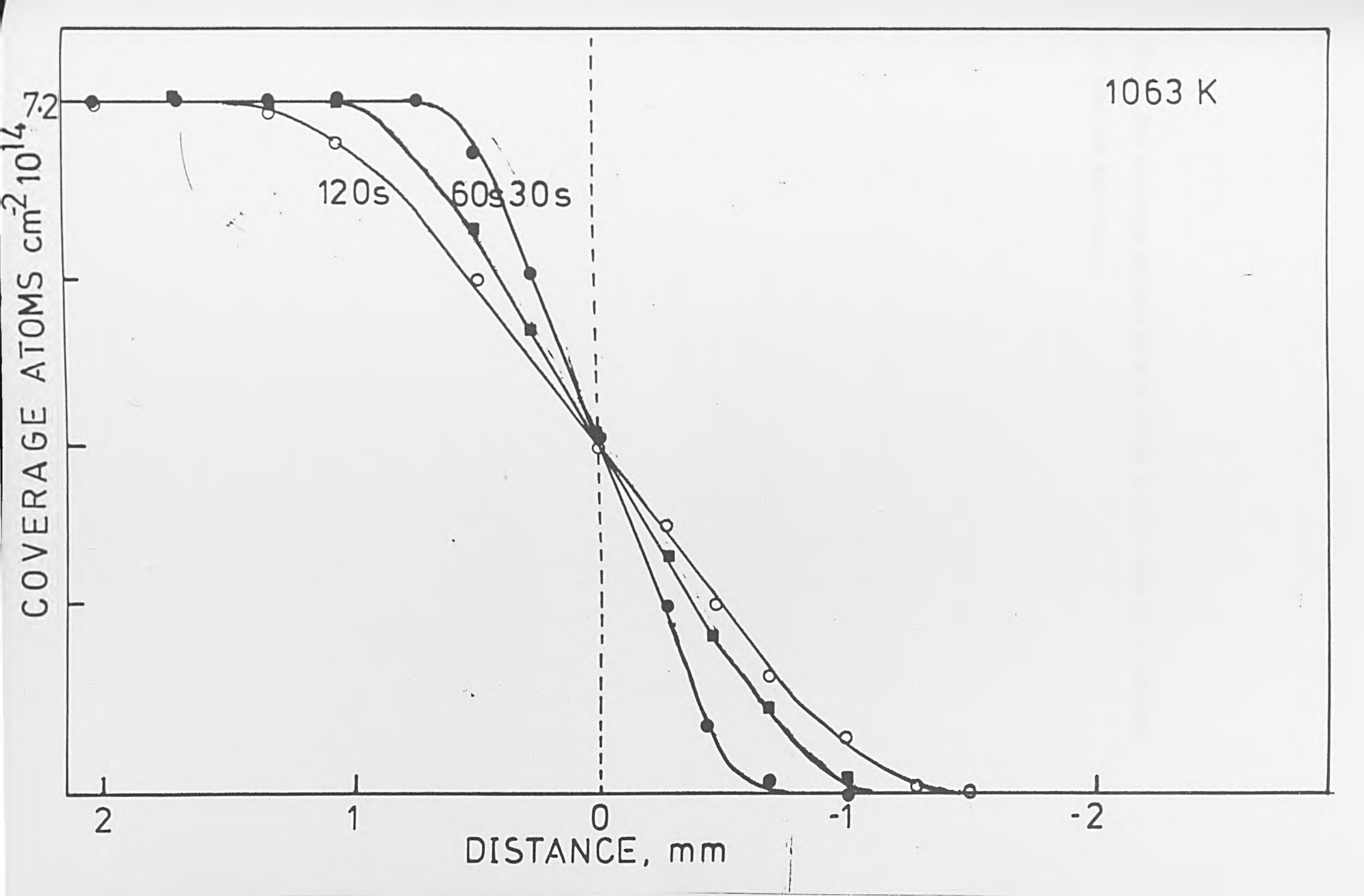
1063 K
7·2
COVERAGE ATOMS cm^{-2} 10^{14}
120s
60s
30s
2
1
0
-1
-2
DISTANCE, mm

Fig.6. The spreading profile of a $\theta = 0.75 / \theta = 0.5$ step as a function of time and temperature.

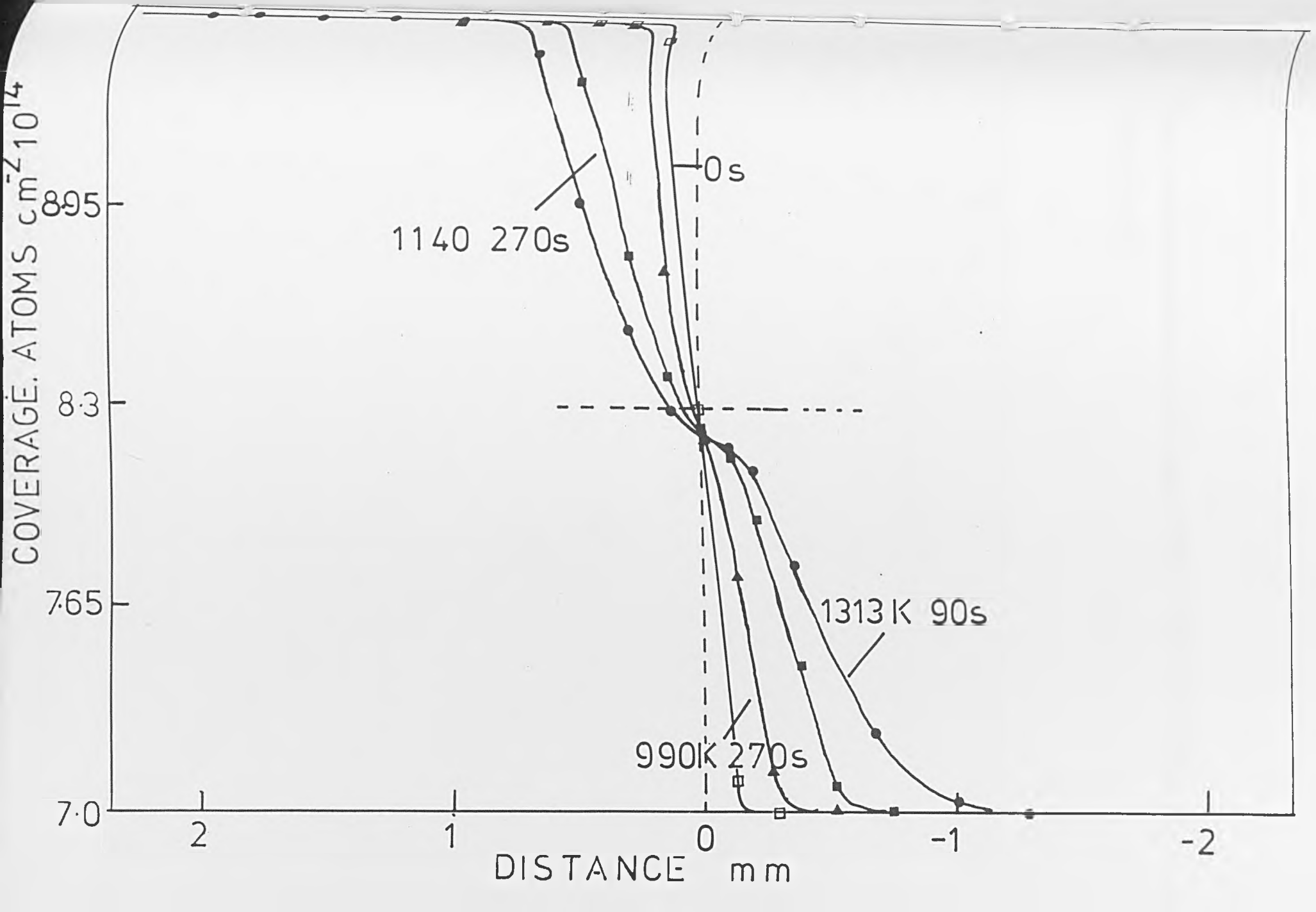
COVERAGE. ATOMS cm⁻² 10¹⁴
8·95
8·3
7·65
7·0
2
1
0
-1
-2
DISTANCE mm
0s
1140 270s
1313 K 90s
990K 270s

Fig.7. A time reduced plot of the data in Fig.5. (Obtained by making the x-axis dimensionless.)

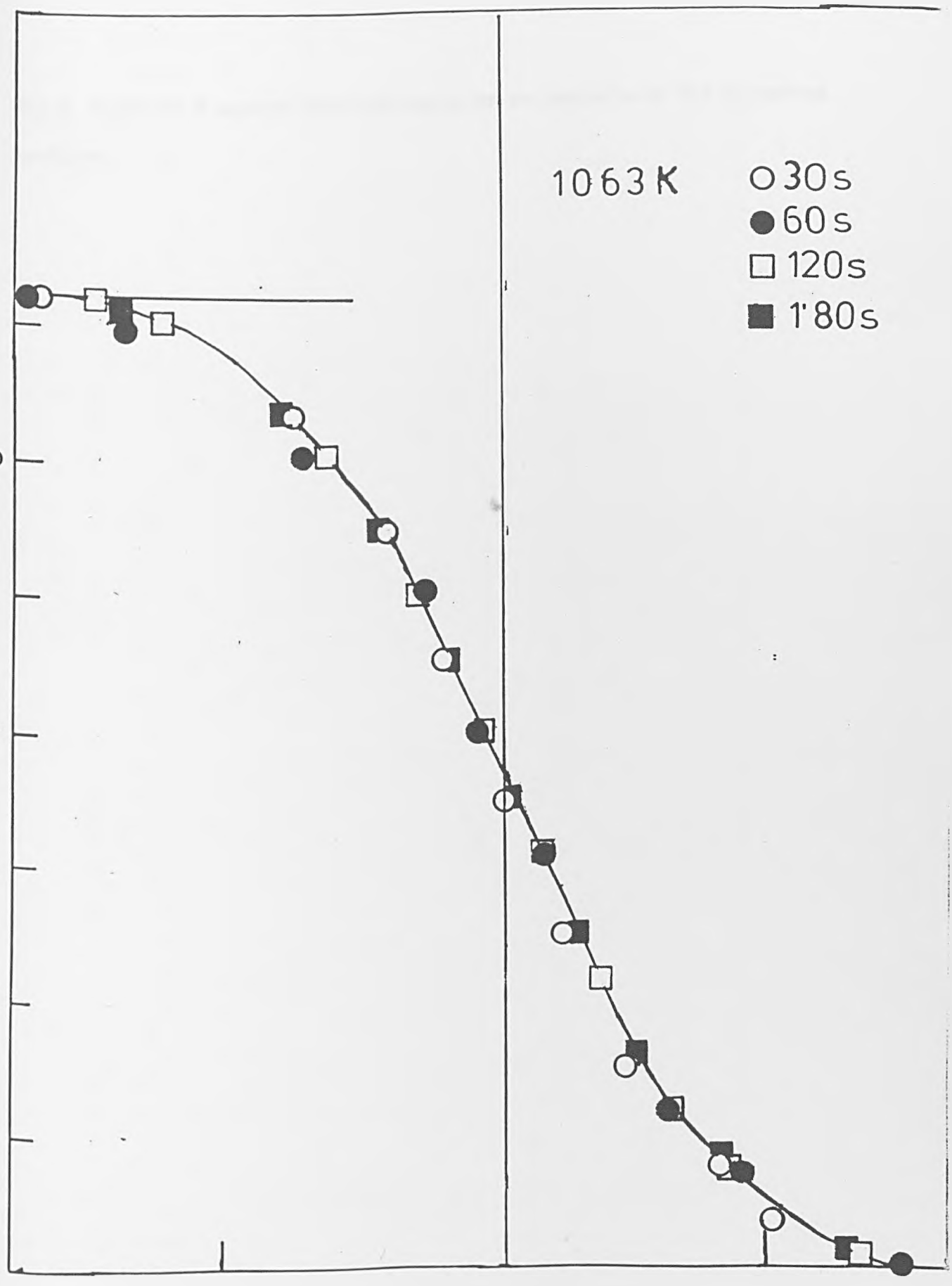
1063 K
30s
60s
120s
1'80s
COVERAGE, ATOMS cm⁻² 10¹⁴
2
4
6
Δx²/t , ARB. UNITS.

Fig.8. Plots of D against coverage based on an analysis of the spreading profiles.

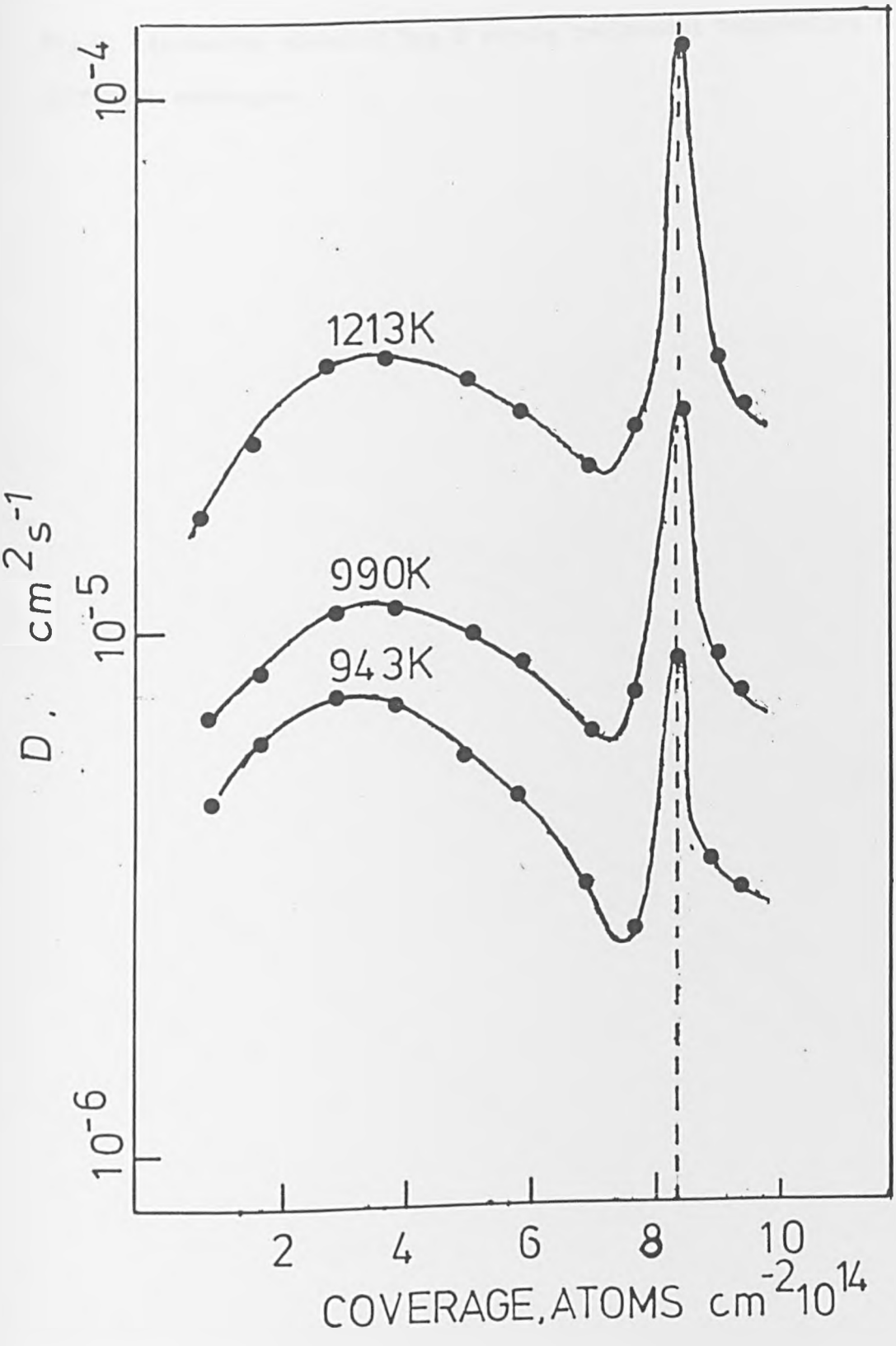
1213K
990K
943K
10^{-4}
10^{-5}
10^{-6}
D, $cm^2 s^{-1}$
2
4
6
8
10
COVERAGE, ATOMS $cm^{-2} 10^{14}$

Fig.9. Arrhenius plots of Log D versus reciprocal temperature for different coverages.

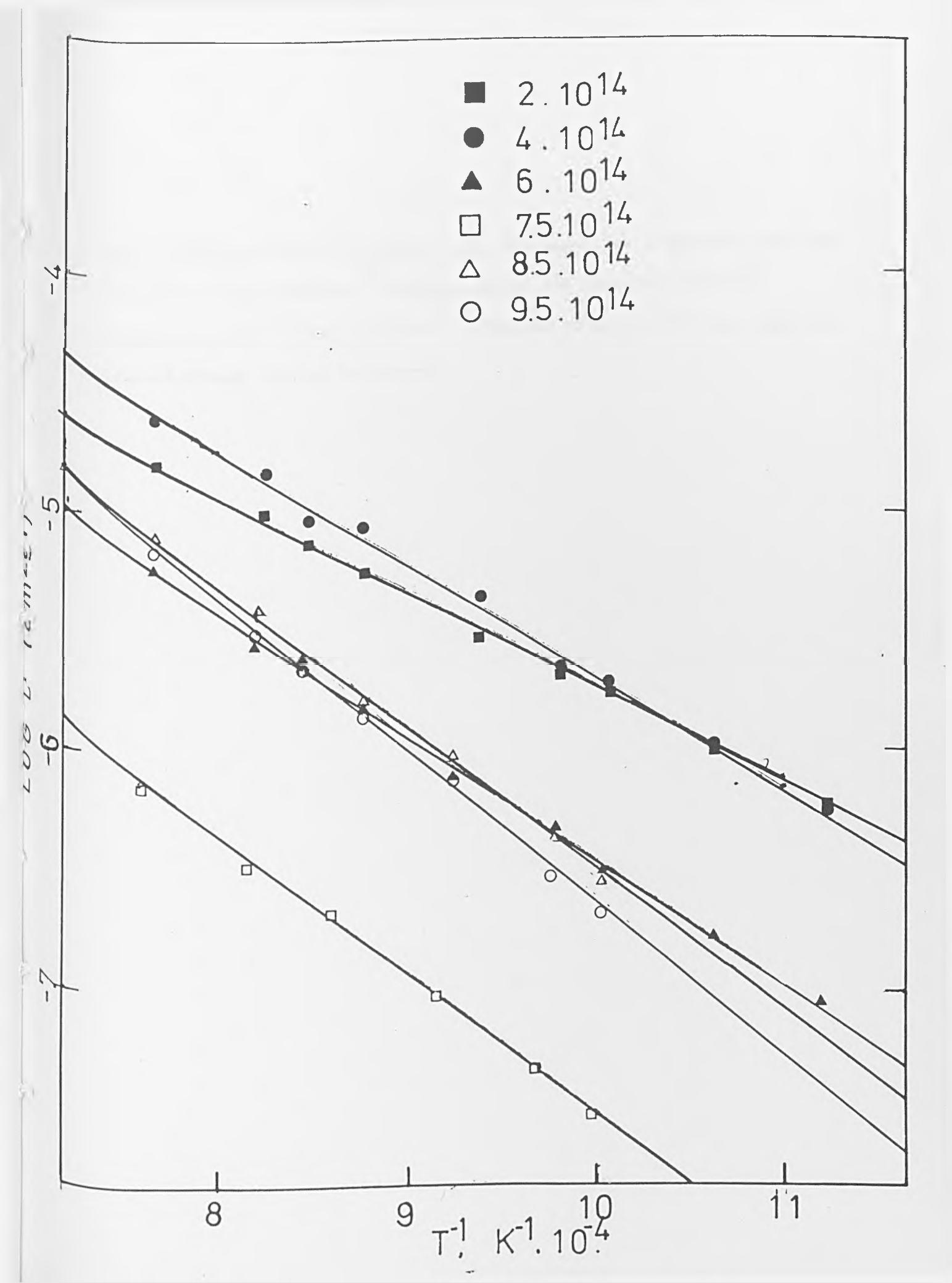
2 . 10^14
4 . 10^14
6 . 10^14
7.5.10^14
8.5.10^14
9.5.10^14
-4
-5
-6
-7
8
9
10
11
T^-1 K^-1 . 10^-4

Fig IO. The variation of E_m and D_o with coverage. For comparison the resu[l]
results of Chen and Gomer [18] are also shown, but note that their D_o
values have been multiplied by 10^4. Chen and Gomers results are drawn as
(-----), present work as (————)

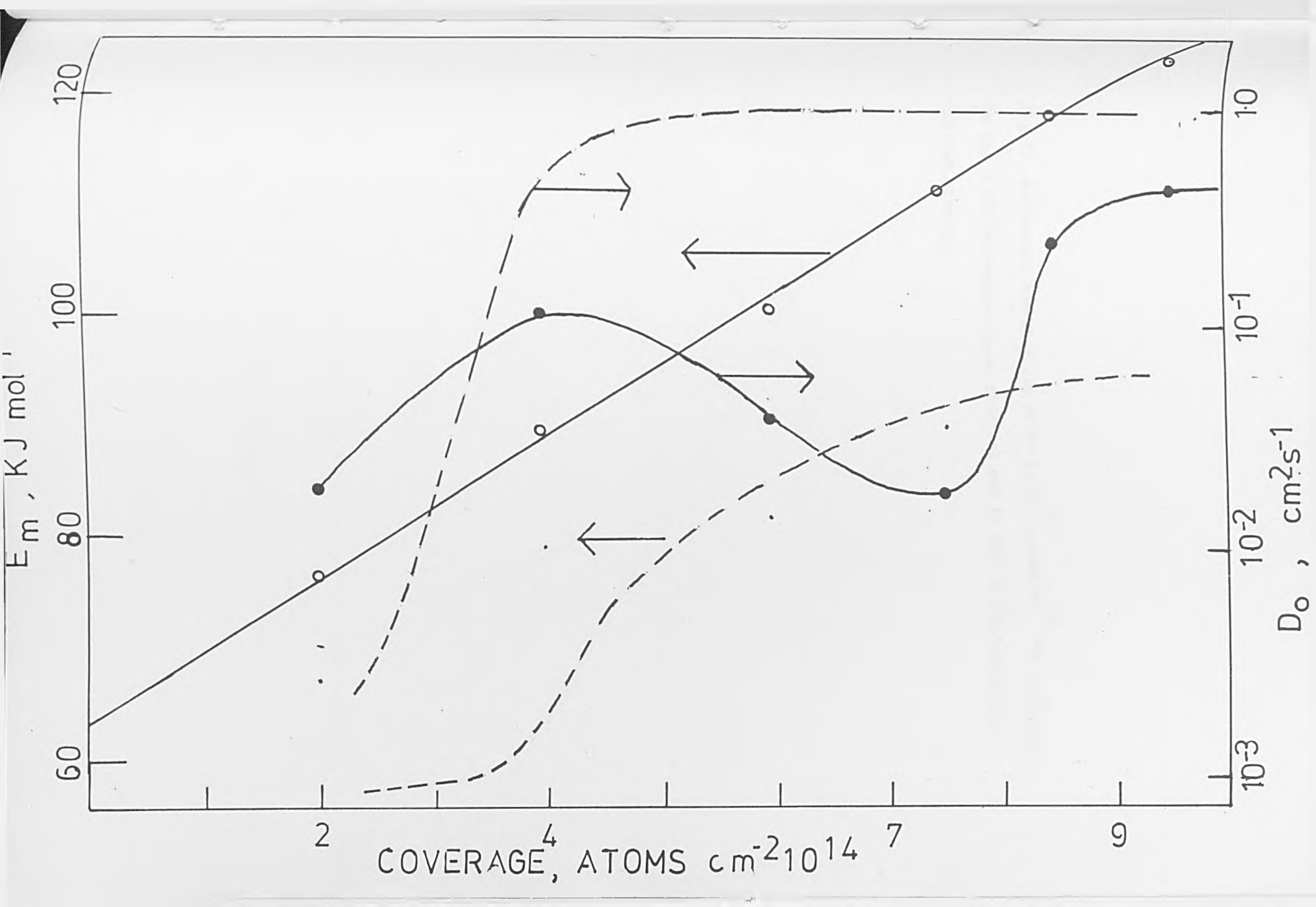
120
100
80
60
E_m , KJ mol'
10
10^{-1}
10^{-2}
10^{-3}
D_o , cm^2s^{-1}
2
4
7
9
COVERAGE, ATOMS $cm^{-2}10^{14}$

Fig.II. Activation energy plots at $N = 4 \times 10^{14}$ atoms cm^{-2} for diffusion in the $\langle 001 \rangle$ direction (open circles) and in the $\langle 1\bar{1}0 \rangle$ direction (filled circles).

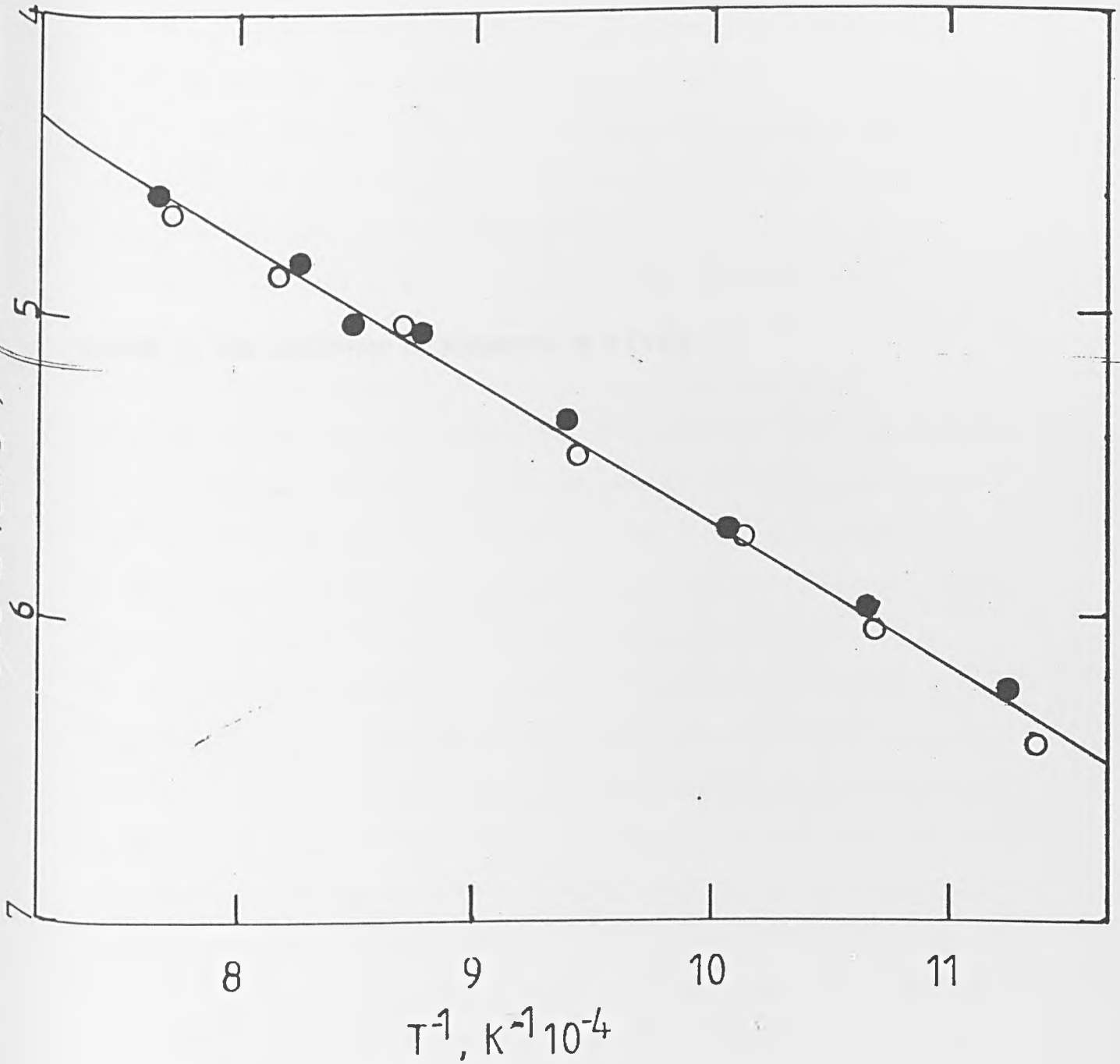
4
5
6
7
8
9
10
11
log D (cm²s⁻¹)
T⁻¹, K⁻¹ 10⁻⁴

CHAPTER 5: THE ADSORPTION OF POTASSIUM ON W{110}.

I. Introduction.

The adsorption of alkali metals on to single crystal planes of metals is one of the most studied fields since the advent of surface science. The interest,here,has been generated because of two important factors. Firstly, they are readily treated theoretically and so have often been used as "ideal adsorbates". The second reason is that they are of great importance industrially; they are often used to increase the emission of certain filaments (they lower the work function of the refractory metals), and the ultra-low work functions they sometimes produce may lead to the development of a near perfect Thermionic Energy Converter.[I]

The most studied of the alkali metals is Cs, due, in part, to the very low work functions observed when it is co-adsorbed with oxygen on to tungsten.[2] It has been well proven that for Cs and the other alkalies that the binding energy of the alkali decreases with the weight of the alkali.[3] Work functions show the opposite trend going to ever more positive values as the group is ascended .Both effects are due ostensibly to the enhanced polarisability as the radius of the atom increases.Li[4-6], Na[7] and Cs[8-10], all form ordered structures on the W{110} surface, many of these displaying order/disorder transitions below room temperature[II] and as a consequence many of the structures can not be observed at room temperature. It would seem[II] that the phase transition temperature increases with the molecular weight of the alkali. From the LEED results we can build up a behaviour pattern for the adsorption of these metals. Firstly, provided the temperature is low enough, ordered commensurate phases are formed at low coverages ($\theta < 1$) and there may be several of these dependent on the coverage. As the coverage nears a monolayer the system exhibits the pattern due to hexagonal, close-packed layers of adsorbate, with no registry with

the surface. These are normally visible at room temperature.

Basing explanations of surface properties of alkali metals on depolarisation effects is being challenged. Many of the alkali metals exhibit work-function minima as a function of coverage; explained using this type of approach. However results for W deposition on to W {110} show similar variations[12], but the explanation is based on terms of surface mobilities. The decreasing binding energy of alkali with increasing coverage may also have a different explanation; similar results have been observed for non-metal adsorbates and the variation is due to lateral interactions between the adspecies[29]. Highly charged alkalies should show similar effects.

Layers of alkali metals are strained due to their large ionic radii and this, coupled to low sublimation energies, ensure that multi-layer growth is rare. To this effect reports of layer growth of Cs on W {100}[13] have been met with some scepticism.

Vast amounts of experimental and theoretical information have been obtained for alkali metal adsorption, but much of it is conflicting. This is due, to a large extent, to the problems of maintaining good surface cleanliness during adsorption; alkalies are extremely sensitive to small impurity concentrations[35]. It has been pointed out that the high order LEED patterns observed for Zr adsorption on W {100} are the result of oxygen contamination[14]. Tables of desorption parameters drawn up by Hurkmans et al[3] have allowed much of the previous work to be classified in this category.

2. Experimental.

The system has been described elsewhere[15]. It consists of a stainless

steel chamber equipped with a 250 ls^{-1} ion pump and a titanium-sublimation pump "firing" on to a liquid nitrogen cooled shroud. Base pressures are in the 2×10^{-11} torr range. There is a mass spectrometer for residual gas analysis and an R.F.A. for LEED and AES. Gas inlet is from a molecular beam source or from the background. The sample was a W{110} single crystal cut and polished to within $\frac{1}{2}^{o}$ of the {110} surface plane, measuring $75 \times 75 \times 5$ mm. Temperatures were measured with a W-Re 5% / W-Re 25% thermocouple located in a small pit drilled into the edge of the crystal. Temperatures > 1000k were obtained using electron bombardment heating, below this resistive heating was used. The thermocouple was part of a feedback circuit so that the sample temperature could be controlled to within 2K. The sample was cooled by liquid nitrogen flowing through a stainless steel reservoir attached to the sample mounting block with a copper braid. Heat losses limited the sample temperature to 220K. The sample was cleaned in the manner associated with W [15] until AES showed the surface to be free of contamination.

Potassium evaporation was from a zeolite source coated on a filament as described by Weber and Cordes [16]. The filament was part of an electron gun like assembly at the end of which was a shield with a small slit cut into it allowing K to be dosed on to the crystal. Large shield to crystal distances resulted in a homogeneous K covering. It has been pointed out that zeolite sources are prone to oxygen impurities, presumably through breakdown of the zeolite itself. Mass spectra taken during the dosing showed only a mass peak at 39 amu, no KO or KO_2 were ever observed. After degassing the source for 100 hours, it could be used without the AES revealing any oxygen on the surface.

3. Results and Discussion.

3.I. Adsorption Results.

AES studies have been performed relatively few times for alkali metals adsorbing onto refractory metals [18-21], in particular, K has only been studied once for adsorption on to Mo {II0} and Mo {I00} [19]. The AES peaks of K were observed in the usual positions of 38 and 25IeV. Fig,I shows a typical AES derivative spectrum for a K covered W {II0} system, recorded with the primary beam energy of 2keV, modulation of 5 volts peak-to-peak and primary beam current of 4 μA. Fig.2 shows the peak-to-peak AES derivative height as a function of dose time for the K 25I peak and the W 347 eV peak. It can be immediately seen that the graph is made up of a number of linear sections with distinct knees where there is a change of slope. This graph is indicative of layer-by-layer growth [25]. We assume that in the initial portion of the graph the first layer is growing and the incoming K ions have a sticking probability of one (recent results have shown this to be true provided that the ion energy is low [35] and in our case the incoming ions had a energy of 2eV). The first observed change in slope occurs at the completion of this monolayer and second layer growth occurs. This layer is completed at the second knee. It is important to note that the time to complete the second layer is greater than the first. This is not due to any source instability, as evidenced by the agreement of two separate runs shown in Fig.2. We explain this fact by assuming a lower sticking probability of second layer ions, and this evaluates to 0.65. After completion of the second layer, third layer growth begins but at this point the AES signal becomes less consistent despite no noticeable decrease in the signal to noise ratio. We believe that this is due to the fact that third layer K is only very weakly bound and that the lifetime is small. Thus the data becomes sensitive to the dose time, the time to measure the signal and the time to move the sample to the AES position.

After this some approximate saturation coverage is reached.

These assertions were checked by repeating the experiments at temperatures other than room temperature. The results for substrate temperatures of 250 amd 350K are shown in Fig.3. At the lower temperature the second layer is completed faster; the sticking probability evaluates to 0.82. At the higher temperature it is incomplete and the signal is again inconsistent. First layer growth is unaffected as would be expected for strong adatom-surface interactions. These results are in support of our model.

The sensitivity of the multilayers to temperature should come as no surprise; using the Frenkel equation,

$$\tau = \tau_0 \exp(E_d/RT)$$

where τ is the residence time, τ_0 the preexponential and T the surface temperature. For $\tau_0 = 1.6 \times 10^{-13}$ s, T = 300K and E_d is the sublimation energy of K, then τ is 150s. If the sublimation energy is raised by 10% (or T lowered by 10%), τ evaluates to around 15 minutes. This also shows that multilayer growth is not unreasonable. It has not been observed for the K/Fe system[22,23] or K/Ni{110}[24] but has been observed for K on W{100}. In using this model we assume that the sublimation energy has been raised slightly, possibly due to some interaction of the second layer K ions with the surface. This seems to be negligable for the third layer. The results here are very similar to results for the Cs/W{110} system[20] where second layer Cs was formed at 250K. Third layer growth was never observed presumably due to the lower sublimation energy of Cs (E_d Cs = 78.7 and K = 90 kJmol^{-1}). The layer-by-layer growth mode observed here is different to the growth of K layers on Mo{110}[19] but this may be due to temperature differences which strongly affect the growth mode[26].

Further evidence was sought that the monolayer point was correctly

assigned. This was done by measuring the drain current of the sample under an impinging electron beam. Fig.4 shows the drain current as a function of dose time. The drain current saturates at a time equal to the time taken to complete the first monolayer. This is good evidence that our assignment is correct, since it is to be expected that such graphs level off after the first monolayer has been completed. The initial decrease of the drain current is very rapid and then slows dramatically. The drain current, I_d, is a measure of the total secondary electron yield current density, I_s. They are related by,

$$I_p = I_s + I_d$$

where I_p is the primary beam current. Clearly the secondary electron yield increases at the exspense of the drain current for an electropositive adsorbate as here. The drain current is a sensitive function of primary beam energy, incidence angle, substrate outer shell electrons, atomic radius and the work function. Since the work function of the system does not show a similar decrease [27] and the other parameters are unaltered, we assume that the drain current is a very sensitive measure of electronic structure. From these results we thus see a very small amount of K alters the electronic properties of the surface drastically. There is some evidence for this in that the presence of small amounts of K cause the sticking probability to increase drastically on certain surfaces [28].

3.2. LEED Observations.

A thorough investigation was made to look for ordered phases developing during the adsorption of K. At temperatures between 225 and 1000K and coverages in the zero to two monolayer range, no new LEED patterns were ever observed. At no point was a Leed pattern observed due to a close-packed K surface. All that was ever observed was a decrease in the intensity of the (1 x 1) clean surface beams and an increase in the background. This is shown in Fig.5, where the intensity of a (1,0) beam and

the intensity of the background (both measured at 75eV) are plotted against exposure time. At the monolayer point the substrate beam has merged into the background. The distance between LEED spots was also monitored during the adsorption regime in order to look for lattice contraction, but there was no evidence for these effects.

It seems likely that the temperature in these experiments was too high to observe any ordered phases at coverages less than a monolayer, however, the lack of the close-packed pattern is disturbing. The usual explanation for this structure is that mobility has decreased by enough to allow the K adatoms to "lock into" an energetically favoured arrangement. We assume that slightly higher adsorption energies may make this less favoured.

3.3. The Desorption of Potassium

An attempt was made to evaluate the desorption energy of K from the W {110} surface. This was done by producing a homogeneous coverage of one monolayer across the surface (the source could produce this type of deposit at large sample to source distances) and heating the surface to successively higher temperatures for a periods of 30s. During this, the coverage was monitored using AES. The results are shown in Fig.6 and indicate that the desorption occurs in two separate stages. It has been shown that the presence of two peaks in a desorption spectra can be explained in terms of lateral interactions between the adatoms [29], one would expect that these are important for the large, highly charged, K ions. The desorption energies of alkali metals have been measured and do show the sort of variation with coverage these theories would predict [22,23].

Using the equation,

$$\frac{d\theta}{dt} = -\nu \theta \exp(-E_d/RT)$$

(where θ is the relative coverage, ν the preexponential and E_d the desorption energy) the desorption parameters can be estimated

if a preexponential of 10^{13} s^{-1} is assumed. For the two stages in the figure this treatment yields; 2.8 (low coverage) and 2.3eV (high coverage). This is well above the value measured in previous work [30,31]. This is because here we measure desorption of ions and neutrals, which takes place at higher energies than neutral desorption. The values here are closer to the values measured in field desorption experiments [32,33], which is a process akin to the one here.

3.4. The Surface Coverage of Potassium.

We have so far failed to mention the surface coverage of K with respect to the W atomic density on this plane. Unfortunately this could not be measured with any accuracy in the present work, thus we assign a value using the work of Blaszczyszyn et al [27]. It was shown that the work function of the system K/ W {110} reached a plateau at the monolayer point and this monolayer coverage was found to be 5×10^{14} atoms cm^{-2}. We adopt this value. This value is very close to the density of the bulk {110} K plane; 4.99×10^{14} atoms cm^{-2}. Some verification was found for this; at an impinging ion current of 0.8×10^{-7} A, the surface reached monolayer coverage in 16.6 minutes, and provided a unity sticking probability this corresponds to a K surface density of 5.2×10^{14} atoms cm^{-2}, in fairly good agreement with the quoted value.

3.5. Surface Diffusion of Potassium.

Diffusion of K on polycrystalline W has been studied a number of times, but the results are conflicting [36-38]. Two of the authors report that the activation energy E_m, for surface diffusion increases with coverage, [37,38] while the third reports the opposite trend [36]. The results of Bosworth and Schmidt and Gomer [38] are summarised in table I. Bosworths results are more in line with what would be expected from a surface covered with adatoms which have a very strong repulsive interaction between them [29], this despite the fact that Bosworth probably worked with a contaminated

surface. The diffusion process can be described by the equation,

$$D = \tfrac{1}{2}\nu l^2 \exp(\Delta S_m/k) \exp(-E_m/kT) = D_o(-E_m/kT)$$

where ν is the effective vibrational frequency of the adatom, l the mean square jump length and D the diffusion coefficient. The overall preexponential D_o is known as the diffusivity and the activation energy for diffusion is E_m.

In this work diffusion was followed in the manner described below. Using a small crystal to source distance a small diameter patch could be deposited onto the sample. This patch could then be measured by turning the sample towards the AES beam and measuring the AES derivative height;using accurate micrometers on the sample manipulator this could be performed at various points along the sample. In this way coverage versus distance profiles could be obtained. By heating the sample diffusion could be monitored by rescanning the profile and looking for peak shape changes. The peak shape analysis used by Bosworth[36] could not be used here to analyse the results because the initial K patch was so large that the large peak shape changes needed for good experimental accuracy would have introduced edge effects. Instead the method used by Bowker and King[39] was followed. This consisted of measuring the change in the width as a function of time and temperature . Typical results at two different coverages are shown in Figs. 7 and 8. At $\theta = 0.2$ for a temperature of 610K and at $\theta = 1.0$ at a temperature of 500K. For a random walk process it is necessary that the increase in width of the patch is proportional to the square root of the heating time. Experimentally this was found to be true,as shown in Fig.9 for both high and low coverage. Arrhenius plots of D (equal to $(\Delta x)^2 / t$, where Δx is the increase in width of a peak) as the temperature varied could be constructed at the two coverages used here and are shown in Figs.10 and 11. The results are

displayed in table I. It can be seen that E_m decreases with coverage but it must be pointed out that these are average values over the coverage range used and that the variation may be larger than these results indicate. The E_m values here appear to be large when compared to the previous results, this may be due to a single crystal plane being used here rather than a polycrystalline sample, due to a higher degree of surface cleanliness used here compared to the older results,or due to an experimental artifact. This may arise from the large error quoted with the low coverage data.This uncertainty is because of the competition of desorption with diffusion at these coverages limiting the temperature range to about 50k when the two processes are readily separated.The high coverage data does not suffer this problem to the same degree and thus is more accurate. The value of E_m at $\theta = I$ is in close proximity to the value measured for Cs diffusion on W $\{110\}$ [34] ; $E_m = 57 kJ\ mol^{-I}$.

Despite the experimental difficulties it has clearly been shown that E_m decreases as θ increases. Following Bosworth [36] we explain this as being due to the large repulsive interactions between these adatoms that exist. The low coverage results approximate to the diffusion energy of a isolated K adatom.and as θ increases the repulsive interactions attain greater significance allowing the adatoms to diffuse more easily.These repulsive interactions are also responsible for the decreasing E_d as the coverage increases.

4. Summary and General Conclusions.

In the present study we have demonstrated that K is able to form multi-layers on W $\{110\}$ at room temperature; however, the stability of these layers is very low. Desorption from the first layer takes place in two stages, each stage presumably due to the presence of strong

repulsive lateral interactions between the adatoms. These lateral interactions strongly affect the diffusion kinetics, causing the activation energy for surface diffusion to decrease as the coverage increases. The decrease found here is opposite to the variation reported by some authors 3738 using the field emission microscope. The results here clearly show the importance of lateral interactions between adsorbed molecules and thus fits the idea that these interactions dominate the desorption, the adsorption and the diffusion in many gas/ single crystal metal surfaces.

REFERENCES.

I. G.N. Hatsopoulus and E.P. Gyftopoulus, Thermionic Energy Conversion, Vol I,Vol. 2, M.I.T., Cambridge, 1974, 1979.

2. C.A. Papergeogopoulus, Surf.Sci.,104(1981)643.

3. A. Hurkmans, E.G. Overbosch. and J. Los, Surf.Sci.,59(1976)488.

4. D.A. Gorodetsky, Yu P. Melnik and A.A. Yusko, Ukr.Fiz.Zh., 12(1967)649.

5. V.K. Medvedev and T.P. Smereka,Sov. Phys, Sol.St., 16(1974)1046.

6. A.G. Naumovets and A.G. Fedorus, Sov.Phys.JETP.,41(1975)587.

7. V.K. Medvedev, A.G. Naumovets and A.G. Fedorus,Sov.Phys.Sol.St. 16(1970)301.

8. A.U. Macrae, K. Muller, J.J. Lander and J. Morrison,Surf. Sci.; 15(1969)483.

9. A.G. Naumovets and A.G. Fedorus, Surf.Sci.,21(1970)427.

10. A.G. Fedorus and A.G. Naumovets,Sov.Phys.Sol.St., 12(1970)232.

11. A.G. Naumovets and A.G. Fedorus,Sov. Phys.JETP.,46(1977)575.

12. P. Hahn, J. Clobes and M. Henzler,J.Appl.Phys. in print.

13. C.A. Papergeogeogopoulus, Surf.Sci.,104(1981)643.

14. P.R. Davis,Surf.Sci.,91(1980)385.

15. M.K. Debe and D.A. King, Surf.Sci.,81(1979)193.

16. R.F. Weber and L.F. Cordes,Rev.Sci.Instrum.,36(1965)112.

17. E. Bauer, in "The Physics of Solid Surfaces and Heterogeneous Catalysis" eds. D.A. King and D.P. Woodruff. Vol 3B, Elsevier,Amsterdam, in press.

18. Yu S. Vedula, V.G. Goichar, A.G. Naumovets and A.G. Fedorus, Sov.Phys.Sol.St.,19(1977)1505.

19. S. Thomas and T.W. Haas,J.Vac.Sci.Tech.,9(1972)840,10(1973)218.

20. J.L. Desplat and C.A. Papergeogeogopulus,Surf.Sci.,92(1980)97,119.

21. G.Broden and H.P. Bonzel, Surf.Sci.,84(1980)106.

22. S.B. Lee, M. Weiss and G.Ertl,Surf.Sci.,108(1981)357.

23. R.L. Gerlach and T.N. Rhodin,Surf.Sci.,19(1970)403.

24. P.W. Steinhage and M. Mayer,Thin Solid Films,28(1975)131.

25. J.A. Venables and G.D.Y. Spiller,"Nucleation and Growth of Thin Films" Surface Diffusion on Solid Materials,ed. V.Thien Binh, NATO-ASI Series, Plenum(1982).

26. E. Gillet and B. Gruzza,Surf.Sci., 97(1980)553.

27. R. Blaszcyzyszyn, M. Blaszcyzyszyn and R. Meclewski,Surf.Sci., 51(1975)396.

28. M. Kitson and R.M. Lambert,Surf.Sci.,109(1981)60.

29. M.A. Morris, M. Bowker and D.A. King, "Kinetics of adsorption,desorption Diffusion at Metal Surfaces" in Comprehensive Chemical Kinetics eds C.H.F. Tipper and C. Bamford, Elsevier,North Holland,(1983).

30. W. Korner, Proc.2nd Intern.Conf on Solid Surfaces,(1974),Jap.J.Appl. Phys.Suppl.2,Pt.2,(1974)75.

31. K. Sendenka and R. Meclewski,Surf.Sci.,70(1978)255.

32. C.J. Todd and T.N. Rhodin, Surf.Sci.42(1974)109.

33. L.D. Schmidt and R. Gomer,J.Chem.Soc.,45(1966)1605.

34. P. Akhter and J.A. Venables,Surf,Sci.,103(1981)301.

35. A. Hurkmans , E.G. Overbosch and J.Los,Surf.Sci.,62(1977)621.

36. R.C.L. Bosworth, Proc.Roy.Soc.,154A(1936)112.

37. R. Meclewski,Acta Physica Poland,A37(1971)41.

38. L.D. Schmidt and R. Gomer,J.Chem.Phys.,42(1965)3573.

39. M. Bowker and D.A.King, Surf.Sci.,94(1980)564.

TABLE I

Diffusion parameters of K on W.

	REF	E_m kJ mol^{-1}	D_o $cm^2\ s^{-1}$	COVERAGE atoms cm^{-2} x 10^{14}
K/W polycrystalline	36	63	40	0.12
		50		1.2
		20		4.8
K/W polycrystalline	38	21	1.6×10^{-6}	0.5
		40	1.3×10^{-4}	1.5
		75	32	2.7
K/W{110}	THIS WORK	128 ± 40	NOT MEASURED, ACCURACY TOO LOW	1.0
		48.5 ± 10	0.16	5.0

Fig.I. Derivative AES spectra for a K-covered W{ 110 } surface.

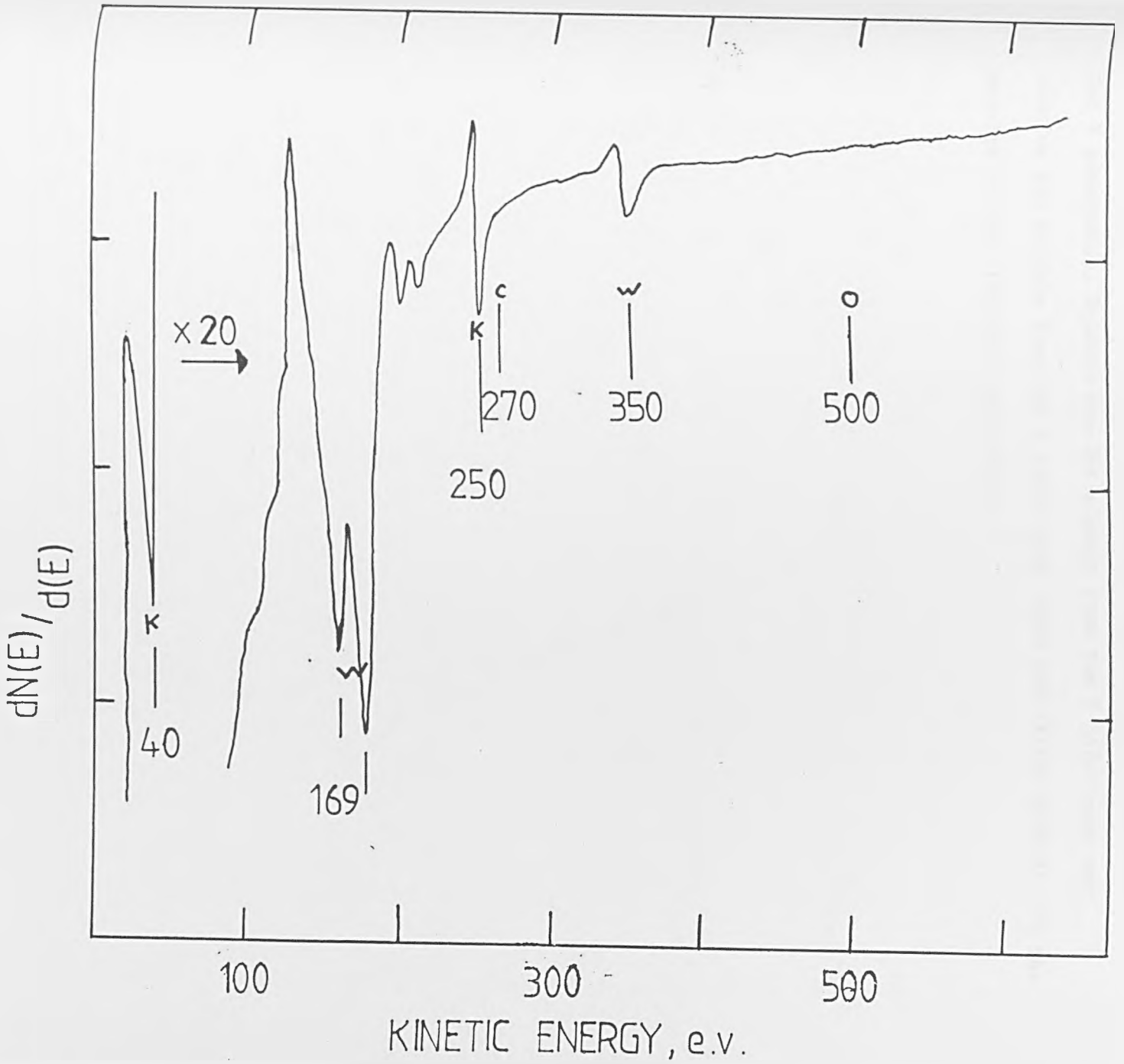
dN(E)/d(E)
× 20
K
40
169
K
C
270
250
350
500
100
300
500
KINETIC ENERGY, e.v.

Fig.2. Derivative AES peak-to-peak heights plotted against dose time for K adsorption. Squares are the signals from the W 347eV peak and circles the signals from the K 251eV peak. Open and filled symbols are the results of two different experiments.

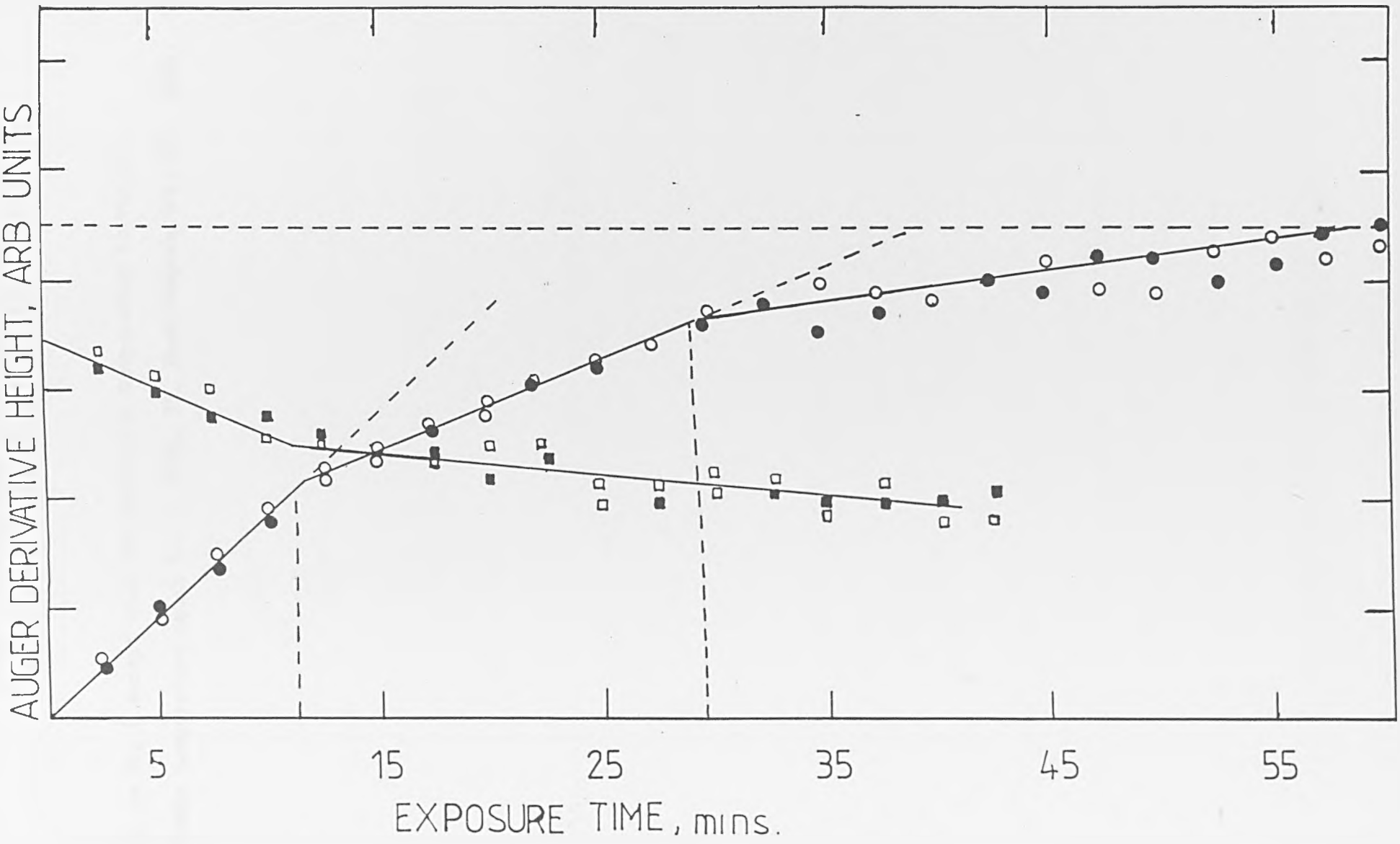
AUGER DERIVATIVE HEIGHT, ARB UNITS
5
15
25
35
45
55
EXPOSURE TIME, mins.

Fig.3. As Fig.2 except that the adsorption temperature is varied.

Substrate temperature equal to: I, 250K, II, Room temperature, III, 350K.

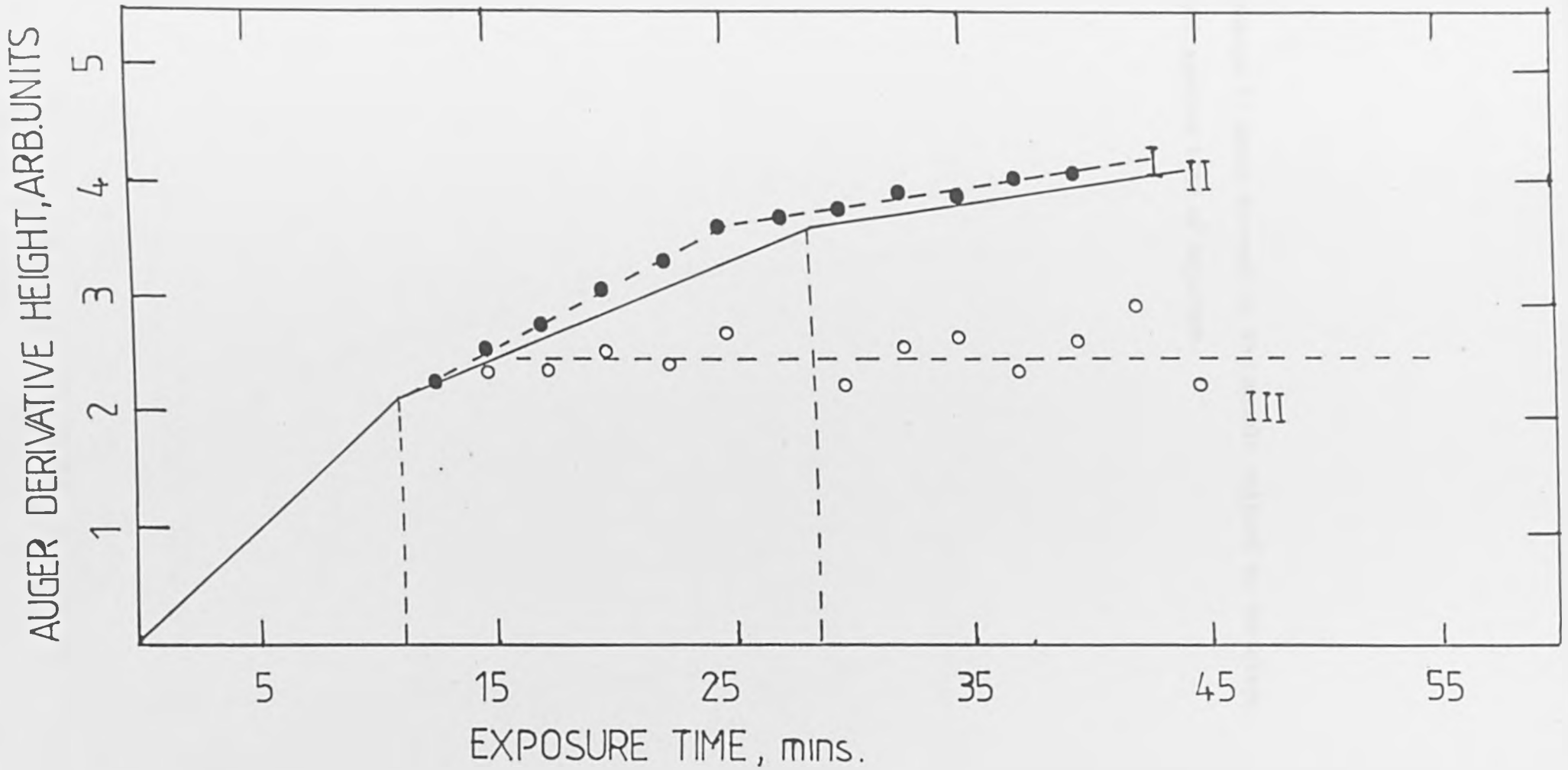
AUGER DERIVATIVE HEIGHT, ARB.UNITS
1
2
3
4
5
I
II
III
5
15
25
35
45
55
EXPOSURE TIME, mins.

Fig.4. The change in drain current at the sample ratioed to the clean surface result against time of exposure.

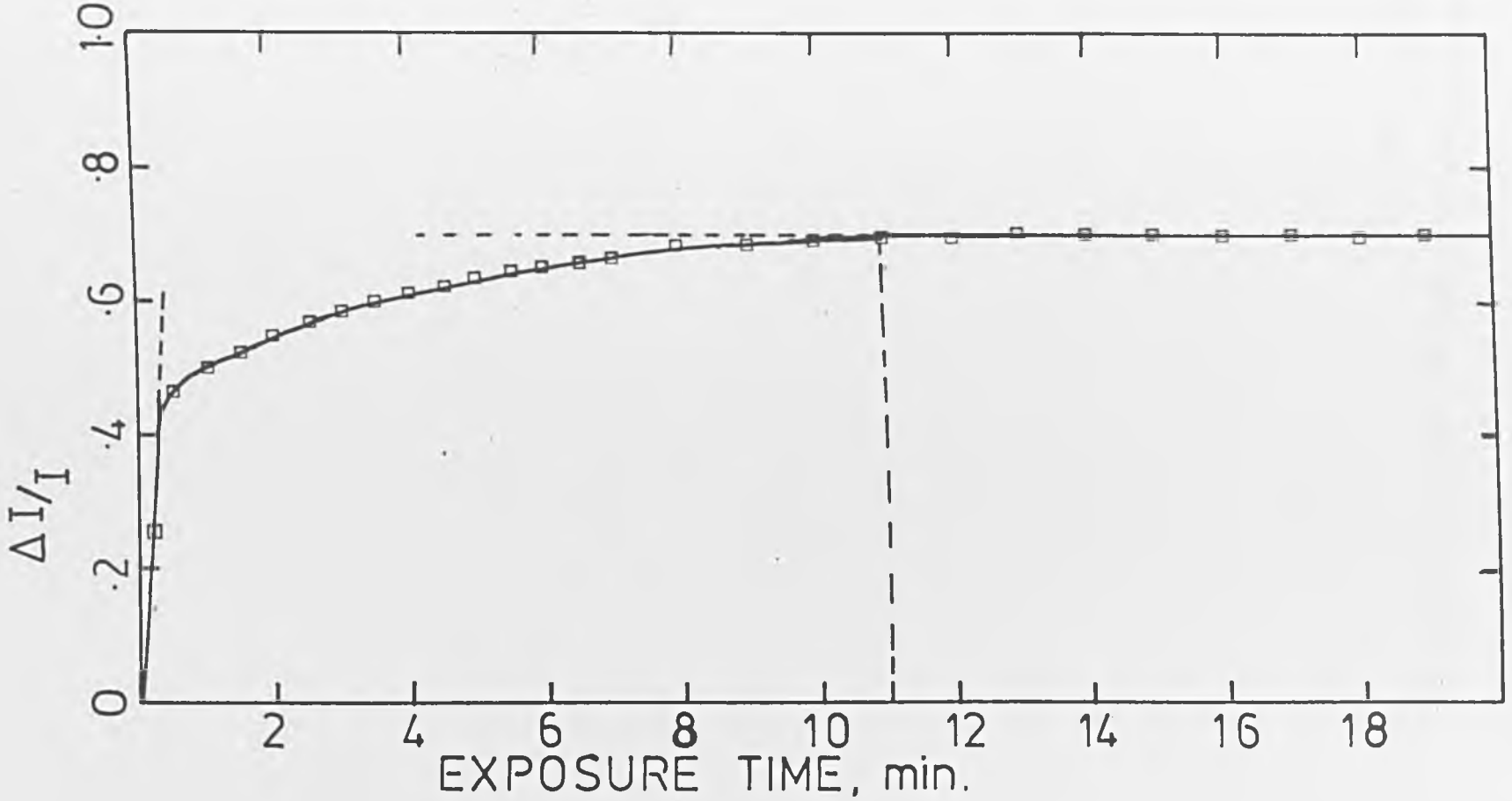
ΔI/I
0
·2
·4
·6
·8
1·0
2
4
6
8
10
12
14
16
18
EXPOSURE TIME, min.

Fig.5. The intensity in a (I,0) LEED spot and the background as a function of exposure time.

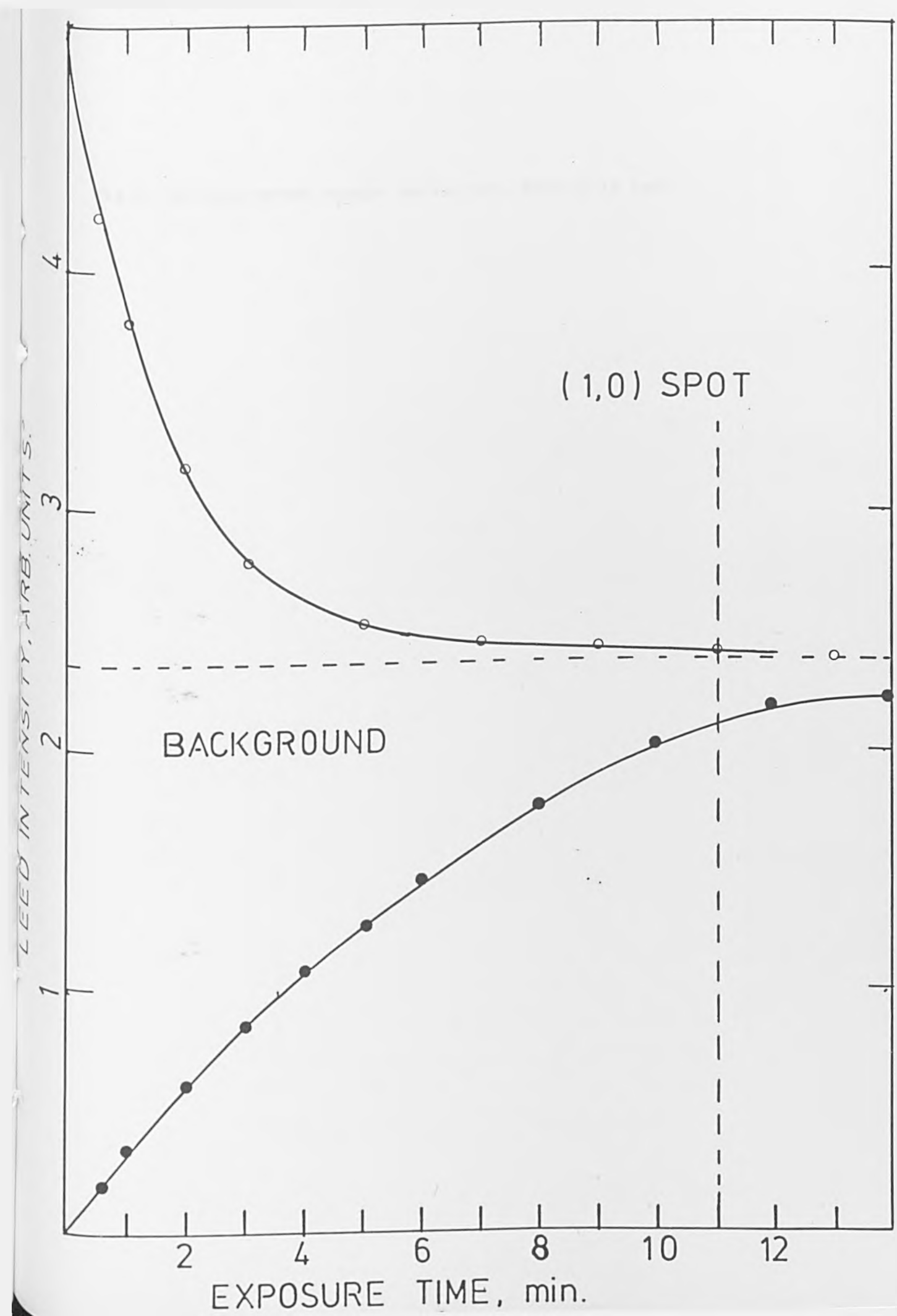
LEED INTENSITY, ARB. UNITS
1
2
3
4
(1,0) SPOT
BACKGROUND
2
4
6
8
10
12
EXPOSURE TIME, min.

Fig.6. Coverage versus sample temperature. Details in text.

COVERAGE, MONOLAYERS.
·2
·4
·6
·8
1·0
400
600
800
1000
1100
TEMPERATURE, K

Figs.7 & 8. Typical coverage versus distance profiles before and after heating, at low and high coverage.

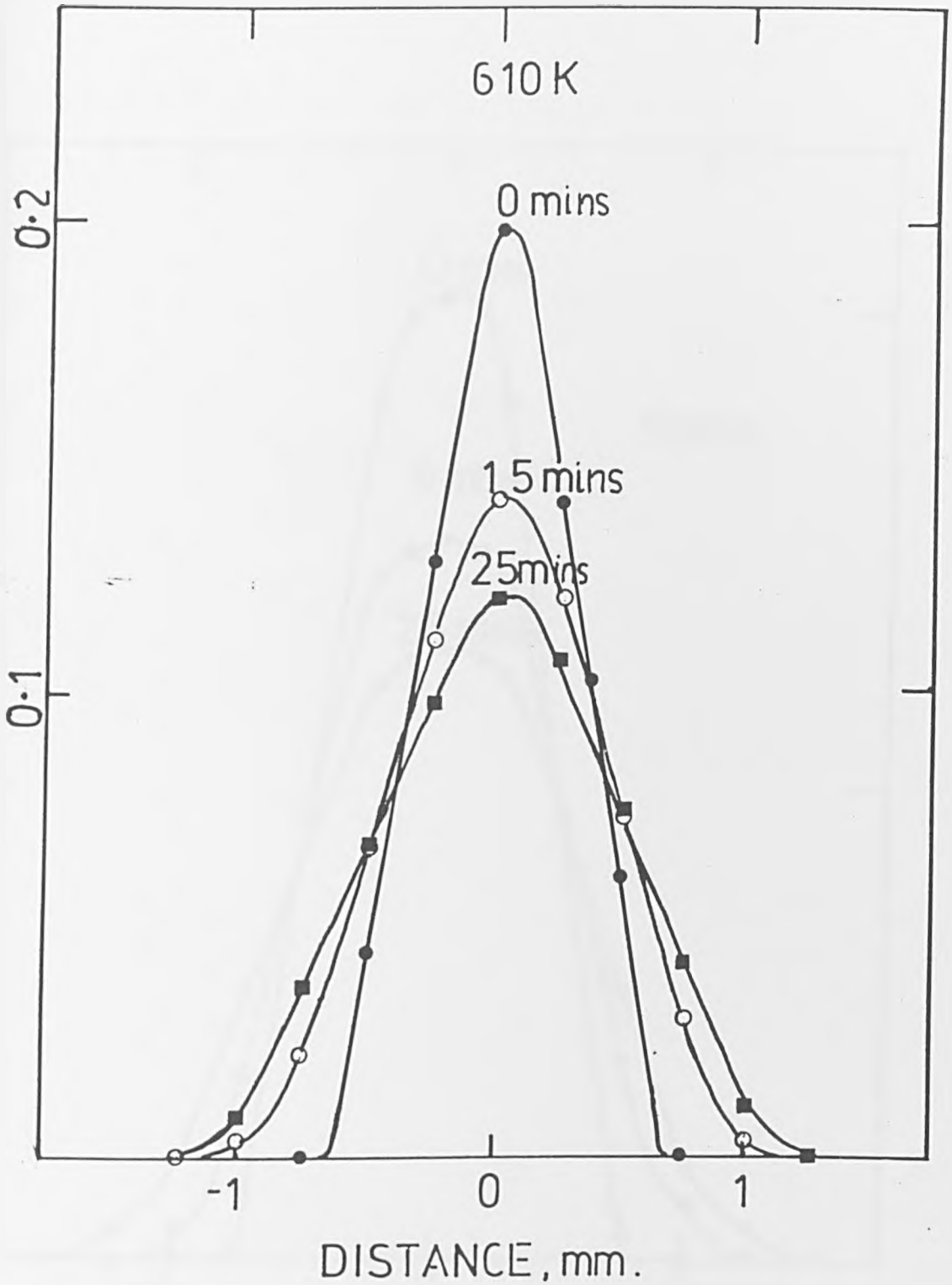
610 K
0 mins
15 mins
25 mins
0·2
0·1
-1
0
1
DISTANCE, mm.

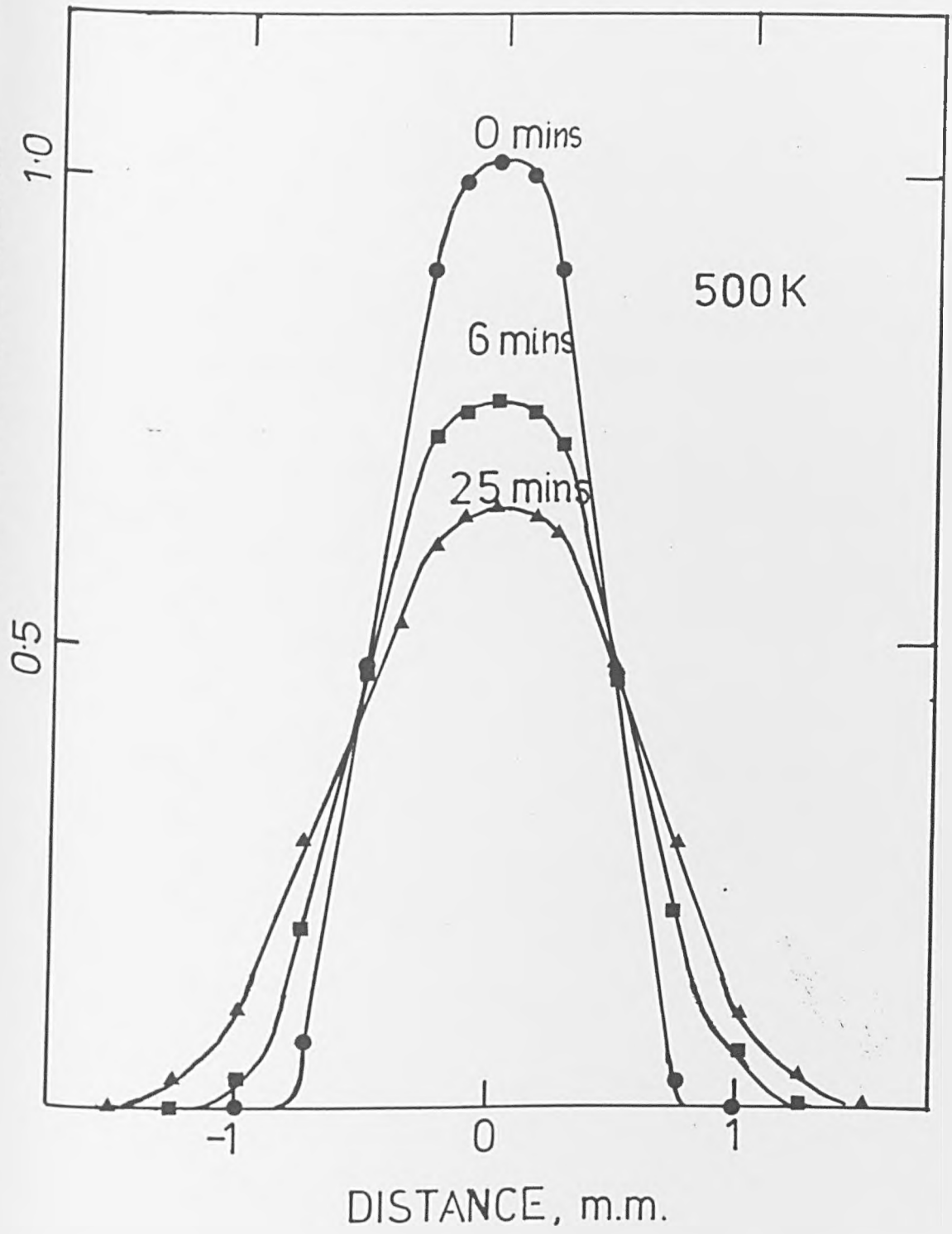
COVERAGE, MONOLAYERS
1·0
0·5
0 mins
6 mins
25 mins
500 K
-1
0
1
DISTANCE, m.m.

Fig.9. Typical $(\Delta x)^2$ versus heating time for the data in Figs.7 & 8.

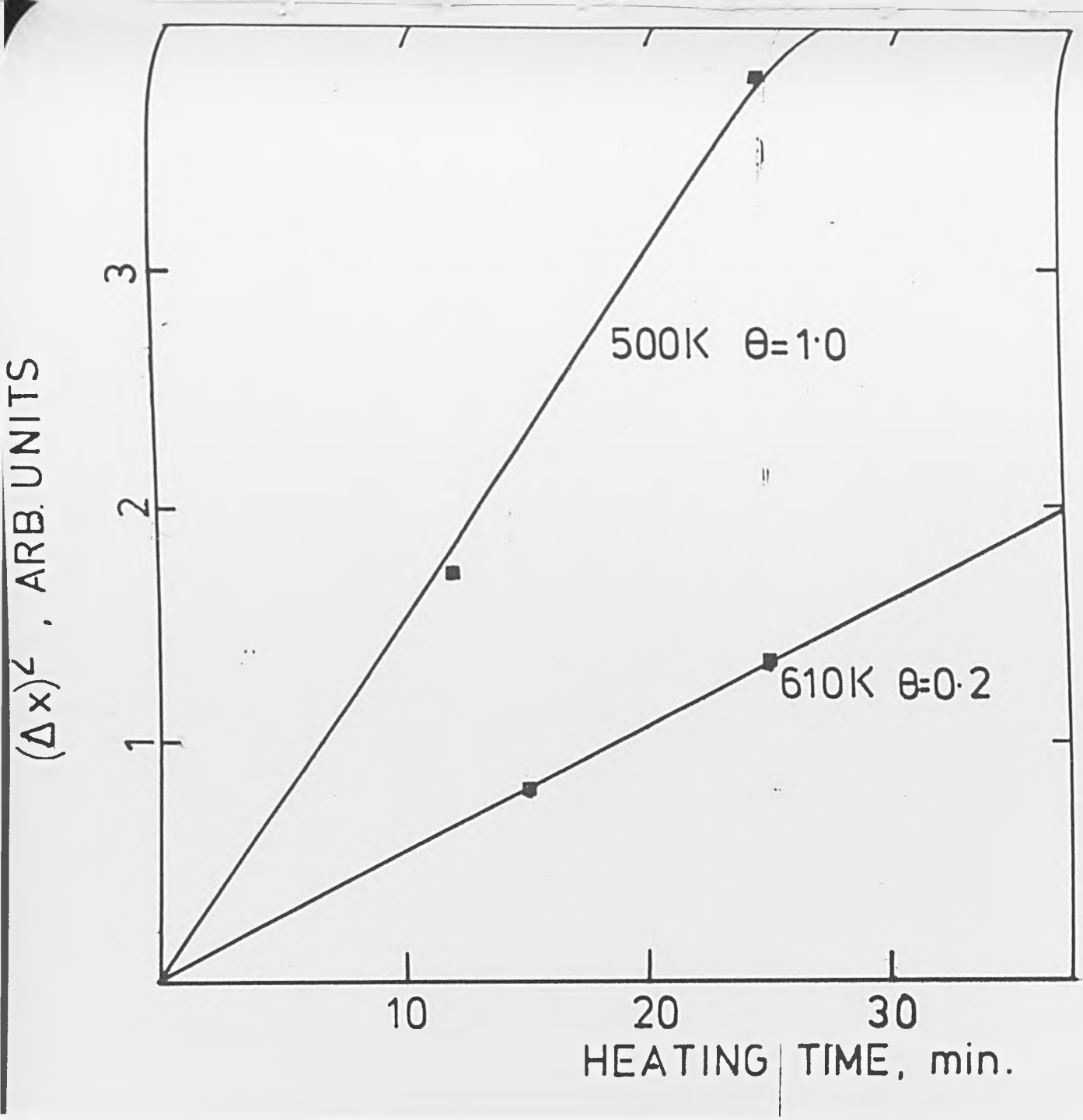
$(\Delta x)^2$, ARB. UNITS
1
2
3
500K θ=1·0
610K θ=0·2
10
20
30
HEATING TIME, min.

Figs.IO & II. Arrhenius plots for diffusion of K at high and low coverage.

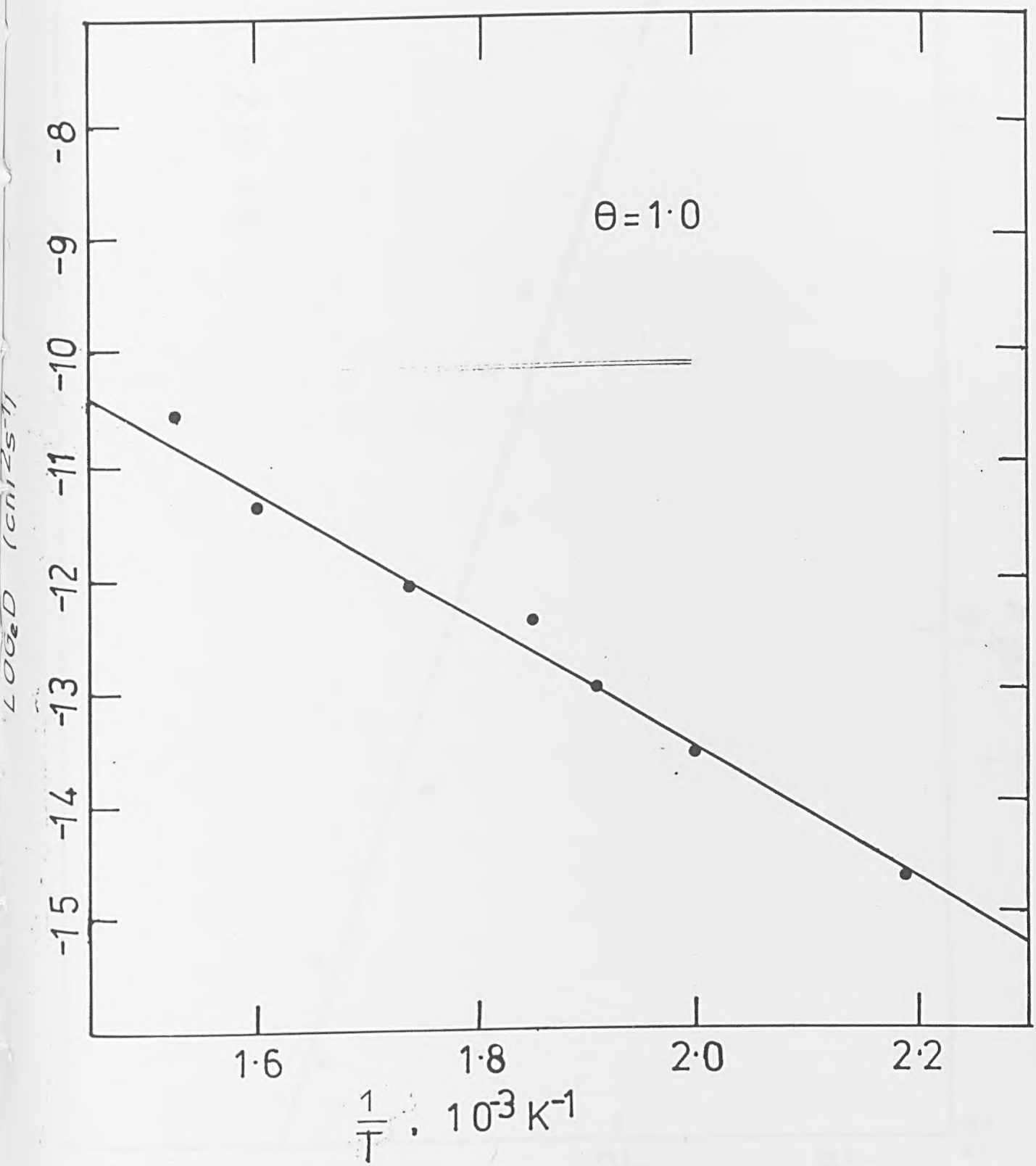
θ=1·0
-8
-9
-10
-11
-12
-13
-14
-15
1·6
1·8
2·0
2·2
$\frac{1}{T}$, $10^{-3}\,K^{-1}$
$\log_e D$ (cm²s⁻¹)

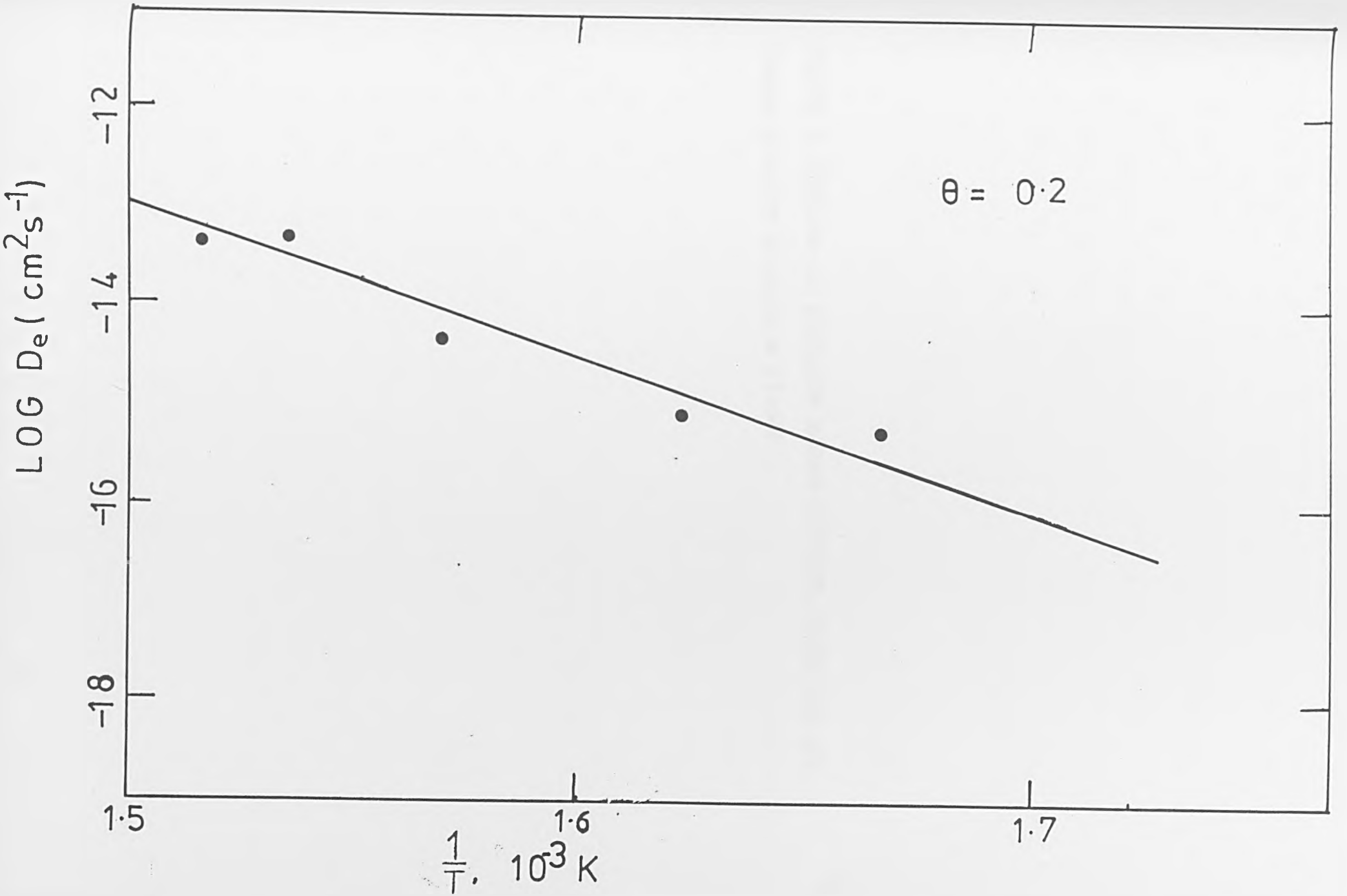
θ = 0·2
LOG D_e ($cm^2 s^{-1}$)
-12
-14
-16
-18
1·5
1·6
1·7
$\frac{1}{T}$, 10^{-3} K

CHAPTER 6: MONOLAYER AND MULTILAYER SURFACE DIFFUSION, GROWTH MODE AND THERMAL STABILITY OF INDIUM ON W{001}.

Monolayer and Multilayer Surface Diffusion, Growth Mode and Thermal Stability of Indium on W{100}.

M.A. Morris, C.J. Barnes and David A. King

The Donnan Laboratories,
Liverpool University,
Liverpool L69 3BX,
England.

1. Introduction

Studies of the surface properties of indium, as substrate or adsorbate, are rare, and are largely limited to its compounds which form III-V semiconductors, particularly InSb and InP. However, indium is often used to coat metals in mechanical engines, as it protects the metal from corrosion and acts as a lubricant.[1,2] No quantitative information is available concerning its diffusion properties, and indeed there is a general paucity of quantitative diffusion studies of adsorbates on single crystal surfaces.[3] In the present work we have attempted to remedy both these deficiencies by using LEED and scanning AES to conduct a detailed investigation of the growth mode the thermal stability and surface diffusion of indium on W{100}. The diffusion studies are of central importance, and form part of a research programme aimed at determining the role of lateral adsorbate-adsorbate interactions in surface diffusion,[4,5] and the role of mobile "precursor" states in adsorption and desorption kinetics.[6]

Indium is a metal forming a body centred tetragonal structure with some distortion. In the bulk, each atom has four nearest neighbours at 3.24 Å and four next nearest neighbours at 3.36 Å. It has the largest temperature range of all the elements between its melting point (429 K) and its boiling point (2340 K).

The {100} plane of tungsten has been very extensively studied, and particular interest has been shown in the discovery that the clean surface undergoes a reversible surface phase transition at ~370 K.[7]

2. Experimental

The uhv system, previously described in detail[8], is equipped with Varian 4-grid LEED optics and a VG Q8 mass spectrometer. LEED intensity measurements were conducted with a Video camera interfaced to a microcomputer, supplied by Data-Quire Corporation. AES measurements were made with the LEED optics, typically operated at a modulating voltage on the crystal of 6 V peak-to-peak. The system was routinely capable of achieving $\sim 2 \times 10^{-11}$ torr.

The tungsten crystal was cut and polished to within $\frac{1}{2}^{o}$ of the {100} plane, and cleaned *in situ* by the usual method until no contaminant peak could be observed using AES and also until the clean surface reconstruction (a very sensitive test of the presence of impurities[9]) could be observed on cooling below 370 K. The sample was heated either by electron bombardment of by resistive heating of the support wires, and temperatures were measured by means of a W-5%Re/W-25%Re thermocouple located in a small hole spark-drilled into the edge of the crystal. The thermocouple output was used as a feedback to accurately control the sample temperature for given time periods. The sample was mounted on a manipulator with Vernier scales, allowing accurate positioning and movement both horizontally and vertically, and thus providing a means of recording AES signals as a function of distance across the sample.

Indium was dosed onto the sample from an evaporation source schematically illustrated in figure 1. It consists of two narrow (1 mm internal diameter) stainless steel tubes,

sealed and spotwelded at one end to feedthroughs. The open ends are attached to each other via a tungsten ribbon, and the tubes are loaded with pieces of indium wire (0.50 mm diameter, 99.999% purity, supplied by Koch-Light Laboratories Ltd.). The source is resistively heated to ~700 K, and steady indium deposition rates, at a source-to-crystal distance of 20 mm. of between 0.02 monolayers per minute and 4 monolayers per minute were readily achieved by controlling the temperature. After an initial degassing period, the source could be used at these deposition rates without an increase in background pressure above 2×10^{-10} torr. It is believed that this evaporation source design is particularly well-suited to elements, such as Ag and Fe, where evaporation takes place close to the melting point. The source is mounted with a collimating shield, and provides a spot of indium on the sample which could be varied between 2 mm and 15 mm in diameter by varying the crystal-to-source distance.

3. The growth mode of indium films on W{100}.

A typical Auger spectrum of the surface after a large exposure (~15 monolayers) of indium is shown in figure 2; the peaks at 345, 403, 417 and 460 eV are in close agreement with previous studies of In. A careful examination in the range 20 to 100 eV revealed no peaks in this range. The film thickness for this spectrum is sufficient to completely attenuate the tungsten Auger peaks.

Both In and W peak-to-peak heights, A, at 403 and 174 eV

respectively, were measured as a function of exposure of the initially clean surface at 300 K to In, as shown in figure 3. Excellent agreement is illustrated between two independent runs with different dosing intervals (30 and 60 sec), which demonstrates the reproducibility of the source.

For dosing times up to 3.8 minutes, the plot of A(In) vs time is perfectly linear, as shown in the inset to figure 3, with a relatively sharp break from linearity at this deposition time. Thereafter, the curve is continuous, showing no further breaks which would be characteristic of a layer-by-layer growth mode[10]; numerous runs of this type were recorded, and no evidence was found for changes in slope at periodic intervals after the first break from linearity. Deposition onto the W{100} surface at 200 K produced an identical result. A thorough investigation was made of the possibility of alloy formation, by annealing the surface at a range of temperatures. No change in the In or W peak width or shape was ever observed; and no change in peak intensity was noted until evaporation of In from the surface. We conclude that alloying does not occur.

The break from linearity in figure 3 is tentatively assigned to the point at which a complete monolayer is formed. Additional support is obtained from escape depth calculations, assuming layer-by-layer growth. Following Seah and Dench[11], the intensity of the In and W Auger peaks may be expressed as

$$A(\mathrm{In}) = A(\mathrm{In})^{\infty} \exp(-m\sec\theta\,\lambda(403))$$

and $$A(\mathrm{W}) = A(\mathrm{W})^{0}\{1-\exp[-m\sec\theta/\lambda(180)]\}$$

where $A(\mathrm{In})^{\infty}$ and $A(\mathrm{W})^{0}$ are the Auger peak intensities from an infinitely think In layer and the clean W surface, respectively; m is the number of monolayers; and $\lambda(403)$ and $\lambda(180)$ are the escape depths in monolayers of 403 and 180 eV electrons, respectively, through indium. The best fits to the experimental data are shown in figure 4, and were obtained with

$$\lambda(403) = 2.5; \quad \lambda(180) = 2.25.$$

The In and W monolayer points show very good agreement with these values for λ.

Linearity up to the monolayer point for $A(\mathrm{In})$ clearly points to completion of the first layer prior to growth of the second layer. However, we note that the attenuation of $A(\mathrm{W})$ as In is deposited onto the clean surface is <u>not</u> linear, as is usually predicted for monolayer growths; the initial decay is less than anticipated from simple considerations. We believe that this non-linearity can be attributed to the geometric effect indicated in figure 5. At low coverages, trajectories of W Auger electrons such as that indicated by path A are attenuated by scattering through an indium atom; while trajectories such as that indicated by path B are unaffected. On the other hand, as the coverage is increased to a monolayer both the trajectories

A' and B' are attenuated by their passage through adatoms. Thus, if a retarding field analyser, with a wide acceptance angle, is used (as in the present work), and if adsorption occurs randomly into surface sites, the attenuation of the substrate signal should be non-linear in surface coverage. On the other hand, if adsorption were to proceed by two dimensional island growth of the first layer, the attenuation should be linear. We therefore conclude that the first layer begins to form by random filling of surface sites.

Finally, the monolayer point was checked by a simple method. The total secondary electron yield, δ, should be a sensitive function of the surface electron barrier,[5] and should therefore change continuously up to the monolayer point, and then remain roughly constant as further layers are formed. The secondary electron yield is readily measured by recording the drain current to the crystal as a primary beam of electrons is impinged on it. In the present work δ was measured at several primary beam energues as a function of indium dosing time. A typical result is shown in figure 6. The secondary electron yield increases with indium coverage (to be expected if In causes a decrease in the work function), and the curve shows a pronounced knee at the monolayer point defined by the AES measurements described above. No change in δ was observed as the film thickness was increased beyond a monolayer.

From the behaviour of the Auger peak intensities with indium deposition time, we conclude that the formation of an indium film proceeds initially by random adsorption into surface sites, Completion of a monolyer is followed by

haphazard development of subsequent layers, possibly in the form of three dimensional islands. This is known as the Stranski-Krastanov growth mechanism, and is commonly observed for metal film formation on metals. Layer-by-layer, or Frank-Van der Merwe growth of films is only expected if the lattice mismatch between the two metals is less than 9%.[12]

4. Surface Structure of Indium on W{100}.

The clean W{100} crystal exhibited a sharp (1x1) LEED pattern with faint half-order beams, attributable to the onset of the low temperature $(\sqrt{2} \times \sqrt{2})R45^{o}$ surface phase[8], just visible at room temperature. The half-order beams are more intense and sharp at 200 K. Adsorption of indium on the surface, at 300 or 200 K, resulted in a loss of the half-order beams at very low In fractional coverages, accompanied by an increase in integral order beam intensity (at a primary beam energy of 75 eV) to a maximum at the monolayer point; the integral order beams then fade with an increase in background intensity until they eventually disappear at ~4 monolayers. No new diffraction beams were observed throughout the deposition sequence. The variation in intensity of the (10) beam and the diffuse background are shown as a function of exposure to indium in figure 7, for a substrate temperature of 300 K. The width of the beams was also monitored, but showed no change with coverage. The maximum intensity occurs at the monolayer point defined by the AES and secondary electron yield measurements, giving further confidence in its assignment.

The intensity of the (01) beam (figure 7) shows a small but very reproducible increase with very small doses of In, amounting to <5% of a monolayer. It has been established[8,9] that very small amounts of impurity adatoms, such as O, C or N, prevent the formation of the low temperature phase. For example, ~2% of a monolayer of N adatoms was sufficient to completely inhibit its formation.[9] We therefore ascribe this initial integral order beam intensity increase to removal of the incipient reconstruction, with the intensity scattered into the half-order beams on the clean surface being returned to the integral order beams. (It has been found that 0.4 monolayers of In adsorbed on Ge{111} completely lifted the (2x8) reconstruction on that surface.[13]) A further increase in In coverage to ~20% of a monolayer results in no change in the (01) beam intensity; random occupation of surface lattice sites, established from AES measurements in the previous section, produces no coherent scattering contribution to the LEED intensity. The sudden subsequent increase in intensity as the In coverage is further increased may be due to two-dimensional island formation at this coverage. At one monolayer of indium, the intensity and sharpness of the LEED beams is strongly suggestive of a well-ordered pseudomorphic layer. This is in agreement with a field ion microscope study of In on tungsten, from which Nishikawa concluded that In overlayers have the same lattice dimensions as the W substrate.[14] At monolayer coverage, we therefore conclude that the In atomic density is the same

as that of the surface atoms in W{100}, i.e. 10 x 10^{14} cm^{-2}.

Above one monolayer, the substrate integral order beam intensity is extinguished, and no other beams are observed. The diffuse background intensity is increased. There is no evidence for epitaxial growth, in contrast with the In/Ge system.[13] This result confirms the conclusion from the AES results in the previous section, that the growth mode is Stranski-Krastonov.

A thorough search was made for LEED patterns which may be formed by annealing at elevated temperatures. The crystal was dosed with In to various coverages and annealed to increasing temperatures. No new LEED beams were observed on cooling the crystal. The LEED pattern was also examined with various coverages at elevated temperatures, and again no patterns otehr than a (1x1) or disordered (1x1) were observed. No evidence was found for an order-disorder surface phase transition.

5. Thermal desorption of Indium

After dosing the crystal with In at 300 K, stepwise desorption was performed by rapidly (< 2 sec) heating the crystal to a preset temperature, holding it at that temperature for 30 sec, cooling the crystal and running an Auger spectrum; the procedure is then repeated, increasing the temperature at each stage, until the surface is clean. The In AES intensity was converted to surface coverage in

monolayers utilizing the calibration described in Section 3. The results of two independent runs are shown in figure 8. In the first (filled circles) the front face of the crystal was covered with In by dosing at a relatively large distance from the In source. In the second (open circles) the crystal was repeatedly dosed at 300 K and annealed at 550-600 K, in an attempt to ensure that both front and back faces of the crystal were covered with In, since, as described in Section 6 below, diffusion of the second layer of In is rapid over macroscopic distances at this temperature. The surprisingly good agreement between the two experiments indicates that there is a negligible influence of diffusion to the back face of the crystal on the overall loss of the adsorbate from the front face as monitored by AES. We conclude that the results in figure 8 refer exclusively to desorption. Also shown in figure 8 is a differential of the coverage vs. temperature plot.

Evaporation from a thick film occurs down to two monolayers over a narrow temperature range, 700 to 800 K; the differential curve, corresponding to a desorption spectrum at $\sim 2\ Ks^{-1}$, produces a peak temperature T_p = 770 K. Desorption of the second and first monolayers occurs over a wide temperature range, from ~800 to 1200 K, giving a broad peak in the differential curve, with T_p = 1050 K. Multilayer evaporation is readily analysed, since, as shown experimentally, by King, Madey and Yates[15], it is a zero order desorption process and can be written as:

$$- d\theta/dt = \nu e^{-E/RT}$$

with both the frequency factor ν and the activity energy E independent of coverage. The data in figure 8 readily yield, from an Arrhenius plot of $\ln(\Delta\theta/\Delta t)$ vs. $1/T$,

$$E = 240 \text{ kJ mol}^{-1}; \quad \nu = 10^{15}\text{sec}^{-1}.$$

The desorption energy is in good agreement with the reported sublimation energy of In (215) kJ mol^{-1}). Analysis of desorption from the second and first monolayers is more complex, since the results are clearly indicative of a strong dependennce of the desorption parameters on surface coverage. However, assuming the same pre-exponential factor as found for the multilayer (10^{15}sec^{-1}), first order desorption, an equivalent heating rate of 2 Ksec^{-1}, and T_p = 1050 K yields $E \sim 340 \text{ kJ mol}^{-1}$. The broad temperature range over which desorption occurs suggests that the desorption energy varies continuously over the range 250 to 350 kJ mol^{-1} as the coverage decreases from θ = 2 to zero.

6. Reactivity of In-covered W{100} to CO and O_2

It was found that a multilayer-dosed surface at 300 K left under uhv conditions over a period of 12 hours showed no impurity peaks in AES. In an effort to investigate the surface reactivity, CO was admitted to a pressure of

5×10^{-8} torr, and Auger spectra recorded after exposures of up to 10^{-4} torr sec. No C or O Auger peaks were ever observed, from which it is concluded that the sticking probability of CO on the indium film is $< 10^{-4}$. The same result was found for O_2. The reactivity experiments were repeated for films with just one monolayer thickness, and the same result was obtained. Clearly all surface W{100} sites are blocked by In at this coverage (since W itself is very reactive in CO and O_2 adsorption.). We conclude that indium very effectively passivates the W{100} surface for CO and O_2 adsorption under these conditions.

7. Surface Diffusion of Indium on W{100}.

7.1 First Layer Diffusion

Surface diffusion of indium was observed and characterised by the following procedure. A small patch (~2 mm diameter) of indium was deposited onto the centre of the cleaned crystal at ~300 K, and the coverage vs. distance profile of the patch was then measured along a fixed azimuth using AES. The crystal was then heated to preset temperatures for increasing periods, quenching to ~300 K after each heating period to again measure the patch profile. A large number of such experiments were performed, varying the diffusion temperature for a given patch coverage, and also varying the patch coverage, over the range $0.5<\theta<2.0$. In all cases, the In AES peak intensity vs. distance profiles were converted to coverage profiles using the calibration

curve, figure 3. The data are analysed to obtain the activation energy for diffusion E_m and the diffusivity D_o, defined by $D = D_o \exp(-E_m/RT)$, where D is the diffusion coefficient.

Data obtained after dosing to coverages at the patch centre of θ_c = 0.5 and 1.0 monolayers, at temperatures of 693 to 750 K, are shown in figures 9 and 10. At these temperatures and coverages no desorption of In occurs, as borne out by the fact that the total area under the coverage vs. distance profiles is independent of annealing time. The shape of the patch after diffusion can be compared with the theoretical predictions of Bowker and King[4]; this gives an immediate qualitative indication that the activation energy for diffusion increases with decreasing coverage. As shown in figures 11 and 12, the change in the full-width-at-half-maximum, Δx, of the patch varies linearly with the square root of time. The gradients of these plots (Δx^2 vs t) may be used in Arrhenius plots to determine the activation energy for diffusion[16], as shown in figure 13. The energy obtained in this way refers to a coverage which is a non-simple average of the coverage across the diffusion boundary. The plot in figure 13 yields E_m = 73 kJ mol^{-1}, and D_o= 0.67 ; the coverage across the profile varies between 0 and 0.5 monolayers, but the value for E is heavily weighted towards ~0.4 monolayers. For the dose with θ_c = 1.0 monolayers, this method yields E_m = 52 kJ mol^{-1}, and D_o = 0.02 cm^2 s^{-1}.

The data can be analysed to yield E_m and D_o as a function of surface coverage, using the expression:[17]

$$\int_a^b (\theta - \theta_o)dx = Dt\left[\left(\frac{d\theta}{dx}\right)_a - \left(\frac{d\theta}{dx}\right)_b\right]$$

where a and b are chosen values of the distance x across the diffusion profile, θ is the coverage at x, and t the diffusion time. θ_o is the value of θ at t = 0. Using this expression to obtain D for a given coverage interval, a plot of lnD vs. 1/T is constructed to produce E_m and D_o corresponding to that coverage (figure 14). This analysis confirms that there is a large decrease in E_m with increasing θ, from $\sim$105 kJ mol^{-1} at θ = 0.25 to $\sim$65 kJ mol^{-1} at θ = 0.75, and, in addition, shows that there is a corresponding decrease in D_o with increasing θ. The data are given in Table 1.

7.2 Diffusion in second and subsequent layers

Preliminary experiments revealed that the second and subsequent layers of In diffused more rapidly that the first layer. For example, figure 15 shows the result of an experiment in which a 2 mm diameter multilayer patch of In was dosed onto the crystal, followed by heating to 700 K for $\sim$80 sec, cooling, redosing, and reheating repeatedly. The patch spreads across the crystal surface, forming a homogeneous monolayer except in the vicinity of the patch itself.

The diffusion of a 2-monolayer patch (θ_c = 2) at 615 K is shown in figure 16. At this temperature, the width of the patch only increases until the coverage across the patch reaches one monolayer, at which point diffusion is effectively terminated. Similar results have been obtained

for Pd and Au[21] diffusion on several tungsten substrates; the results are also strongly reminiscent of the "unrolling carpet" diffusion observed from multilayers of CO and N_2[22] on tungsten field emission tips. Quantitative analysis of the data, such as that in figure 16, is more complex than suggested by previous workers[23], since a distinction must be made between atoms in the second layer, diffusing over first layer atoms with an activation energy E_m', which may be dependent on the second layer coverage, and atoms diffusing in the first layer with the larger activation energy barrier E_m. The diffusion of the two species cannot be readily uncoupled, since there are two coverage gradients and second layer atoms reaching bare sites are instantly converted into first layer atoms. An approximate procedure was used to analyse the data, in which it was assumed that diffusion in the first layer over the times and temperatures employed (510 to 730 K) could be ignored; the coverage in the diffusing second layer species is then obtained as $(\theta - 1)$. Arrhenius plots constructed from the profiles derived in this way are shown in figure 17, and the values of D_o and E_m are given in Table 1. A more satisfactory experiment was performed to obviate the difficulties in this analysis. A homogeneous monolayer of indium was produced across the whole surface of the crystal by repeated high temperature diffusion. A patch of In was then deposited onto this surface, corresponding to $\theta_c = 7$ monolayers, and the patch profile was measured as a function of time at temperatures between 510 and 715 K (figure 18). From

linear plots of $(\Delta x)^2$ vs time obtained from this set of data, an Arrhenius plot was again constructed (also shown in figure 17). The agreement between the results obtained by the two procedures, shown in Table 1, is considered to be very satisfactory. It is concluded that D_o and E_m for In layers beyond a monolayer are insensitive to coverage.

8. General Discussion

The properties concerning the growth, thermal stability and surface diffusion of In films on W{100} which have been determined in this study may be summarised as follows.

1) The growth of an indium film on W{100} by vapour deposition proceeds with a sticking probability which is independent of coverage or layer thickness.

2) At very low fractional coverages of In (<0.02), the W{100}$(\sqrt{2} \times \sqrt{2})R45^o$ surface phase is converted to the (1x1) surface phase.

3) Up to a fractional coverage of ~0.2, In atoms randomly occupy surface sites, forming a two-dimensional lattice gas. As the coverage is increased further, two dimensional islands are formed.

4) The first monolayer is completed before the growth of the second and subsequent layers, and forms a well-ordered (1x1) structure. This complete monolayer renders the surface inert to O_2 and CO adsorption at 300 K.

5) Desorption (or evaporation) of the monolayer occurs over the broad temperature range 900 to 1200 K, indicating a strong dependence of the activation energy for desorption, E_d,

on surface coverage, in the range $350<E_d<250$ kJ mol^{-1}.

6) No incorporation of In into the tungsten crystal, or alloy formation, was observed at any temperature.

7) Surface diffusion up to monolayer coverage occurs with an activation energy E_m and diffusivity D_o which are both strongly dependent on fractional coverage. At $\theta = 0.25$, $E_m = 106$ kJ mol^{-1}, dropping to 64 kJ mol^{-1} at $\theta = 0.75$. The activation energy barrier to diffusion is thus roughly a constant fraction of that to desorption, i.e. ~30%.

8) As the film thickness is increased beyond a monolayer, no sharp AES break points are observed which could be associated with layer-by-layer growth, indicating an uneven development of film thickness. Even after annealing to relatively high temperatures, no ordered structures could be observed. Beyond the first monolayer, the film is disordered.

9) Evaporation from a thick film down to the monolayer region occurs over a narrow temperature range, 700 to 800 K. The desorption energy (240 kJ mol^{-1}) is close to the reported sublimation energy for In.

10) Surface diffusion in the second and subsequent layers occurs with $E_m = 23$ kJ mol^{-1} and $D_o = 3 \times 10^{-3}$ $cm^2 s^{-1}$, i.e. E_m is ~10% of the desorption energy.

Combining the diffusion study with the results pertaining to the growth mode of the indium film produces a coherently detailed model. Indium atoms colliding with an indium-covered region of the surface apparently have the same trapping probability as those arriving at free tungsten sites; but

they are highly mobile (with a hopping frequency of 10^8 s^{-1} even at 200 K) and are therefore rapidly equilibrated with the surface layer. If the total coverage is less than a monolayer, equilibration strongly disfavours the retention of multilayer atoms, since the adsorption energy for monolayer atoms ($\sim$300 kJ mol^{-1}) is significantly greater than that for multilayer atoms (240 kJ mol^{-1}). (This energy difference gives a Boltzmann factor advantage, $e^{\Delta E/RT}$, at 300 K of 10^{10}). Formation of the monolayer thus proceeds via the mobile precursor mechanism originally proposed by Taylor and Langmuir[18] from studies of Cs adsorption on W, and presently favoured for many adsorption systems. The unrolling carpet effect noted in the diffusion studies from initial multilayer patches is a clear manifestation of this effect, coupled with the relative immobility of the first layer. The radom development of layers subsequent to the first is a reflection of the insensitivity of adsorption energy to layer thickness, at least beyond the second layer. There is no energy advantage from layer-by-layer growth.

The absolute values of the diffusion parameters obtained in the present work bear some comment. The strong coverage dependence in the activation energy for diffusion is paralleled by a strong variation in the desorption activation energy (and hence the adsorption energy) with coverage. Both results are consistent with a repulsive nearest neighbour lateral interaction energy of $\sim$20 kJ mol^{-1}.[4] The values of E_m in the monolayer region are consistently $\sim$30% of the In bond energy; in contrast studies of the diffusion of individual

metal adatoms in the field ion microscope on W and Rh [19] single crystal surfaces have yielded diffusion energyes which are consistently in the region of 5 to 10% of the bond energy. Clearly, the energy profile for In atoms across W{100} shows an unusually high degree of roughness, with presumably a strong preference for the four-fold hollow site. The repulsive interaction between adatoms is a consequence of the lattice misfit in the eptiaxial layer: the n.n. distance in bulk In is 3.24 Å, which is compressed to 3.16 Å in the first (ordered) layer on W{100}.

There is an apparent discrepancy between our conclusion that there are strong repulsive interactions between n.n. In adatoms in the first layer, and our prior conclusion that growth of the first layer proceeds by island formation above a fractional coverage of ~ 0.2. However, film growth was observed at temperatures of 200 and 300 K, where the first layer is immobile and hence non-equilibrated. The distribution of occupied first layer sites is entirely determined by the adsorption kinetics, and island growth is a direct consequence of trapping into a mobile second layer at filled sites, and spillover into the immobile first layer at the island boundary.

In the multilayer region, the energy barrier to surface diffusion is considerably smaller than in the first layer, and is also a smaller percentage of the bond energy ($\sim$10%). In this sense the value is more in line with metal atom surface diffusion energies reported in the literature, although it is the lowest absolute value reported to date.

The diffusivities D_o also vary strongly with coverage. Absolute values can be discussed in relation to the expressions

$$D_o = \nu a^2/2\alpha$$

and $$\nu = (kT/h)\exp(\Delta S/R)$$

where $\alpha = 1$ for diffusion in one dimension, and $\alpha = 2$ in two dimensions; a^2 is the mean square jump distance, over a barrier with an activation entropy ΔS. The observed variation in D_o between 0.64 cm^2s^{-1} at $\theta = 0.25$ and $1.3 \times 10^{-3} cm^2s^{-1}$ in the multilayer region thus corresponds to a variation in the frequency factor ν from $2 \times 10^{16} s^{-1}$ to $7 \times 10^{13}\ s^{-1}$, which can in turn be attributed to a coverage-dependent ΔS, between 80 J $mol^{-1}K^{-1}$ and 20 J $mol^{-1}K^{-1}$. There would appear to be a strong correlation between E_m and ΔS, which can be empirically represented as:

$$\Delta S = E_m/T_b,$$

where T_b is a constant with the units of K. This relation has often been previously reported from kinetic studies on surfaces, and is known as a compensation effect[20]; this is, however, the first time it has been noted in relation to diffusion.

REFERENCES.

I. C.F. Smart, Trans.AIME,Tech.Publ. 900(I938).

2. J.M. Freund, H.B. Linford and P.W. Schutz, Trans.Electrochem.Soc. 84(I943)650.

3. D.A. King, J.Vac.Sci.Tech.,I7(I980)24I.

4. M. Bowker and D.A. King,Surf.Sci. 7I(I978)583, 72(I978)208.

5. M. Bowker and D.A. King,Surf.Sci.,94(I980)564.

6. A. Cassuto and D.A. King,Surf.Sci.,I02(I98I)288.

7. D.A. King, Physica Scripta, in press.

8. M.K. Debe and D.A. King, Surf.Sci.,8I(I979)I93.

9. K. Griffiths and D.A. King, J.Phys.C.Solid State Phys.,I2(I979)L34.

I0. E. Bauer and H. Poppa,Thin Solid Films,I2(I974)I67.

II. M.P. Seah and W.A. Dench,Surface and Interface Analysis,I(I979)2.

I2. J.M. Van der Merwe,Proc.Roy.Soc.,(London)I98A(I949)205,2I6.

I3. T. Ichikawa, Surf.Sci.,III(I98I)227.

I4. O. Nishikawa,M. Wada and M. Konishi, Surf.Sci.,97(I980)I6.

O. Nishikawa,Jap.J.Appl.Phys.Suppl 2,Pt. 2,(I974)37.

I5. D.A. King, T.E. Madey and J.T. Yates,J.Chem.Phys.,55(I97I)3247.

I6. J. Crank,The Mathematics of Diffusion, Clarendon Press,London,I956.

I7. R.C. Bosworth, Proc.Roy.Soc.,AI54(I936)II2.

I8. J.B. Taylor and I. Langmuir, Phys.Rev.,44(I933)423.

I9. G. Ehrlich and F.G. Hudda,J.Chem.Phys.,44(I966)I039.

G. Ayrault and G. Ehrlich,J.Chem.Phys.,60(I974)28I.

20. M.A. Morris, M. Bowker and D.A. King, The Kinetics of Adsorption, Desorption and Diffusion, in Comprehensive Chemical Kinetics, eds, C.H.F. Tipper and C.H. Bamford, Elsevier, North Holland.

21. R. Butz and H. Wagner, Surf.Sci., 87(1979)69,85.

22. R. Gomer, R Wortman and R. Lundy, J.Chem.Phys., 26(1957)1147.

23. P. Akhter and J. Venables, Surf.Sci., 103(1981)301.

Table 1

The activation energy for diffusion, E_m, and diffusivity D_o for In on W{100}

Coverage θ (monolayers)	E_m (kJ mol^{-1})	D_o cm^2 s^{-1}
0.25	106	0.64
0.50	79	0.179
0.75	64	0.030
1-2	22.2	0.003
1-7	24.9	0.0013

Fig.I. The indium source. W is a W ribbon and T the In loaded tubes.

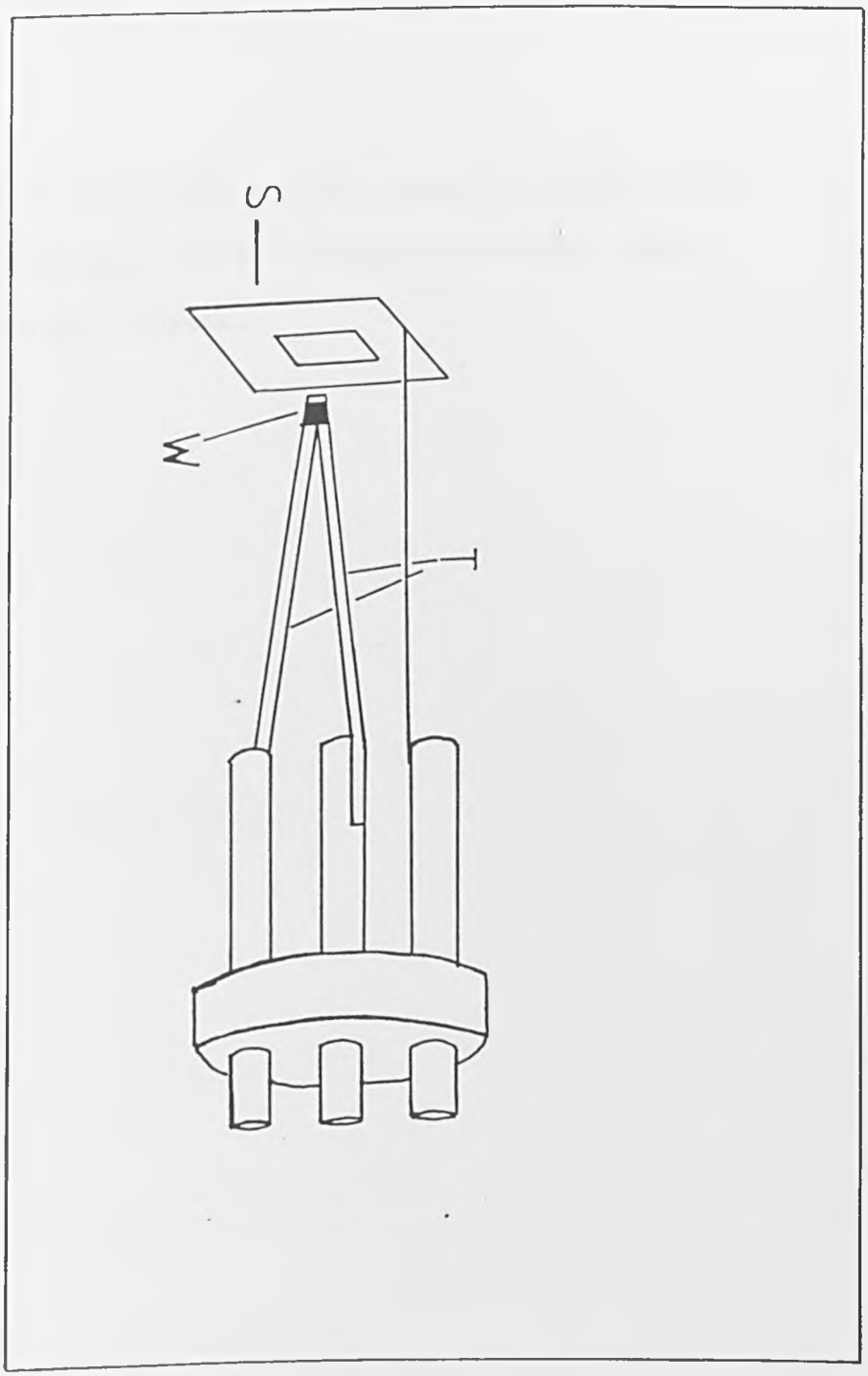
S
W

Fig.2. Auger spectrum from an In dosed W {100} crystal (derivative mode). Primary beam energy of 2keV at a current of 5μA and recorded with a modulation voltage of 5V peak-to-peak.

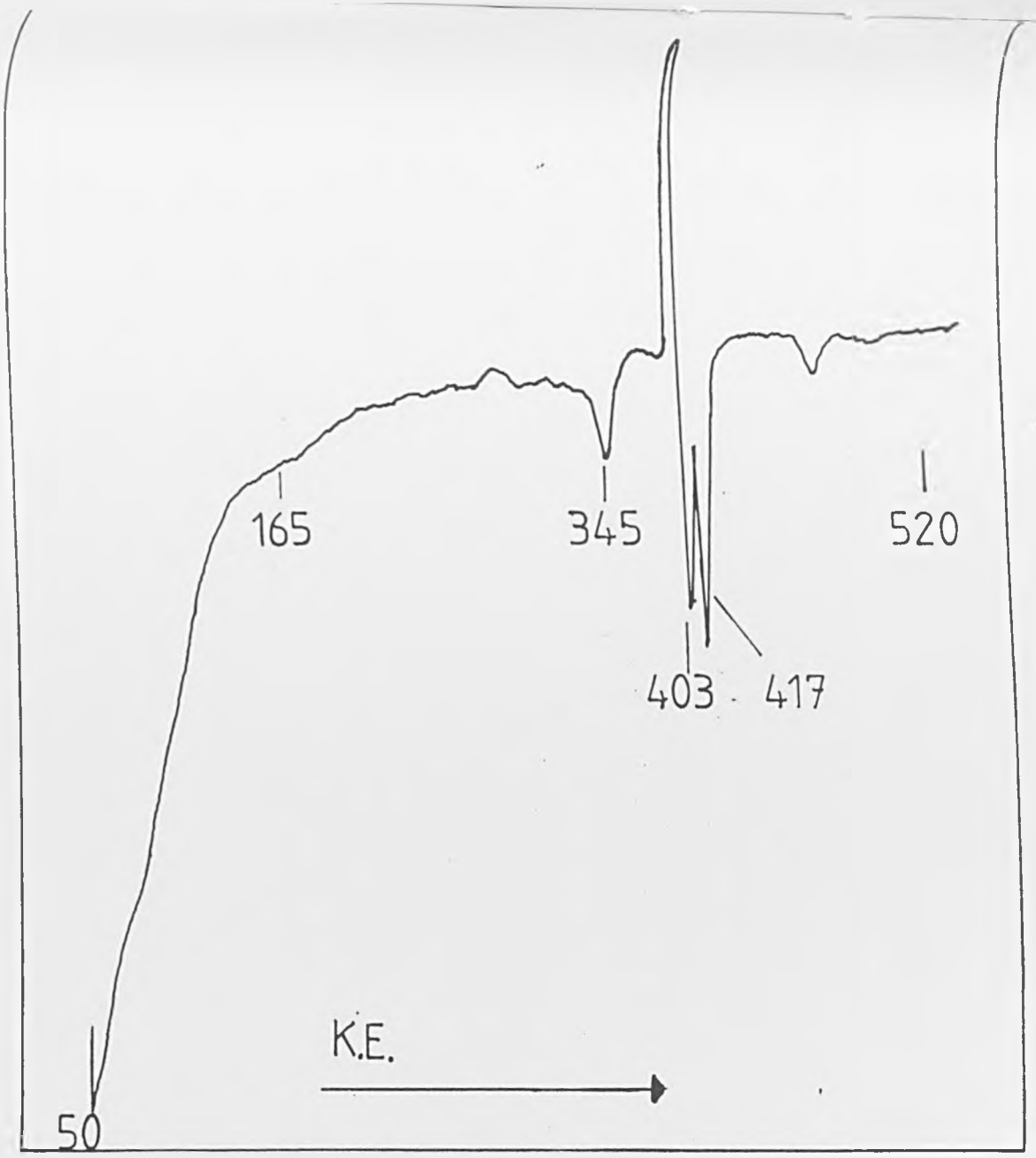
165
345
520
403
417
50
K.E.

Fig.3. The increase in the AES peak-to-peak height as a function of dose time. The inset is an exspansion of the data at low dose times (0-5min).

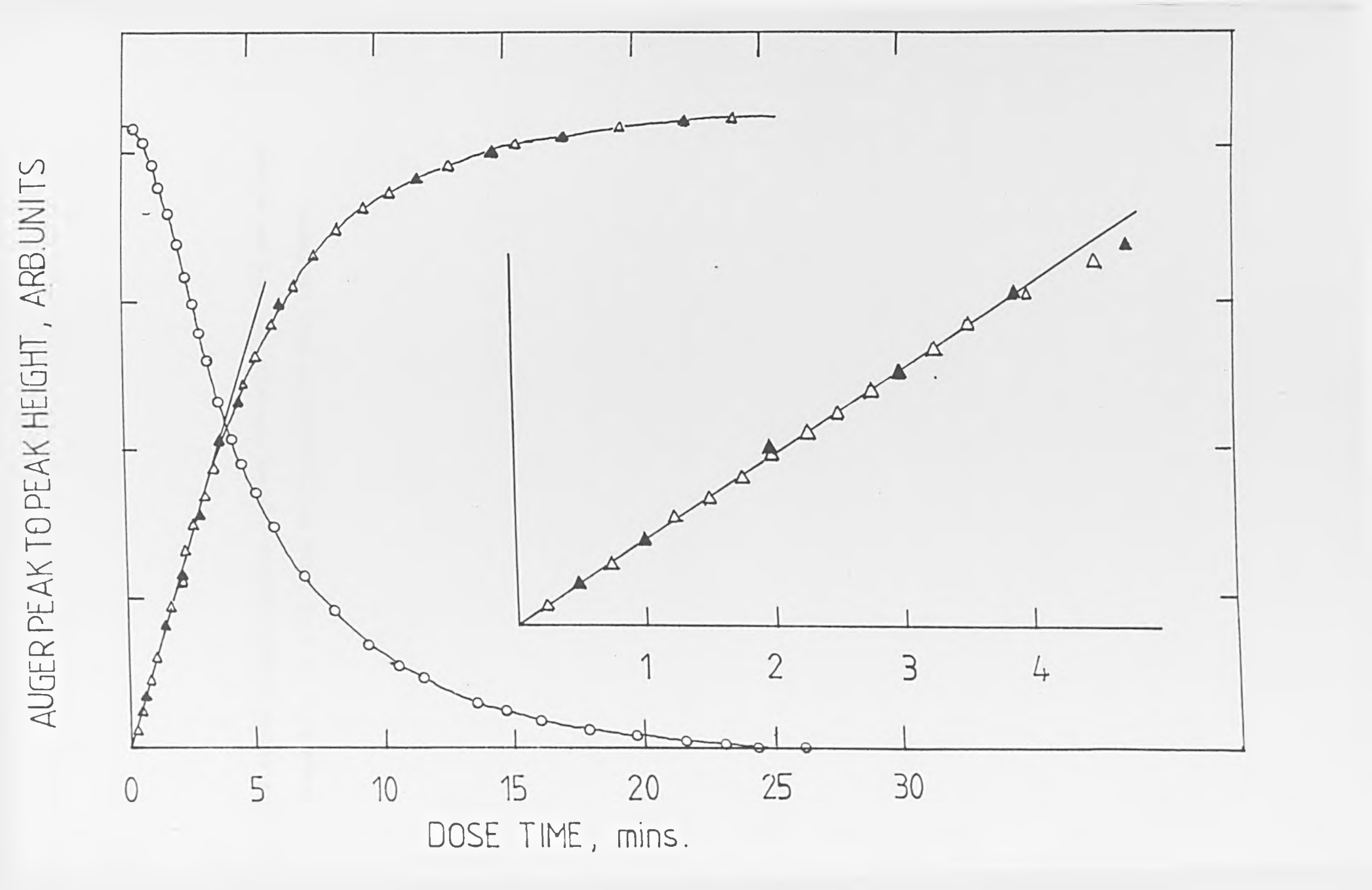
AUGER PEAK TO PEAK HEIGHT, ARB.UNITS
0
5
10
15
20
25
30
DOSE TIME, mins.
1
2
3
4

Fig.4. AES signal heights plotted against coverage (————) and a best fit lineshape (- - - - - -) using the formulism of Seah and Dench.

AUGER PEAK TO PEAK HEIGHT, ARB. UNITS.
1
2
3
4
5
6
7
8
COVERAGE, MONOLAYERS.

Fig.5. The geometric effect in AES.

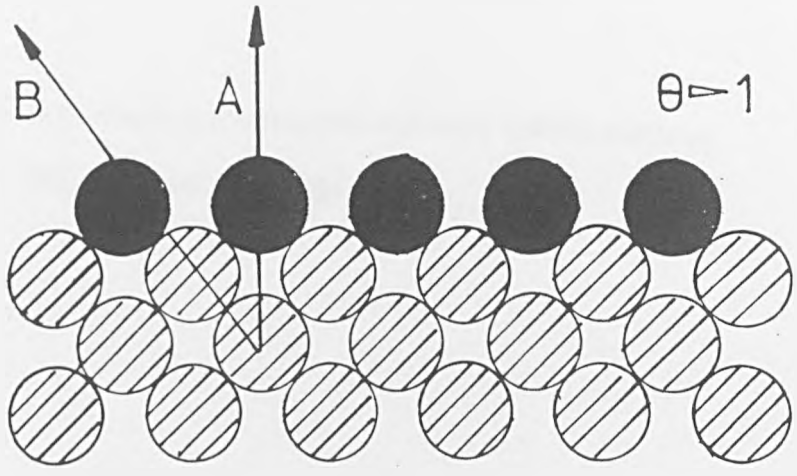
B
A
θ=1

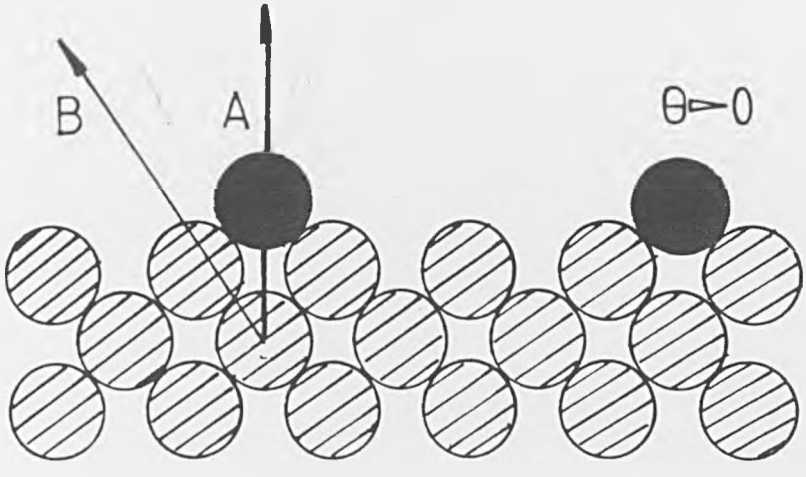
B
A
θ=0

Fig.6. The change in secondary electron emission current (ΔI), ratioed to the total drain current (I), versus coverage.

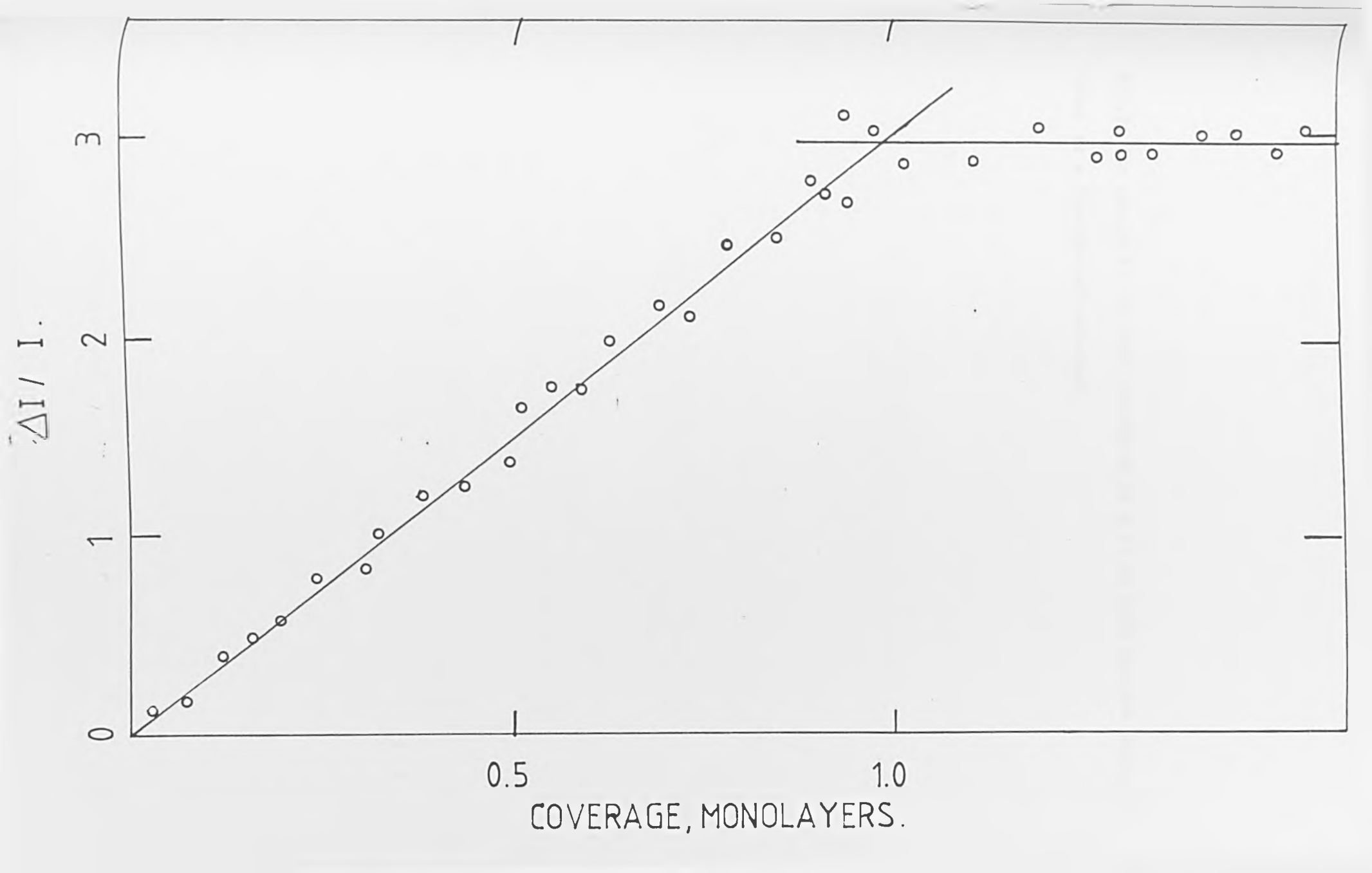
ΔI / I.
0
1
2
3
0.5
1.0
COVERAGE, MONOLAYERS.

Fig.7. The change in the LEED intensity of a (I,O) beam and the background level as a function of coverage.

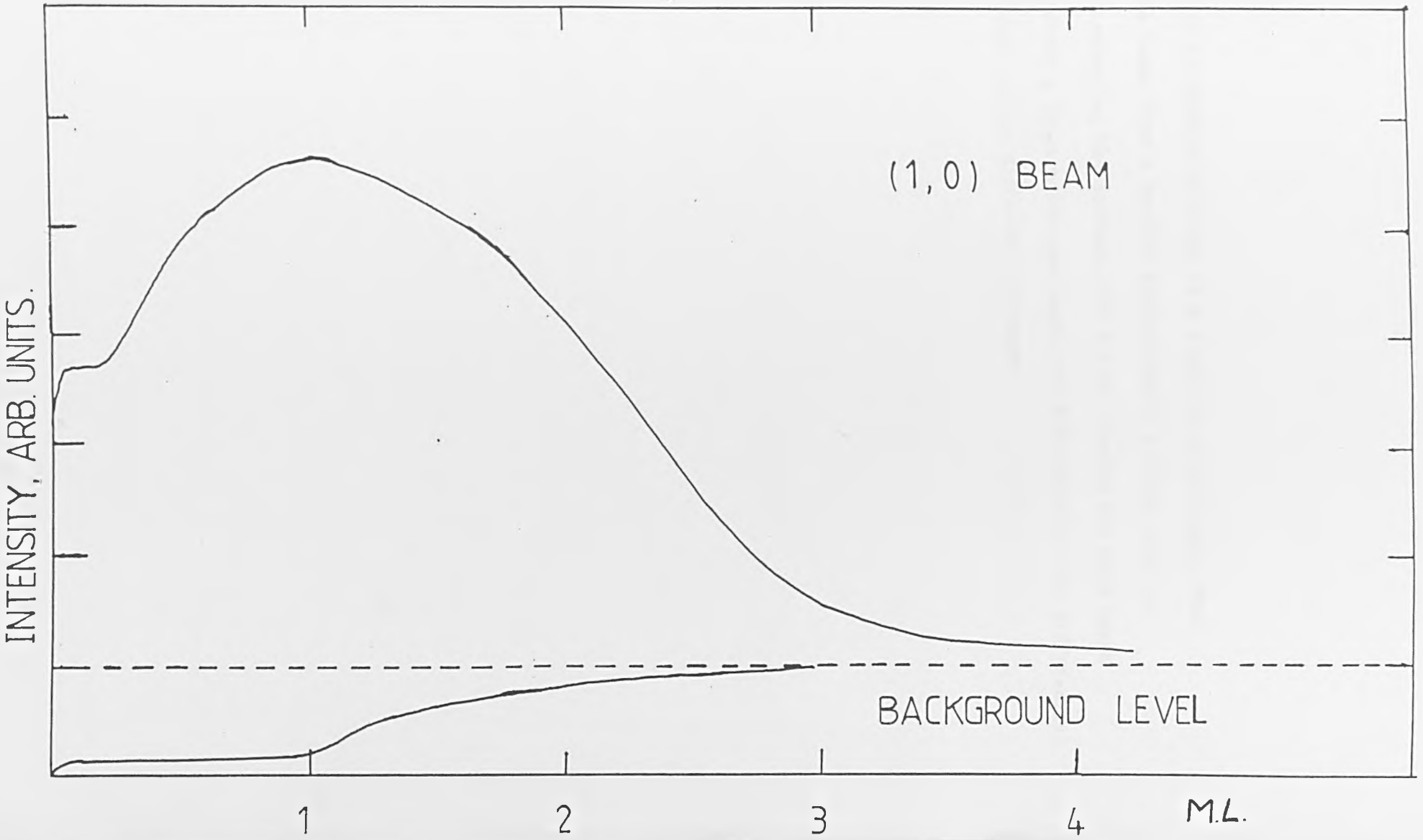
(1,0) BEAM
INTENSITY, ARB. UNITS.
BACKGROUND LEVEL
1
2
3
4
M.L.

Fig.8. The change in surface coverage as a function of coverage. Open circles are data taken from a surface homogeneously covered with In from dosing and annealing the surface. The filled circles are data taken from a surface where a large patch was deposited. Also shown is the differential form of these graphs at two different coverages.

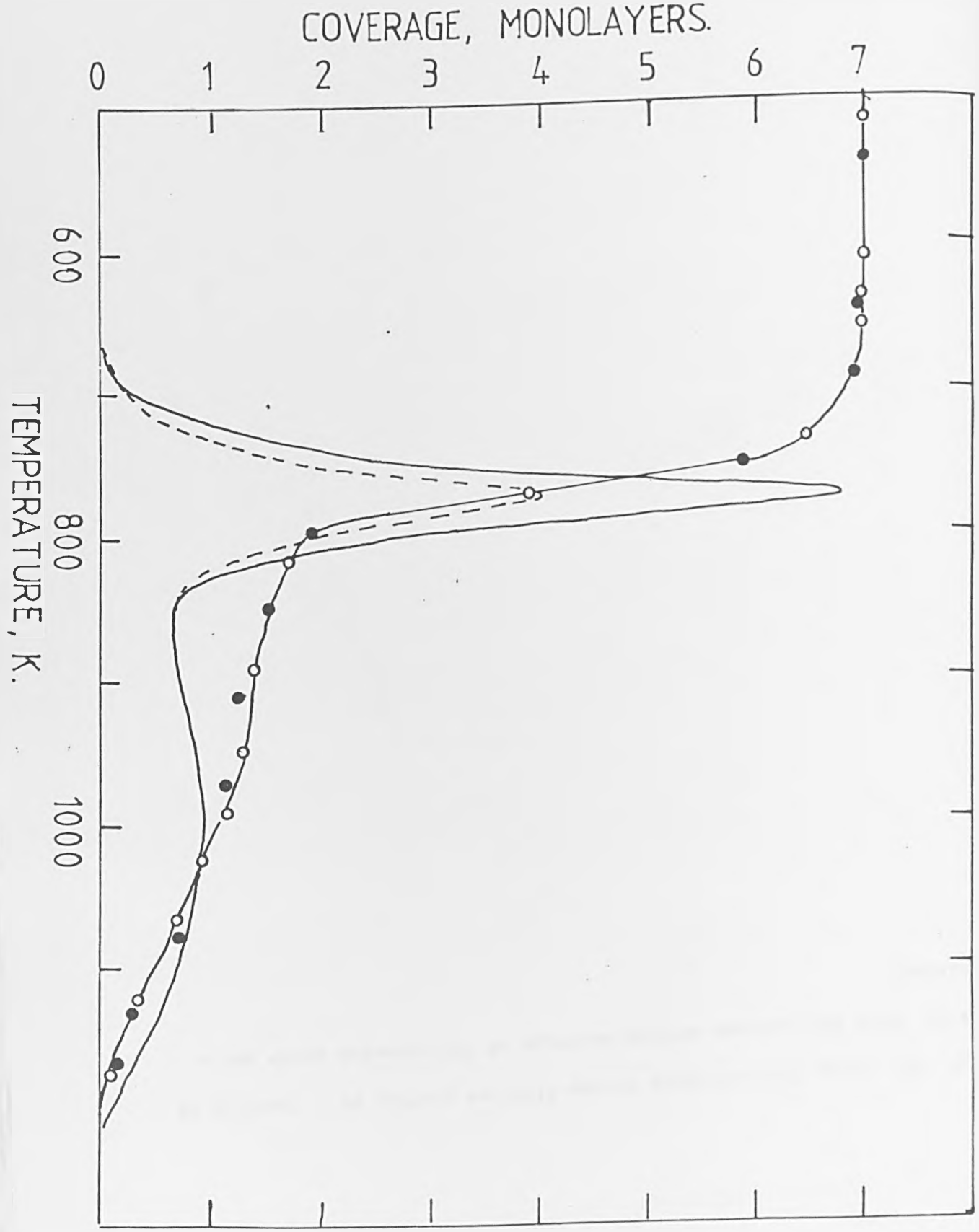
COVERAGE, MONOLAYERS.
0
1
2
3
4
5
6
7
600
800
1000
TEMPERATURE, K.

Fig.9. The change in a coverage versus distance profile as a function of heating. Here the maximum surface coverage of the unheated patch was a monolayer.

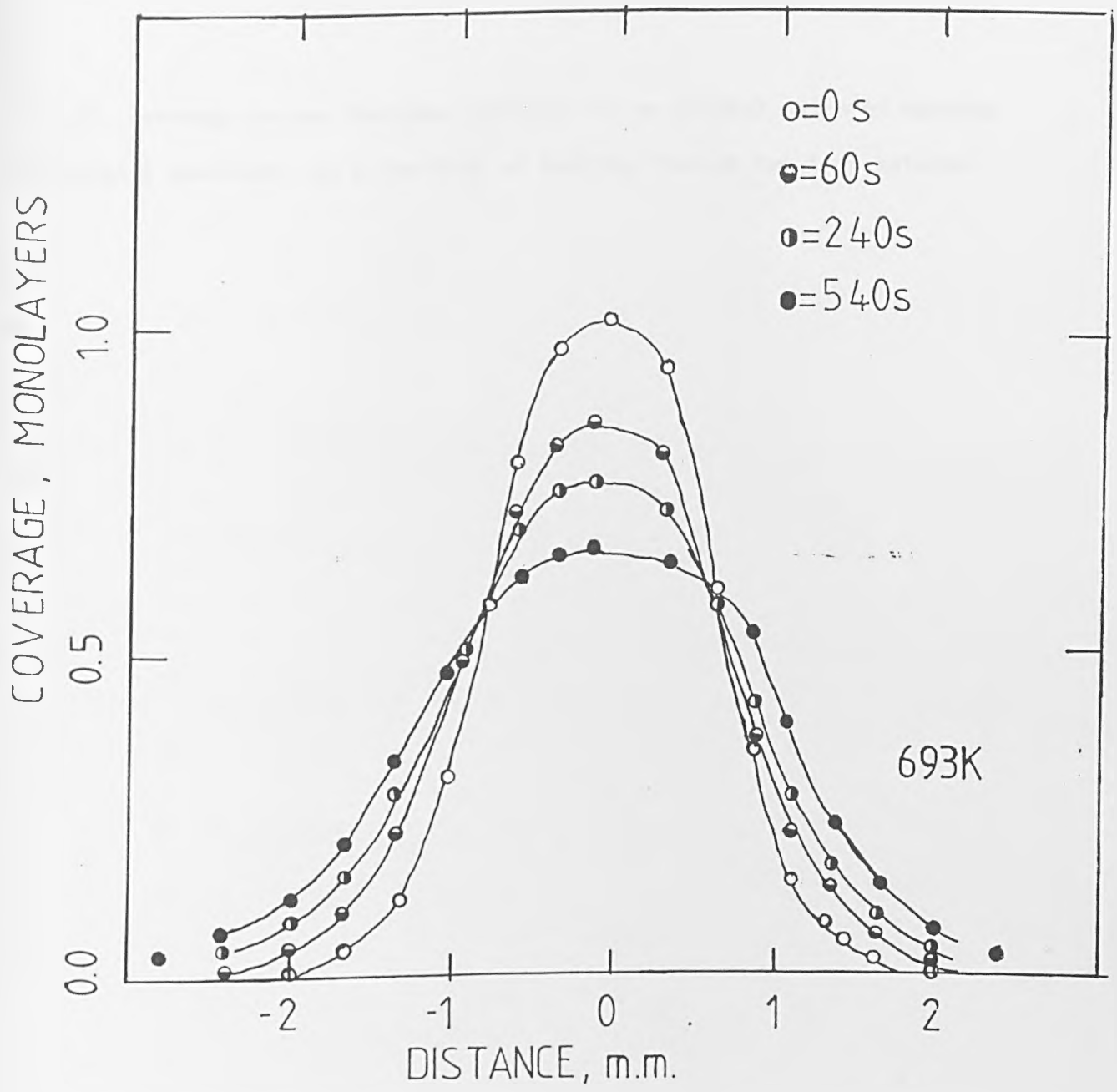
o=0 s
=60s
=240s
=540s
693K
COVERAGE, MONOLAYERS
0.0
0.5
1.0
-2
-1
0
1
2
DISTANCE, m.m.

Fig.IO. Coverage versus distance profiles for an initial patch of maximum coverage $\frac{1}{2}$ monolayer, as a function of heating time at two temperatures.

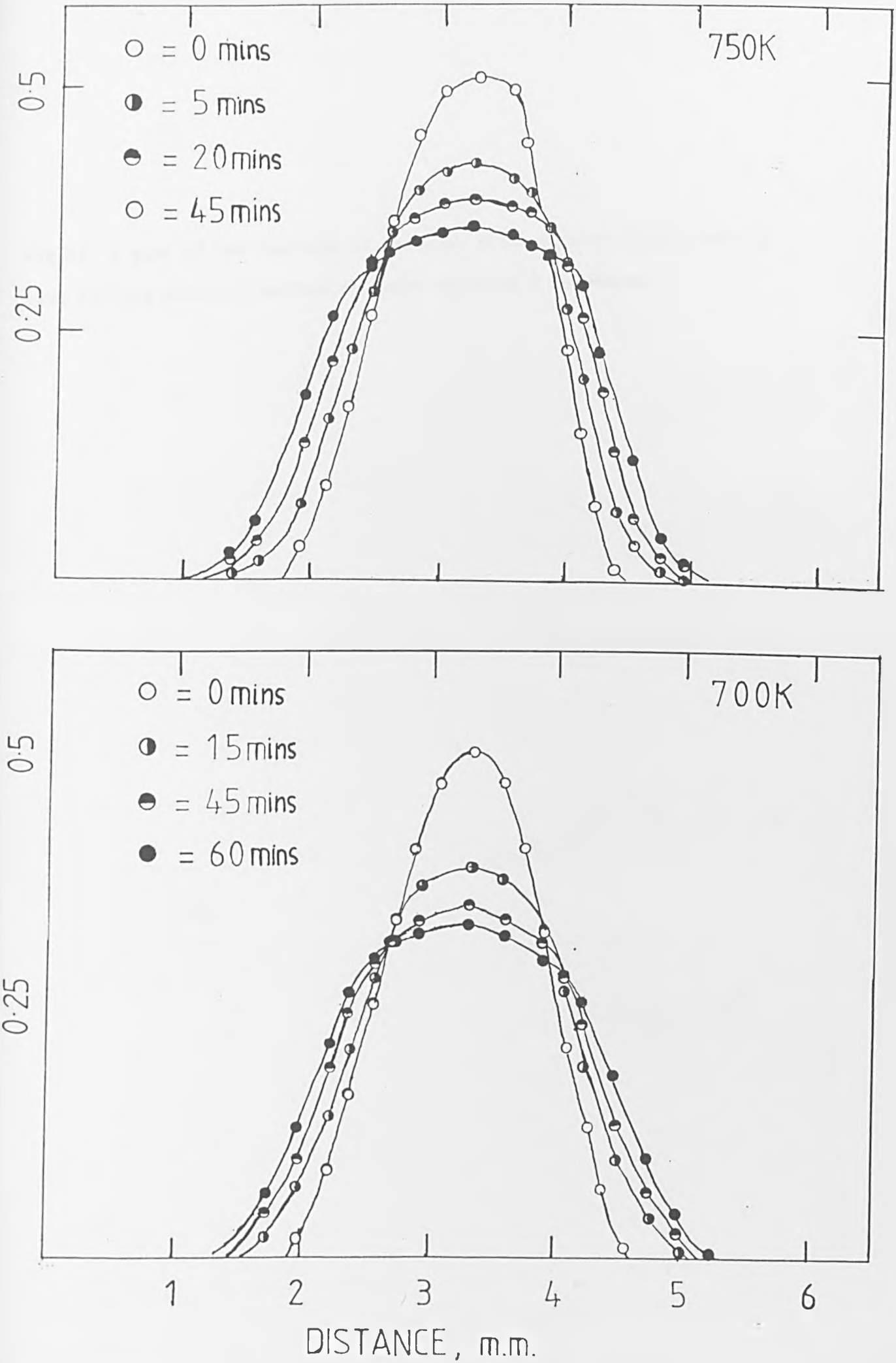

COVERAGE, MONOLAYERS.

Fig.II. A plot of the increase of the peak width squared versus heating time for the patch of maximum coverage equal to $\frac{1}{2}$ monolayer.

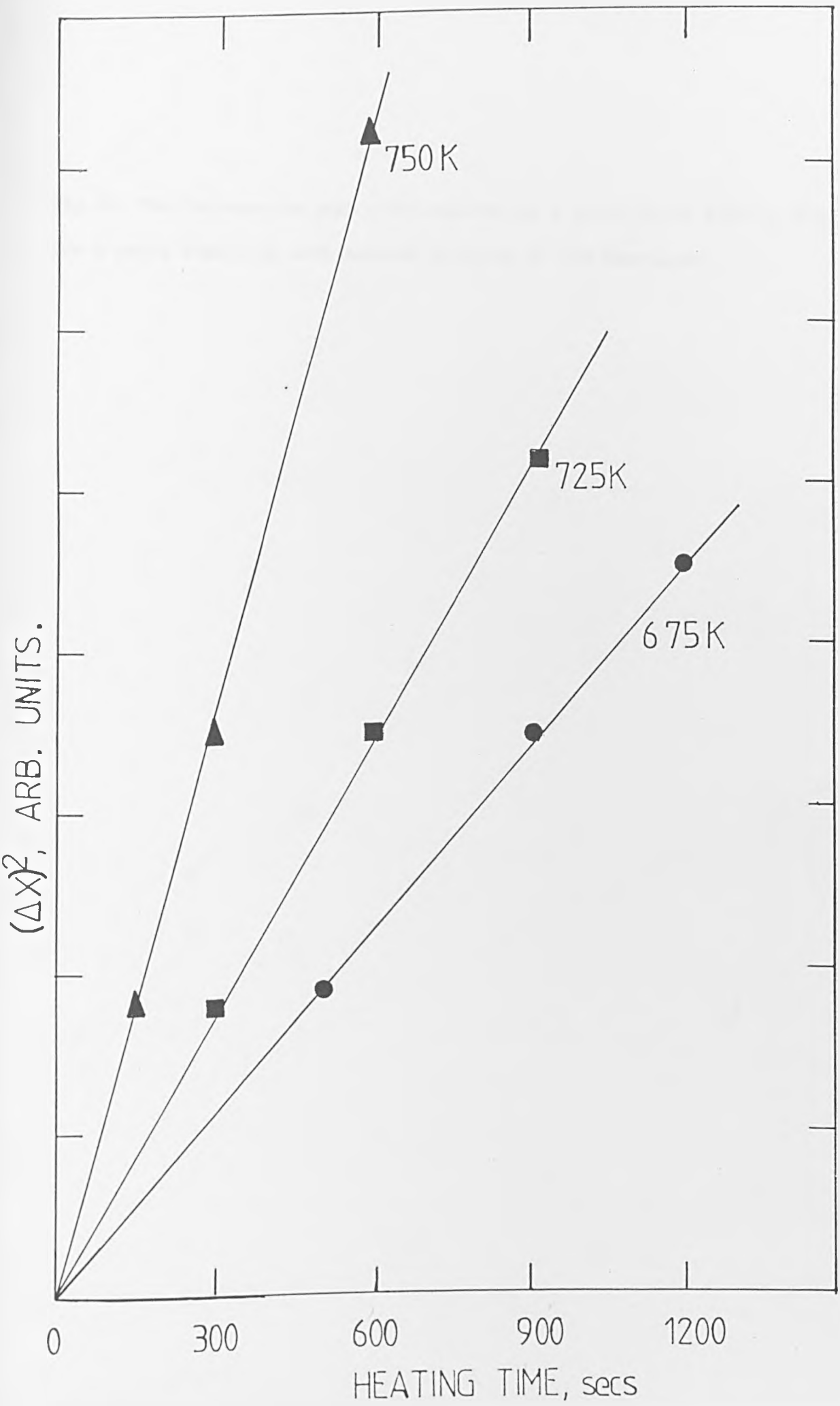
750 K
725K
675K
$(\Delta x)^2$, ARB. UNITS.
0
300
600
900
1200
HEATING TIME, secs

Fig.I2. The increase in peak width squared as a function of heating time for a patch deposited with maximum coverage of one monolayer.

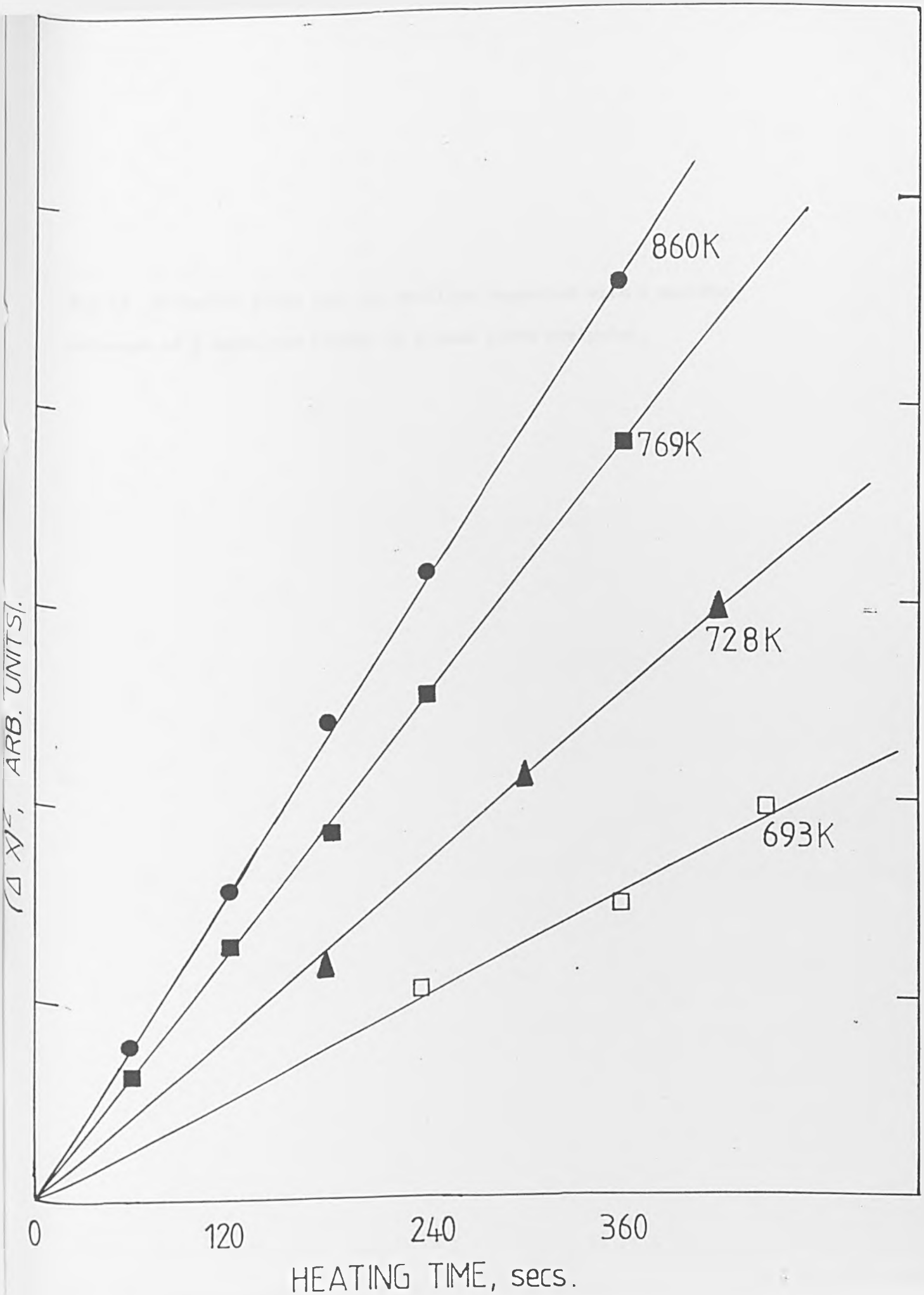
860K
769K
728K
693K
0
120
240
360
HEATING TIME, secs.
(Δ X)², ARB. UNITS].

Fig.13. Arrhenius plots for the profiles deposited with a maximum coverage of $\frac{1}{2}$ monolayer (based on a peak width analysis).

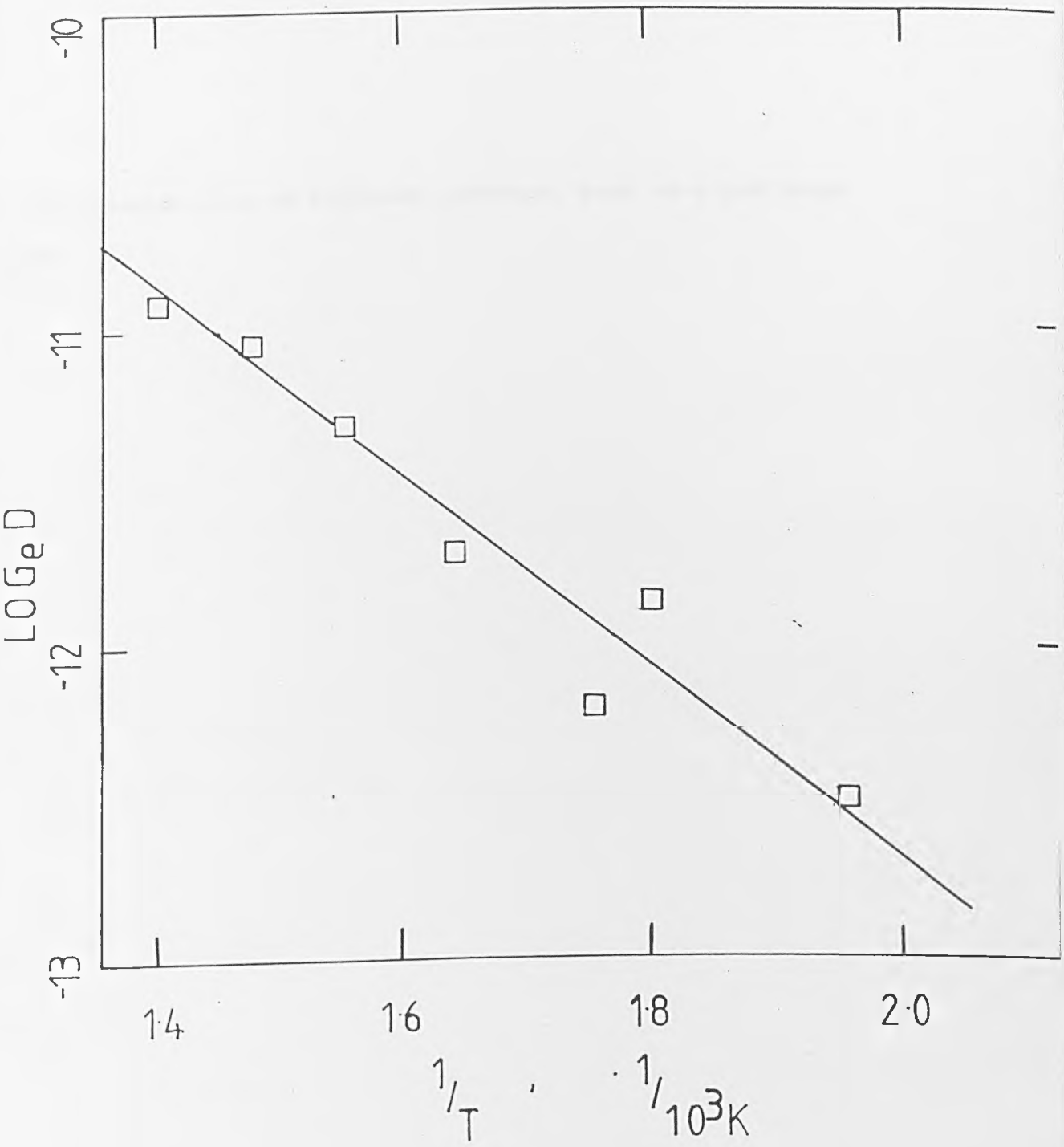
-10
-11
-12
-13
LOGeD
1·4
1·6
1·8
2·0
1/T
1/10³K

Fig.I4. Arrhenius plots at different coverages, based on a peak shape analysis

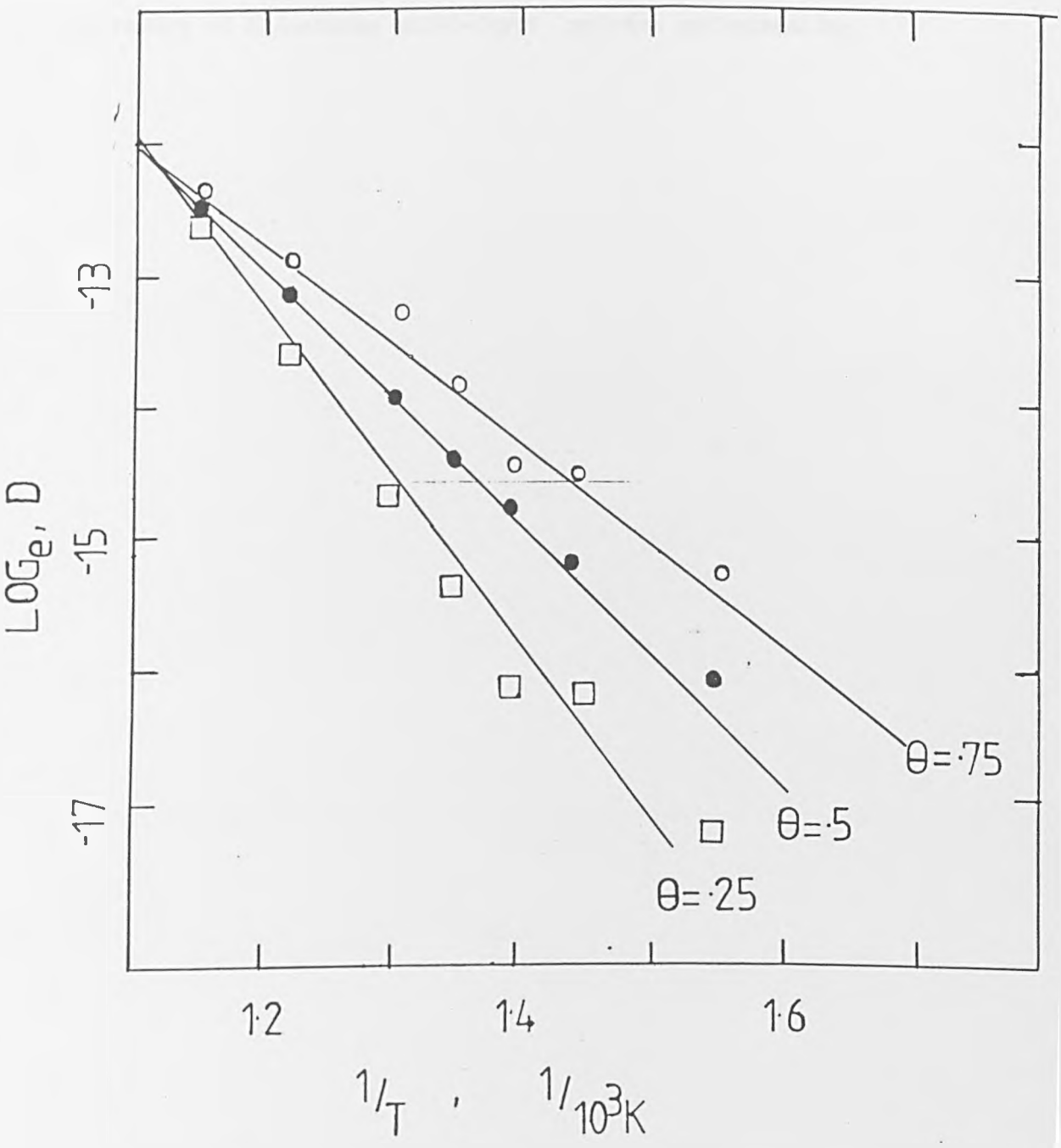
LOG$_e$, D
-13
-15
-17
θ=·75
θ=·5
θ=·25
1·2
1·4
1·6
1/T , 1/10^{3}K

Fig.15. The result of depositing multi-layer patches and annealing to 700K.

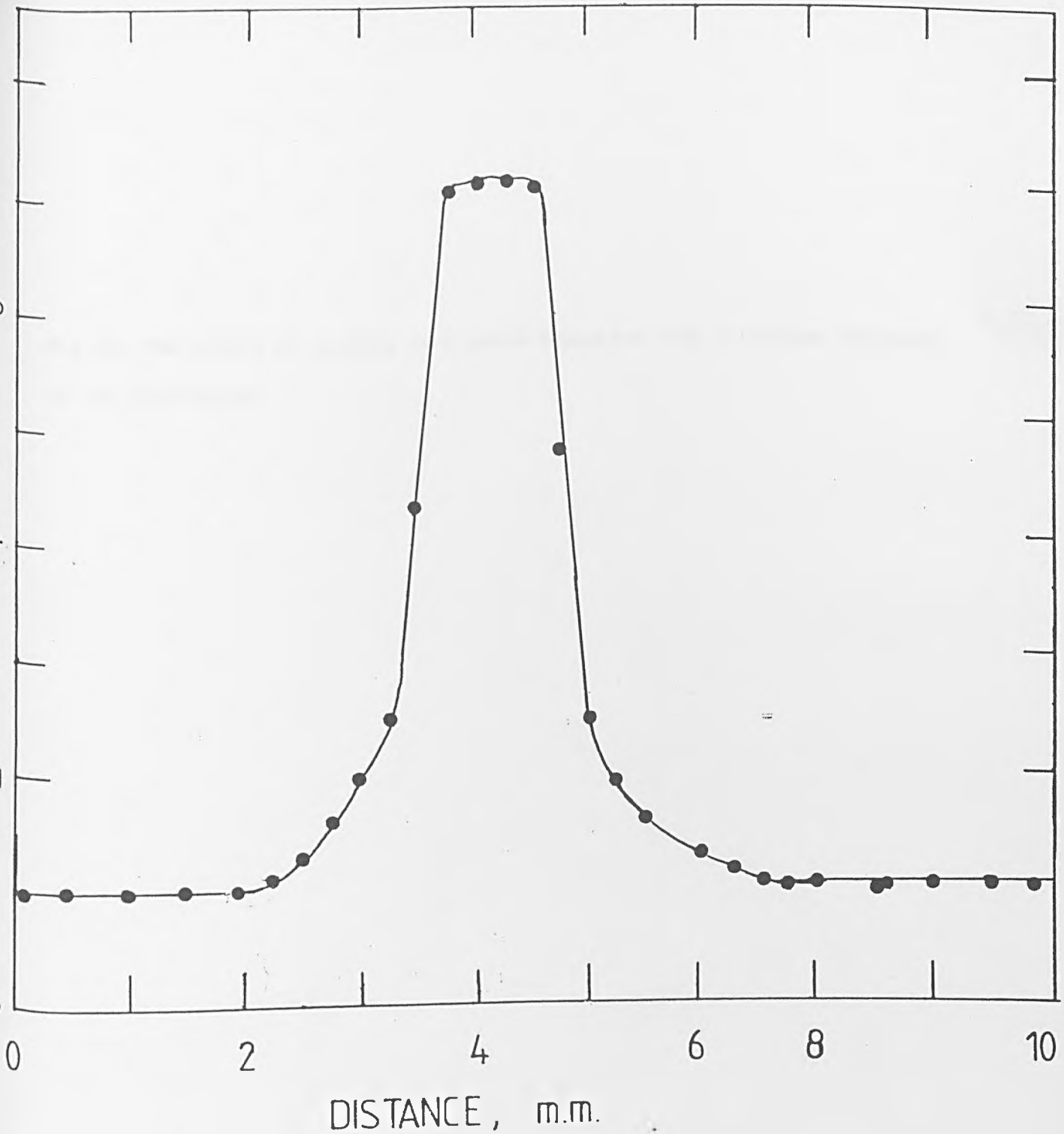
0
2
4
6
8
10
DISTANCE, m.m.

Fig.16. The effect of heating on a patch deposited with a maximum coverage of two monolayers.

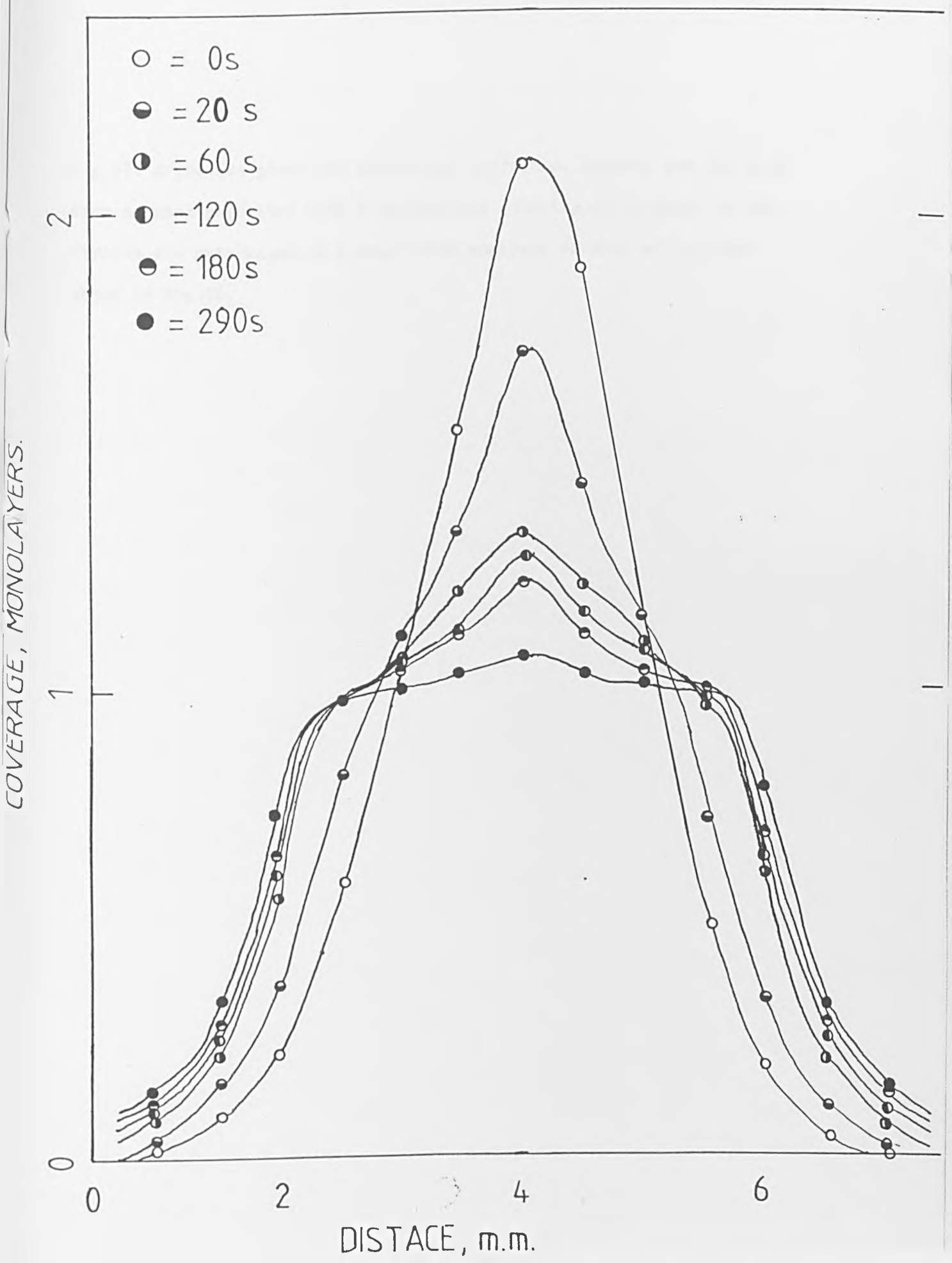
○ = 0s
◒ = 20 s
◑ = 60 s
◐ = 120 s
◓ = 180s
● = 290s
COVERAGE, MONOLAYERS.
0
1
2
0
2
4
6
DISTACE, m.m.

Fig.I7. Arrhenius plots for multilayer diffusion. Squares are the data from a patch deposited onto a homogeneous covering of In equal to one. Circles are data based on a peak width analysis of data of the type shown in Fig.I6.

LOG e D
-10
-11
-12
-13
1·4
1·6
1·8
2·0
1/T . 1/10³K

Fig.I8. The change of a In patch deposited onto a surface, covered with a one monolayer layer of In, as a function of temperature.

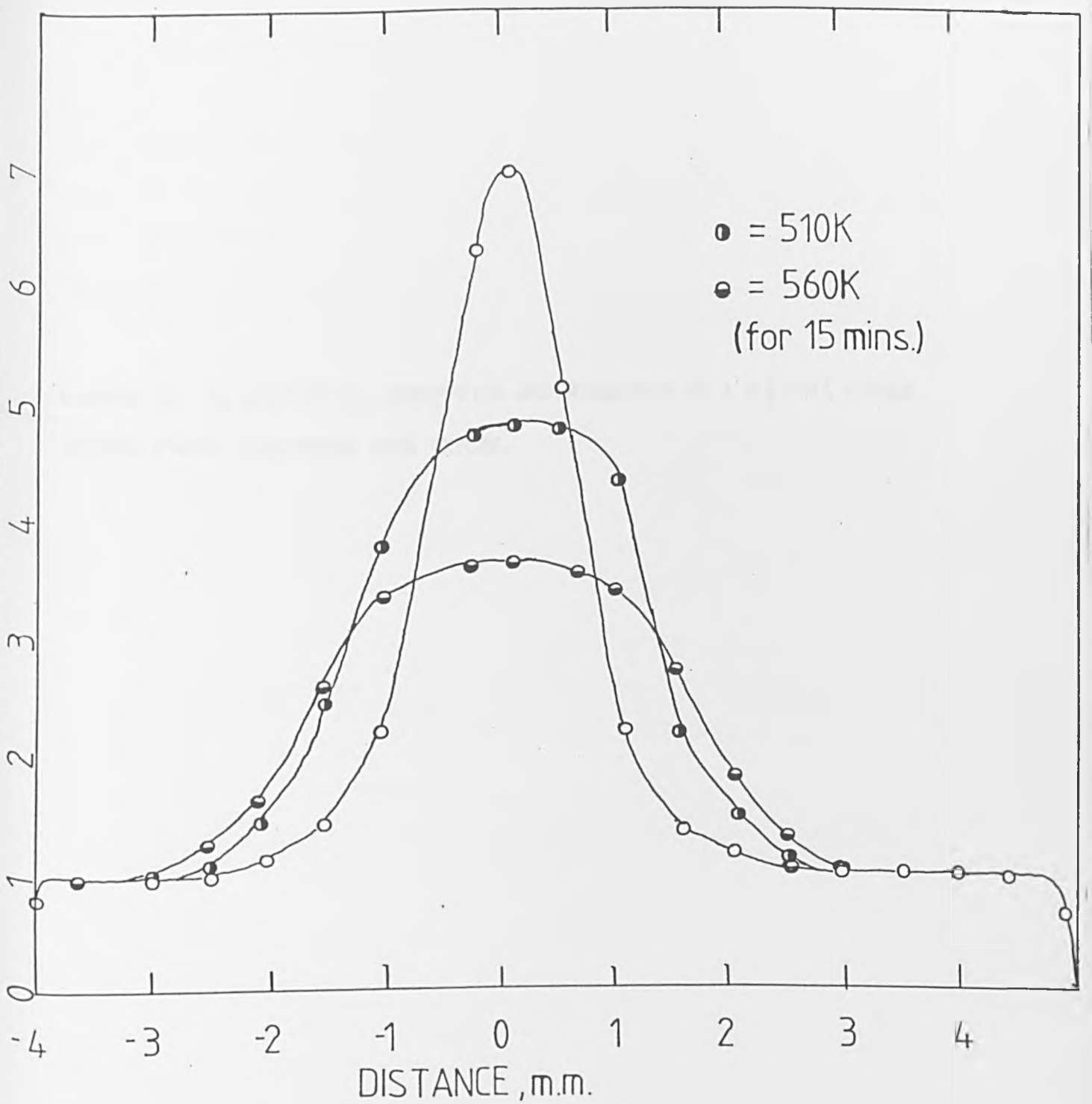
= 510K
= 560K
(for 15 mins.)
0
1
2
3
4
5
6
7
-4
-3
-2
-1
0
1
2
3
4
DISTANCE, m.m.

CHAPTER 7: In ADSORPTION, DESORPTION AND MIGRATION AT A W {100} SINGLE CRYSTAL PLANE. PRECOVERED WITH OXYGEN.

Indium adsorption, desorption and migration at a W{100} single crystal plane precovered with oxygen.

M.A. Morris, C.J. Barnes and D.A. King.

The Donnan Laboratories,

Liverpool University,

Liverpool, L69 3BX,

England.

I. Experimental.

The stainless steel UHV system, the retarding-field-analyser for LEED and AES, and the gas dosing arrangement has been described elsewhere.[1] The sample in both investigations was the same, a 1.5 x 0.5 cm W single crystal cut and polished to within $\frac{1}{2}^{o}$ of the {100} plane. The crystal was cleaned by the usual methods[2]. Oxygen adsorption was achieved via random dosing through a large diameter gate valve. O_2 is admitted to the system through a mercury pumped, UHV, gas-handling line from research grade gas bottles, the purity being checked using a mass spectrometer[1]. Sample temperature control and measurement was as described earlier[1].

2. Introduction.

In a recent study the adsorption of In on to a W {100} single crystal plane was investigated[1] and the results are summarised here.

a) Initially In adsorbs into a pseudomorphic (1 x 1) layer with the number of In sites equal to the number of {100} sites.

b) The first layer grows via 2D island growth. Subsequent layers condense via the formation of 3D islands and these layers are disordered.

c) In films show no signs of alloying with the W surface.

d) In passivates the layer to CO and O_2 adsorption.

e) Desorption takes place in two stages, one corresponding to the loss of In multilayers, the other to the loss of In from the first layer. The desorption energies are 200 and 275 KJ mol^{-1} respectively and the former value is close to the sublimation energy of In.

f) As the surface coverage of In increases the migration of In, in the first layer, takes place with a continually decreasing activation energy.

g) Diffusion in the second and higher layers is very much faster than in the first layer.

h) Within the first layer repulsive lateral interactions exist between the adatoms.

The present study has been prompted by two major reasons. Firstly, the coadsorption system Metal/Oxygen-Metal has shown many interesting effects for some alkali metals [3] e.g. the formation of a double layer for Cs/O/W [6], and the formation of high order LEED patterns for mixed adsorption layers [3]. Secondly, the diffusion of an electropositive species in the presence of an electronegative species should be interesting both, theoretically and with an aim to explain material transport in catalytic systems.

3. Results.

Formation of the precovered oxygen surface took place as follows. The crystal was saturated at a pressure of 10^{-7} torr and then annealed at this pressure, at 1400K. On cooling a sharp p(2 x 2) LEED pattern was observed. It is well known that the O/W {100} system shows a number of structures at various temperatures, [5-12] and these are associated with surface reconstruction, overlayer and oxide formation. In the current investigation the highest temperature phase was used so that the surface was stable when heated in diffusion experiment. The p(2 x 2) has been shown to be made up of contributions from a p(2 x 1) and a c(2 x 2) [8] and the coverage in this phase can be taken as 1.25 monolayers. The surface structure of this phase is uncertain but almost certainly the substrate {100} structure has undergone severe reconstruction [5-12].

AES was used to investigate In adsorption on to the p(2 x 2)-O surface. The peak-to-peak derivative heights of Auger spectra were used as a measure of coverage using the calibration curves reported earlier [I]. With the same bombardment rate as used in the earlier investigation, the rate of growth of the In signal was the same up to the monolayer point. After this the In signal increased slowly compared to the results for In deposition on the clean W {100} surface. The results are shown in Fig.1.

The horizontal scale is in τ ,the time taken to complete a monolayer on the clean surface. The surface reaches a maximum coverage of I.6 monolayers (ML).Such a result may be explained in terms of a decreasing sticking probability [13], but this is not so here. Fig.2. shows the apparent coverage of the surface as a function of heating time at 700K. Clearly the surface coverage of In increases as the surface is heated, and the coverage reached is close to the value that would have been achieved for clean surface adsorption. After this the coverage drops again, presumably due to desorption. Similar curves were taken at various temperatures and an Arrhenius plot of the log reciprocal time to reach a monolayer versus the reciprocal time can be used to estimate the activation energy of this process. This is shown in Fig.3 and yields a value of 62 ± 8 KJ mol^{-1}. Information on this process can be found by close examination of the oxygen peaks. Formulism developed by Seah [14] allows the escape depth of electrons λ_e to be calculated from the distance and the type of material through which the electrons have to pass. It can be written,

$$\lambda_e = (538d/E^2) + 0.4Id(dE)^{\frac{1}{2}},$$

where E is the escaping electron energy and d the monolayer distance, normally taken as the cube root of the volume per atom. So λ_e for 5I0eV electrons escaping through In is 3.3 monolayers. The attenuation of an AES signal is given by,

$k = \exp(-H/\lambda_e \cos\theta)$ where H is the number of monolayers and θ is an angle to account for the collection of electrons and the analyser geometry($\theta = 42^o$ for an RFA); k can be evaluated as 0.66 if H=I This compares with an experimentally measured value of 0.68 ± 0.05, thus it seems that the first layer of In sits above the oxygen-tungsten surface.

Auger peak lineshapes and their positions have long been known to be

sensitive to chemical enviroment . In the present work, no shifts in the O,W or In peaks were ever observed, although the high modulating voltages used here (5V peak-to-peak) may have obscured such effects, and for the same reason lineshape comparisons were not made. Instead the width of the recorded Auger peaks was used. These results are shown in Fig.4. The In peak is not shown since its width remained unchanged by the presence of O or annealing and the O peaks were not recorded because of a lack of sensitivity. The figure shows that the W peak broadens considerably when the p(2 x 2)-O phase is formed, presumably because of the reconstruction of the W {100} surface. In adsorption on to this surface causes the peak to narrow and if the surface is annealed to restore the In to the surface, the width decreases to a value close to that recorded on the clean {100} surface.

LEED observations were also made. The p(2 x 2)-O pattern $\frac{1}{2}$ order spots fade as the In coverage increases until at a coverage of $\theta = 1$ only the (1 x 1) spots can be seen. During this process the background continually increases. Further adsorption seems to produce a negligible change in the pattern. Heating the surface to ever increasing temperatures maintains (1 x 1) symmetry until faint c(2 x 2) spots associated with the clean surface appear.

Desorption experiments were performed using the AES derivative height to monitor the coverage. The p(2 x 2)-O layer was prepared and then dosed with In for excessively long times. The surface was then annealed to increasing temperatures for 30s intervals monitoring the amount remaining after each heating interval. These results are shown in Fig.5. The first process occuring is the restoration of the In to the surface layers and it is important to note that that the O signal does not attenuate very strongly during this process, indicating that the O remains close to the

outermost layers or spread throughout the In multilayers. The In signal then drops very suddenly from the maximum value until the coverage reaches $\theta = 1$ when the rate of decrease slows considerably. During the rapid decrease of the In signal the O AES signal is also strongly attenuated. Using the sudden decrease of the In signal an approximate value of the desorption energy can be found using the equation,

$$\frac{d\theta}{dt} = -\nu\theta \exp(-E_d/RT)$$

where θ is the relative coverage, t the heating time, R the gas constant and T the temperature. If ν, the preexponential is assumed to be 10^{13} s^{-1}, E_d evaluates to about 260 kJ mol^{-1}. For the slower In loss the corresponding value is 308 kJ mol^{-1}. Treatment of the O data yields a value of 230 kJ mol^{-1}.

Because of the effects noticed here it was only possible to calculate diffusion parameters below $\theta = 1$. This was done by depositing an In patch on to the surface and scanning the patch across the AES beam using accurate micrometers on the manipulator. The crystal could then be heated and the patch rescanned to look for diffusion effects. The maximum coverage in the patch was set at $\theta = 1$ ML. Typical results for a spreading patch at a temperature of 680k for differing times is shown in Fig.6. The general diffusion equation can be written,

$$D = D_o \exp(-E_m/RT)$$

where D is the diffusion coefficient, D_o the diffusivity and the activation energy for diffusion is E_m. The diffusion mechanism can be found by plotting the increase in peak width squared versus heating time; if the process is a random walk type then these plots should be straight lines. Experimentally this was found to be true as Fig.7 shows. The slopes of these graphs can be used as the Y-axis in Arrhenius plots and such a plot is shown in Fig.8. From this graph $E_m = 27.9$ kJ mol^{-1} and $D_o = 1.45 \times 10^{-3}$ $cm^2 s^{-1}$, but note that

these are average values over the whole coverage range.

Bosworth [16] has derived a method to obtain activation energies as a function of coverage from profiles such as obtained here. Using the equation,

$$\int_a^b (c-c)dx = Dt \left[(dc_o/dx)_a - (dc_o/dx)_b \right]$$

dc/dx is the change in coverage with distance and a and b are two ordinates of c in a coverage versus distance graphs; c_o is the initial value of the coverage at t = 0. Thus, the integral on the left hand side is the change in the total amount of adsorbate from a to b. E_m can be found at any coverage by plotting the log of D versus I/T at this coverage. Results were evaluated at θ = 0.75, 0.5 and 0.25. The Arrhenius plots are shown in Fig.8 and the resultant activation energies and diffusivities are shown in table I.

4. Discussion.

Results are presented here for the adsorption of In on the W {100} p(2 x 2)-O surface and these indicate that the system is far from simple. Adsorption up to θ = I appears to be fairly simple; In layer sitting above the O is formed. The Leed pattern is a simple (I x I) at all energies and this persists as the In is desorbed, indicating that the In layer in some way rearranges the oxygen layer so that a In layer, pseudomorphic with the substrate (I x I) surface, can grow. The rearrangement of the oxygen-tungsten layer is reflected in the decrease in width of the W AES peak.

Above θ = I the rearrangement becomes even more complicated. Very little of the adsorbing In is equilibrated near the surface. Since the oxygen signal is only weakly attenuated during this incorporation stage

we can conclude that the oxygen remains close to the surface but the In is incorporated into the W lattice. The transport of In may be via grain boundaries but it is more likely that the first layer of In causes the pathway to be opened by substrate rearrangement, since there was no sign of any similar effects for the In/W {100} system[I].

Whatever the structure of this arrangement it is clear that by imputing an energy of about 62kJ mol^{-1} it can be dramatically altered and most of the incorporated In can be equilibrated at the surface again. These multilayers formed are not of the same type as the condensed multilayers examined earlier[I]. This is apparent since, the desorption energies are higher; the oxygen AES signal is not strongly attenuated by the multilayer formation (indicating that the oxygen is distributed through the overlayers); and the persistence of the (I x I) leed pattern is much greater than for adsorption on the clean surface. These results lead us to postulate that this structure is some In-O alloy bound to the W substrate. The desorption energies of these layers for both O and In are fairly close and it is likely that the "alloy" rather than separate species is desorbed. The activation energy needed to form this structure may be associated with the energy necessary to break the strong W-O bonds.

The diffusion results are much more easily explained. The diffusion energy is considerably reduced compared to diffusion at the same coverages observed on the clean surface, although the diffusion energy still decreases as a function of coverage. The decrease in diffusion energy can be explained in terms of electron transfer to the O layer, increasing the charge on the In adatoms and thus increasing the repulsive lateral interactions between the In atoms and lowering the diffusion energy[17.] This effect may be combined with a surface roughening effect which has been shown to reduce the activation energy for surface diffusion[18,19,20].

The values of D_o noticed here are close to those predicted if the

entropy of the activation is negligible and that the length of the surface hop is close to the lattice spacing.[21] As the coverage increases there is an increase in the value of D_o but it is very small, in contrast with the clean surface results which showed a large increase. This may be because of the difference in the chemistry of the surfaces; if the peak in D_o for the clean surface is associated with the increased disorder of the 2nd and subsequent layers this peak will be very much reduced because of the stronger order noticed in the In multilayers earlier. This is, of course, only a very tentative explanation.

REFERENCES.

I. M.A. Morris, C.J. Barnes and D.A. King, to be published.

2. M.K. Debe and D.A. King, Surf. Sci.,8I(I979)I93.

3. P.R Davis,Surf.Sci.,9I(I980)385.

4. W Jost,Diffusion in Solids,Liquids and Gases, Academic Press, New York, I980.

5. P.J. Estrup and J. Anderson,Surf.Sci.,8(I967)IOI.

6. C.A. Papergeorgopoulus and J.M. Chen,Surf.Sci.,39(I973)3I3

7. A.M. Bradshaw, D. Menzel and M. Steinkilberg, Jap.J.Appl.Phys.Suppl. 2.Pt 2(I974)84I.

8. E. Bauer, H. Poppa and Y. Viswanath, Surf.Sci.,58(I976)5I7.

9. T.E. Madey,Surf.Sci.,33(I972)355.

IO. S. Prigge, H. Niehus and E. Bauer, Surf.Sci.,75(I978)635.

II. H. Kramer and E Bauer, Surf.Sci.,92(I980)53, 93(I980)407.

I2. J. Holz and J. Schafer, Surf.Sci.,I08(I98I)L387.

I3. M.A. Morris, M. Bowker and D.A. King, The Adsorption,Desorption and Diffusion at Metal Surfaces, in Comprehensive Chemical Kinetics, eds. C.H.F. Tipper and C.H. Bamford, Elsevier, North Holland.

I4. H.P. Seah, Surf.Sci.,32(I972)703.

H.P. Seah and W.A. Dench, Surface Interface Analysis,I(I979)2.

I5. J.P. Coad and J.C. Riviere, Proc.Roy.Soc.London A 33I(I972)403.

G.F. Amelio, Surf.Sci.,22(I970)30I.

I6. R.C. Bosworth, Proc.Roy.Soc.,I54A(I936)II2.

I7. M. Bowker and D.A. King,Surf.Sci.,7I(I978)583.

I8. M. Drechsler, L. Elektrochem,58(I954)340.

I9. L.W Swanson,R.W Strayer and L.E. Davis, Surf.Sci.,9(I968)I65.

20. C.F. Kirk and G. Ehrlich, J. Chem.Phys.,48(I968)I465.

2I. H.Uttsugi and R. Gomer,J.Chem.Phys,37(I962)I706.

TABLE I.

θ	0.75	0.5	0.25	
E_m	25.0 ± 5	25.0	47.0	$KJ\ mol^{-1}$
D_o	4.23×10^{-4}	4.23×10^{-4}	8.25×10^{-3}	$cm^2\ s^{-1}$

Fig.I. The apparent surface coverage of In (I_{In}) (estimated from a calibration reported earlier) versus the monolayer time.

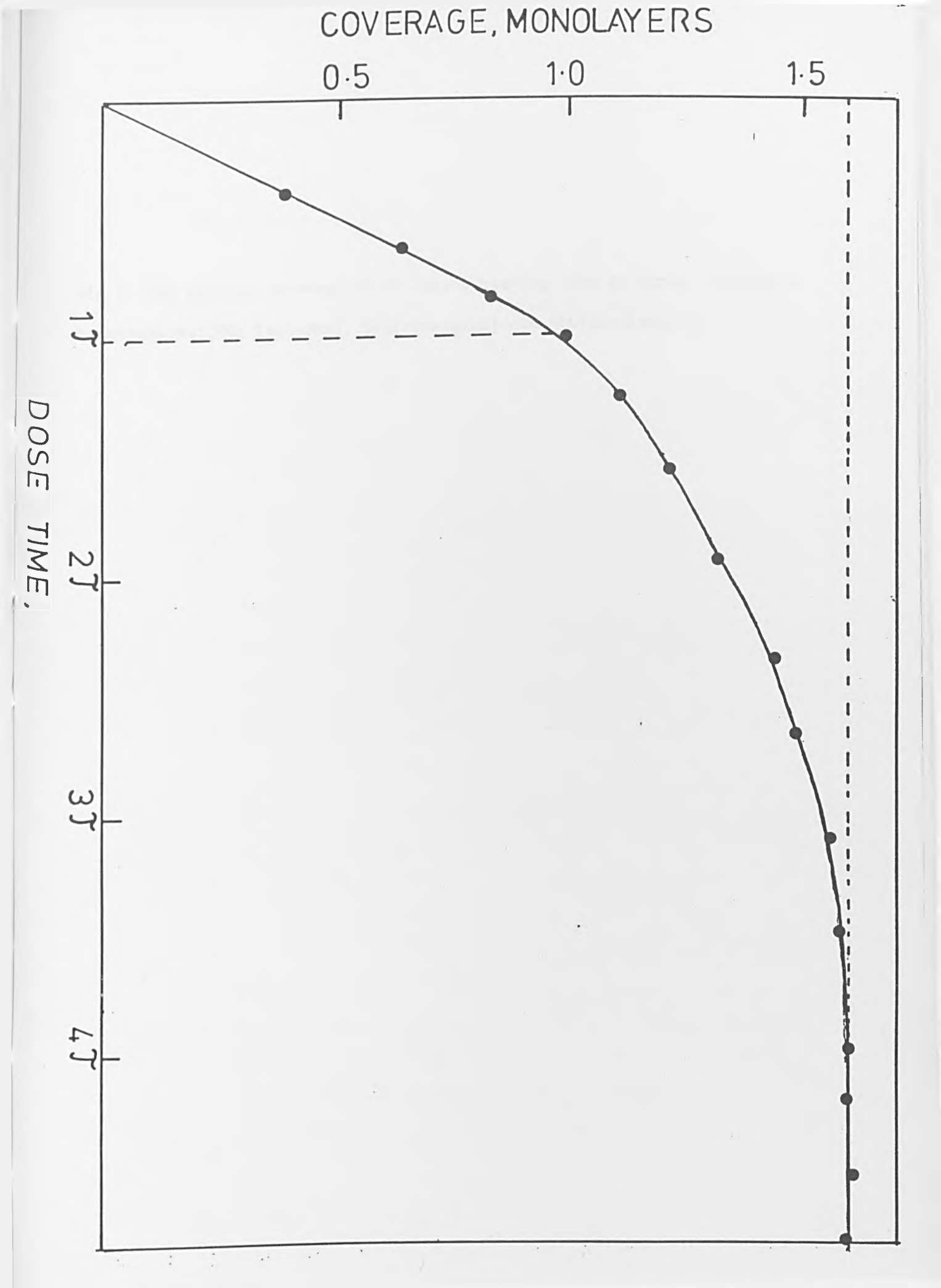
COVERAGE, MONOLAYERS
0·5
1·0
1·5
DOSE TIME,
1τ
2τ
3τ
4τ

Fig.2. The surface coverage of In versus heating time at three different temperatures;700k (squares), 585(triangles) and 560(circles).

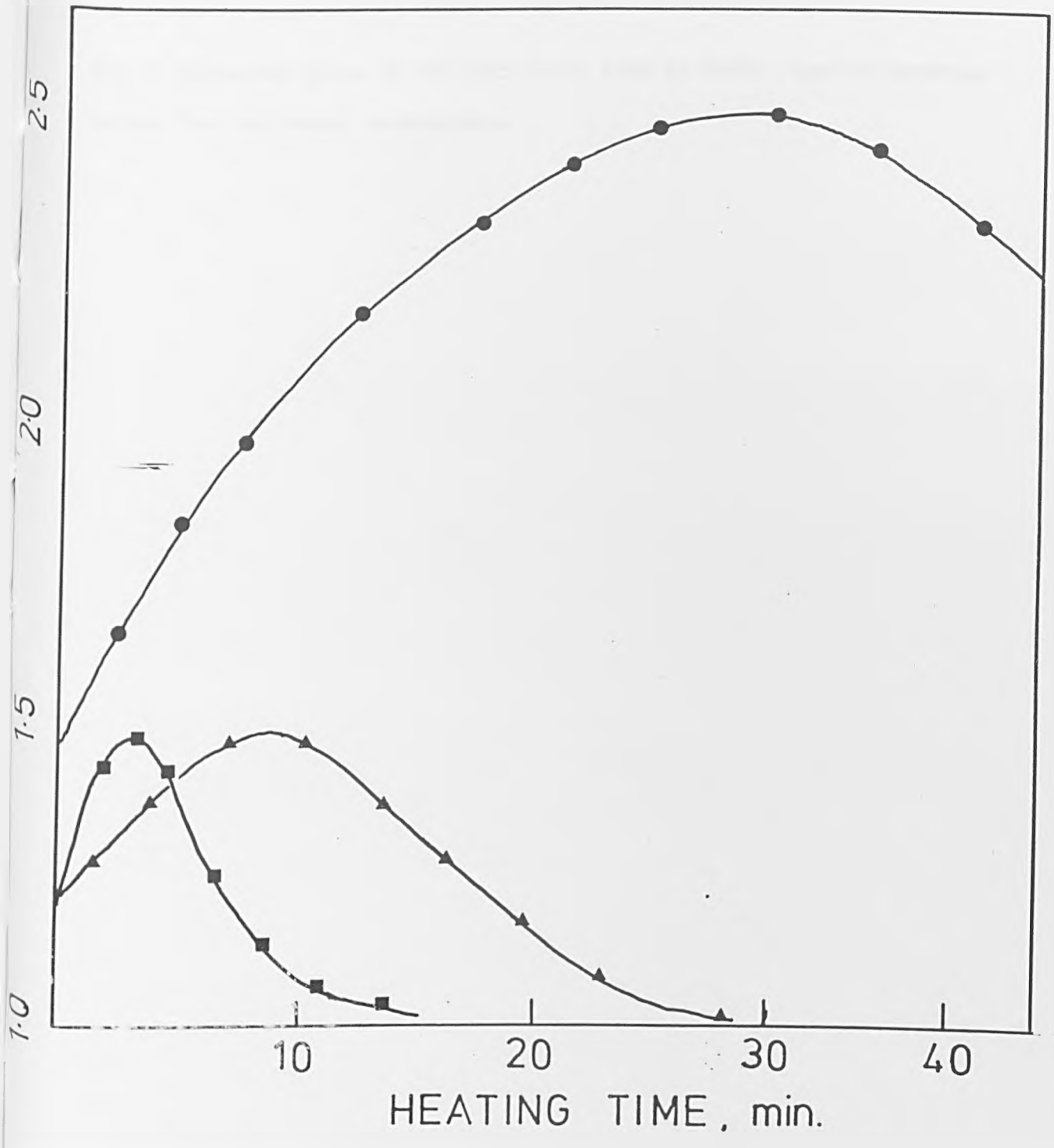
2·5
2·0
1·5
1·0
10
20
30
40
HEATING TIME, min.

Fig.3. Arrhenius plots of the reciprocal time to reach maximum coverage versus the reciprocal temperature.

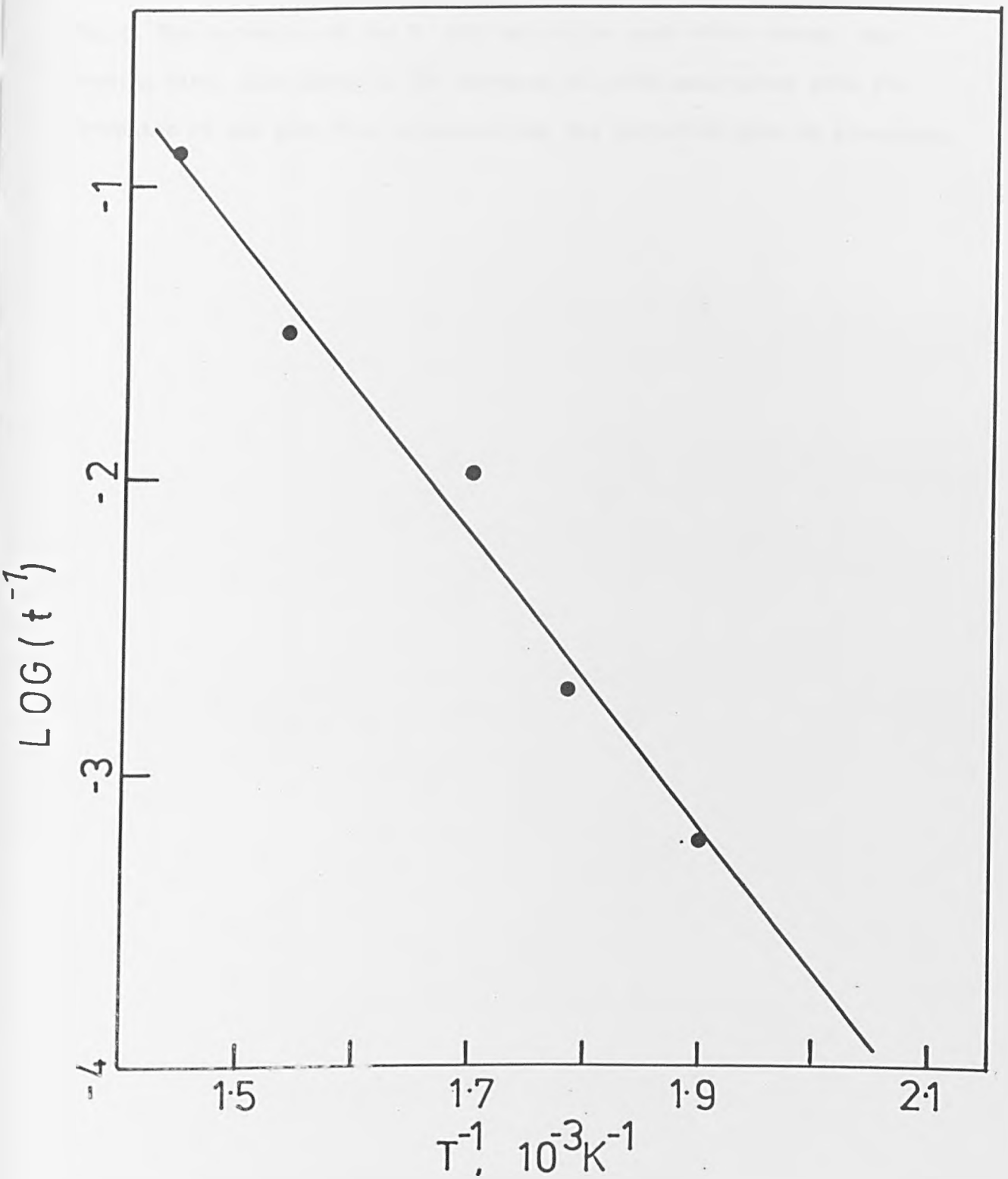
LOG(t⁻¹)
-1
-2
-3
-4
1·5
1·7
1·9
2·1
T⁻¹, 10⁻³K⁻¹

Fig.4. The variation of the W AES derivitive peak width versus the heating time. Also shown is the increase in width associated with the formation of the p(2× 2)-O structure and the p(2×2)-O plus In structure.

W PEAK WIDTH, ARB. UNITS.
710K
clean
p(2x2)
p(2x2)
+
In
5 10 15 20 25
HEATING TIME, min.

Fig.5. The variation in O (- - - -) and In(———) coverage, as measured using AES, as a function of temperature for successive anneals of 30s.

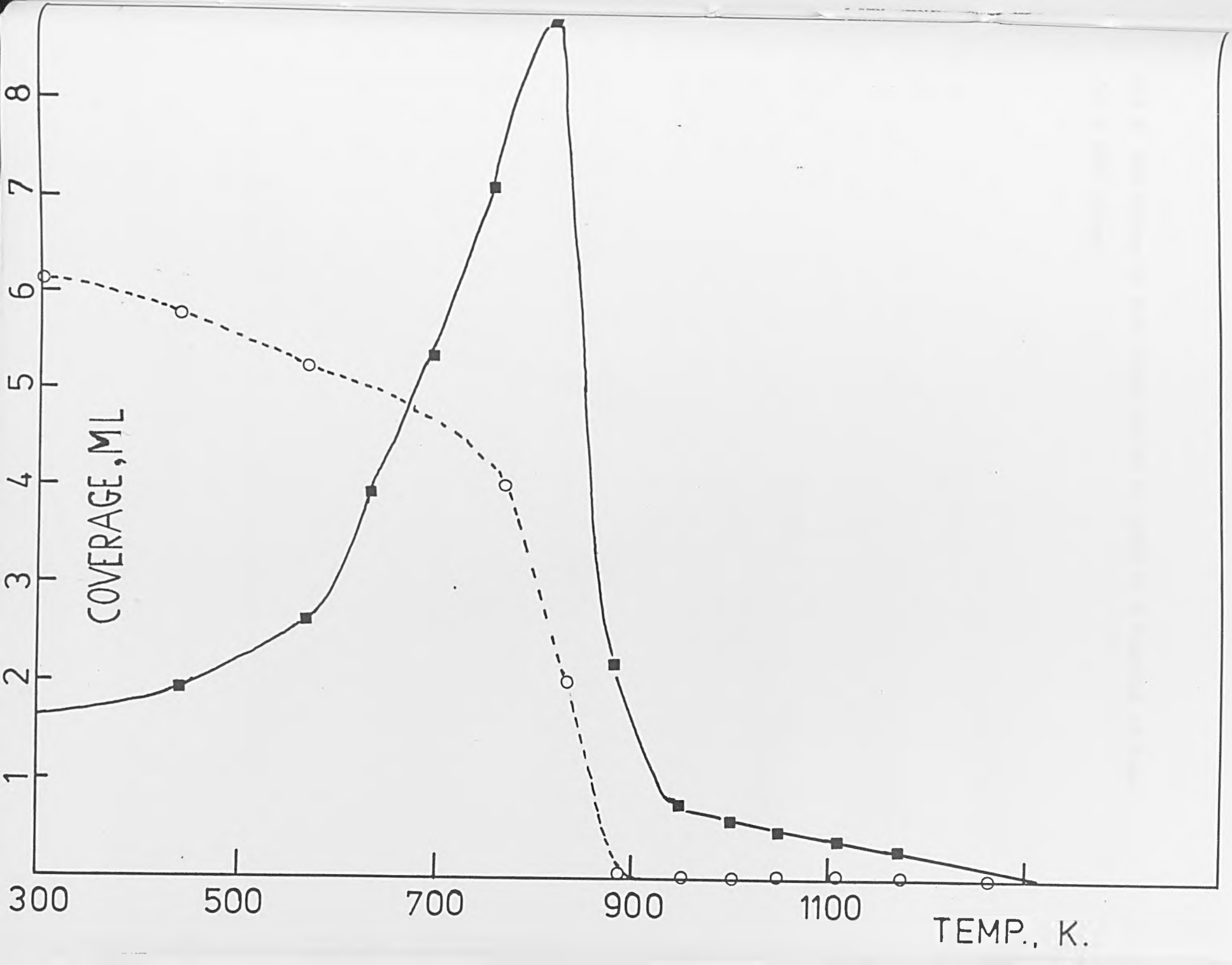
COVERAGE, ML
1
2
3
4
5
6
7
8
300
500
700
900
1100
TEMP., K.

Fig.6. The change in peak shape for an In patch as a function of time for a 680K anneal.

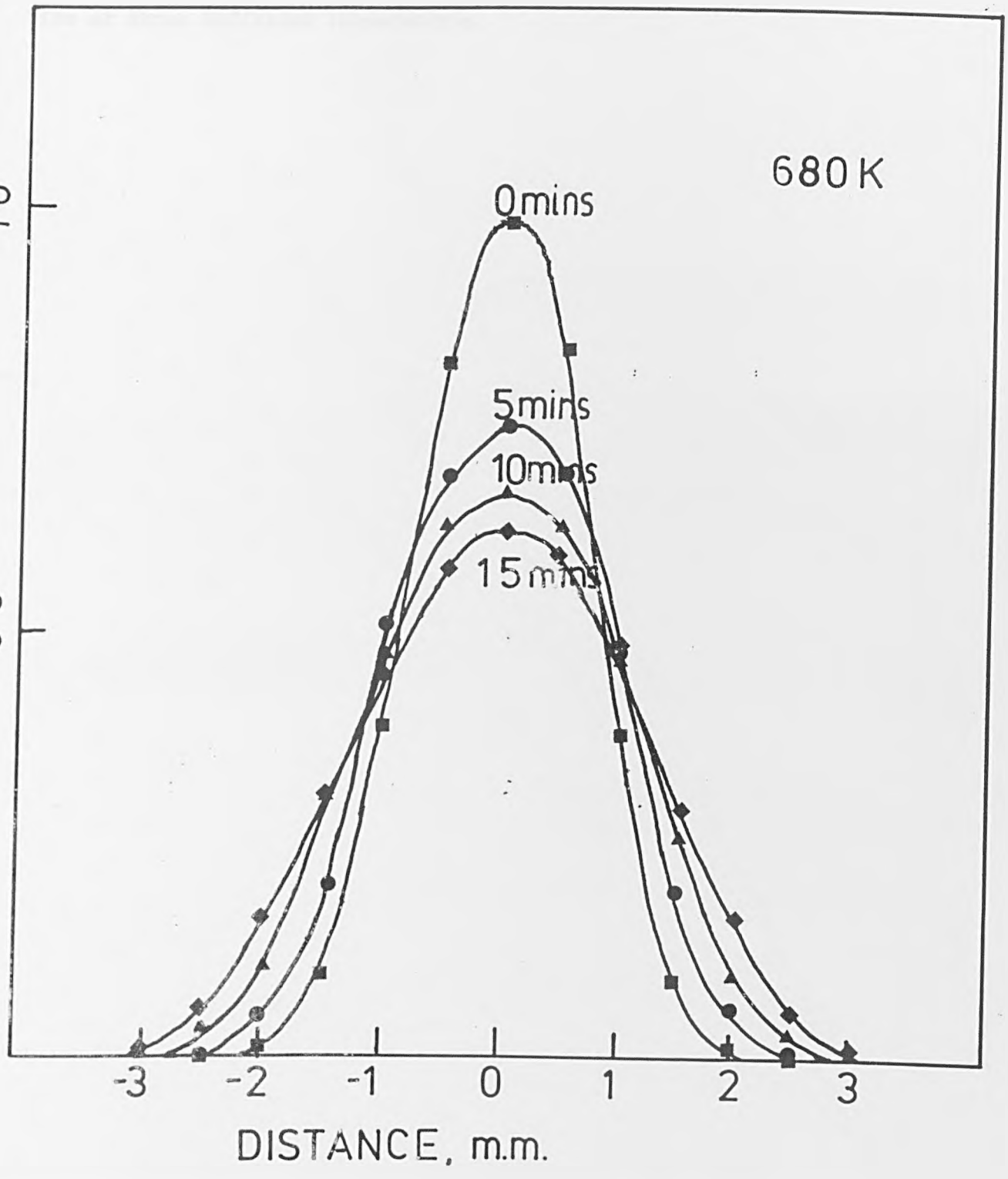
680 K
0 mins
5 mins
10 mins
15 mins
1·0
0·5
-3
-2
-1
0
1
2
3
DISTANCE, m.m.

Fig.7. A plot of the increase in peak width squared versus the heating time at three different temperatures.

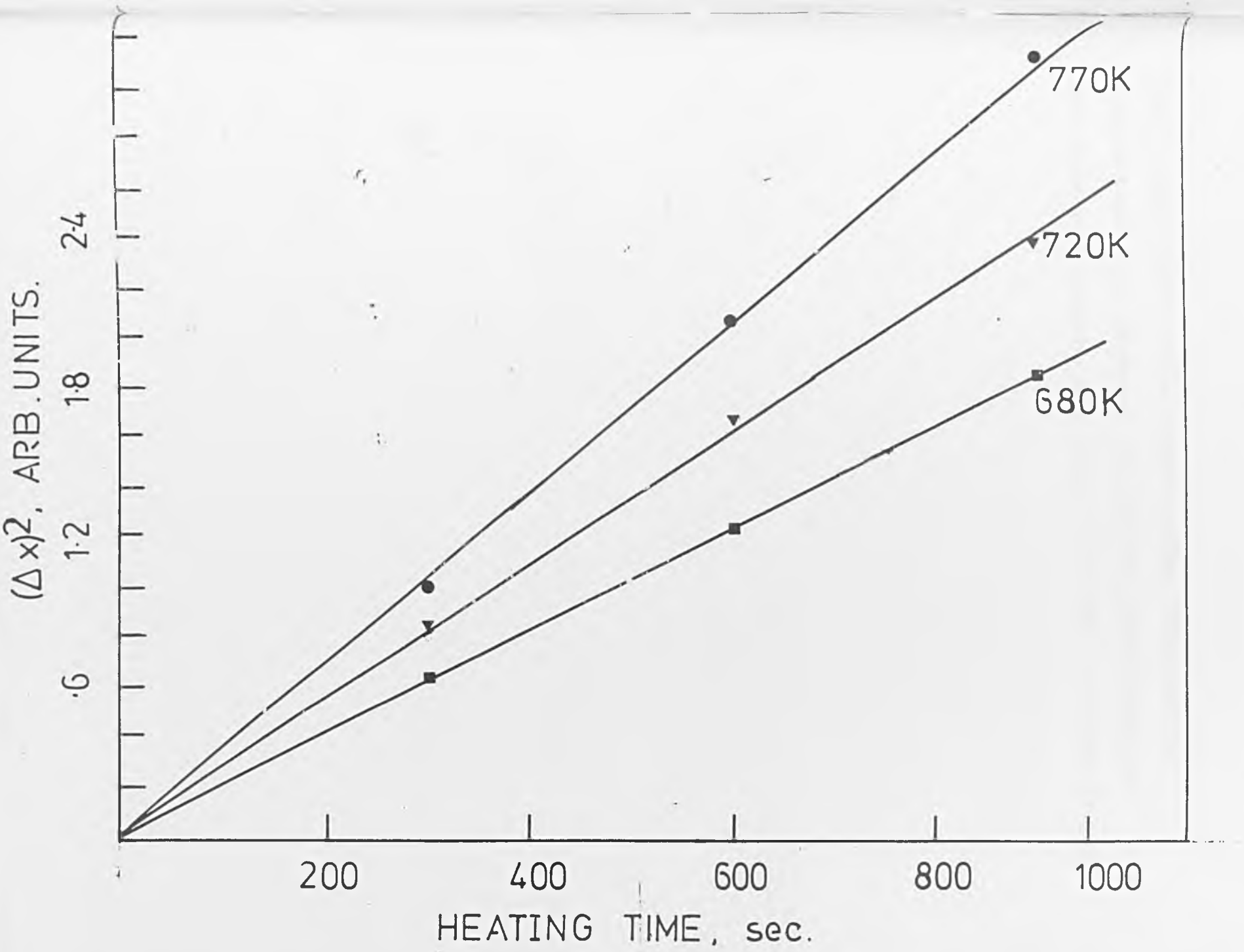
770K
720K
680K
$(\Delta x)^2$, ARB. UNITS.
·6
1·2
1·8
2·4
200
400
600
800
1000
HEATING TIME, sec.

Fig.8. Arrhenius plots for the diffusion process. ● represents an analysis based on the increase of the peak width, other symbols are from a peak shape analysis. These are; ▲, $\theta = 0.75$; ■ , $\theta = 0.5$; ◆, $\theta = 0.25$.

LOG$_e$ D (cm^{-2}s^{-1})
-13
-12
-11
-10
1·2
1·4
1·6
T^{-1} K^{-1} 10^{-3}

CONCLUDING REMARKS.

The diffusion and adsorption kinetics of four systems have been measured; these are O/W {110} , K/W {110} , In/W {100} , and In/W {100} + p(2×2)-O. The three adsorbates are very different in their physical and chemical properties and these differences are reflected in their adsorption properties. Oxygen is typical of many gaseous adsorbates; it saturates the surface at a density equal to the substrate atom density and displays a number of ordered structures through the coverage regime. Multilayers of O do not form at room temperature. K is like many of the alkalies in that it forms very few ordered structures at room temperature and none were observed in the present study. Multilayer growth is unstable. In is an excellant example of the metal/metal adsorption system. It condenses with a sticking probability equal to one and multilayer growth is highly favoured. The first layer is pseudomorphic and layers after this grow via the formation of three-dimensional islands.

This work has shown that these adsorption properties are mirrored in the diffusion kinetics, of the adatoms, across the surface. This is to be expected since it is the properties of the adatom which dominate the adsorption and desorption properties. Hopefully, this work emphasised that to picture the surface realistically it is essential that the three events are not considered as separate. More specifically the work presented here has shown that there is a very strong relationship between the measured diffusion kinetics and the surface structure. The reason for this is clear, both diffusion and ordering are critically dependent on the lateral interactions between the adsorbed species.

The diffusion/desorption/adsorption kinetics show that the K/W {110} system is dominated by the very strong repulsive lateral interactions between the adatoms, and the lack of ordered structures observed is because of the same reason. The O/W {110} system is dominated by the attractive

next-nearest-neighbour interactions that exist. In this system the oscillatory nature of the interactions, i.e. repulsive nearest-neighbour, attractive next-nearest and so on, results in several ordered phases as a function of coverage; the $p(2\times1)$, $p(2\times2)$ and (1×1). In shows a sudden decrease in diffusion energy after the first monolayer is complete. This is associated with the enhanced mobility of second layer adatoms as they attempt to reach equilibrium with more strongly bound 1st layer sites (and so cause a lowering of the total energy of the system). No change in diffusion kinetics was noticed as a function of coverage above $\theta = 1$ and this is strongly associated with the haphazard 3-dimensional island growth seen in the multilayer region. Below $\theta = 1$ the diffusion is dominated by repulsive interactions between the adatoms, the diffusion energy continually decreasing with coverage.

The In/W {100} -p(2×2)-O system is very much more complicated; whereas In shows no sign of alloying with the clean W{100} substrate lattice, this is not true for the p(2×2)-O system where dramatic changes in the nature of the adlayer are noticed as a function of temperature. Further investigations for this system are strongly indicated; XPS, ISS and SIMS depth profiling would give detailed information on the surface rearrangements noticed here. This system may have a commercial importance in that it could be related to the Al_2O_3 surface, which is important as a catalyst and support. Proposals have been made by the author to examine this system by the techniques listed above. Only at coverages $< \theta = 1$ can the In be maintained, over the temperature range necessary, at the surface -vacuum interface and so only at these coverages can the diffusion be studied. The activation energy for surface diffusion decreased with coverage as for the clean surface but the magnitude of the energy was reduced and this lowering of the diffusion barrier may be crucial in the

absorption processes seen after $\theta = 1$. The lowering of the surface diffusion activation energy barrier is associated with a surface roughening effect and/or electron donation to the O adatoms increasing the repulsive interactions between the adsorbed In.

For many years, surface diffusion has been very much neglected, apart from the work of a few isolated laboratories. This is probably due to the work being very demanding and time consuming. However, the rewards can be great, no surface will be fully understood until high quality diffusion measurements have been made. The new techniques that are being continually discovered and the improvement of older ones should make the experimentalists task easier and the results of these experiments will be important academically and commercially.